An Investigation of the Circulation in a Numerical Model using Tracer Distributions

Peter Murray Douglas

Doctor of Philosophy
The University of Edinburgh
1997

Declaration

This thesis has been composed by myself, and all work reported herein is my own except where otherwise stated.

To Tim

Acknowledgements

I wish to thank Prof. R. S. Harwood for his supervision and invaluable feedback throughout this work. I acknowledge W. G. Read of the Jet Propulsion Laboratory for his assistance with the MLS water vapour. Thanks go to the British Atmospheric Data Centre, particularly Sam Pepler, for providing the ECMWF analyses. I thank J. S. Kinnersley for his patient help concerning the 2-D model. Thanks to M. W. Morrey for his plot of PV gradient in Chapter 5. A big thanks to the Meteorology Department and the UGAMP community for the technical support and excellent working environment.

On a more personal note, I'd like to thank my family, particularly Mum and Dad, for their support over the years. Thanks to my best friend, Matthew Hurst, for everything. Thanks also go to Claudio Russo and the rest of the Strathfillan Road crowd for an excellent time. Thanks to Forbidden Planet for giving me more than just a part-time job. My thanks to Maureen for making it possible - I won't forget. Finally, a very special thank-you to Tim Taylor - I couldn't have done it without you.

Abstract

Recent observations of trace constituents were used as a basis for comparing the circulation of the UGAMP General Circulation Models with that of the real atmosphere. Measurements of two different constituents were used; upper-tropospheric water vapour and the volcanic aerosol injected into the stratosphere by Mt. Pinatubo.

The study of upper-tropospheric water vapour in the UGCM was motivated by reports of an interhemispheric asymmetry in aircraft measurements; the northern winter hemisphere contained 2 to 4 times more H_2O than the southern winter hemisphere [*Kelly et al.*, 1991]. The UGCM did exhibit an interhemispheric asymmetry in water vapour fields between 200 and 300mb, but to a lesser degree than claimed by *Kelly et al.* A further analysis of water vapour in the UGCM revealed that, due to the longitudinal variability of the distribution, a different choice of measurement sites could significantly alter claims made about interhemispheric asymmetry. Confidence in the severity of the asymmetry was further decreased after examining MLS retrievals of H_2O at 215mb which showed very little difference in water vapour mixing ratios between the two winter hemispheres.

The UGCM and EUGCM were used to simulate the dispersal of the Mt. Pinatubo aerosol cloud. With a lifetime of years in the stratosphere and a well documented evolution, the Pinatubo cloud serves as a good test for model dynamics. Both models showed evidence of the two different mixing regimes seen in the real atmosphere; material mixing into the northern mid-latitudes below 20km and material mixing into the southern mid-latitudes above 20km. The two Pinatubo simulations developed a tropical stratospheric reservoir, similar to that in the real atmosphere. The tropical confinement of material was maintained in the EUGCM by steep PV gradients, acting as a barrier to isentropic transport, situated in the low latitudes. Material only escaped from the tropics into the mid-latitudes via a channel of low PV gradient.

The Pinatubo simulation did contain one major flaw, and that was a severe interhemispheric asymmetry in the tracer dispersal; not enough material was reaching the southern latitudes. The cause of the problem was narrowed down to a lack of cross equatorial transport near the beginning of the model run. An equatorial PV barrier was found to be responsible for this lack of transport and if material had reached the southern tropics in the first few weeks of the model run, the interhemispheric asymmetry would diminish. It is shown that the equatorial gradients of PV in the EUGCM are stronger than those in the ECMWF analyses in the months following the Pinatubo eruption. Further investigation reveals that this is due to a split in the tropical-stratospheric easterly jet in the EUGCM which is not present in the analyses.

A simple experiment, using a 2-D model with interactive radiation, dynamics and chemistry, contributed to the debate of whether including the radiative effects of volcanic aerosol is necessary to accurately simulate the poleward spread of the aerosol. It was found that the additional heating did promote transport south, across the equator. Any UGAMP model experiments involving transport of sulphate aerosol should include aerosol heating.

Contents

Chapter 1

Introduction and Motivations

The stratosphere is important to human life because it contains the ozone layer which filters out ultraviolet radiation. Prolonged exposure of human skin to ultraviolet radiation can cause skin cancer. The amount of ozone in the stratosphere is a result of a number of chemical processes of which catalytic destruction is important. The species which are involved in the catalysis are mostly released in the troposphere and pass into the stratosphere in equatorial regions. They are then transported around the rest of the stratosphere by the motion systems present there. Therefore, it is important when modelling the ozone layer to be sure that the motion systems behave in a realistic way.

A good opportunity for testing that numerical models get the transport processes right was afforded by the eruption of Mt. Pinatubo in 1991. The volcano put a pronounced tracer into the stratosphere, the spread of which was extensively monitored. We compare the spread of tracers in the UGAMP model with that of the Pinatubo cloud in the real atmosphere. A focus of this comparison will be the method of tropical/mid-latitude exchange and the role that PV barriers play in it. Another opportunity for testing the circulation in the UGAMP model was provided by recent measurements of water vapour in the upper-troposphere. Specifically, we check the model for an interhemispheric asymmetry in upper-tropospheric H_2O reported in the literature.

The thesis is structured in the following way. The next chapter revises what is currently understood about middle-atmosphere dynamics, giving a context for the work presented here. Chapter 2 also describes the main features of the UGAMP general circulation model, the principal numerical model used in this thesis.

An initial comparison between observed trace fields and equivalent fields in the UGCM is made in Chapter 3. Both aircraft measurements and satellite retrievals of upper-tropospheric water vapour are used for the study. The main purpose of the comparison is to ensure that the UGCM represents the interhemispheric asymmetry in the water vapour fields reported by *Kelly et al.* [1991].

The bulk of the work concentrates on the ability of the UGAMP models to simulate the dispersal of the Mt. Pinatubo cloud. As the volcanic cloud entered the stratosphere in the tropics, it is an excellent device for testing tropical/mid-latitude exchange. We want to see if the model can reproduce the dynamical processes necessary to accurately simulate the poleward dispersal of volcanic material. Chapter 4 describes simulations of the Pinatubo cloud conducted in two different versions of the UGAMP GCM. Chapter 5 addresses some of the issues raised by those simulations. In particular, the EUGCM is investigated for evidence of steep gradients of potential vorticity acting as barriers to isentropic transport. We want to see if there are PV barriers in the low latitudes of the model and if they are responsible for maintaining the tropical, stratospheric reservoir of volcanic tracer. In Chapter 6 we use a 2-dimensional model to run a simple experiment to ascertain the significance that including aerosol heating has on the Pinatubo simulation.

The final chapter sums up what has been learnt through the course of the thesis and the possibilities for further work are discussed.

Chapter 2

Overview of Atmospheric Science and the UGAMP GCM

2.1 Current understanding of the middle atmosphere

2.1.1 The structure of the atmosphere

A standard model for the mean mid-latitude temperature profile is shown in Figure 2.1. The atmosphere is divided height-wise into different sections and these sections can be identified by certain features in the mean vertical distribution of the temperature, T. The mean temperature profile can be roughly explained in terms of absorption and emission of radiation. Infrared emission by water vapour and clouds is primarily responsible for the minimum temperature at the tropopause. The temperature peak at the stratopause is due to the absorption of solar ultra-violet radiation by ozone. Our work concentrates on the lower-stratosphere and upper-troposphere.

Most of the atmosphere is stably stratified; the stratosphere has the strongest stable stratification. Dynamical constraint due to stable stratification is one of the most critical considerations for the global-scale mean mass circulation (the other being height dependence of solar uv fluxes).

2.1.2 General mean circulation

Figure 2.2 shows the typical latitude and height dependence of the longitude and time-averaged mass circulation of the stratosphere. The mean circulation is for

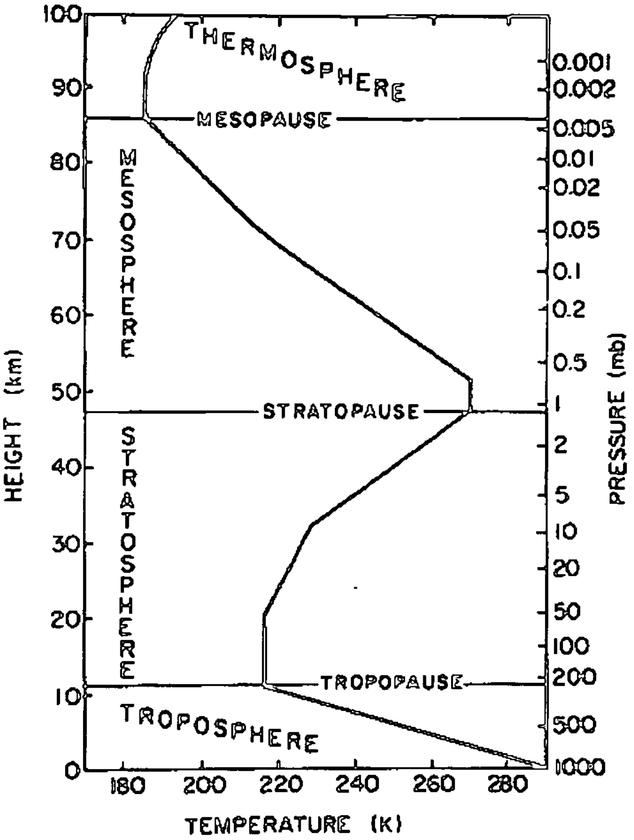

Figure 2.1: Mid-latitude temperature profile. Taken from *Andrews et al.* [1987]

January 1979 and is thought to be typical of other northern hemispheric winters (taken from *McIntyre* [1992]). The northward mean velocities at the top right of the plot (not including the mesospheric circulation) are of the order of 2 or 3 ms^{-1}. The vertical velocities in the tropics of the lower stratosphere are much smaller, in the order of a fraction of a millimetre per second. Air parcels entering the stratosphere at the tropical tropopause will generally take about two years to reach 40km. At the top of the stratosphere, the circulation flows predominantly towards the winter pole. This meridional circulation is induced by a difference in heating between the poles, with more heating occurring in the upper stratosphere above the summer pole. However, the circulation is primarily driven by eddy forcing, not radiative heating directly.

Fels [1985] showed that if there was no eddy flux divergence the mean circulation would not get driven and the atmosphere would come to radiative equilibrium. For example, air in the descending branch of the circulation in Figure 2.2 gets compressed. This raises the temperature of the air parcel meaning that the temperature of the descending branch is above the radiative equilibrium. Therefore that part of the atmosphere cools. The reverse happens in the ascending branch of the circulation. So this heating (or cooling) is a direct result of the mean circulation which is driven by the eddy flux convergences. The eddy forcing is caused by atmospheric waves, some of which are discussed in section 2.1.4.

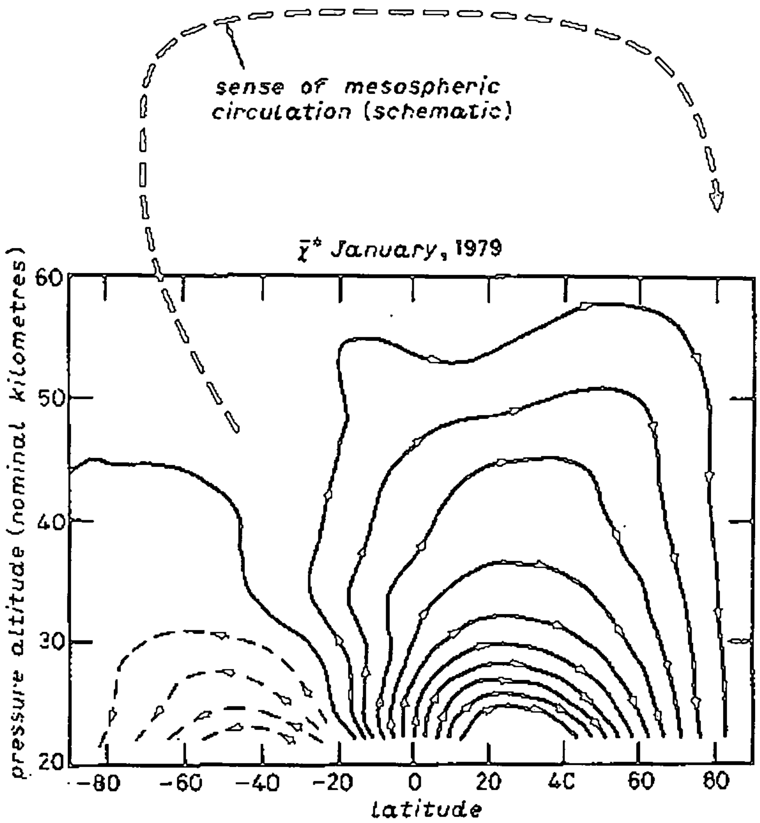

Figure 2.2: Mass transport streamlines of the global-scale mean circulation for January 1979 estimated using satellite data. The heavy dashed line indicates the qualitative sense of the mesospheric circulation deduced from other observational evidence. *McIntyre* [1992]

2.1.3 Potential vorticity

Potential vorticity (PV) is a quantity of considerable dynamical importance because it is conserved in adiabatic, frictionless motion. This was shown by *Ertel* [1942] who defined PV as

$$PV = \rho^{-1}\zeta_a \cdot \nabla\theta, \tag{2.1}$$

where ρ denotes density (mass per unit volume), θ is potential temperature and ζ_a is the three-dimensional definition of absolute vorticity.

Throughout most of the atmosphere, the isentropic surfaces are almost horizontal (due to stable stratification). This means that the vector, $\nabla\theta$ (the potential temperature gradient), is usually directed nearly vertically. So generally speaking, the PV of an air parcel can be considered as a measure of it's spin about the vertical.

The combination of $\nabla\theta$ (representing the inverse length of the air column), absolute vorticity and density (allowing for compressibility of air parcels) shown in equation 2.1 means that this definition of PV is conserved for all adiabatic motion. The ability to characterise quasi-horizontal motion largely in terms of the two scalar fields, PV and θ, with an evolution that is easy to visualise and understand, greatly simplifies atmospheric dynamics and this technique is used in Chapter 5.

2.1.4 Atmospheric waves

Of great significance when looking at transport processes in the middle atmosphere are atmospheric waves. The waves in question propagate upwards from the troposphere and dissipate in the middle atmosphere. Accompanying the wave propagation is a flux of momentum. The effect of the waves is to transport momentum (flux) from where they are generated in the atmosphere to where they dissipate. The process which occurs when the waves dissipate is sometimes known as momentum deposition or, more accurately, momentum flux deposition [*McIntyre*, 1981]. This irreversible transport of momentum affects, to a significant degree, the mean circulation described earlier.

Atmospheric waves significant to middle atmosphere dynamics include Rossby waves, gravity waves and equatorial Kelvin waves. Rossby waves play a particularly important role in the dynamical processes relevant to the transport of volcanic aerosol in the stratosphere so they will be discussed in more detail in the next section. The main features of the other waves can be summarised as follows.

Gravity waves are caused by the buoyancy restoring force associated with stable stratification so can only be generated in a region where there is a vertical gradient of θ. The gravity waves form in the troposphere and are activated by vertical undulations of isentropic surfaces. They are generated when there is stably stratified flow over orography or local diabatic heating, for example. Once generated, the gravity waves propagate upwards and have a propagation time of hours from the troposphere to the mesosphere. The irreversible angular-momentum transport due to gravity waves is thought to drive the upper mesospheric branch of the circulation featured in Figure 2.2 [*Haynes et al.*, 1991]. Gravity waves break just before reaching their critical level, much the same as ocean waves break before they reach the edge of the beach. The critical level is the theoretical location of zero intrinsic frequency. A consequence of gravity wave breaking is that the isentropic surfaces deform irreversibly instead of undulating; this results in three-dimensional turbulence.

Equatorial Kelvin waves are thought to originate from oscillations in the large-scale convective heating in the tropical troposphere [*Holton*, 1972], but this link has not been fully established. The Kelvin waves propagate vertically and are the predominant disturbances in the equatorial stratosphere due to their vertical energy and momentum transport [*Holton*, 1992]. Equatorial Kelvin waves along with equatorial Rossby-gravity waves drive the quasi-biennial oscillation (QBO). The QBO is discussed in section 4.3.4 and section 7.3.1.

2.1.5 Rossby waves

While gravity waves involve small-scale, relatively fast, vertical displacements of θ-surfaces in time scales of minutes to hours, Rossby waves involve large-scale, relatively slow, nearly horizontal displacements of air parcels along θ-surfaces with time scales of days. In the extra tropics, relatively slow means $\hat{\omega}^2 \ll \mathrm{f}^2$, where $\hat{\omega}$ is the intrinsic frequency of the wave and f is the Coriolis parameter.

The existence of Rossby waves depends on the presence of an isentropic gradient of potential vorticity (in a stably stratified atmosphere). The generation of Rossby waves occurs when air undulates on an isentropic surface in a manner similar to that illustrated in Figure 2.3. The contours in Figure 2.3 represent constant lines of PV on an isentropic surface. The x-axis is longitude and the y-axis is latitude.

The undulations of air create cyclonic and anticyclonic PV anomalies which are due to air parcel displacements across a positive isentropic latitudinal-gradient

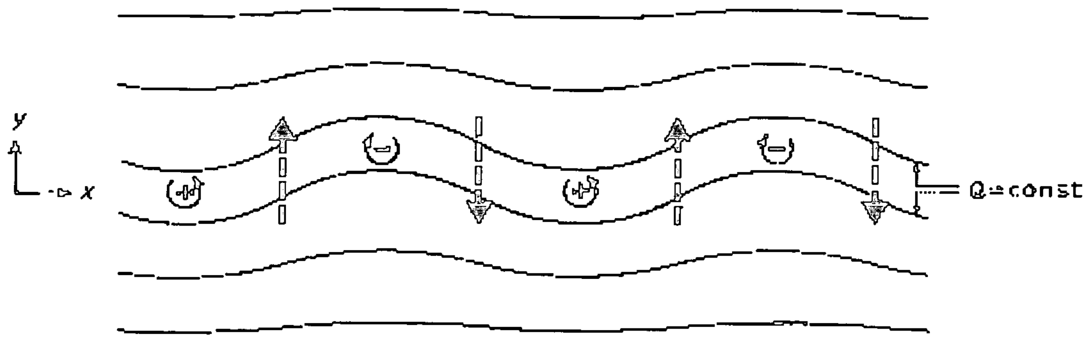

Figure 2.3: The generating of Rossby waves. PV contours on an isentropic surface in the northern hemisphere. The + and - signs, respectively, indicate the centres of the cyclonic and anticyclonic PV anomalies due to air parcel displacements. The heavy dashed arrows indicate the induced velocity field - see main text for details. From *Hoskins et al.* [1987]

of PV. Also marked on the diagram are the areas where the maximum latitudinal velocities occur, induced by the PV anomalies. Note that the maximum velocities occur a quarter of a wavelength out of phase with the displacement. These velocities move the PV contours in such a way that the wave propagates in a westward direction in relation to the mean flow (the intrinsic phase propagation). Since the intrinsic phase propagation must be westward, stationary Rossby waves can only exist for westerly mean flows. Due to the easterlies in the summer hemisphere, the Rossby waves only affect the winter stratosphere. The time that Rossby waves take to propagate through the depth of the stratosphere is on the scale of days.

As with gravity waves, small intrinsic phase speeds of Rossby waves are related to wave breaking. Rossby waves, however, break either side of the critical line, not just before it. The effect of Rossby wave breaking is to mix PV irreversibly along isentropic surfaces. Note that this mixing is layerwise two-dimensional as distinct from the three-dimensional turbulence caused by gravity wave breaking. As well as irreversibly mixing the PV, chemical substances are affected in the same way.

2.1.6 Rossby-wave breaking and the surf zone

Rossby wave breaking is characterised by rapid and irreversible deformation of material contours as distinct from the undulation of material contours associated

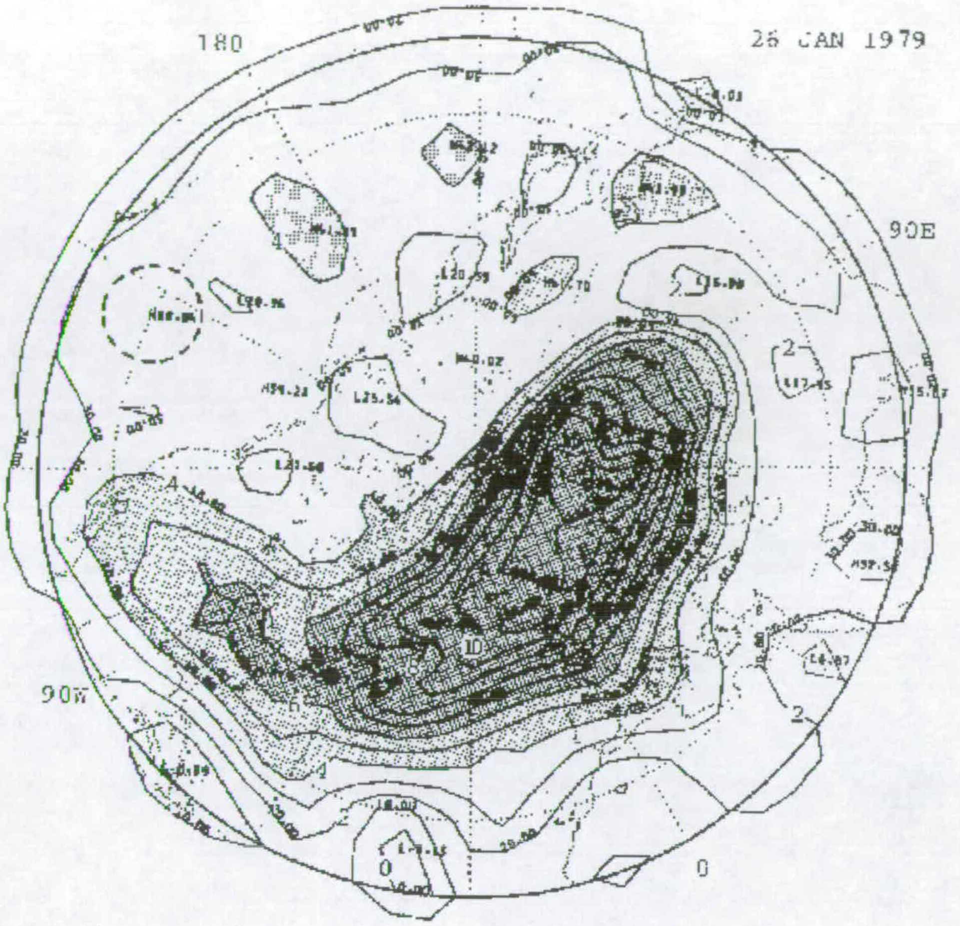

Figure 2.4: An example of a planetary wave breaking event as shown in *McIntyre and Palmer*, [1984]. The figure shows a polar stereographic (outer circle is 20°N) map of potential vorticity (divided by gH/p_0) on the isentropic surface, θ=850K for January 26, 1979. The shaded region represents high values of PV.

with wave propagation. A good example of wave breaking was presented by *McIntyre and Palmer* [1984] using isentropic maps of Ertel's PV (Figures 2.4 and 2.5). The sequence of two plots shows a tongue of high PV being pulled off the polar vortex and stretching westward into the mid-latitudes. Knowing that the potential temperature, θ, and PV of air parcels are conserved in adiabatic, frictionless processes within a time scale of up to 5 days, we can say that the tongue in Figure 2.4 represents material being dragged out from inside the polar vortex. We can see that the tongue breaks up as it is mixed irreversibly into the mid-latitude air. This example gives an idea of the planetary scale of Rossby wave breaking events. *McIntyre and Palmer* [1984] suggested that isentropic mixing associated with events of this kind are responsible for eroding the main polar

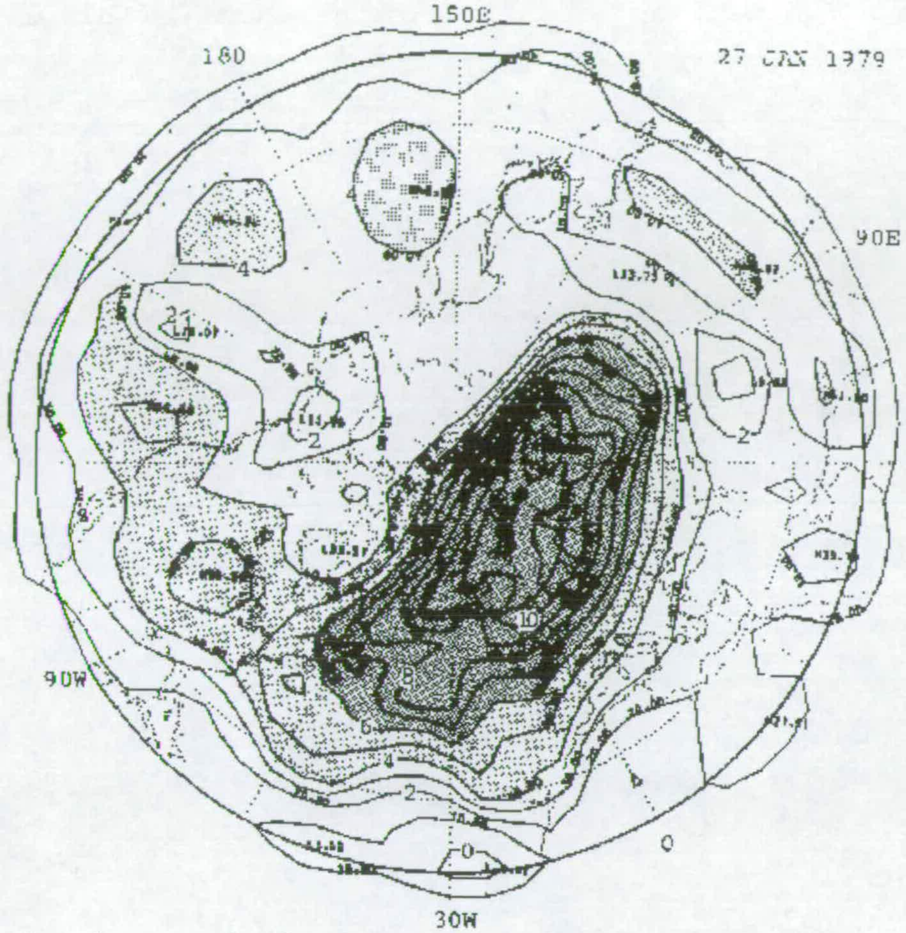

Figure 2.5: An example of a planetary wave breaking event as shown in *McIntyre and Palmer*, [1984]. The figure shows a polar stereographic (outer circle is 20°N) map of potential vorticity (divided by gH/p_0) on the isentropic surface, θ=850K for January 27, 1979. The shaded region represents high values of PV.

winter vortex to produce the region of uniform potential vorticity that is often observed to surround the polar vortex.

The following simple example illustrates what Rossby wave breaking does to an isentropic PV field with uniform latitudinal gradient. The Rossby wave breaking occurs in the shaded area in Figure 2.6a. When continuous wave breaking of the type illustrated in Figure 2.5 occurs, then the PV in the shaded area is mixed irreversibly, to the extent that the PV gradient there diminishes to almost nothing (see Figure 2.6b). This area is known as the "surf zone".

Norton [1994] provide us with a very good example of what happens to a passive tracer while the planetary waves break in the surf zone (Figure 2.7). The experiment involves contour advection in a single-layer, shallow-water model. A

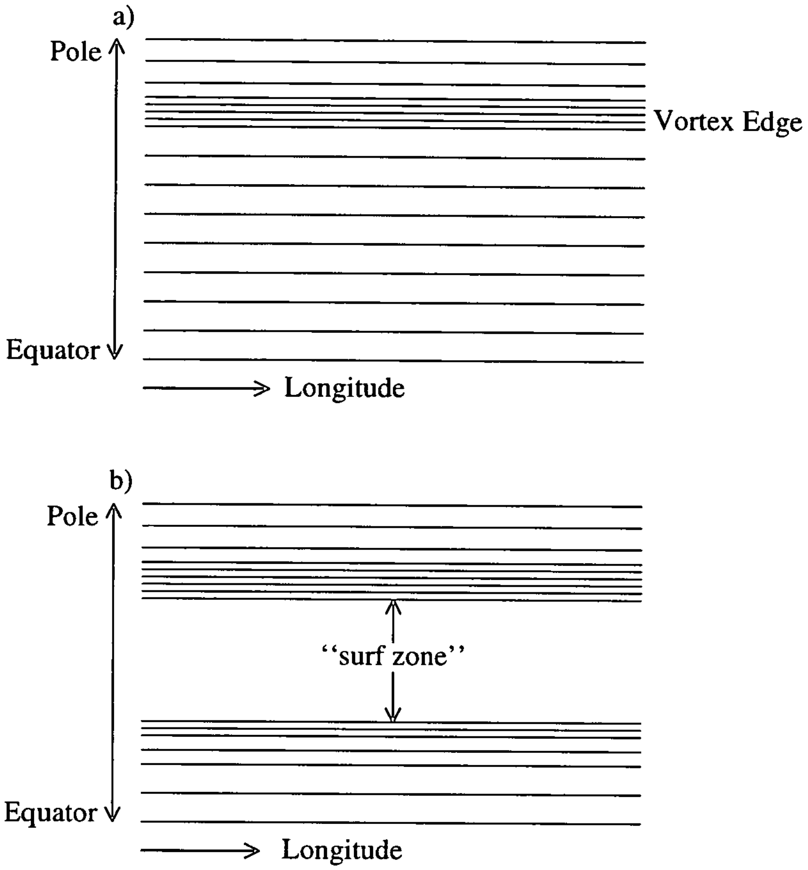

Figure 2.6: The formation of the "surf zone". Both diagrams show PV contours on an isentropic surface in the middle to upper stratosphere located in the northern hemisphere. a) shows an idealised structure of PV contours in winter with the vortex edge indicated by a tight latitudinal gradient. The shaded area indicates the area where the wave breaking will occur. b) the PV field after wave breaking.

material contour is defined by a series of particles that are advected by the velocity field of the model. This method uses an algorithm, "contour advection with surgery", developed by *Dritschel* [1989], which prevents the material contours from becoming ill-defined; particles are redistributed along the contour and new particles are added to areas of high curvature. Figure 2.7 shows the first 30 days evolution of ten initially circular material contours. The areas between the material contours are shaded to distinguish between the different air masses.

At day 10 there has been some folding of the material contours. From day 20 we can see some very fine structure in the surf zone. This includes a tongue of air extending into the mid-latitudes from the polar regions. This is a similar phenomenon to what was seen in Figures 2.4 and 2.5, but the contour advection

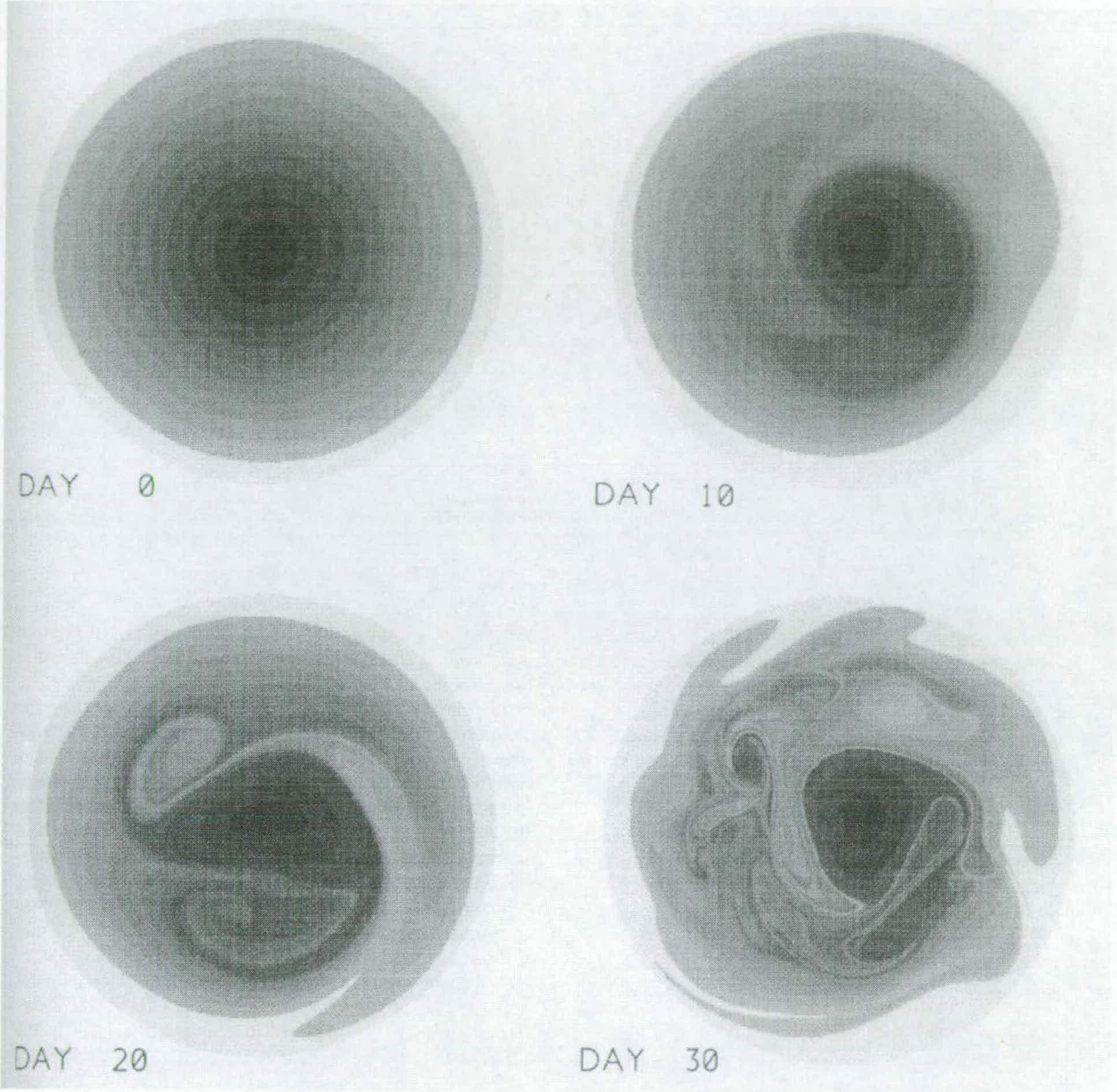

Figure 2.7: Contour advection results for ten material contours using a shallow-water model [*Norton*, 1994], days 0 to 30. Contours are advected using the velocity fields from the model. The edge of each plot represents the equator.

scheme allows us to see the chaotic and fine-scale nature of eddy advective transport. A conspicuous tongue of material is also being detrained from the tropics. It is features such as this that play an important part in the poleward transport of volcanic aerosol in the real atmosphere and we will want to see how the UGAMP model copes with these dynamical processes. By day 30, the material in the surf zone is well mixed. The polar vortex is easily identified in the tracer field with the relatively undisturbed polar material surrounded by the turbulent, mid-latitude air. Notice also that the material contours in the tropics are only slightly folded, indicating very little eddy advective activity there.

Rossby wave breaking is not evident in the polar and tropical latitudes for the following reasons. The edge of the polar vortex which forms in the winter stratosphere (see next section) can be seen as a sharp gradient in an isentropic PV field. This means that the Rossby wave restoring mechanism is concentrated and the vortex edge acts like a barrier to eddy advective transport of mid-latitude air into the core of the vortex [*McIntyre*, 1992]. There is no planetary-wave mixing in the tropics because the waves cannot propagate through the easterlies which exist there.

A second sharp latitudinal gradient in PV appears at the edge of the surf zone, dividing the mid-latitudes from the tropics. The dynamical significance of this low-latitude PV gradient is investigated in Chapter 5. It is thought that the low latitude PV gradients may be acting as a barrier to eddy advective transport in the same way that the polar vortex edge does [*Trepte and Hitchman* 1992, *Hitchman* 1994]. For the purpose of studying the dispersal of volcanic aerosol (of which there is a reservoir in the tropics) it is important to establish what effect, if any, this steep PV gradient has on tropical/mid-latitude exchange. As well as confirming the existence of PV barriers in the UGAMP model, we will want to see if they are situated where we would expect them to be.

2.1.7 The polar vortex

The polar vortex is an important dynamical phenomenon and it plays a significant role in ozone depletion. In the polar region of the winter stratosphere the temperatures become very low (lack of solar heating in the polar night). This lowering of temperatures causes the zonal winds in the area to increase in magnitude (thermodynamic balance) which, in turn, results in the formation of the polar-night jet or polar vortex. As we have already mentioned, the wall of the vortex acts as a barrier to any adiabatic motion so the constituents inside the vortex are cut off from any outside influences for as long as the vortex exists.

The environment inside the polar vortex is ideal for ozone-depleting reactions to occur. The low temperatures within the vortex allow the formation of Polar Stratospheric Clouds (PSC's). The surface of the PSC's provides the necessary conditions for the production of chlorine by heterogeneous chemistry. The chlorine molecules, through a series of reactions described in the literature [*WMO*, 1995], destroy ozone. The air in which the ozone destruction is occurring is trapped within the polar vortex; the mixing ratios of ozone noticeably dwindle in this region. Although the ozone does not actually disappear altogether this region of low ozone values is known as the ozone hole and is most prominent in the latter half of winter; the lowest values occurring just before spring. The polar vortex breaks down when the temperatures rise again (the onset of spring) allowing ozone-depleted air to escape into the more populated mid-latitudes. Chapter 5 investigates how effective the vortex edge is at inhibiting the poleward transport of volcanic tracer in the UGAMP model.

2.2 The use of numerical models in atmospheric science

Mathematical models of the atmosphere play an essential role in the advancement of understanding in atmospheric science. Models can tell us information which satellite observations cannot provide. While satellite observations can show transport processes, they often have a poor spatial or temporal resolution, a limitation which can be overcome using a numerical model. The most important contribution that models make to atmospheric science is identifying causal relationships. For example, we see from observations that the Mt. Pinatubo aerosol cloud is mostly confined to the tropics. We use a numerical model to investigate the dynamical processes which facilitate this confinement (Chapter 5).

The emphasis throughout this thesis will be on transport mechanisms and these are represented in numerical models in different ways, depending on the kind of model used. One-dimensional models consist of a single vertical column and vertical transport is usually represented by diffusion. The diffusion varies with height and is designed to give agreement with observations. In 2-dimensional models (as used in Chapter 6) the meridional circulations can be divided into an eddy flux and a zonal mean term and the eddy flux is normally based on some diffusion parametrization. 1-D and 2-D models are limited for investigations of transport processes because there is no satisfactory theory of the eddy diffusion.

While assumptions still need to be made for three-dimensional models, a broader selection of transport processes can be simulated. For example, the 3-D model can simulate advective eddy motions instead of a parametrised diffusion, an ability which is essential for studying dynamical events detraining air from the tropics. It is a 3-D general circulation model which is used for most of the work here.

2.2.1 UGAMP GCM

The General Circulation Model (GCM) featured here is the UK Universities Global Atmospheric Modelling Programme (UGAMP) GCM. There are two different versions of this model, the UGCM (UGAMP GCM) and the EUGCM (Extended UGAMP GCM). Both models are used at some point in the thesis.

The main difference between the two versions of the model is the height range which they cover. Both models extend upwards from the surface, but the UGCM's top level lies in the mid-stratosphere at 10mb, while the EUGCM, a troposphere-stratosphere-mesosphere model has a top level of 0.0017mb. The two topics of research deal with upper tropospheric water vapour and the Mt. Pinatubo aerosol cloud. Both constituents lie within the domain of the UGCM and the EUGCM so either model can be used.

The UGCM is clearly suitable for the study with tropospheric water vapour but the upper level of the UGCM proves to be a limitation with respect to the volcanic cloud study. However, with the EUGCM comes a large computational expense. Both models were used for the volcanic cloud study.

2.2.2 UGCM

The UGAMP GCM is a 3-dimensional, primitive equation model, based on the cycle 27 forecast model of the European Centre for Medium-range Forecasts (ECMWF). The model consists of prognostic equations for vorticity, divergence, temperature, specific humidity and surface pressure.

The model uses a spectral transform technique for horizontal advection, with the evolution of certain variables represented by a truncated series of spherical harmonics [*Simmons et al.*, 1989]. There are particular difficulties when advecting tracers in a spectral model and they are discussed later in Chapter 4 (section 4.3.5). The dynamical equations are integrated in time using the leap-frog scheme while physical parametrization uses the forward time-stepping scheme; both schemes are semi-implicit. The UGCM runs have a time step of 45mins (32 steps per day).

The runs of this thesis were performed at either T21 or T42 horizontal resolution, corresponding approximately to grid resolutions of 5° by 5° and 2.5° by 2.5°. The Gaussian grid is used for initialising the tracer distributions in Chapter 4.

The UGCM has 19 levels in the vertical, from the surface to 10mb (approximately 30km). The vertical coordinate scale is a hybrid of pressure and sigma, where sigma equals pressure over surface pressure. In the troposphere, where isobars may intersect the Earth's surface, sigma is used, while higher up, pressure is used.

The vertical advection of momentum, temperature, moisture and tracers in the model is handled by the total variation diminishing (TVD) scheme. This scheme is important for our purposes as it eliminates any undershoot and overshoot errors usually associated with traditional 2nd order centred difference schemes when advecting quantities with a steep vertical gradient. Tropospheric water vapour and the Pinatubo cloud are both examples of fields with a strong vertical gradient. As the TVD scheme is particularly relevant to our studies, it is described more fully in Appendix A of this thesis.

Model runs are given a seasonal cycle by varying the solar zenith angle and using monthly climatology data for deep soil temperature and sea surface temperatures. The Earth's orography is used as a boundary condition for the model.

The radiation scheme in the UGCM is that which was developed by *Morcrette*

[1990] used in conjunction with seasonally varying climatological ozone profiles. Clear sky longwave fluxes are calculated with an emissivity method and shortwave fluxes are calculated using a photon path distribution method to separate the contributions of scattering and absorption processes to the radiative transfer. Clouds are treated as grey bodies with a longwave emissivity dependent on the cloud liquid-water path. Cloud shortwave parameters are optical thickness and single scattering albedo which have been fitted to actual measurements of stratocumulus clouds.

The convection scheme used in the model is a point of discussion in Chapter 3, comparing two different schemes with respect to tropospheric water vapour. The scheme used for deep convection in the main water vapour analysis and in all the volcanic tracer simulations is the *Kuo* [1974] convection scheme where the heating and moistening by cumulus clouds is determined by the local moisture supply from large scale convergence of moisture and surface evaporation. Shallow cumulus convection is represented in the way shown by *Tiedke et al.* [1988]. One run uses the Betts-Miller scheme [*Betts and Miller*, 1993] for deep convection and that is discussed briefly in section 3.5.

The gravity wave scheme used in the UGCM is based on *Palmer et al.* [1986] and consists of a single, orographically forced wave with zero horizontal phase speed in each column.

The UGCM runs are initialised using fields obtained from ECMWF daily analyses, interpolated to suit the UGCM. The analyses are for June 15th, 1991 (start of the Mt. Pinatubo eruptions).

2.2.3 EUGCM

The EUGCM is based on the UGCM with the following differences:

The number of levels in the vertical is increased to 47, extending over a height range of approximately 0 to 90km. The vertical resolution in the lower stratosphere is about 2km which is considerably finer than the UGCM (see Figure 2.8).

Physical processes which are irrelevant for the middle atmosphere, for example deep convection, are switched off above a certain level.

The radiation scheme is adapted to cope with higher altitudes. The Morcrette radiation scheme while effective for the troposphere, is unsuitable for use

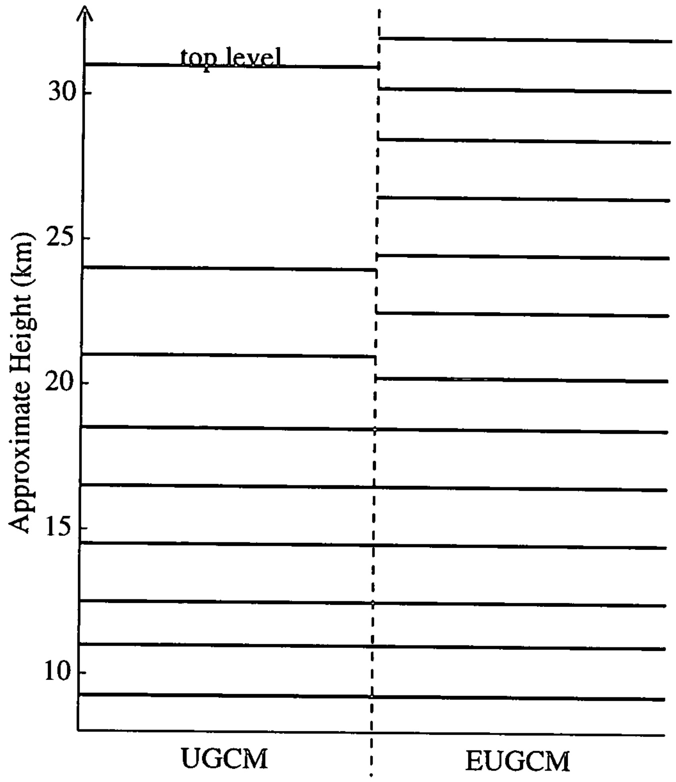

Figure 2.8: Comparing the vertical resolution of the UGCM with that of the EUGCM. The vertical scale is an approximate height (in km).

throughout the middle atmosphere. An example of how the Morcrette scheme is not suitable for the middle atmosphere is that the absorption of shortwave radiation by O_2 is not represented. At higher levels a solar radiation scheme developed and documented by *Shine et al.* [1987] is used. This scheme does take into account shortwave heating due to ozone and oxygen as well as a Curtis matrix method to determine the longwave heating due to ozone and carbon dioxide. The two distinct radiation schemes are effectively fused together in the EUGCM by taking a linear combination of heating rates calculated by the two schemes. This merging of the two schemes occurs over several model levels above the tropopause.

In the EUGCM experiments, the TVD scheme is based on fourth order differences which is of a higher order than the scheme used in the UGCM runs.

The gravity wave scheme is more complex. The EUGCM includes the ability to specify additional, non-orographic waves in an extension of the Palmer et al., gravity wave scheme. The particular configuration used in our EUGCM run is as follows. In addition to the orographic wave (zero phase speed) included in the UGCM, 16 non-orographic waves, each with momentum flux $0.5\text{x}10^{-4}\text{Nm}^{-2}$, are released from a height of 250mb. The waves are launched with phase speeds of 10ms^{-1} and 20ms^{-1} and in eight different directions (45° apart, starting from eastward) with a view to better representing the broad spectrum of waves thought to be present in the real atmosphere.

The EUGCM is initialised using fields obtained by “spinning up” the model from a previous EUGCM run which, in turn, had been initialised from ECMWF synoptic analysis fields for Jan 15th, 1987.

Chapter 3

Interhemispheric Differences in Upper-tropospheric Water Vapour

The aim of the work in this chapter is to test whether the UGAMP model is compatible with the claims made in *Kelly et al.* [1991] pertaining to interhemispheric differences in upper-tropospheric water vapour. The comparison between model and observations is extended to MLS measurements in section 3.4. A further study is carried out to establish the sensitivity of the model water vapour fields to the convective scheme used.

3.1 Motivations

The findings of *Kelly et al.* [1991] are based on aircraft measurements made as part of the Airborne Antarctic Ozone Experiment (AAOE) and Airborne Arctic Stratospheric Expedition (AASE) campaigns. Profiles of water vapour were obtained in the upper troposphere above six different sites (three in the southern hemisphere, three in the northern hemisphere) the locations of which are given in Figure 3.1. Four times as many profiles were taken at Punta Arenas and Stavanger than at the four other sites. All the measurements were taken in the winter of each hemisphere, August to September, 1987, for the southern hemisphere and late December to February, 1988-89, for the northern hemisphere. Most of the readings were taken within the height range of 300 to 200mb.

Average profiles of two main sites can be seen in Figure 3.2. From these two profiles and the others, *Kelly et al.* conclude that the northern winter hemisphere

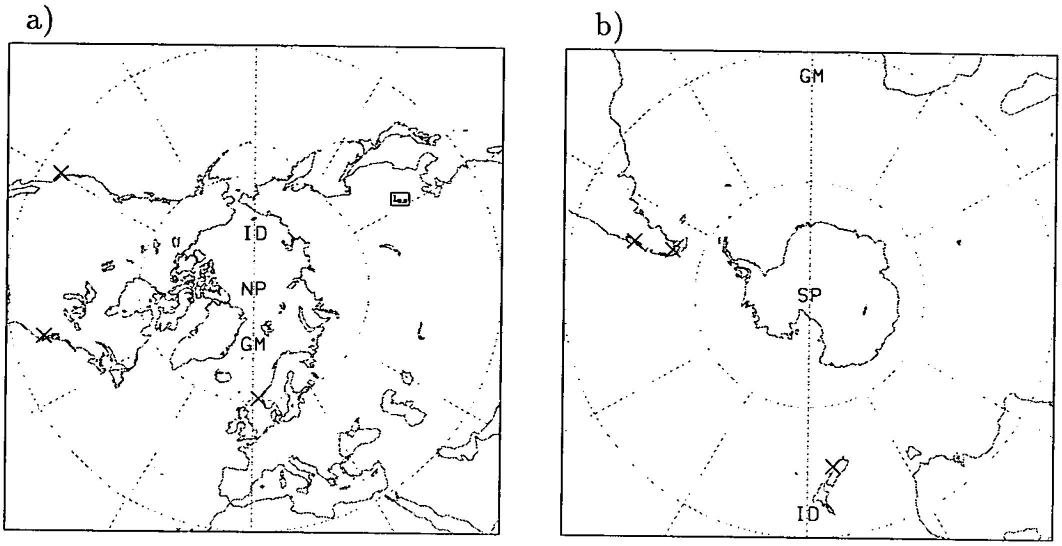

Figure 3.1: The six sites at which water vapour profiles were taken. The two main sites were Punta Arenas (53°S, 71°W) and Stavanger (59°N, 6°E). A lesser amount of readings were also taken at Puerto Montt (41°S, 73°W), Christchurch (44°S, 172°E), Moffett Field (37°N, 122°W) and Wallops Island (38°N, 75°W).

contains 2 to 4 times more water vapour than the southern winter hemisphere (in the upper troposphere).

Kelly et al. go on to explain (and attempt to verify) that this interhemispheric difference is for the following reason:

"As the lower-latitude air moves towards the pole in austral winter, it is forced to cool to lower temperatures than in the north - more of the water vapour therefore condenses to form ice crystals, which then precipitate, thereby removing the moisture from the air mass" (sloping convection during cyclogenesis dries the poleward moving air providing a sink for water vapour). Once the sloping convection during cyclogenesis has dried the poleward moving air, it finds its way back to the mid-latitudes (shown in *Kelly et al.* using trajectory experiments).

If there is an asymmetry in water vapour, as the paper suggests, then this implies an asymmetry in the production rate of the OH free radical, with probable consequences for the rate of methane loss. Upper-tropospheric water vapour is important as it has large effects on the flux of infrared radiation near the tropopause. The distribution of water vapour is central to cloud formation; clouds also have an effect on the radiation flux. With the implications that this asymmetry in water vapour has on the radiative budget and some chemical reactions, it is important

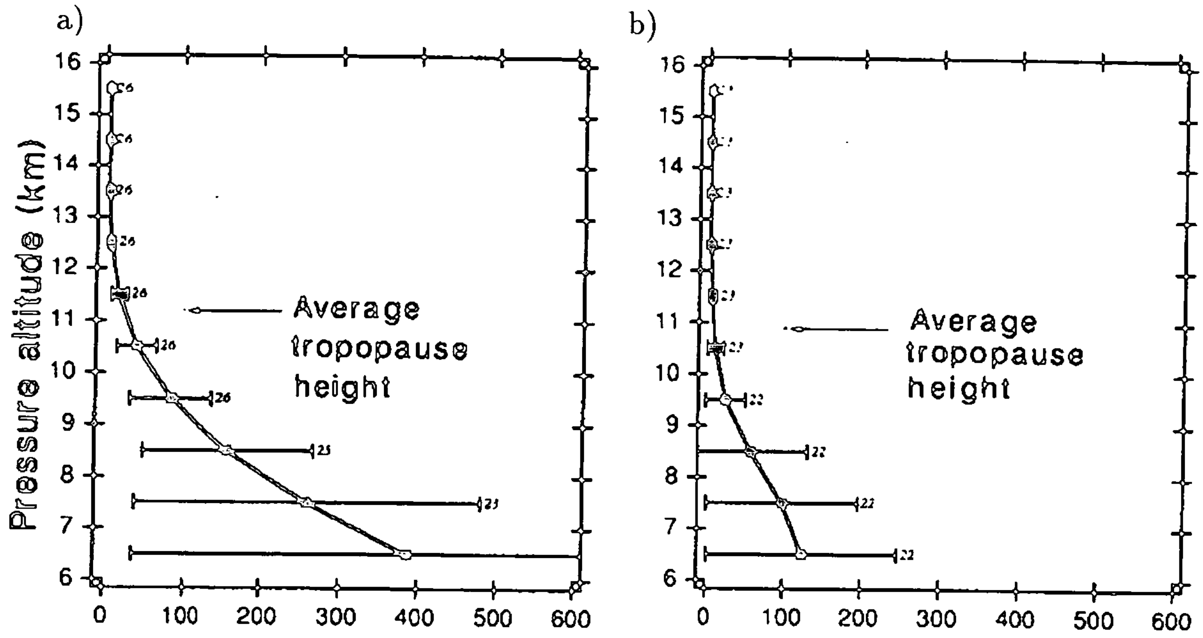

Figure 3.2: Average profiles of water vapour presented in *Kelly et al,.* [1991] from the two main sites, a) Stavanger and b) Punta Arenas. The horizontal axes are water vapour (in ppmv). The bars are standard deviations and represent atmospheric variability. The number to the right of each bar is the number of ER-2 flights contributing to the average at that altitude.

that the UGAMP model can simulate this feature to a competent degree or model experiments relating to water vapour will not be satisfactory.

Accordingly we investigate the water vapour distribution in the UGAMP model to answer two specific questions.

i) Does the UGAMP model exhibit the interhemispheric asymmetry which, according to *Kelly et al.*, is a necessary feature when conducting related modelling experiments?

ii) Are there signs of longitudinal variations in the water vapour fields that would lead to an interpretation that *Kelly et al.*'s interhemispheric differences are really an example of inadequate sampling of the entire hemisphere?

3.2 The model version used

The version of the UGAMP GCM used for this chapter is the UGCM which has 19 levels in the vertical from the surface to 10mb. With a horizontal resolution of T21, this is the simplest and cheapest version of the model. The model was run for a year with seasonal cycle using initial fields from June 15, 1991.

Many of the important features of the UGAMP model are discussed in Chapter 2, but here, particular attention should be drawn to the convection scheme used. For the initial comparison with observations, the Kuo convection scheme is used, but a further comparison is made between the Kuo and Betts-Miller schemes (see section 3.5).

The model water vapour and satellite/aircraft water vapour are in different units; the model output gives a mass mixing ratio, while all the measurements are in units of volume mixing ratio. Throughout this chapter, the model output has been converted into volume mixing ratio using the following:

$$mmr = \frac{5}{8} vmr \tag{3.1}$$

where *mmr* is mass mixing ratio and *vmr* is volume mixing ratio [*McIntosh and Thom*, 1983]. All plots of water vapour in this chapter are in units of ppmv (with the exception of Figure 3.7).

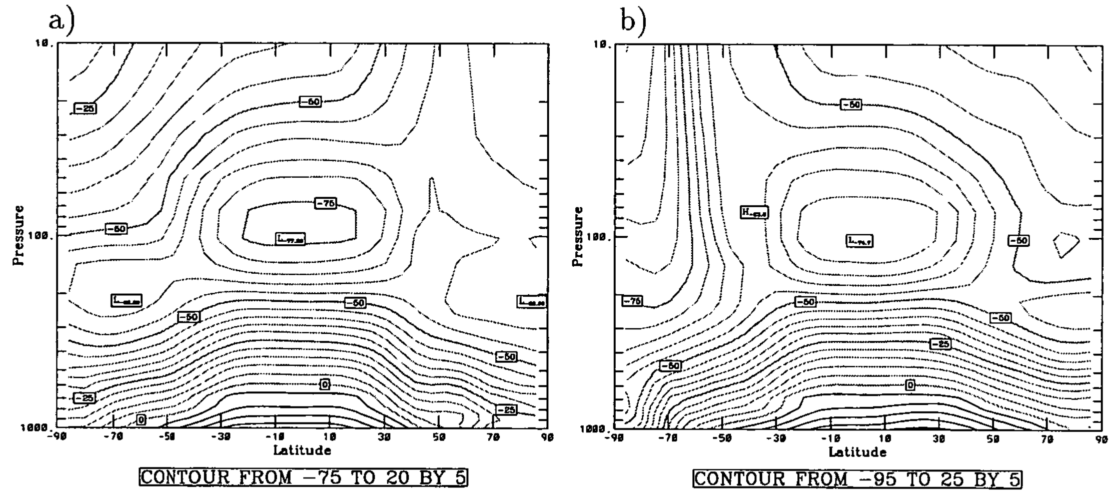

Figure 3.3: Sample zonal mean temperatures (°C) in the UGCM for a) January and b) August. Pressure scale is in mb.

3.3 Comparison between UGCM and *Kelly et al.* measurements

Averages were taken over the relevant periods of time (August to September and end of December to February) in the model run to give comparable data. As the

NORTH		SOUTH	
Site	H_2O (ppmv)	Site	H_2O (ppmv)
Stavanger	29	Punta Arenas	13
Moffett Field	35	Puerto Montt	30
Wallops Island	75	Christchurch	24

Table 3.1: Water vapour mixing ratios taken from the UGAMP model at a height of 251mb (see Figure 3.4)

emphasis of the study is on the upper troposphere it is important that the fields being compared are situated in the upper troposphere of the model. Figure 3.3 shows sample zonal mean temperatures from the model for the two time periods being used in the study. The two plots show that for the high winter latitudes the tropopause is above the fields being compared (the highest field being 215mb).

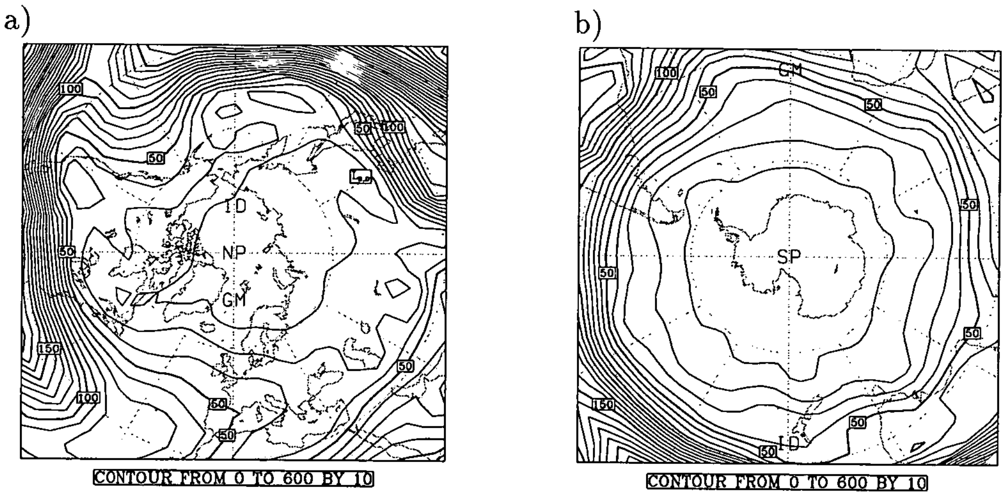

Figure 3.4: Polar stereographic projections of water vapour (in ppmv) at a height of 251mb in the UGCM averaged over a) end Dec to Feb (northern hemisphere) and b) Aug to Sept (southern hemisphere)

Figure 3.4 shows water vapour on the pressure surface 251mb which is the central height at which most aircraft measurements were taken. Table 3.1 contains the mixing ratios of water at each measurement site, as portrayed by the model fields in Figure 3.4.

Taking the average mixing ratio of each group of three sites we get 46.3ppmv for the northern winter and 21.7ppmv for the southern winter. This would seem to confirm the claim of *Kelly et al.*

That was for the average of the sites. Looking at the sites individually, however, gives a less clear-cut impression. The value at Moffett field is not much larger than those at Puerto Montt and Christchurch while Wallops Island produced a value 2 to 4 times higher than the southern sites. There is a gradient in water vapour with respect to latitude but this is not the main cause of the variation in values.

Figure 3.5 contains two plots; one for austral winter and the other for boreal winter. They show water vapour at specific latitudes plotted with respect to height and longitude. Figure 3.5a is plotted at 59°N, which corresponds to the latitude where Stavanger is situated, and Figure 3.5b is plotted at 53°S (latitude of Punta Arenas). They give a clear indication of the longitudinal variation occurring in the model.

The northern hemisphere has much more longitudinal variation than the southern hemisphere. This is due to the northern hemisphere having a more disturbed winter than the southern hemisphere. Water vapour at 251mb, around the latitude 59°N, ranges from 16ppmv to just over 40ppmv while at 53°S the values range from 10ppmv to 21ppmv. If the same kind of variation is occurring in the real atmosphere then doubts could be raised over the claims made by *Kelly et al.* as they are based on a limited number of measurement sites.

The model can be used to test the hypothesis on a more general basis using zonal averages of water vapour. Figure 3.6 contains two plots of zonally averaged water vapour, one for each hemisphere. Both plots are for a limited latitude range (35° to 60° in each hemisphere) which includes the latitudes at which the aircraft measurements in *Kelly et al.* were taken. The altitude range is also limited based on where the majority of measurements were made.

In Figure 3.6a the values range from around 17ppmv to 145ppmv and in Figure 3.6b they range from 7.5ppmv to 105ppmv. The plots clearly show an asymmetry between the hemispheres but not to the degree that *Kelly et al.* suggested. Table 3.2 gives sample values from Figure 3.6 at three different heights and the two latitude extremes. At the low latitudes, the northern values of water vapour are higher than the southern values, but not 2 times higher. The greatest difference is at 300mb where the mixing ratio at 35°N is just under 1.4 times that at 35°S. At the higher latitudes though, the difference between the hemispheres is much greater. Water vapour at 60°N is more than two times that at 60°S for all pressures

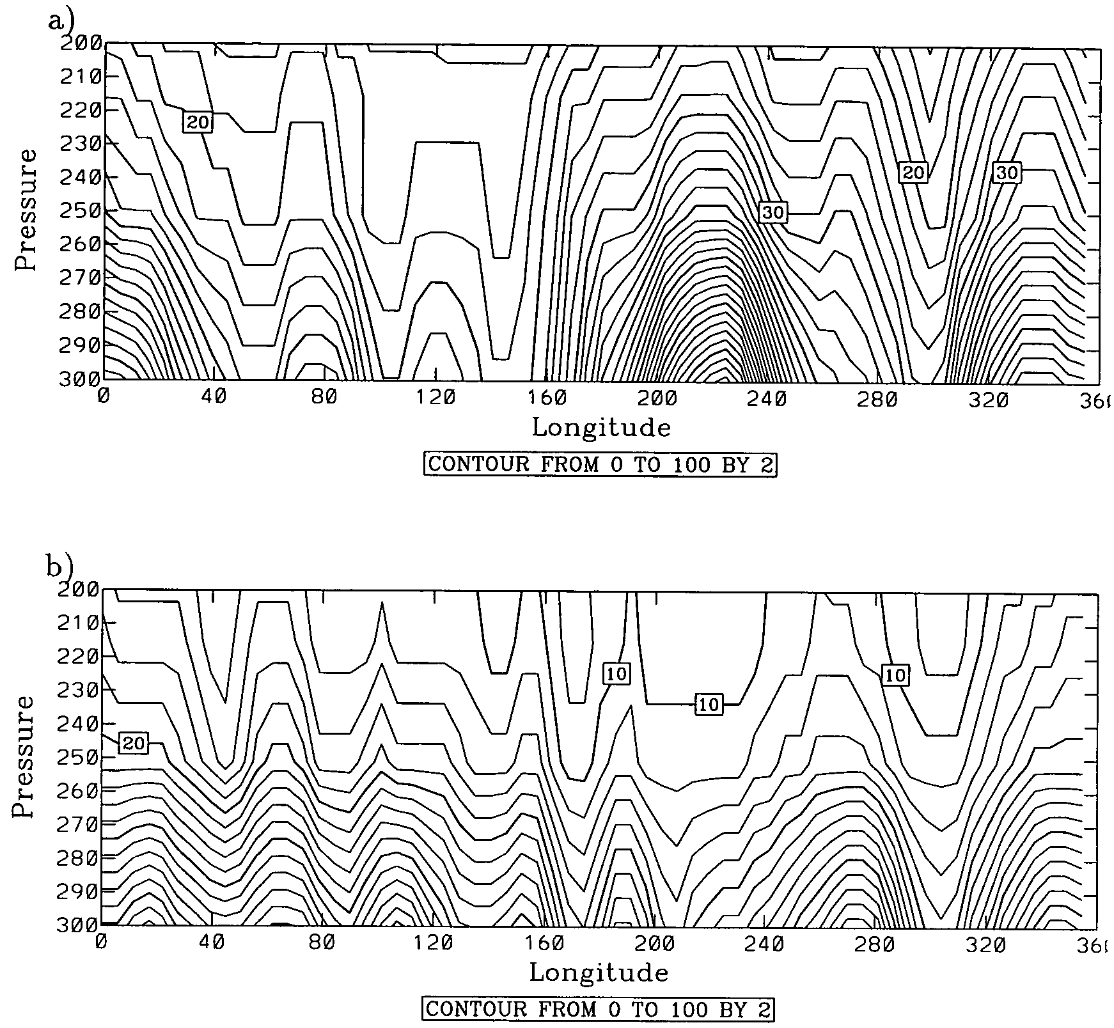

Figure 3.5: UGCM water vapour (in ppmv) plotted along a single latitude to demonstrate longitudinal variability. The slices are along the latitudes a) 59°N and b) 53°S. The values of water vapour are averaged over a) end Dec to Feb and b) Aug to Sept. Pressure scale is in mb.

	Northern Winter		Southern Winter	
	35°N	60°N	35°S	60°S
200mb	37.5	17.0	31.5	7.5
251mb	66.0	26.5	52.5	8.0
300mb	145.0	39.0	105.0	16.0

Table 3.2: Water vapour mixing ratios, in ppmv taken from the UGAMP model at specific latitudes and heights (see Figure 3.6)

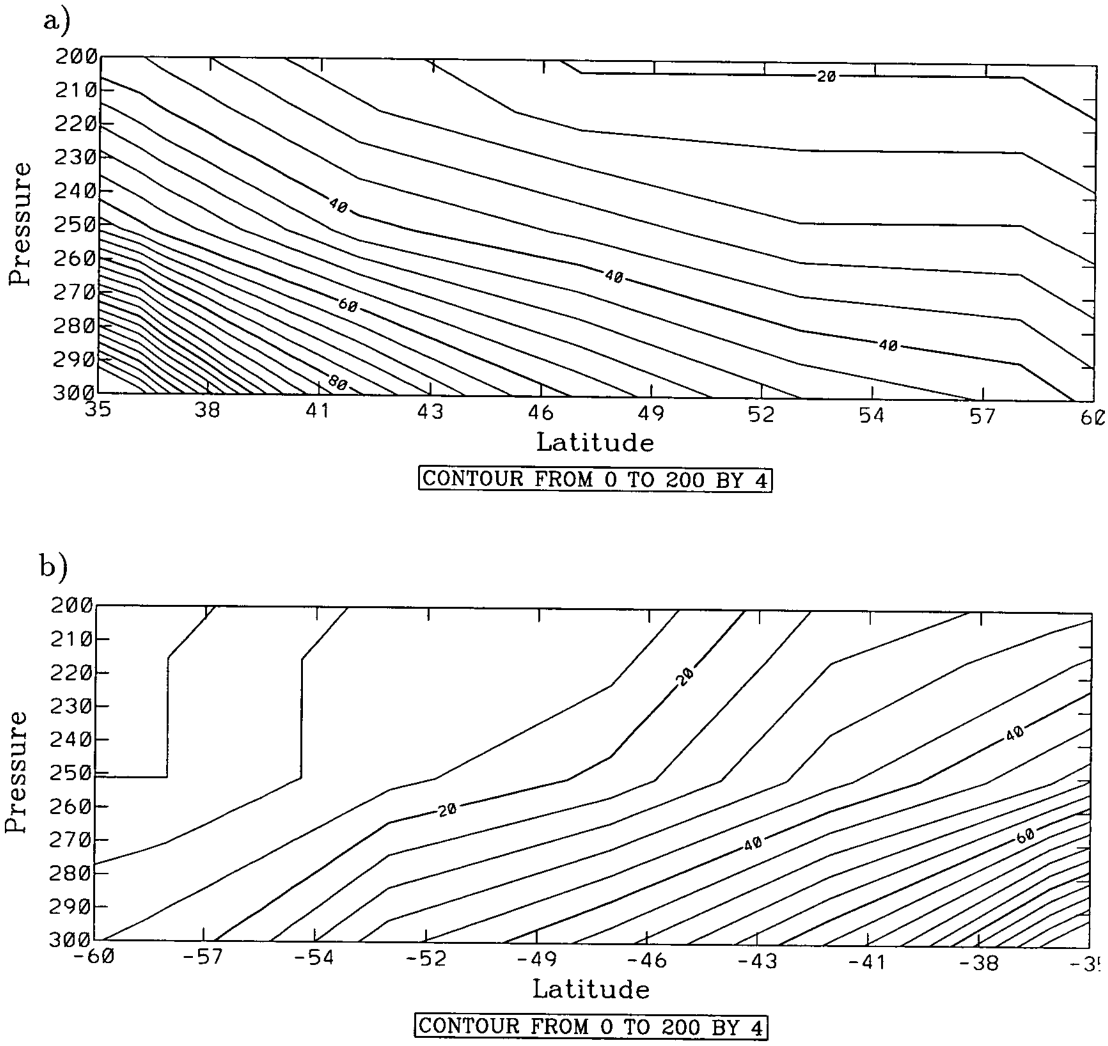

Figure 3.6: Zonally averaged water vapour in the UGCM over a limited altitude (300 to 200mb) and latitude range; a) 35°N to 60°N and b) 35°S to 60°S. Values are time averaged over a) end Dec to Feb and b) Aug to Sept. Pressure scale is in mb.

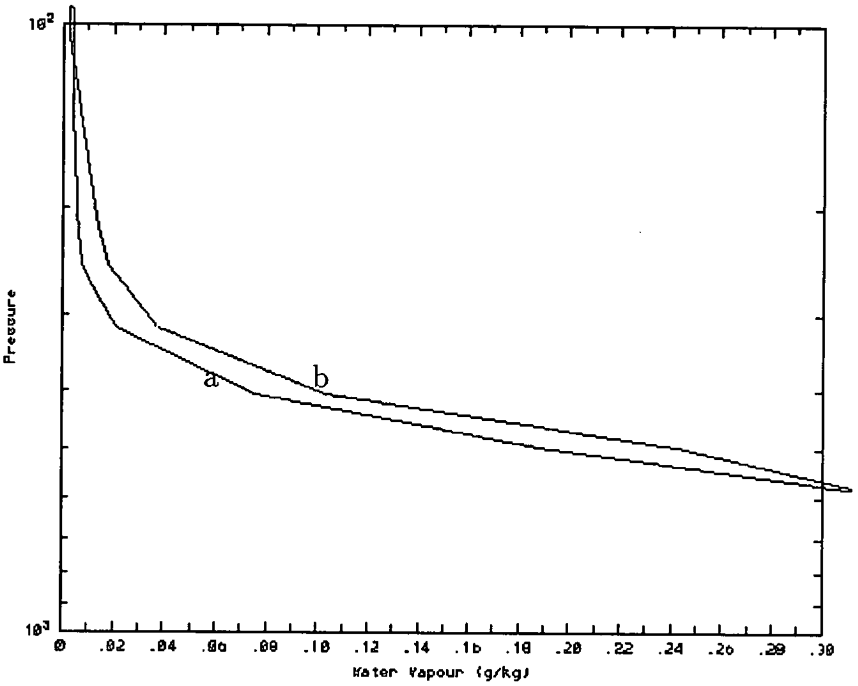

Figure 3.7: Profiles of water vapour (in g/kg) in the UGCM. a) Time averaged (Aug to Sept) at Punta Arenas (53°S, 71°W). b) Time averaged (end Dec to Feb) at Stavanger (59°N, 6°E). The pressure axis is from 1000mb to 100mb (logarithmic scale).

being considered here. In fact at 251mb the difference is more than a factor of three. In the UGCM the degree of asymmetry between the hemispheres varies with latitude.

Finally, a direct comparison is made between the observations and the model output (Figure 3.7), particularly comparing the vertical gradient of water vapour in the UGCM to that in the model. This time a much larger altitude range is being considered, but just for the two main measurement sites, Punta Arenas and Stavanger. Note that Figure 3.7 expresses water vapour in units of g/kg rather than ppmv.

There was a clear difference between the profiles at Stavanger and Punta Arenas for the aircraft measurements, especially below 9km (see Figure 3.2); the vertical gradient of water vapour at Punta Arenas is noticeably greater than that at Stavanger. The same can be not be said of the profiles in Figure 3.7. The gradients are quite similar and although there is around twice the water vapour at Stavanger than Punta Arenas between 200 and 300mb, the relative difference becomes much less, lower in the troposphere.

In summary, using the UGCM, we see that the choice of measurement sites could affect general statements made about the interhemispheric asymmetry of water vapour. It is reasonable to assume that the same may be true of the real atmosphere, and so this casts some doubt on the degree of asymmetry suggested by *Kelly et al.*, but certainly not its existence. With the implications that the asymmetry in water vapour has in relation to climate change it is important to be able to quantify this asymmetry more precisely than *Kelly et al.* were able to. This could mean using more measurement sites (although expensive) or another method of measuring water vapour this low down in the atmosphere which would give a greater degree of coverage. The next section about MLS measurements may offer some help with this.

On the other hand, the model does show evidence of an interhemispheric difference in water vapour in the upper troposphere. The difference in the model however is not as much as the 2 to 4 times that was seen in the aircraft measurements. The difference between the hemispheres in the UGCM is even less below 300mb.

3.4 Comparison between UGCM and MLS retrievals

A further comparison between model water vapour and measurements was motivated by the availability of upper-tropospheric H_2O measurements from the Microwave Limb Sounder (MLS) instrument on the UARS satellite. Although not designed for this purpose, MLS detects tropospheric water vapour through the 205GHz band. Measurements of water vapour at this height are valuable as they provide data for the poorly monitored tropical troposphere.

The measurement is a difficult one for a couple of reasons. MLS water vapour is usually measured at the 183GHz band but this frequency cannot penetrate as low as 215mb due to the large amounts of water vapour present. However, when the band that usually measures ClO (205GHz) scans through the troposphere, its dominant signal is thermal emission from water vapour. It is the process of extracting the data from the chlorine monoxide band which is technically difficult.

Another problem is that in the upper troposphere the vertical gradient of water vapour is very steep and so a small error in pointing leads to a large error in H_2O. *Read et al.*, [1995] gives a full explanation of how MLS water vapour is retrieved.

It was decided to use the model as a rough guide for testing the measurements at this height. This comparison can actually be seen as a two-way test between model and satellite measurements. The MLS measurements can also cast light on the interhemispheric asymmetry seen by *Kelly et al.*, discussed in the last section. This study is divided into two parts based on the type of plots being analysed, zonal and latitude-longitude.

3.4.1 Analysis using zonal fields

Figures 3.8 and 3.9 show H_2O in July and January respectively, at an altitude of 215.4 mb. The green crosses represent each measurement taken by the MLS instrument on two different days. The reason that two different days are used is due to the fact that the satellite does not have global coverage. The satellite has two different yaws and it switches between them approximately every 30 days. The MLS instrument can see between 34°S and 80°N in one yaw and between 80°S and 34°N in the other. Combining retrievals from two different days (which are close to each other), each from a different yaw, gives the closest to global coverage as can be obtained.

The green line running through the crosses is the average water vapour mixing ratio for each latitude. The red line is the zonal average of water vapour in the UGCM for the same altitude. The red shaded area indicates the range of values (of water vapour) which could be found at each latitude in the model. Also marked are the aircraft measurements used in the *Kelly et al.* aircraft measurements.

In many respects the MLS measurements and model output fields of water vapour compare favourably. The figures for MLS and model water vapour are similar in the mid-latitudes and tropics for both January and July, particularly when comparing the two average lines on the plots. Certain features can be seen in both the model data and the real data.

The highest values of water vapour are found in the tropics, on the summer side of the equator in both cases. The model places these high values slightly further poleward than the MLS measurements. However, although the zonal average of

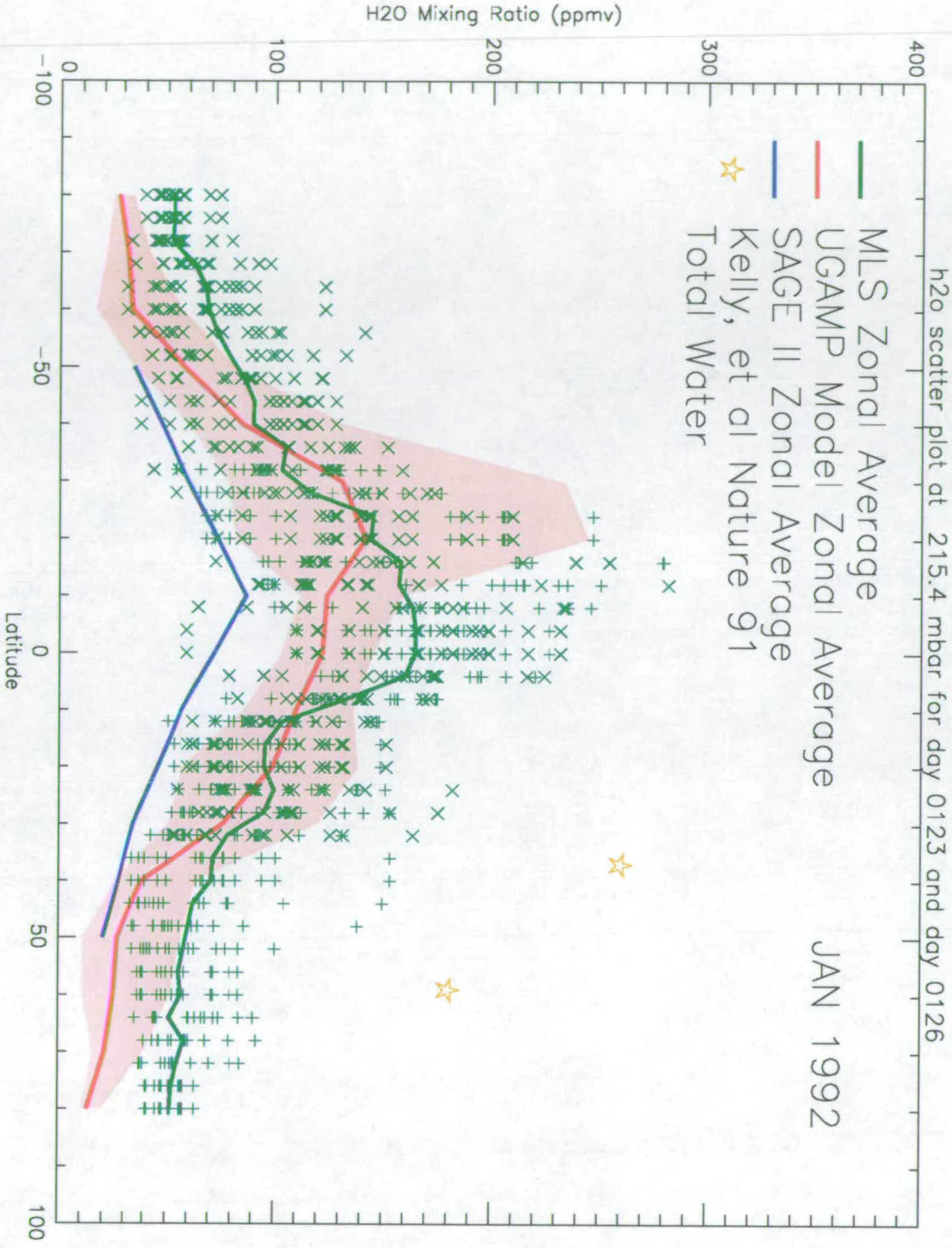

Figure 3.8: UGCM water vapour versus MLS measurements for January 1992. The green crosses represent individual MLS measurements and the red shaded area shows the range of values to be found at each latitude in the UGAMP model. The aircraft measurements used in *Kelly et al.*, [1991] are included as yellow stars

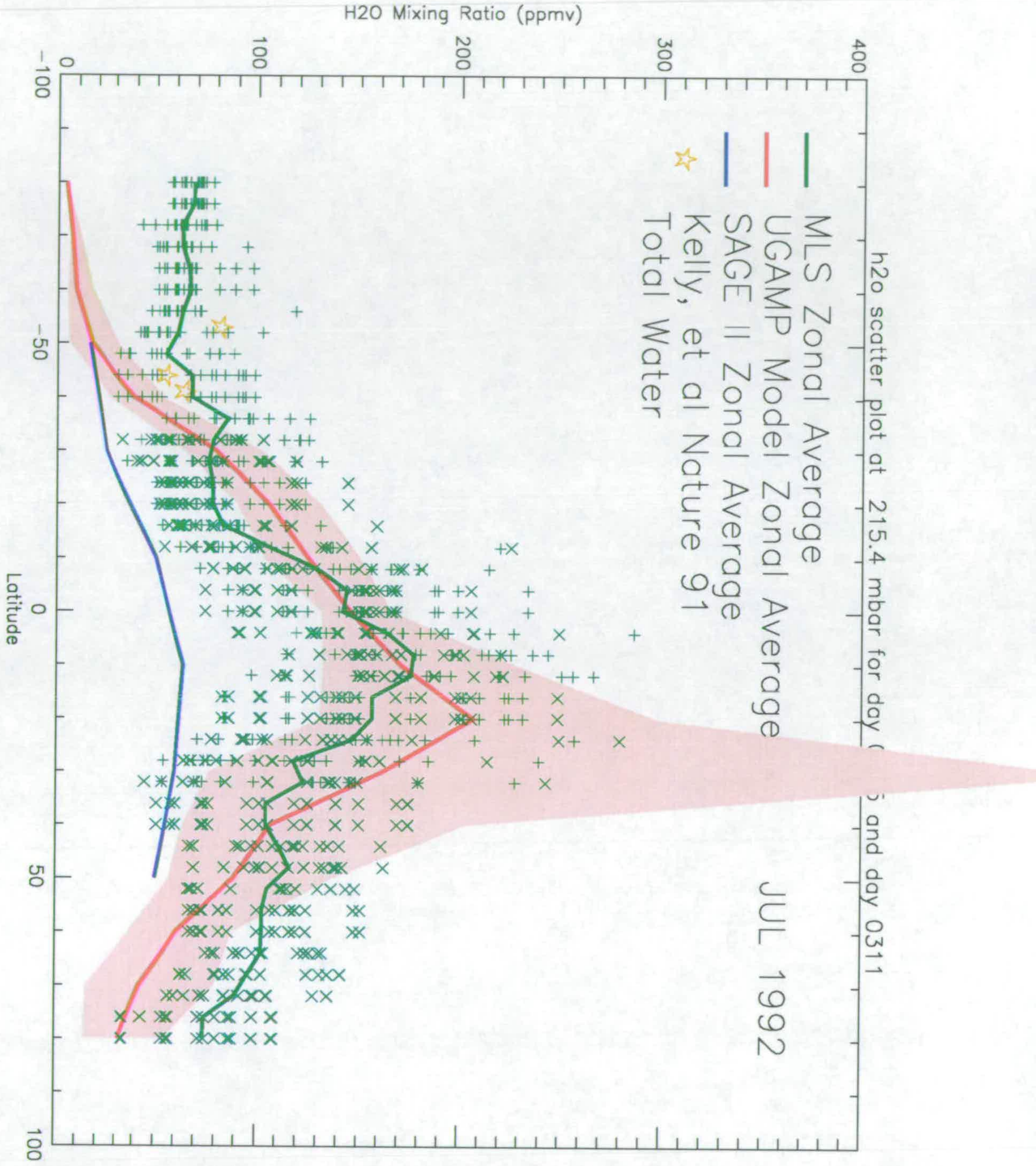

Figure 3.9: UGCM water vapour versus MLS measurements for July 1992. See previous figure for additional information.

model water vapour is not too far from the satellite values, for July at 30°N the extreme values of water vapour produced by the model far exceed those found by MLS.

One reason why there are high values of water vapour in the tropics is convection. Air is transported here from lower in the atmosphere where the mixing ratios of water vapour are much higher. This movement is part of a general circulation, which, as well as lifting air up over the tropics, transports it gradually towards the summer pole (see Figure 2.2 in Chapter 2). Further evidence of this circulation can be seen in the same plots for both MLS and the model in the form of an arch over the tropics in the lower extremes of both sets of data.

Another probable reason that values of water vapour are higher in the tropics has to do with the position of the tropopause relative to the 215mb isobaric surface. In the tropics, the tropopause is above 215mb while at high latitudes, the tropopause is below 215mb. The high H_2O values are upper-tropospheric water vapour while the lower values over the polar regions are stratospheric values.

Over the polar regions, the two fields do not compare well. The model produces much drier mixing ratios, particularly over the winter poles. The average value of water vapour seen by MLS over the polar regions is a factor of 2 to 3 times that seen in the model run. It is thought that the very cold (compared to the real atmosphere) polar vortex in the UGCM excessively dries the air, producing low values of water vapour over the southern polar regions of the model. Very low temperatures in the vortex can cause polar stratospheric clouds (PSCs) to form, reducing the amount of water vapour present in that region. This could explain some of the difference.

Unlike the model, however, the MLS measurements do not exhibit the asymmetry brought to our notice by *Kelly et al.* The aircraft measurements are represented in Figures 3.8 and 3.9 by yellow stars. For July, the stars lie close to the line of average water vapour as measured by MLS and lie inside the two extreme values measured by the satellite instrument at those latitudes. The stars in the plot for January are situated well above the values retrieved by MLS. It is unlikely that natural variability would cause such a difference in measurements (remembering that the measurements used in *Kelly et al.* were taken in '87 and '88 and the MLS measurements are for '92). It is difficult to say what we can conclude from the lack of asymmetry in the MLS measurements; it possibly casts some doubt over the strength of the interhemispheric asymmetry seen in *Kelly et al.*

At this point, we can say that the MLS H_2O retrievals, at a height of 215mb, produce values in the same range as UGCM fields for the tropics, agreeing less towards the poles. Also, there are features which occur in both model fields and MLS water vapour, but this is just in the zonal sense. In the next section latitude-longitude plots are used to determine if the correspondence between features also occurs with respect to longitude.

3.4.2 Analysis using isobaric maps

We turn now to consider longitudinal variations of H_2O at 215mb, using isobaric maps of H_2O.

Figure 3.10 shows MLS water vapour for the same times (January and July) as Figures 3.8 and 3.9. Figure 3.11 contains equivalent plots of UGCM fields within two days of the MLS plots. The first thing to be noted from all the plots in Figure 3.10 and Figure 3.11 is the large longitudinal variability of water vapour in the tropics. This variability is important to the overall comparison between MLS and the UGCM.

Comparing the two plots for January first, the highest values of each field are both just over 280ppmv. Not only are the highest values very similar (Figures 3.8 and 3.9 told us this already), the areas in each field at which the highest values are occurring are the same. Those areas are over the middle of South America, the western edge of Africa and to the north-west of Australia. Both MLS and the model have a series of significantly large mixing ratios linking the larger mixing ratios over Africa and Australia. In fact, the two fields correspond very well indeed, except for the aforementioned problem with polar values of water vapour in the model. This similarity in the fields suggests that the model is accurately representing the physical processes which are placing the high values of water vapour in the tropics at specific longitudes.

The plots for July also show a strong correspondence between areas of high water vapour mixing ratios; this time, a high over central America and a large area of high values over India. Although the areas of large mixing ratios correspond

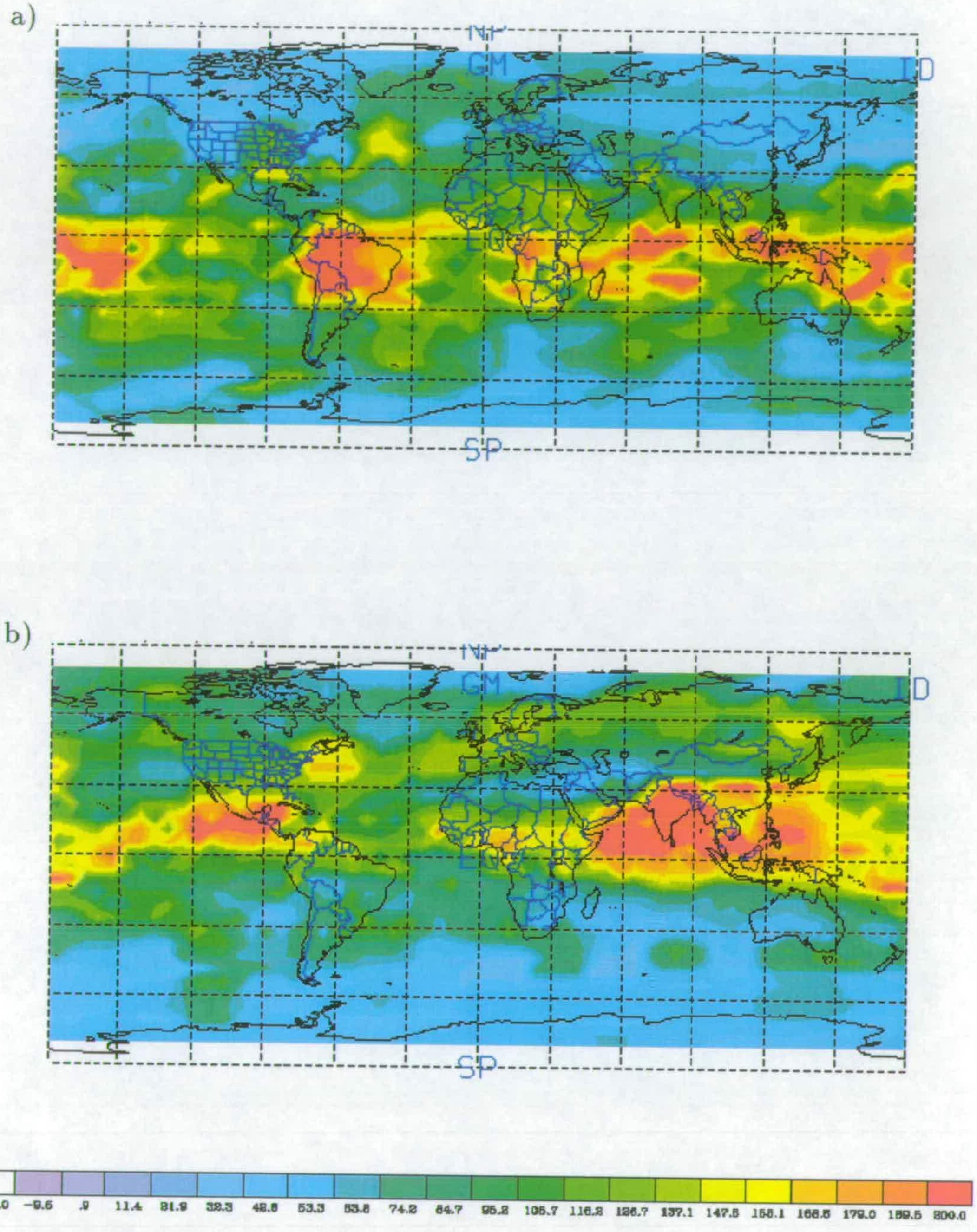

Figure 3.10: Latitude-longitude fields of water vapour (in ppmv) as retrieved by MLS for a) mid-January 1992 and b) mid-July 1992 at a height of 215mb.

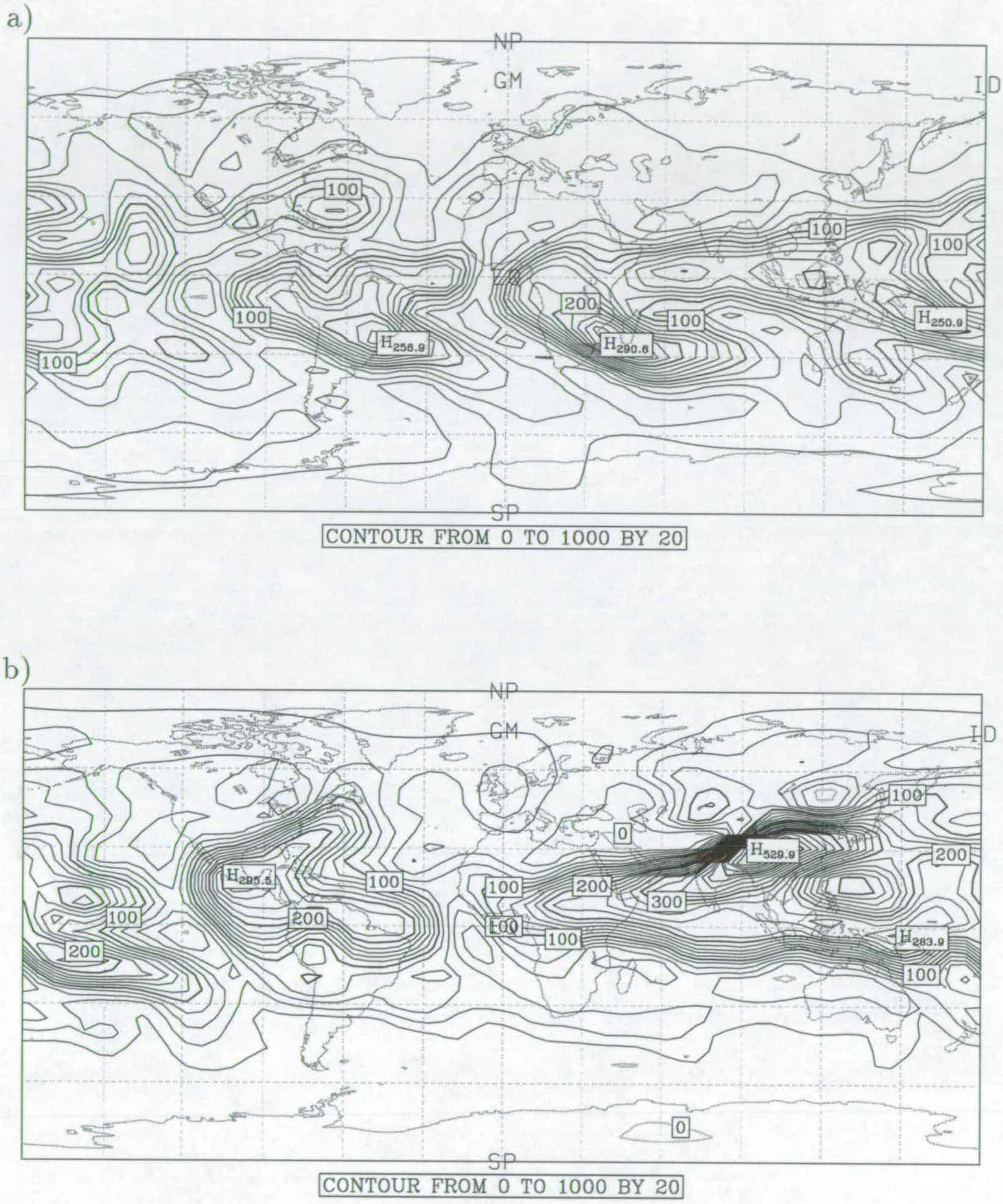

Figure 3.11: Latitude-longitude plots of water vapour (in ppmv) in the UGCM for a) mid-January 1992 and b) mid-July 1992 at a height of 215mb

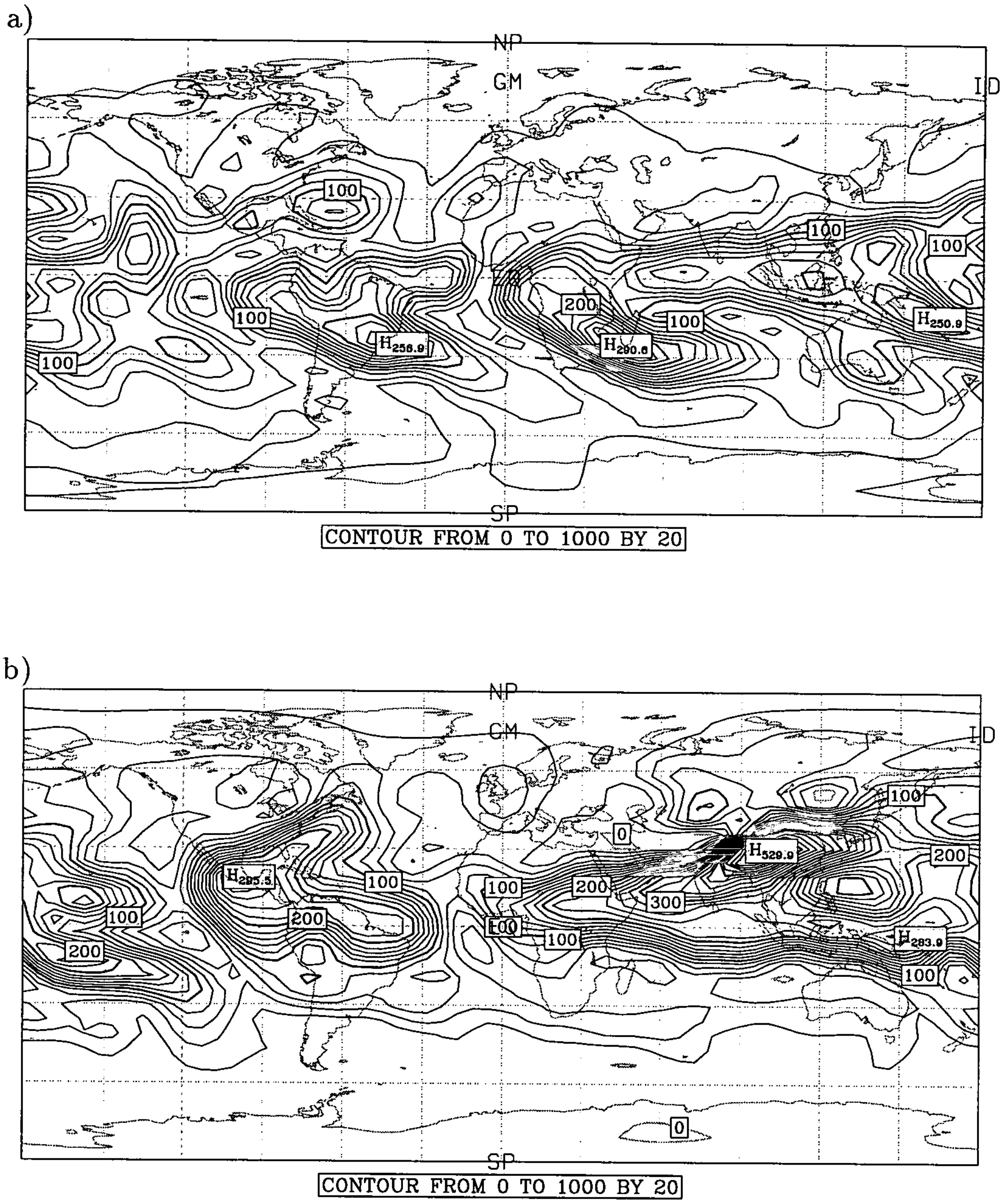

Figure 3.11: Latitude-longitude plots of water vapour (in ppmv) in the UGCM for a) mid-January 1992 and b) mid-July 1992 at a height of 215mb

very well, the size of them do not. The MLS high over India is 277ppmv while the UGCM high is 530ppmv (the high extreme value seen in Figure 3.8), just under twice the amount. The high values over central America do agree well.

In summary, there is very good agreement between MLS water vapour retrievals and the UGCM at 215mb bar two exceptions. Those are the overly dry polar regions of the UGCM and the extremely high concentrations over India in July. An equivalent study using fields from 316mb (not shown here) shows a massive difference in mixing ratios. The UGCM has values over four times the amounts seen by MLS. This could explain the dramatically high values over India at 215mb in the UGCM, the H_2O rich air being convected from below. Beyond that we need to look to other measurements to understand the discrepancies between the MLS data and the model output.

As convection is the origin of some of the higher values of water vapour at 215mb, the choice of convection scheme used in the UGCM could affect the results to some degree. The next section addresses this issue by conducting a comparison between the convection scheme used in this section and another convection scheme.

3.5 Sensitivity to convective parametrization

The previous comparison was based on runs using the Kuo convection parametrization. A Run was also performed using the Betts-Miller scheme. These schemes are described in full in *Kuo* [1974] and *Betts and Miller* [1993] respectively. The Betts-Miller scheme is a convective-adjustment scheme which relaxes to observed thermodynamic states. The main differences between the schemes in the UGAMP model are described by *Slingo et al.* [1992]; the Betts-Miller scheme was deemed a suitable alternative to the Kuo scheme. However, this study makes the comparison specifically for the water vapour fields used for the analysis in the last sections. We need to establish to what degree the comparisons which have been carried out are sensitive to the convective scheme in the model.

Figure 3.12 shows two different plots of the zonally averaged water vapour in the UGCM model for a very limited altitude range centred around 251mb. The seasonal placement of the largest values of water vapour in the tropics is still very much in evidence but slightly closer to the equator, which is more in line with the

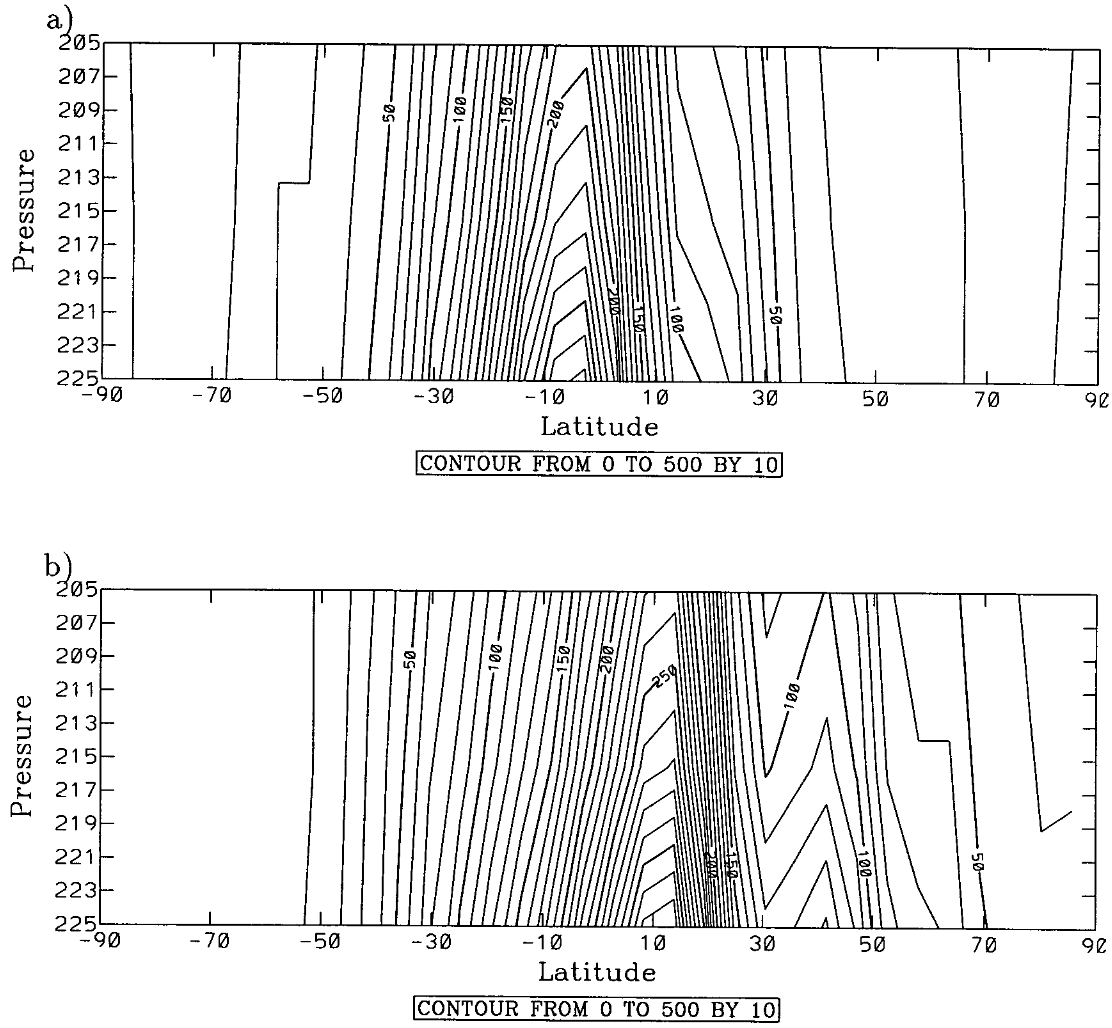

Figure 3.12: Zonal mean plots of water vapour (in ppmv) from the Betts-Miller run for a) mid-January 1992 and b) mid-July 1992. The vertical scale covers the narrow range of 225mb to 205mb.

largest MLS values. These values are around 225ppmv for January and 270ppmv for July, which is far higher than the average values for either MLS measurements or the Kuo run of the UGCM (Figures 3.8 and 3.9). The values for the higher latitudes are very similar to those of the Kuo run including the dry polar regions, with higher values (more than 2 times) in the boreal winter.

We turn to isobaric maps of water vapour again to aid the comparison between the two convection schemes. Figures 3.13a and 3.13b show latitude-longitude plots of H_2O at 215mb for January and July respectively. These two plots are the equivalent (same days and height) of the plots in Figure 3.11.

For January, the locations of the highest range of values in the Kuo field are also the same for the Betts-Miller field. The magnitude of the high values over west Africa is the same for each run, but the same is not true for the highs over northeast Australia and South America. For example, the high over South America in the Betts-Miller run is just over 60% larger than that in the Kuo run. In addition to this, there are other areas of high values which were not seen in the Kuo run, adding to the very high tropical zonal average. The same can be said for the July fields.

In summary, with respect to the comparison with *Kelly et al.*'s findings the Betts-Miller scheme makes very little difference; the inter-hemispheric asymmetry is still evident. However, with respect to the comparison with the MLS measurements, using the Betts-Miller scheme makes a huge difference. Extremely high values of water vapour (compared with both the Kuo model run and the MLS measurements) are produced in the tropics of the Betts-Miller run. The large sensitivity of tropospheric water to the convection scheme used will be due to the steep vertical gradient of the water vapour profile in the upper troposphere. In comparison with the MLS retrievals, the Kuo convection scheme produces the best water vapour fields in the UGCM.

3.6 Conclusions

The UGAMP model has been compared with two different sources of water vapour measurements and has shown the ability to represent certain features to a satisfactory extent.

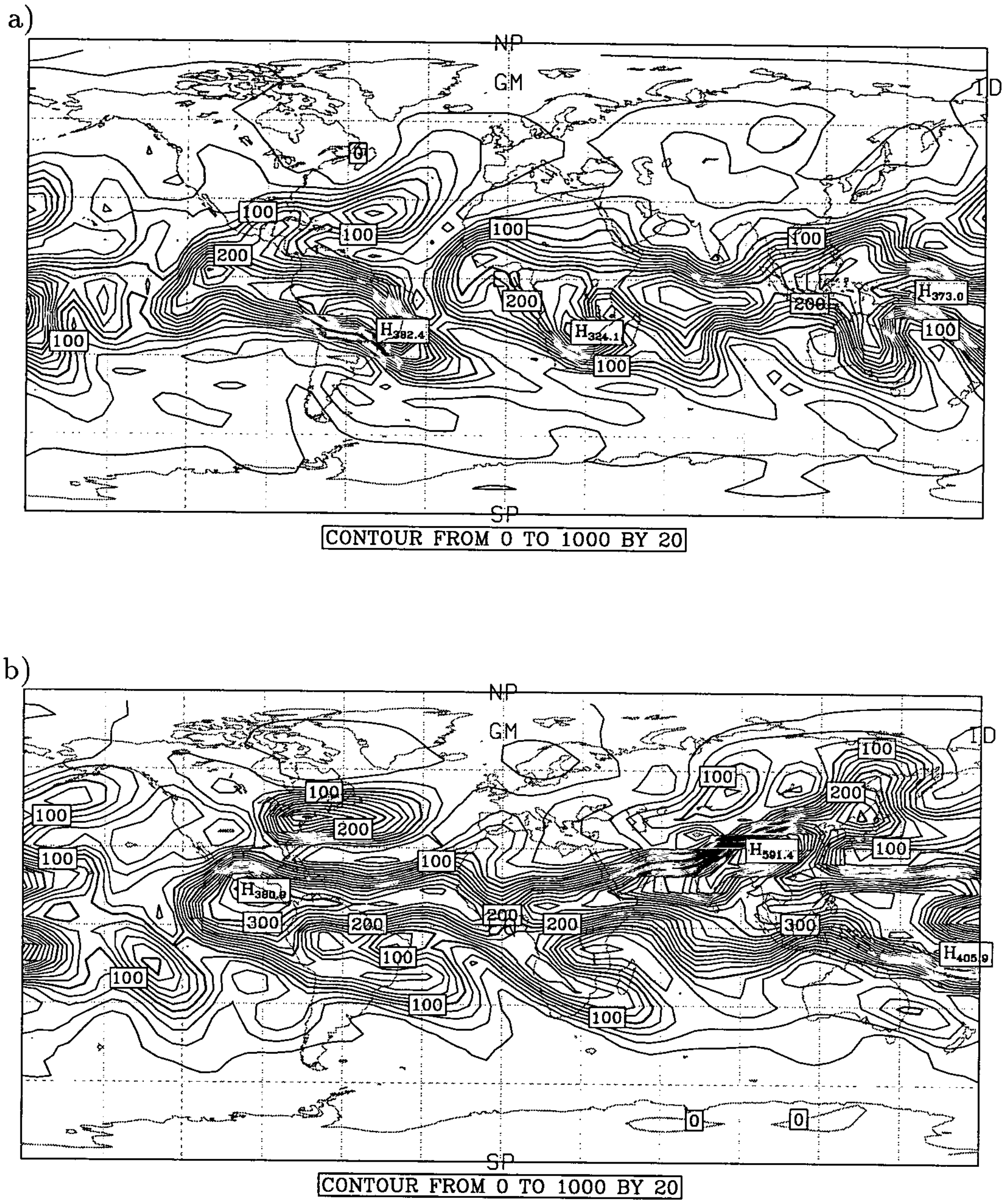

Figure 3.13: Latitude-longitude plots of water vapour (in ppmv) at 215mb from the Betts-Miller run for a) mid-January 1992 and b) mid-July 1992.

In the comparison with the aircraft measurements presented in *Kelly et al.*, the UGCM, although not agreeing with the measurements quantitatively, does support the idea of an interhemispheric difference in upper tropospheric water vapour. The UGCM also indicates that due to the nature of the water vapour distribution (like high longitudinal variability) more extensive measurements need to be taken to quantify the asymmetry more confidently.

The UGCM was also compared with some newly calculated MLS retrievals from 215mb. The comparison showed that the model and measurements agreed well, both quantitatively and qualitatively, apart from the polar regions. A further comparison between UGCM runs with the Kuo and, the more recently developed, Betts-Miller schemes showed that the model is very sensitive to the convective parametrization used (mostly with respect to tropical values). The Kuo scheme produced the closest fields to the MLS measurements. The Betts-Miller scheme gives unsatisfactory fields of tropical H_2O in the upper troposphere, with mixing ratios far greater than those observed.

These results highlight that the UGCM is capable of representing important dynamical processes affecting tracer fields, particularly in the tropics. This is very encouraging as the dynamical processes in and around the tropics (albeit in the stratosphere) are the focus of most of the investigations throughout this thesis.

Chapter 4

Modelling the Spread of Mt.Pinatubo Volcanic Cloud

The last chapter used observations of water vapour to test the model properties. The next three chapters are based on the same idea, but using the sulphate aerosol cloud which was injected into the stratosphere by Mt. Pinatubo. Several different observations were made of the cloud's spread by instruments on satellites and ground based apparatus. This chapter makes a direct comparison between these observations and a tracer designed to simulate the volcanic cloud in the UGAMP model. The experiments highlight certain features in the model, both good and bad, and Chapters 5 and 6 investigate these further. Chapter 5 looks at the existence of PV barriers in the EUGCM and Chapter 6 studies the effects of radiative heating on the transport of a volcanic cloud.

4.1 Motivations for Studying the Volcanic Cloud

Mount Pinatubo is a volcano situated in the Phillipines (15°N, 122°E). On June 15th and 16th, 1991, a series of massive eruptions occurred ejecting an estimated 20 million tonnes of sulphur dioxide (SO_2) into the stratosphere [*Bluth et al.*, 1992]. Once the SO_2 is in the lower stratosphere it slowly converts into sulphate aerosol by the following reactions:

$$SO_2 + OH + M \rightarrow HSO_3 + M \tag{4.1}$$

$$HSO_3 + O_2 \rightarrow SO_3 + HO_2 \tag{4.2}$$

$$SO_3 + H_2O + M \rightarrow H_2SO_4 + M \qquad (4.3)$$

where M is an inert reaction partner (mostly N_2 or O_2). The rate-limiting reaction is 4.1 where the SO_2 reacts with OH to give sulphurous acid [*McKeen et al.*, 1984]. The process of changing the SO_2 into H_2SO_4 has an *e*-folding rate of about a month [*Bluth et al.*, 1992]. That would mean that by mid-July only 42% of the original SO_2 would remain and by August 1st only 21% would remain.

The volcanic cloud, in the form of H_2SO_4, has a lifetime in the stratosphere thought to be of the order of years [*Rosen et al.*, 1994]. What dictates this lifetime is the rate at which the aerosol particles merge together to form larger particles. The larger particles have higher settling velocities than the original, smaller particles. The altitude of the particles is partially maintained by the general upwards circulation which occurs in the lower, tropical stratosphere (Figure 2.2). Eventually the settling velocities become so high as to remove the particles from the stratosphere. The stratospheric aerosol loading decays at an exponential rate [*Lambert et al.*, 1993] and *Rosen et al.* [1994] estimate that the aerosol would return to background levels after three and a half years.

With a lifespan of this magnitude, the volcanic cloud is a useful trace species. That is to say, any movement the volcanic cloud makes is due almost entirely to dynamics. The implications of this are significant for both the study of the stratosphere and the development of GCMs such as the UGAMP model. A tracer injected into the UGAMP model with a similar distribution to the Mt. Pinatubo cloud, at the same time of year, would ideally be transported around the globe in exactly same way as the real Pinatubo cloud. If there are major differences between the two, then this could point to an inadequacy in the model, perhaps failing to represent a certain dynamical process (or an inadequacy in the way the experiment is set up).

One particular dynamical feature to which close attention will be paid is the theoretical barrier preventing motions between the tropics and mid-latitudes [*Trepte and Hitchman* 1992, *Hitchman et al.* 1994]. The Mt. Pinatubo cloud, having originated in the tropics provides an excellent opportunity, both in the real atmosphere and in the model, to investigate whether such a feature does exist.

Although the volcanic cloud is a good device to test the GCM it is not only that. It also absorbs radiation, with implications for the radiative balance. Moreover, heterogeneous chemistry may take place on the cloud's surface which can affect the ozone profile.

4.1.1 The influence volcanic aerosol has on ozone profiles

Several sources have reported an increase in ozone depletion following the Mt. Pinatubo eruption. *McGee et al.* [1994] reported a 10% reduction in total ozone (40% at some heights) over Haute Provence (43.9°N, 5.7°E) in July and August, 1992. The areas of ozone depletion corresponded well with the distribution of H_2SO_4. *Grant et al.* [1992] also reported ozone losses above Brazzaville, Congo (4°S, 15°E) and Ascension Island (8°S, 14°W), just three to six months after the Pinatubo eruption. In this case, the ozone losses were said to have peaked at 20% at a height of 24km.

The method by which the sulphate aerosol enhances ozone depletion is a point of debate within the scientific community. *Stolarski et al.* [1988] was one of many to report losses in total ozone (of up to 10% in some regions of the mid-latitudes) in the December and January following the eruption of El Chichón in late March/ early April, 1982. In response to these findings, *Hofmann and Soloman* [1989] suggested that one of the causes of ozone reduction was heterogeneous chemistry.

Heterogeneous chemistry involves the type of chemical reactions which occur on the surface of an aerosol cloud. The reactions which are most relevant to volcanic sulphate aerosol are the two heterogeneous reactions (equations 4.4 and 4.5) presented in *Rodriguez et al.* [1991] and *Prather et al.* [1992].

$$N_2O_5 + H_2O \rightarrow 2HNO_3 \tag{4.4}$$

$$ClONO_2 + H_2O \rightarrow HNO_3 + HOCl \tag{4.5}$$

These reactions ultimately reduce the amount of NO in the stratosphere (with exposure to light). This affects the balance between ClO and HCl in the following reactions (equations 4.6 and 4.7).

$$ClO + NO \rightarrow Cl + NO_2 \tag{4.6}$$

$$Cl + CH_4 \rightarrow HCl + CH_3 \tag{4.7}$$

The reduction in NO means that less ClO is taken out of the stratosphere. We would expect reactive chlorine to be enhanced in volcanically perturbed regions. This increase in ClO would cause a reduction in ozone.

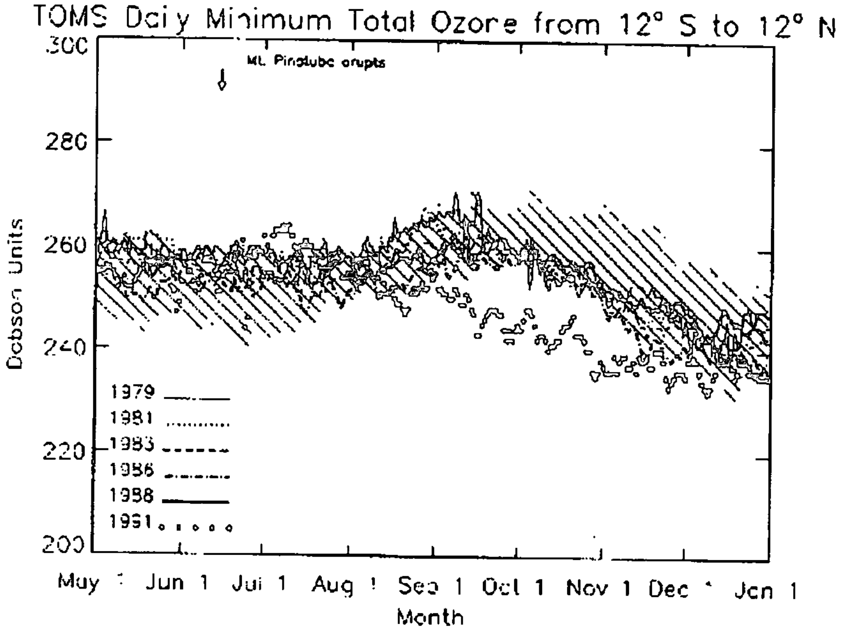

Figure 4.1: Minimum total ozone amounts recorded on a total ozone map in the region 12°N to 12°S as measured by TOMS (taken from *Schoeberl et al.*, [1993]). The data range for all the years from 1979 to 1990 are indicated by the hatching. The eruption of Mt. Pinatubo is marked with an arrow.

Prather et al. go on to note that the stratospheric chlorine has increased by more than 30% since 1983. Considering this, and the fact that El Chichón emitted only a third of the material that Mt. Pinatubo did, then the potential for ozone loss in the tropics after Pinatubo's eruption is even greater.

However, although TOMS (Total Ozone Mapping Spectrometer) measurements do show ozone reduction after the Pinatubo eruption between 24 and 28km in the tropics (Figure 4.1), *Schoeberl et al.* [1993] argue that the heterogeneous loss mechanisms described by *Prather et al.* are not the major mechanisms causing the reported ozone changes. Instead they attribute the ozone profile change mainly to an uplift mechanism caused by an increase in temperature of the aerosol region.

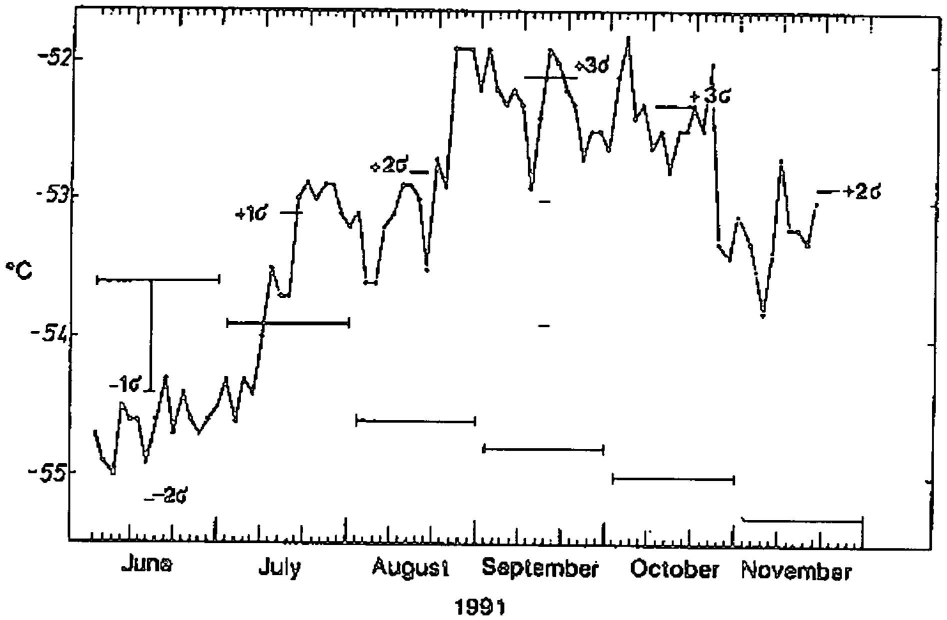

Figure 4.2: Time series of daily zonal mean 30mb temperatures (°C) at 20°N as measured by Raman lidar [*Labitzke and McCormick*, 1992]. Horizontal lines with end bars are 26-year means for the respective months.

Labitzke and McCormick [1992] discuss how the volcanic cloud can affect the temperatures in the atmosphere. The cloud particles scatter solar radiation back to space, causing the Earth's surface to cool, and they absorb upwelling infrared radiation, warming the stratosphere where the particles are situated. Evidence of these temperature increases have already been found (Figure 4.2) using rawinsonde-derived data and they correspond very well with aerosol locations derived from SAGE II (Stratospheric Aerosol and Gas Experiment II) measurements. The effects of radiative heating on the volcanic aerosol are studied in Chapter 6.

Whether the aerosol causes ozone depletion, heating, or possibly both, it ultimately has an effect on the ozone profile. If the UGAMP GCM is to be used for calculating ozone depletion in the mid-latitudes then the ability to simulate the transport of the volcanic aerosol is of utmost importance.

Thus there are a number of good reasons for simulating the transport of the

Mt. Pinatubo cloud in the UGAMP model.

4.2 Observed Behaviour of Mt. Pinatubo cloud

The following is a summary of the volcanic cloud's movements from the day of the eruption onwards. An attempt has been made to divide the cloud's dispersal into distinct phases.

4.2.1 The first month after the eruption

When Mt. Pinatubo erupted on the 15 June, 1991, volcanic plumes reached up to 30km in some cases with the bulk of the SO_2 cloud between the altitudes of 20 and 28km [*Bluth et al.*, 1992]. At this time the local tropopause height was 15km [*Labitzke and McCormick*, 1992], so clearly, the SO_2 got well into the stratosphere. The peak values of aerosol were found at approximately 22km [*Trepte et al.*, 1993].

The cloud drifted west of the eruption and had traveled completely round the earth in 22 days [*Bluth et al.*, 1992 and *Stowe et al.*, 1992]. The time to travel around the earth varies, depending on height. 22 days was the fastest time while lower down in the stratosphere the cloud travelled westward at a slower rate. Although starting at 15°N, the cloud quickly travelled south of the equator and a strong meridional gradient formed at 20°S [*Trepte et al.*, 1993]. The volcanic material remained in the tropics and was fairly zonally mixed by mid-July.

4.2.2 Tropical confinement of aerosol

As late as mid-August material was still mostly confined to the tropics with most reports stating a latitude range of 20°S to 30°N. SAGE II data [*McCormick and Veiga*, 1992] show that there was substantial isolation between the tropics and mid-latitudes in this period with aerosol occasionally escaping into the middle latitudes due to events of planetary and synoptic scale (see Figure 4.3).

This isolation was seen more prominently at the southern edge of the aerosol cloud which was constrained quite uniformly with respect to longitude. The northern edge of the cloud showed a lot of longitudinal variation, a point which was also noted by *Hayashida and Sasano* [1993]. This could be seen as evidence for the existence of two different mixing regimes. The smooth edge indicative of a

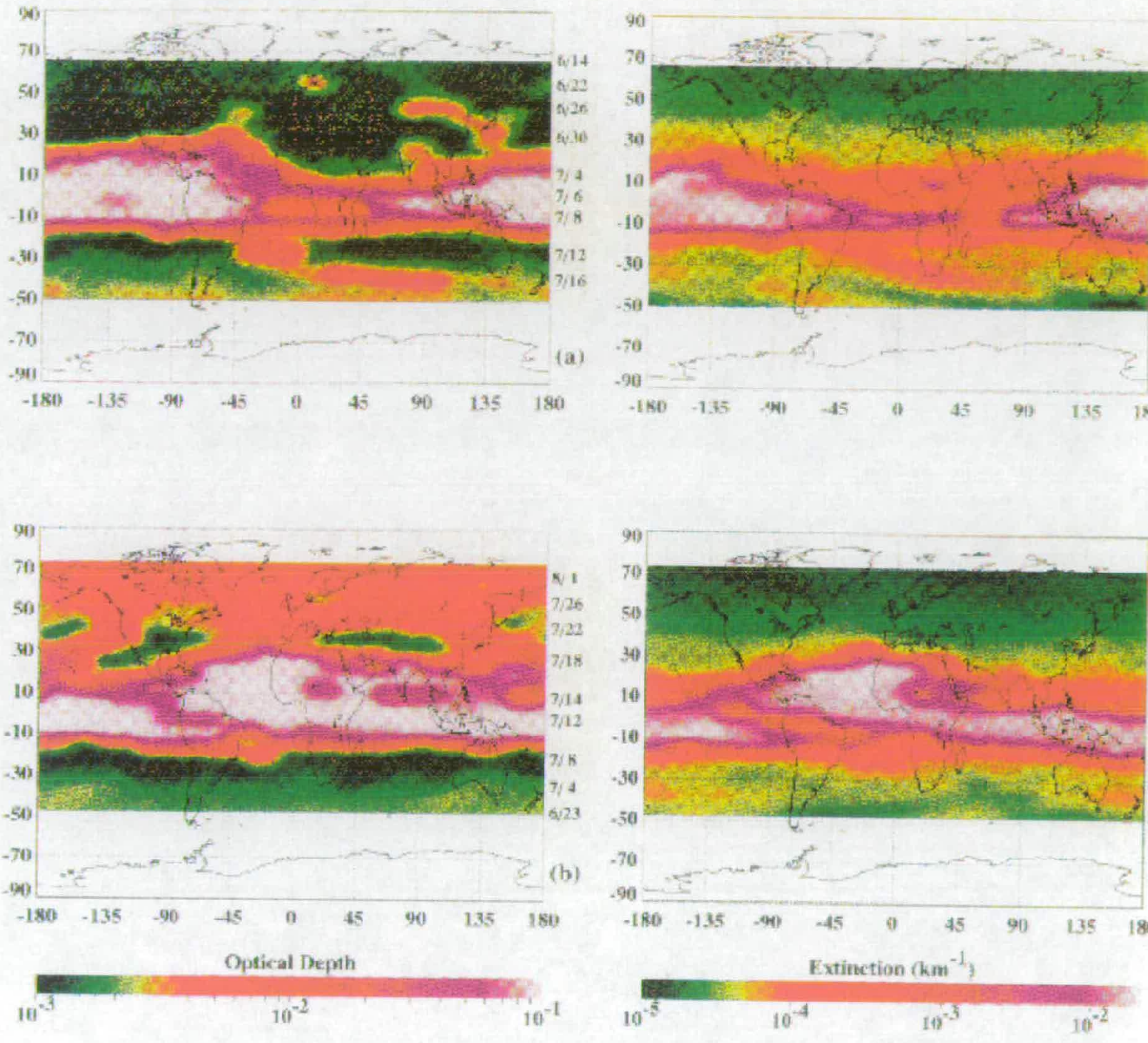

Figure 4.3: Longitude-latitude cross-sections of SAGE II 1020nm stratospheric optical depth and aerosol extinction for the sunset measurements of June 14 to June 26, and the sunrise measurements of June 23 to August 8 [*McCormick and Veiga*, 1992]. a) optical depth for sunsets, b) optical depth for sunrises, c) extinction at 24.5 km for sunsets, and d) extinction at 24.5 km for sunrises.

smooth dynamical barrier (see section 5.2), while the variable edge is caused by small-scale mixing associated with the summer hemisphere [*Trepte et al.*, 1993]. This is discussed further in section 4.2.3. The tropical confinement, although most apparent in the first two months before any major poleward transport of material, remains very much in evidence throughout the first year after the eruption.

The tropical confinement is not 100% and material escapes into the middle latitudes throughout the year. The method of transport from the tropics to the middle and high latitudes in the UGAMP GCMs is a key focal point throughout the following work.

4.2.3 Latitudinal spread of the cloud

During early to mid-August the volcanic cloud started to make a considerable move polewards, both north and south [*McCormick and Veiga*, 1992]. Below 20km the aerosol progressed northwards. Small amounts of aerosol reached far northerly latitudes by October but significant amounts of the cloud were slower, reaching about 50° N by the end of November [*Ansmann et al.*, 1993]. *Trepte et al.*, [1993] show that this transport has the form of mixing due to tropospheric, synoptic-scale disturbances. Only a small fraction of aerosol got as far as the polar latitudes before the polar vortex formed [*Rosen et al.*, 1992]. Aerosol levels within the vortex remained steady until a vortex disturbance developed in the middle of January, after which the aerosol increased rapidly.

At altitudes above 20km, about half a month later than the northward movement, a southward movement becomes noticeable. As for the northern hemisphere, only small amounts of aerosol were detected in the southern mid-latitudes at first. Throughout the end of August and September there was a large and steady increase of aerosol in the southern mid-latitudes [*Trepte et al.*, 1993]. The mixing in this hemisphere is attributed to the breaking of planetary waves and is most apparent at a height of 22km. This mixing does not occur in the northern hemisphere at this time as planetary waves cannot propagate in summer easterlies [*Charney and Drazin*, 1961 and *Andrews et al.*, 1987]. As the mixing was mostly occurring at the same height as the maximum values of aerosol, the southern hemisphere experienced a greater increase in aerosol loading than the northern hemisphere. The greatest amounts of material above 20km are centred above 15°S [*Trepte et

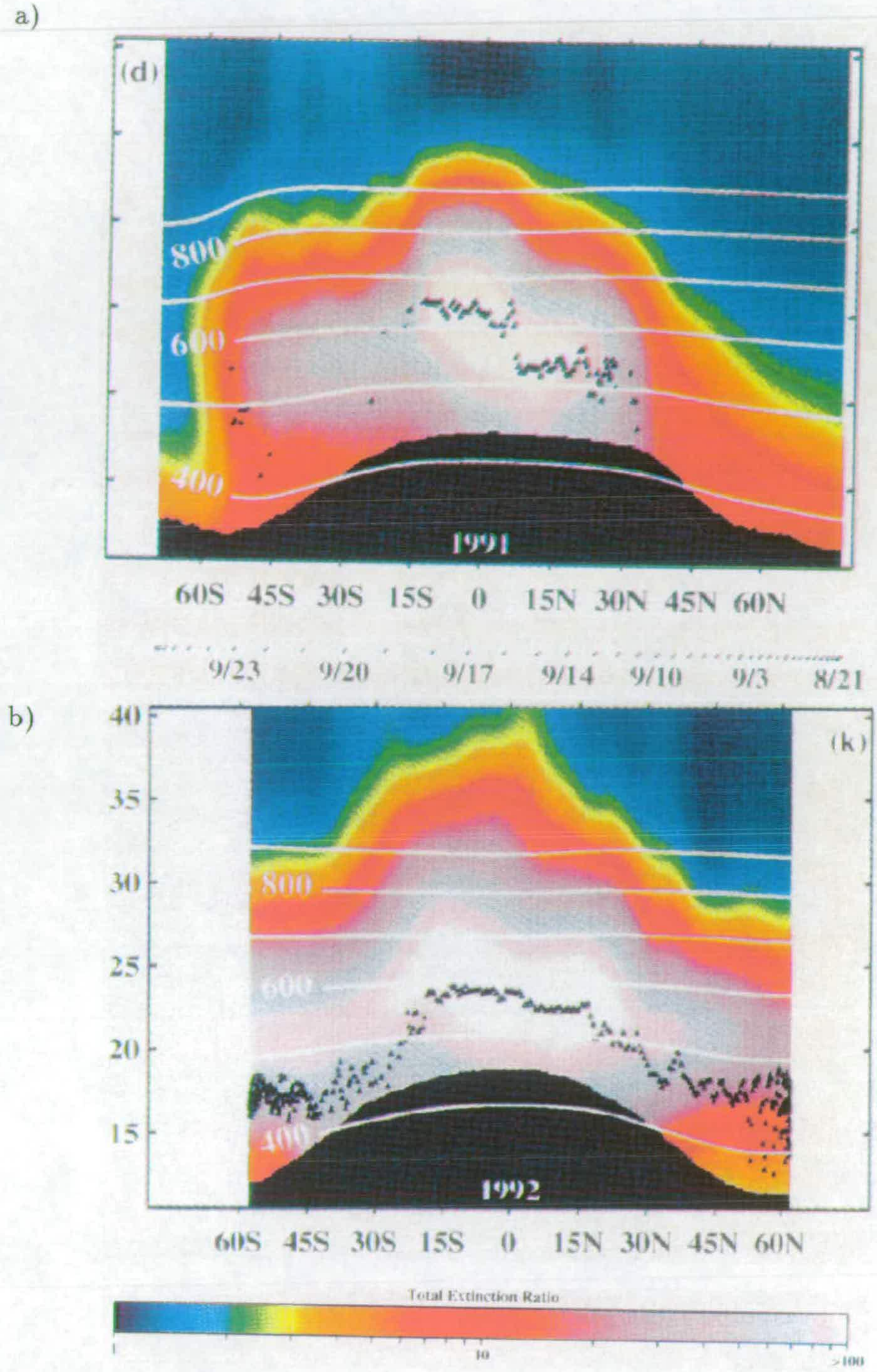

Figure 4.4: Latitude-altitude cross-sections of SAGE II extinction ratios for a) August 20th to September 30th showing material being prevented from moving into southern polar regions and b) March 11th to April 11th showing more material in the southern hemisphere than the northern hemisphere (*Trepte et al.*, [1993]). Vertical scale is in altitude (km).

al., 1993] as a result of the upper mixing regime. Figure 4.4a shows this difference between upper and lower mixing regimes very effectively (looks like two blobs of material, the higher of the two centred further south than the other).

MLS measurements of SO_2 presented in *Read et al.*, [1993] illustrate best the height dependency of poleward spread (see Figure 4.5). Material at 21km biased towards the north while material at 31km is biased to the south. The same skewed nature of the distribution can be seen in ISAMS measurements too (Figure 4.6a).

The plot in Figure 4.4a also shows that material is prevented from moving into the southern polar latitudes by the polar vortex. According to *Cacciani et al.*, [1993], the main cloud reaches the southern polar latitudes by December, 1991. The data presented by *Trepte et al.*, [1993] is in close agreement, with material present in southern polar regions from the middle to end of November onwards.

To reiterate, *Lambert et al.* [1993] state that the dispersal of the cloud was more rapid in the southern hemisphere and penetration to the southern polar latitudes occurred earlier than transport to the corresponding northern area which was inhibited by the northern polar vortex (see Figure 4.6c).

By late winter/early spring 1992, the volcanic aerosol could be found at all latitudes with more aerosol evident in the southern hemisphere [*Trepte et al.*, 1993, *Lambert et al.*, 1992]. The zonally averaged distributions change very little from this point until a year after the eruption, including the persistence of tropical confinement. *Lambert et al.* state that the decrease in aerosol peak extinction is approximately exponential. Figures 4.4b and 4.6f give an indication of the distribution of the cloud 10 months to a year after Mt. Pinatubo erupted.

4.2.4 Spread of the cloud with respect to altitude

When the cloud was first injected into the atmosphere it covered an altitude range from the troposphere to about 28km. The top of the cloud was gradually lifted higher until after December 1991 when a rise to 40km occurred [*Trepte et al.*, 1993]. This ridge of high aerosol values occurred over 15°S and persisted until late March. After March the ridge broadens and drops to a lower altitude. ISAMS measurements [*Lambert et al.*, 1993] show a double peaked structure in the upper edge of the cloud above the tropics from January 1992 onwards (Figure 4.6). This is a feature of the mean meridional circulation at this time [*Trepte and Hitchman*,

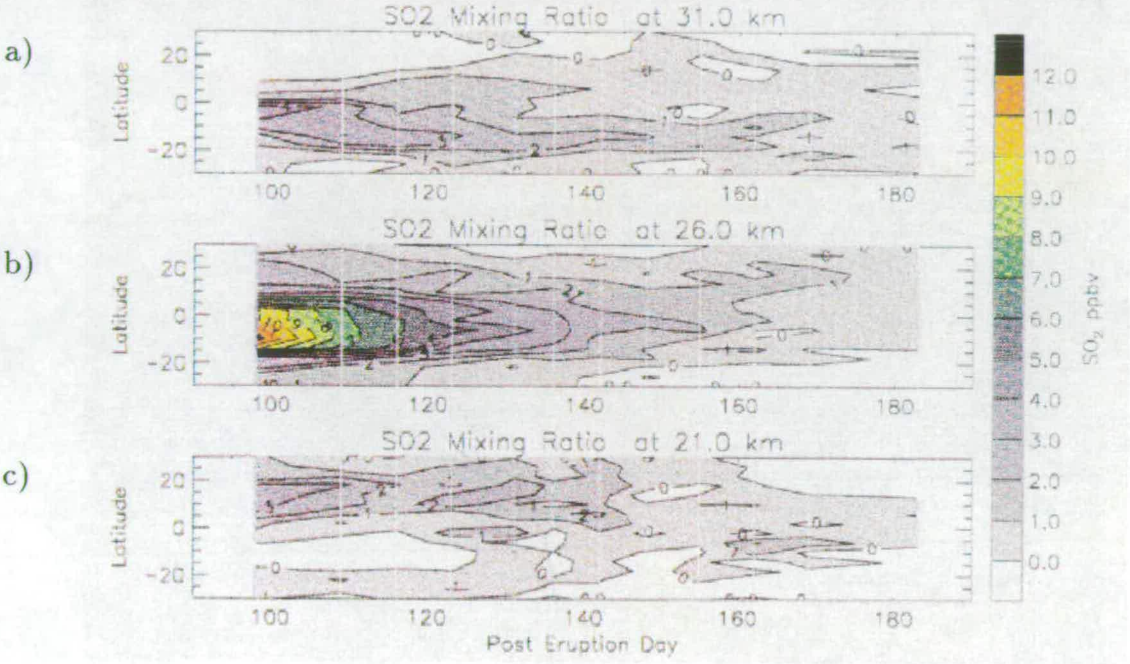

Figure 4.5: Temporal evolution of zonally averaged SO_2 (in ppmv) between 32°S and 32°N at a) 31km, b) 26km and c) 21km (taken from *Read et al.*, [1993]).

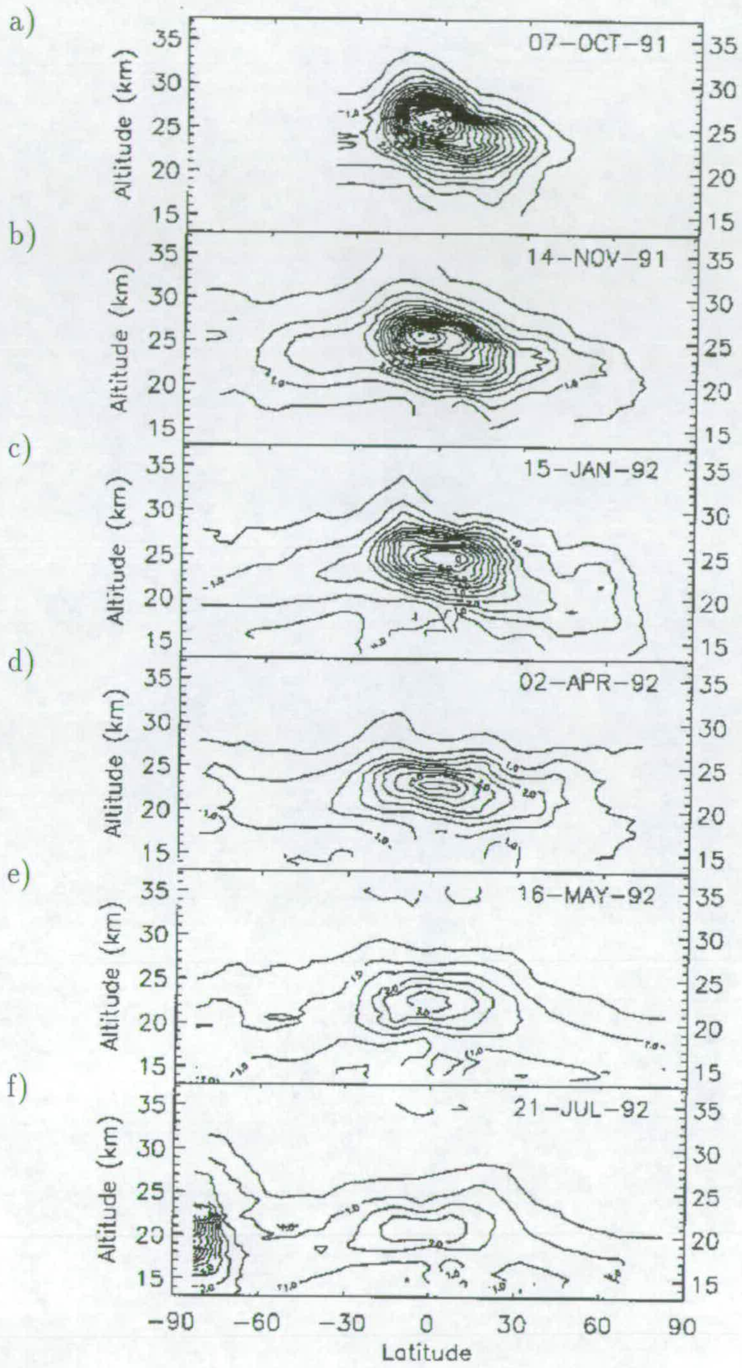

Figure 4.6: Six zonal means of the 12.1 micron extinction observed by ISAMS in the period October 1991 to July 1992 (*Lambert et al.*, [1993]).

1992].

The aerosol reservoir in the tropics is partially maintained against sedimentation by mean upward motion from the Brewer-Dobson circulation [*Trepte and Hitchman*, 1992 and *Trepte et al.*, 1993] and is enhanced by the QBO mean meridional circulation during descending easterly shear.

4.2.5 Particle size of Pinatubo aerosol cloud

Deschler et al., [1992], based on ISAMS measurements, tell us that there were two different particle sizes in the volcanic cloud in late July. The cloud can be thought of in two sections. The higher section of cloud, centred at 23km contains particles with average size, 0.3 microns while the lower section, centred at 17km consists of particles with average size 0.07 microns, significantly smaller than those above.

Lambert et al., [1993] use the observed change (with respect to time) in altitude of the peak equatorial aerosol extinction, and compare it with calculated settling velocities for various particle sizes to estimate the Pinatubo average particle size at .25 to .30 microns.

Thomason, [1992] confirms the existence of the smaller particle size using the SAGE II instrument. The smaller particles were found mostly in the northern hemisphere, below 20km. Knowing that these particles were mostly centred around 17km, then this is further evidence that a lower mixing regime exists, transporting material only northwards from the tropics. *Thomason* suggests that the small aerosol mode represents a transitional phase between a very small aerosol produced by the conversion of SO_2 to H_2SO_4 and the quasi-steady state aerosol size which eventually sets in after a volcanic eruption.

4.2.6 Key features of Pinatubo cloud dispersal

To summarise, there are many aspects of the spread of the volcanic cloud in the real atmosphere which we will be looking for in the model simulation. The following points are significant features of the aerosol dispersal just described. They will be paid particular attention when looking at the simulated distributions in sections 4.4 and 4.5.

The main features are as follows:

- A tropical stratospheric reservoir of material existing for at least a year after the eruption. The edge of the reservoir is usually well defined at the edge of the tropics although, the southern edge is more uniform than the northern edge
- Height dependency of poleward spread: below 20 km, material was transported north and above 20 km, material was transported south from the tropics
- Two separate mixing regimes transporting material from tropics in the first few months after the eruption. Southward transport is due to the breaking of planetary waves while northward mixing is associated with upwardly decaying tropospheric disturbances
- Prevention of poleward spread by the edge of the polar vortex
- Sudden rise of top of cloud over the tropics in December
- More material in the southern hemisphere, after one year, than in the northern hemisphere

Having described the observations of the Pinatubo cloud, we shall go on to try and model it.

4.3 About the model runs

In the following sections of this chapter an attempt to model the spread of the tracer in the UGAMP model is made. Before analysing the model runs an explanation of how they were set up is needed.

There are two main experiments using different versions of the model and they are described in section 4.3.1. An initial comparison between the ECMWF analyses and the two different model runs is made in sections 4.3.2 and 4.3.3. The lack of a quasi-biennial oscillation in the model is considered in section 4.3.4. Of particular importance to an experiment like this is the way the tracer is initialised in the model and the problems this may entail, and so this point is discussed in section 4.3.5.

	RUN A	RUN B
No. of levels	19	47
Horizontal Resolution	T42	T21
Initial fields	June 15 1991	Generic mid-June
Time Step	45mins	15mins

Table 4.1: Properties of the two model runs, highlighting the main differences between Run A and Run B.

4.3.1 The differences between the two model runs.

As already mentioned, there are two distinct model runs used in this investigation and we shall call them Run A and Run B. They use the two different versions of the UGAMP GCM; the 19 level UGCM and the 47 level Extended UGCM (EUGCM). The main characteristics which differ between the two runs are listed in Table 4.1.

To some extent the reason for choosing two experiments is historical because the 47 level model was not available at the beginning of the project but it serves to identify certain features of the runs.

The 19 level model, with T42 horizontal resolution, offers a good opportunity to look at, in detail, events transporting material from the tropics. The small number of vertical levels (reaching only 10mb) proves to be a serious restriction in modelling the volcanic cloud. There is no such restriction with EUGCM, so the model continues to produce useful (for comparison with the real atmosphere) fields indefinitely. This enables us to take a more extensive look at the poleward spread of the tracer over the first year.

Due to expense, however, the EUGCM was not run with a T42 horizontal resolution - it would cost about twelve times the amount in computer time to run EUGCM with T42 instead of T21. This means that the experiment with the UGCM is still useful in its own right for looking closely at mixing events.

Another difference between the Run A and Run B is the initial fields used. Run A uses initial fields from ECMWF for 15th June 1991, the day that the Pinatubo eruption began. The equivalent files were not available for the EUGCM so Run B is initialised using fields from a generic mid-June.

As will become apparent when the model experiments are described, the two model runs complement each other rather well. The work will show that the

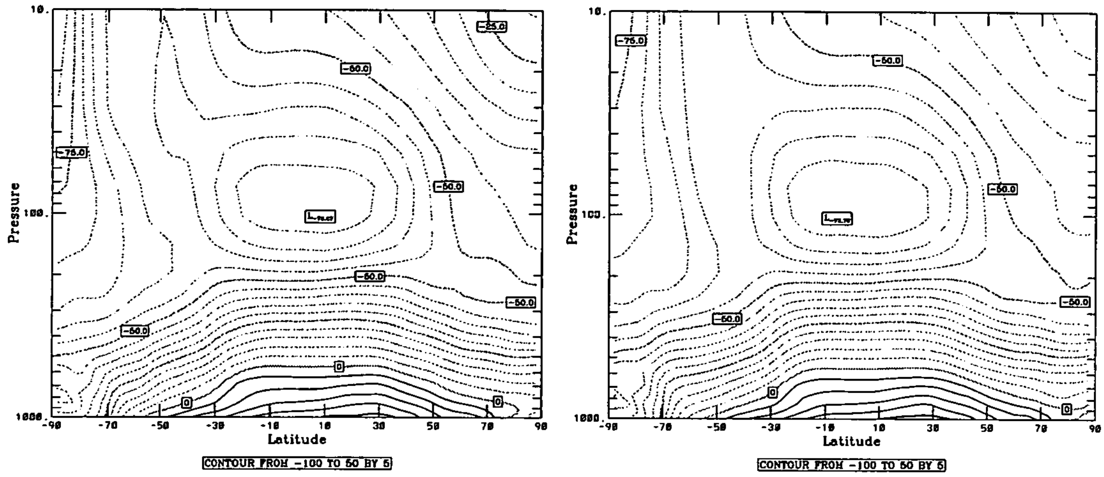

Figure 4.7: Zonally averaged temperature (°C) fields from Run A for a) mid-July and b) mid-August.

behaviour of the cloud over the tropics in the first few weeks is crucial to the poleward spread of the tracer. Run A provides the detailed fields required to look specifically at the transport of the cloud in these initial few weeks, while Run B gives a more general look at the poleward spread of the cloud throughout the first year after the eruption.

The next section presents an initial comparison between the model fields (zonal winds and temperatures) with the ECMWF analyses for the period after the eruption of Mt. Pinatubo. The European Centre for Medium-Range Weather Forecasts (ECMWF) produce operational analyses using a spectral model with T213 resolution and 31 levels in the vertical. The ECMWF model has a three dimensional semi-Lagrangian advection scheme. The data set used here contains data for the 12 months following 15th June, 1991 and is on a 2.5 degree resolution regular grid.

A more detailed comparison between the real atmosphere and the EUGCM run is made later (in Chapter 5) in the light of experiment results.

4.3.2 Run A comparison with analyses

At the start of Run A, the zonal winds and temperatures of the model agree very well with the corresponding ECMWF analyses (since the model was initialised with ECMWF fields). In general, the zonally averaged temperature fields are

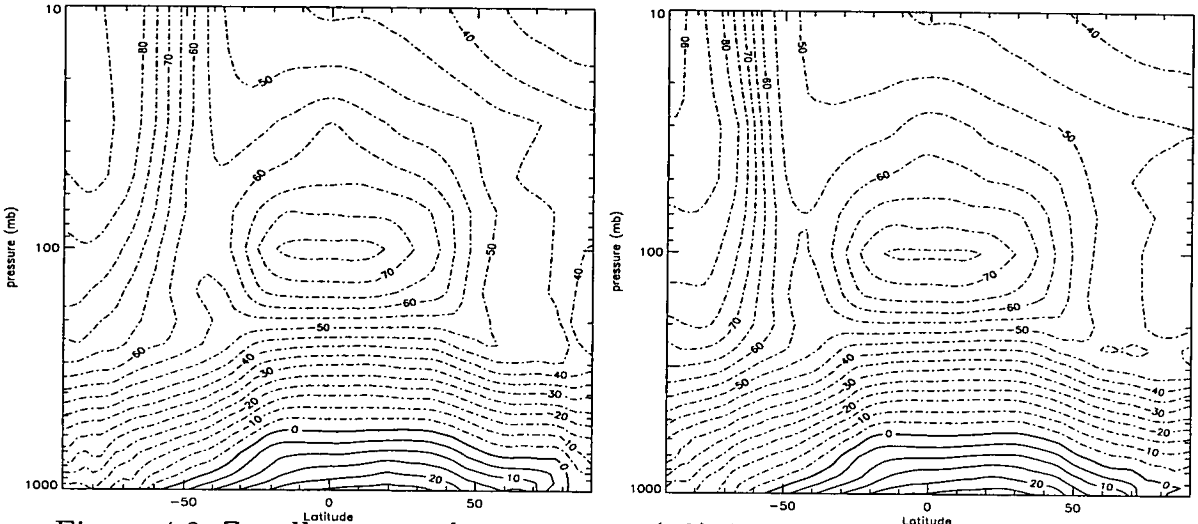

Figure 4.8: Zonally averaged temperature (°C) fields from the ECMWF analyses for a) mid-July,1991, and b) mid-August,1991. The contour interval is 5°C.

in good agreement throughout the entire model run, but by the beginning of August the temperatures above the south pole are warmer than those seen in the analyses. Figures 4.7 and 4.8 show the zonally averaged temperature fields from the ECMWF analyses and from Run A respectively. In July the agreement is very good, but by mid-August the stratospheric southern hemisphere looks quite different. The stratospheric south pole is about 15°C warmer in Run A than it is in the analyses at mid-August and there is a more pronounced meridional gradient in temperature at the edge of the polar vortex in the analyses.

Looking at the zonally averaged winds (Figures 4.9 and 4.10), the easterly jet in the tropics looks a reasonable strength throughout Run A, although it is centred about 10° further north in the model than it is in the ECMWF analyses. The polar jet in the southern hemisphere looses a lot of the strength as Run A progresses. Even by mid-July, the jet is approximately 50 % weaker, in places, than that seen in the analyses, although it does regain its strength half a month later. This is consistent (through the thermal wind equation) with the difference in temperatures between the model and analyses. At times in Run A, (an example of which can be seen in Figure 4.9b), the westerlies in the stratospheric southern hemisphere intrude further into the tropics than they do in the ECMWF analyses. Note also that the polar jet has lost some of its strength again.

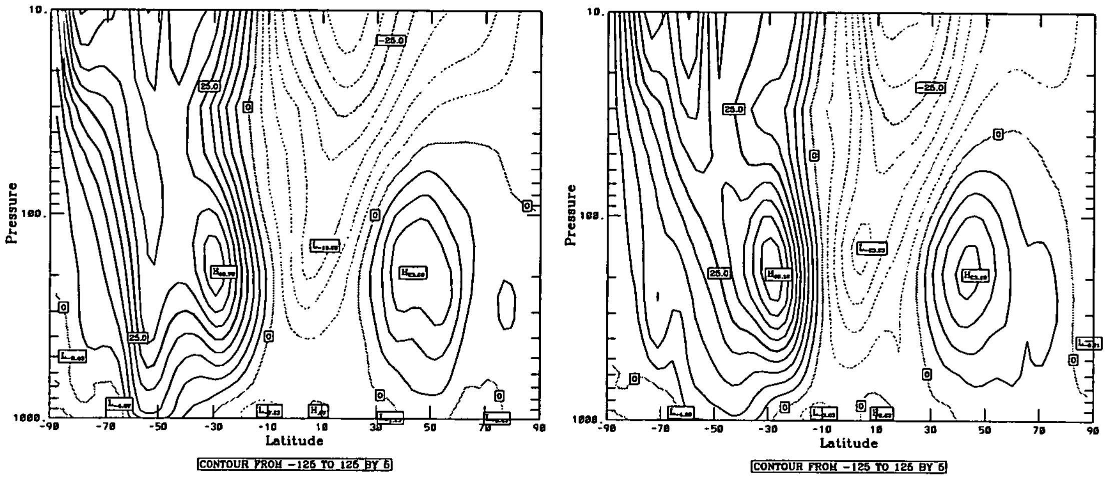

Figure 4.9: Zonally averaged winds ($m^{-1}s$) from Run A for a) mid-July and b) mid-August.

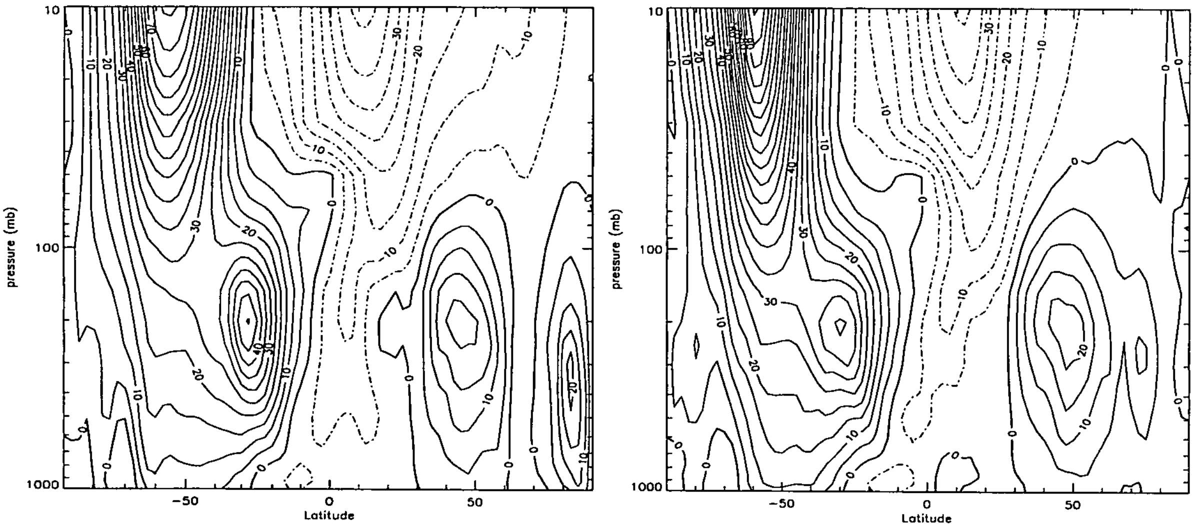

Figure 4.10: Zonally averaged winds (ms^{-1}) from the ECMWF analyses for a) mid-July, 1991, and b) mid-August, 1991. The contour interval is $5ms^{-1}$.

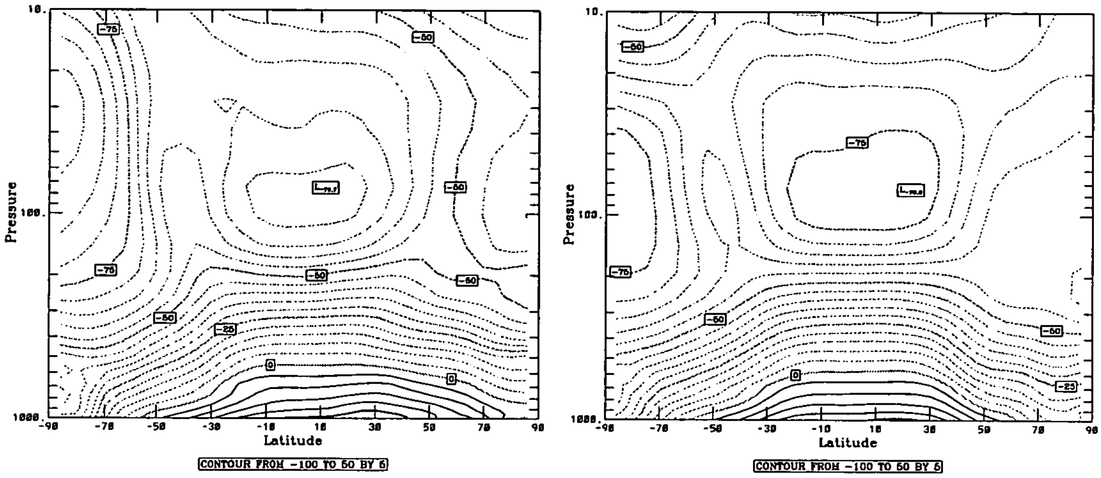

Figure 4.11: Zonally averaged temperature (°C) fields from Run B for a) mid-June and b) mid-September.

4.3.3 Run B comparison with analyses

At the start of Run B the temperature fields agree fairly well except the tropics above 50mb are cooler in the model than they are in the analyses (see Figures 4.11a and 4.12a). By September (Figures 4.11b and 4.12b) fairly good agreement remains below 50mb, but above 50mb, the model is warmer than the analyses above the south pole and colder (by about 15°C) than the analyses at all other latitudes.

Three months later the difference in stratospheric temperatures between the model and the analyses is quite large. In the model (Figure 4.13), the stratospheric southern hemisphere is, in general, colder than the analyses (Figure 4.14), as is the tropics above 50mb (up to 20°C colder in some places). In the northern, polar latitudes, the actual structure of the fields is different. The meridional gradient in temperature in the stratosphere, seen in the analyses, is not present in Run B. Throughout the rest of the run, the stratosphere of Run B remains significantly cooler than in the analyses, particularly in the southern hemisphere.

At the start of Run B, the zonally averaged winds look a bit different from the ECMWF analyses (Figures 4.15a and 4.16a). The easterly jet over the tropics is approximately 15% weaker than the analyses and is centred about 20° further north. There is a split in the westerly jet in the southern hemisphere of the analyses which is not present in the model. However, this split does appear a

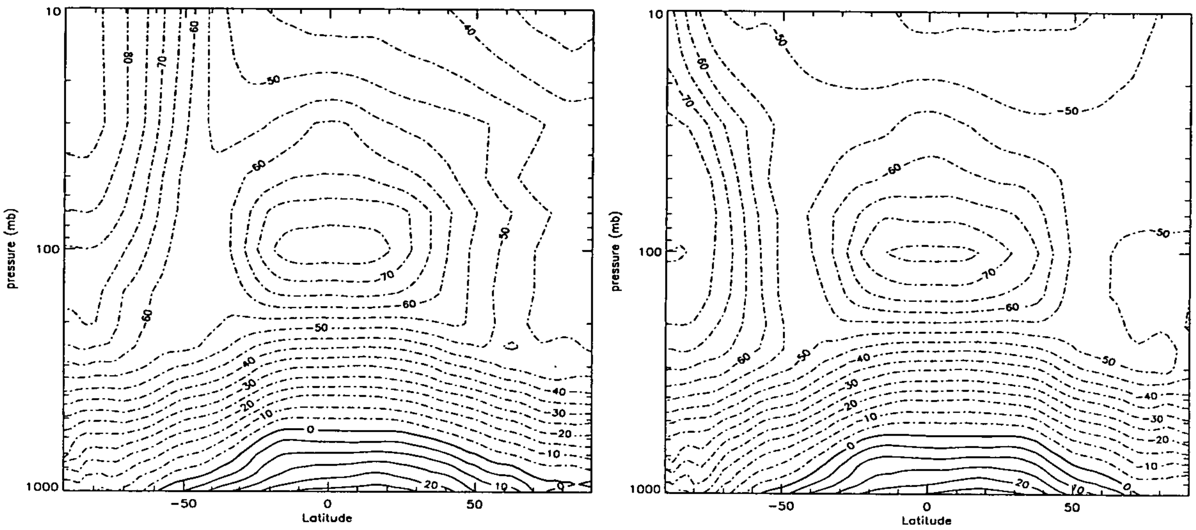

Figure 4.12: Zonally averaged temperature (°C) fields from the ECMWF analyses for a) mid-June,1991, b) mid-September,1991. The contour interval is 5°C.

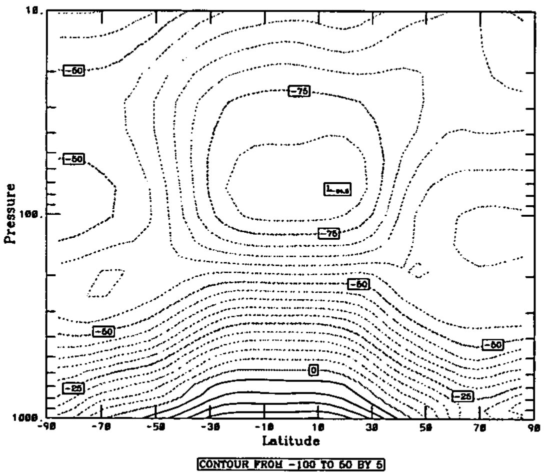

Figure 4.13: Zonally averaged temperature (°C) field from Run B for mid-December

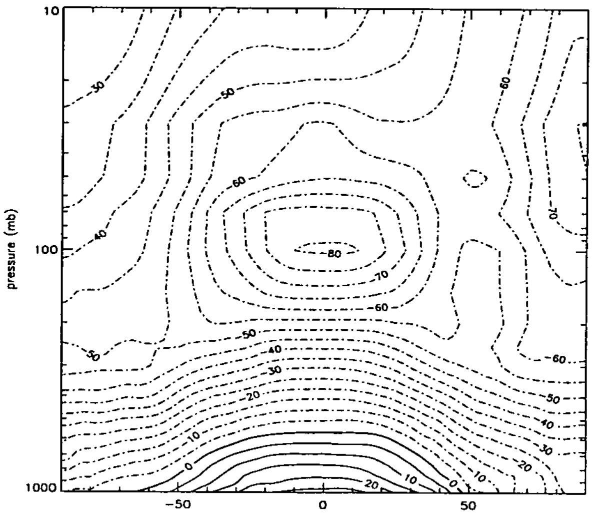

Figure 4.14: Zonally averaged temperature (°C) field from the ECMWF analyses for mid-December,1991. The contour interval is 5°C.

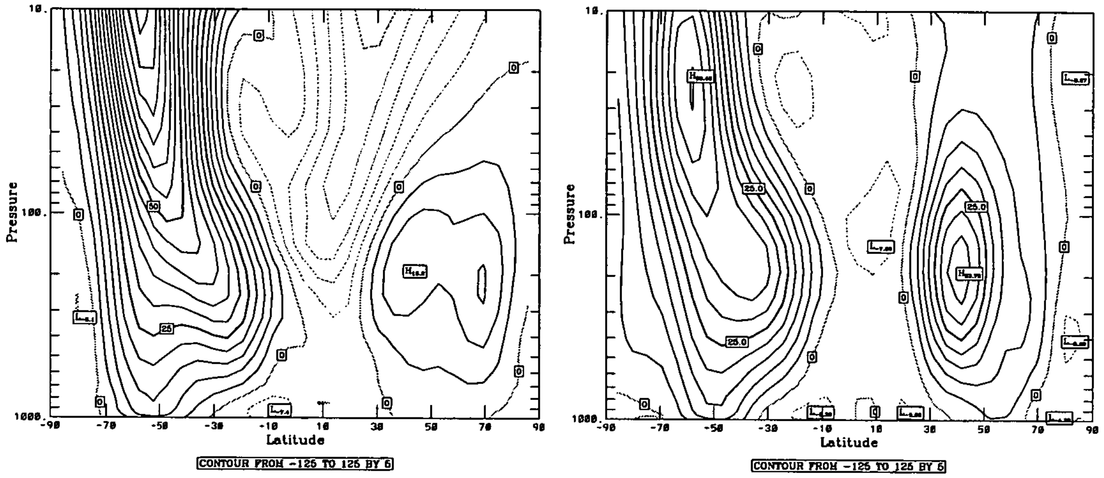

Figure 4.15: Zonally averaged winds (ms^{-1}) from Run B for a) mid-June (start of model run) and b) mid-September.

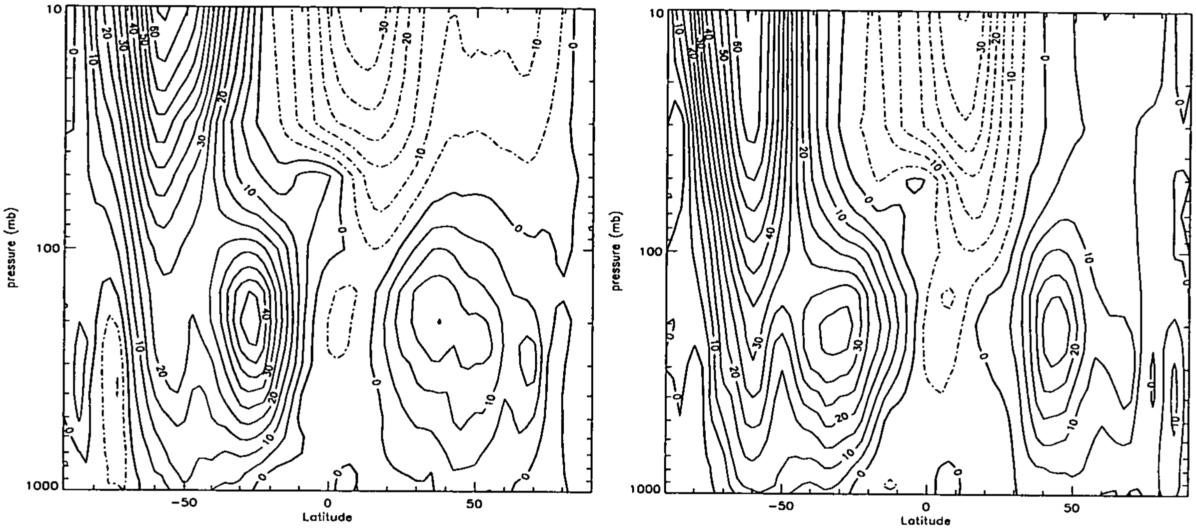

Figure 4.16: Zonally averaged winds (ms^{-1}) from the ECMWF analyses for a) mid-June,1991, and b) mid-September,1991. The contour interval is 5ms^{-1}.

month later in Run B. The structure of the winds over the tropics is quite different between the model and the analyses. In the lower stratosphere, westerlies are present in the tropics of analyses, but in the model there are easterlies.

The difference in the zonal wind over the tropics can be better illustrated by plotting the difference between the model and analyses fields (see Figure 4.17). We can see that over the tropics, the model winds are more westerly (by up to 20ms^{-1}) than the analyses above 30mb, and more easterly (by up to 15ms^{-1}) below 30mb. This difference in the model and analyses can be attributed to the model not being able to represent the QBO and we discuss this later, in section 4.3.4.

During the first three months of Run B, the easterlies present in the tropical stratosphere become progressively weaker while in the analyses they maintain their strength. The plots for mid-September (Figures 4.15b and 4.16b) show how dissimilar the easterlies in the two different data sets become; the model easterlies are at least 80% weaker than those in the analyses. The areas where westerlies exist agree well, although the southern westerlies are weaker in the model (by approx. 10ms^{-1}) and the northern westerlies are stronger in the model (by approx. 10ms^{-1}).

The easterlies in Run B continue to be much weaker than in the analyses until December. For mid-December (Figures 4.18 and 4.19) the easterlies are of similar strengths although, over the southern polar latitudes, the analyses easterlies are

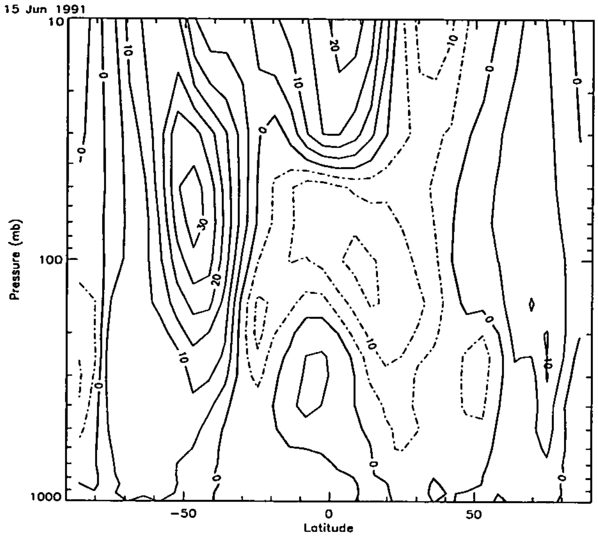

Figure 4.17: The difference between zonally averaged winds (ms^{-1}) taken from the EUGCM and ECMWF analyses for 15th June. The difference was obtained by subtracting the ECMWF analyses field from the model field. The contour interval is 5ms^{-1}.

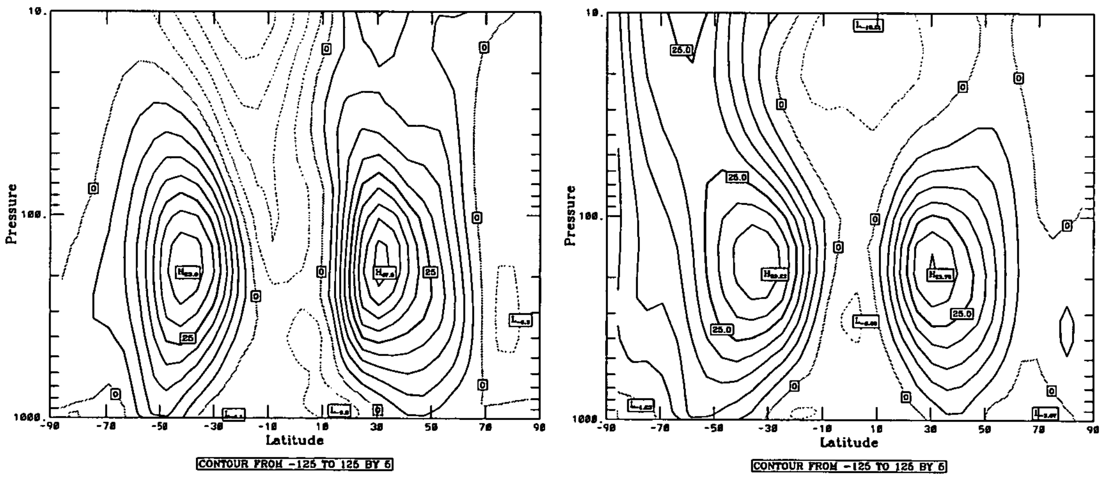

Figure 4.18: Zonally averaged winds (ms^{-1}) from Run B for a) mid-December and b) mid-March.

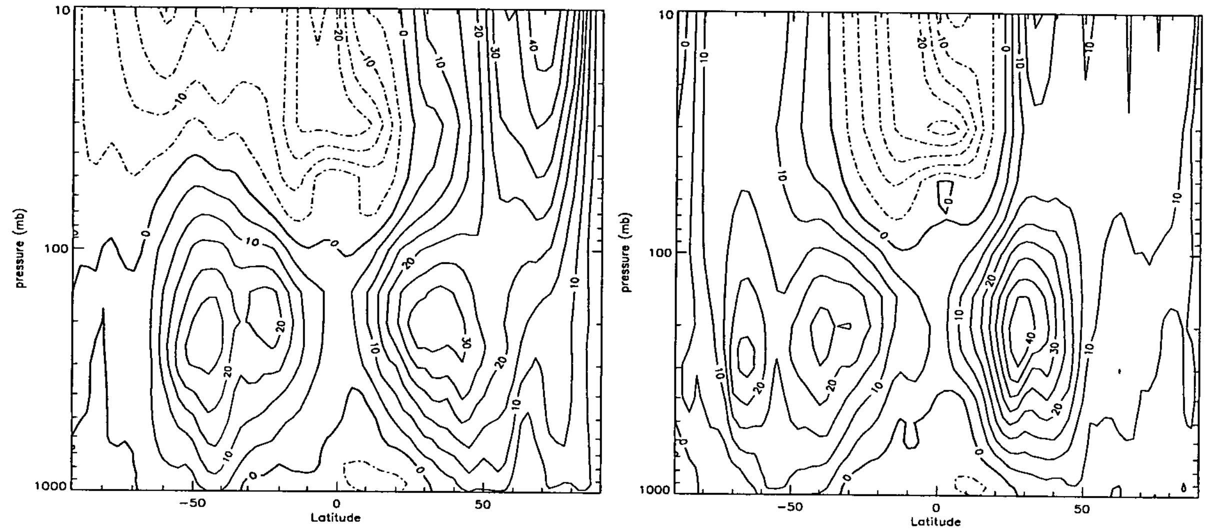

Figure 4.19: Zonally averaged winds from the ECMWF analyses for a) mid-December,1991, and b) mid-March,1992. The contour interval is 5ms^{-1}.

more dominant. The southern westerlies at this time, however, exist at higher altitudes in Run B than they do in the analyses. Of greater concern though is the different form that the westerly jet takes in the northern hemisphere in the model. In the analyses a split jet is apparent with a fairly strong jet (maximum is over 40ms^{-1}) in the stratospheric polar regions. Such a strong jet is not present in the model at this time, nor at any point during the northern winter.

By March, the weaker easterlies above the tropics in Run B have become the biggest difference (up to 20ms^{-1}) between the model and the analyses. The westerly jet in the southern hemisphere of the model is stronger than the analyses by about 10ms^{-1} in the stratosphere. There are also westerlies present in the analyses in the northern stratosphere which do not appear in Run B.

Over the next couple of months the easterly jet in the model shifts its centre further north, which is in disagreement with what happens in the analyses (remains centred near equator). By May (Figures 4.20 and 4.21 the structure and strength of the zonal winds in the southern hemisphere in the model and analyses seems fairly similar. However, in the northern hemisphere the two fields are quite different. The tropospheric jet in the northern hemisphere is 50% weaker in the model than the analyses. In the model, the easterlies are centred further north than in the analyses.

As a guide for later in the work, Figure 4.22 shows a latitude/height plot of potential temperature at the start of Run B. When discussing PV distributions

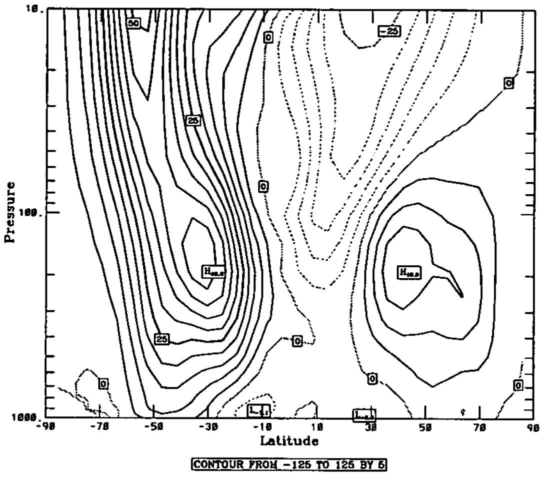

Figure 4.20: Zonally averaged winds (ms^{-1}) from Run B for mid-May

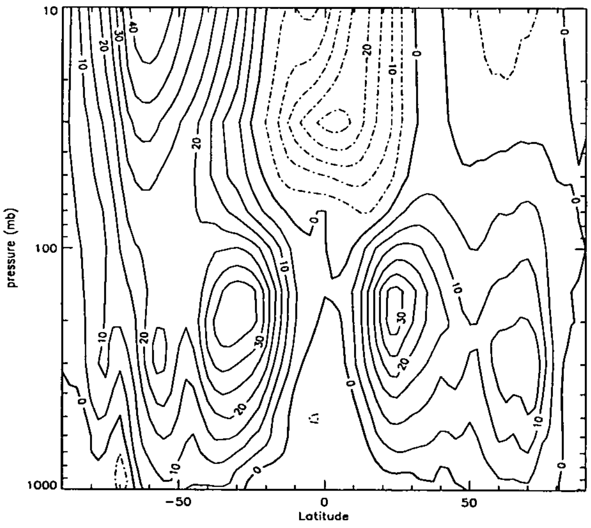

Figure 4.21: Zonally averaged winds from the ECMWF analyses for mid-May,1992. The contour interval is $5ms^{-1}$.

later, isentropic surfaces are used frequently and it helps to have a sense of where they are in relation to pressure surfaces. With the exception of the polar regions, the heights of these isentropic contours are fairly constant throughout the model run. While this plot is for Run B, the agreement with the equivalent plot for Run A is good and so this can be used as a rough guide for both model runs.

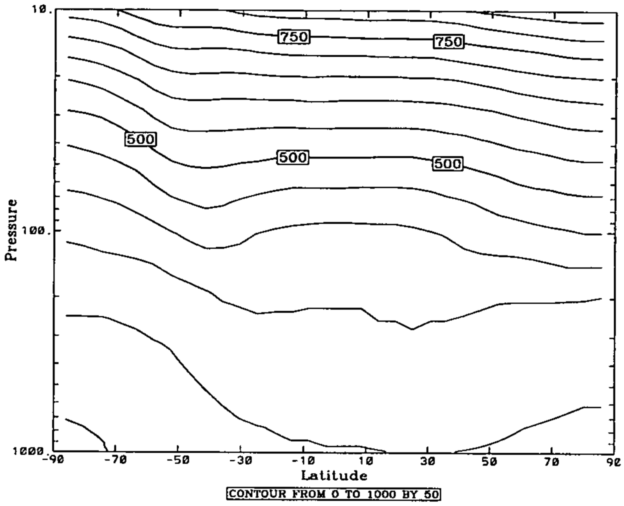

Figure 4.22: Latitude/height plot of zonally averaged potential temperature (K) at the start of Run B. The contour interval is 50K.

It is clear from this brief comparison between the model runs and the ECMWF analyses that although, in general, the model behaves in a realistic way, there are some noticeable differences. The effect that some of these differences have on the Pinatubo simulations is investigated in greater depth in the next chapter.

4.3.4 Considering the QBO

The quasi-biennial oscillation (QBO) is a feature seen in the zonal winds of the equatorial stratosphere. The QBO is driven by vertically propagating equatorial waves [*Holton*, 1992]. The main feature of the QBO is zonally symmetric easterly and westerly wind regimes alternating with periods varying from about 24 to 30 months. The regimes appear above 30km and propagate downwards at a rate of 1 km per month. Figure 4.23 depicts the QBO as seen at the equator.

The UGAMP models do not represent the QBO (something which is true of many GCM's), but this is not an immediate concern. At the height where the Pinatubo cloud was situated, the QBO had just entered the easterly phase (see Figure 4.23). The tropical zonal winds in the UGAMP model runs are also

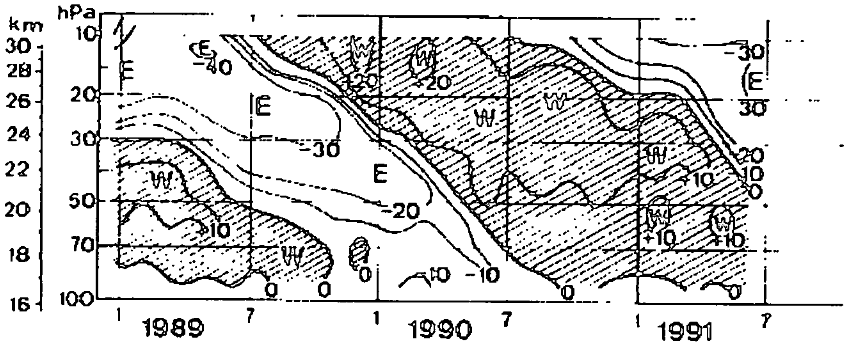

Figure 4.23: Time-altitude section of monthly mean zonal wind component at Singapore (1°N, 104°E) for January 1989 to June 1991, showing the quasi-biennial oscillation in the equatorial lower stratosphere. Contour interval is 10 ms^{-1}. Where the contours stop on the right of the plot is when Mt. Pinatubo erupted. Taken from *Holton* [1992].

easterly at this time (see previous section) and they remain easterly throughout the model runs. The easterly phase of the QBO persists for at least a year which is the length of the longest model experiment. This gives us more confidence for a realistic Pinatubo simulation. The QBO is discussed further in section 7.3.1 when we consider its possible effects on the meridional transport of volcanic tracer.

The configuration for the two main experiments have now been described, apart from the initialisation of the volcanic cloud within the model. Due to the nature of the spectral model, initialising a distribution such as the Pinatubo cloud requires careful consideration and the next section deals with that issue.

4.3.5 Initialising the volcanic cloud in the model

The aerosol cloud generated by Mt. Pinatubo was injected into the stratosphere over a vary small area compared with the typical resolution scales of the model. This causes problems when using a spectral model as negative values develop for two reasons.

The first is "dispersion errors". If you break the tracer profile down into its Fourier components and consider what the scheme does to each component (this is valid because the advection scheme is linear, so that advecting the components then adding them together is the same as just advecting the whole profile), it turns out that the different Fourier components travel at different speeds, i.e.

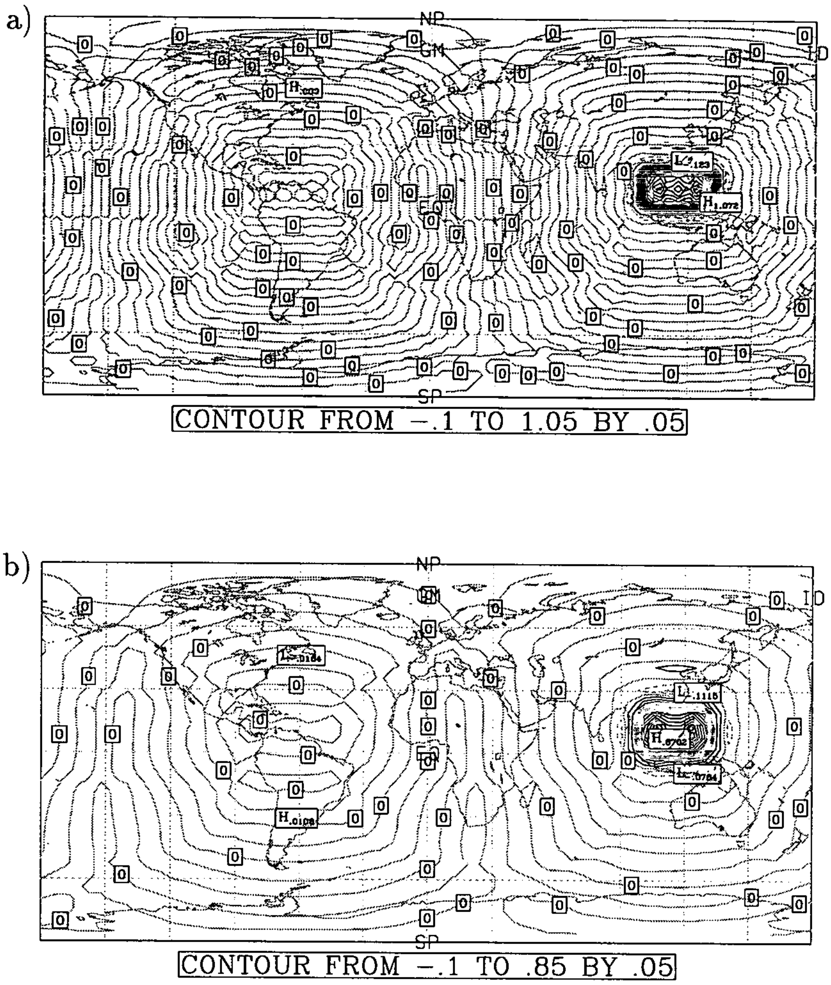

Figure 4.24: Two isentropic (500 K) maps of tracer (in vmr) a) from Run A and b) from Run B, both showing examples of Gibbs fringes. The tracers seen here are not smoothed. Significant negative values occur before the first time step has even been reached.

they disperse [*Haltiner and Williams*, 1980]. If the scheme were perfect, of course, all the components would travel at the speed of the flow. This becomes serious when steep gradients occur in the tracer field, particularly if there is a strong flow parallel to the steep gradient. The result is negative values of the tracer occurring upwind from the steep gradient.

The second reason is "Gibbs fringes". In the case of the UGAMP GCM, the representation in grid space has more degrees of freedom than the spectral representation. If you start with a field in grid space and transform to spectral space, usually some information will be lost. When the field is transformed back to grid space it will be different from the original field. In some cases (e.g. if the original field has a step like the Mt. Pinatubo cloud) there will be spurious oscillations which are known as Gibbs fringes. Figure 4.24 shows two examples of Gibbs fringes, one for T21 resolution, the other for T42 resolution.

So far, all mention has been of the problems caused by the horizontal advection scheme. The equivalent problem in the vertical is not an issue due to the Total Variation Diminishing (TVD) scheme which the UGAMP model now employs. The TVD scheme is an important aspect of the model in relation to these experiments and is explained in Appendix A. To reiterate briefly, the scheme stops negative values from developing by preventing new maxima and minima developing in the tracer field. Unfortunately such a scheme is not available to compensate for the problems caused by the two-dimensional horizontal advection scheme.

For both the model runs, an inert tracer is included as part of the initial data. This represents an instantaneous release of material into the stratosphere which is not what actually happened. The eruptions really occurred over a few days. However, while it is possible to represent this in the model it makes very little difference to the tracer distributions (including the magnitude of the negative values) throughout the run and certainly no difference to the poleward spread of the cloud (based on experiments not shown here).

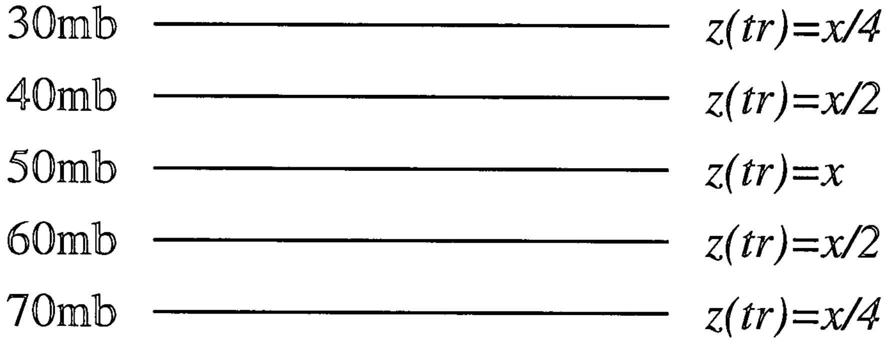

Figure 4.25: The initial distribution of tracer (for Run A and Run B) with respect to pressure.

Although the TVD scheme solves any problems with negative values of tracer in the vertical, the initial distribution is given some vertical structure as this was seen in the real Pinatubo cloud. The initial distributions of the tracers in Run A and Run B both have the same vertical structure. The vertical distribution of the clouds can be expressed as a function of whatever value the tracer is at 50mb, say

x (50mb is the centre of the tracer distribution with respect to pressure). x varies in longitude and sometimes in latitude, depending on the distribution. Figure 4.25 shows the vertical distribution in terms of x which is then interpolated onto the model levels.

Both the problems with horizontal advection in a spectral model (discussed earlier) are at their most serious when a large step occurs in the tracer field, a situation which is inevitable when dealing with the Mt. Pinatubo cloud. The negatives are impossible to eliminate but they can be greatly reduced by making the distribution less of a step.

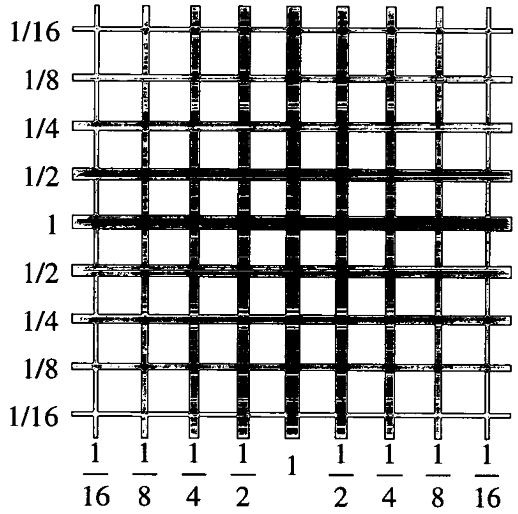

Figure 4.26: A description of the horizontal distribution of tracer at 50mb for Run A. Where two lines cross is a gridpoint in the model. The value of tracer (in volume mixing ratio) which is assigned to each gridpoint is the multiple of the values assigned to the two lines associated with that gridpoint. The distribution is smoothed in the same way at all heights, but the values involved are dictated according to the previous figure.

Figure 4.26 shows how the chosen distribution is represented in the EUGCM. The version for the UGCM is very similar but over less gridpoints. In both model runs, the initial tracer distribution is centred over the site of Mt. Pinatubo as near as possible, depending on gridpoint positions. Note that the maximum value (volume mixing ratio) of the distribution is 1 which has been chosen arbitrarily. The value chosen is not important as the tracer advection equation is linear in the tracer and therefore can be arbitrarily scaled. This also means that subsequent experiments in Chapter 5 using some zonal distributions will be comparable with experiments in this chapter.

The fact is, the negative values of tracer are always going to appear with a spectral advection scheme but, in this case, they do not detract from the validity of information gained from the experiments. The initial tracer distributions have been chosen such that the negative values are not significant enough to cause any major problems. Throughout the rest of this thesis, tracer fields are presented with any zero or negative contours omitted. This is not an effort to hide the negative values, but to make interpretation of the evolution of the volcanic cloud (the positive values) much clearer. The Gibbs fringes cause many zero contours to appear (see Figure 4.24) and this makes the tracer fields look more confusing than is necessary. Figure 4.27 shows the initial tracer distribution of Run A without negative or zero contours.

Having looked fairly extensively at the experiment conditions, we proceed with the analysis of the model runs. In this chapter, most of the focus is on the direct comparison between the model fields and observations of the Pinatubo cloud. The next section deals with Run A (the 19 level, T42 run) and then section 4.5 presents the results from Run B (the 47 level, T21 run).

4.4 Analysis of Run A

The analysis is split in to different parts, similar to those in section 4.2.

4.4.1 Rate at which the cloud circles the globe

The cloud starts heading West at different rates, depending on latitude and altitude. After 5 days (Figure 4.28b), for example, the part of the cloud which was initialised near the equator at θ=500K has not traveled nearly as far West as material initialised further north, ; the zonal winds at 20°N being stronger than those at the Equator (see Figure 4.28a).

Also, the higher the altitude, the faster the cloud travels West. Figure 4.29 shows a cross-section of the volcanic cloud at the latitude 15°N at day 15 in the model run. Near the top of the model the cloud has just completed one circuit of the Earth while, at the altitude of the initial cloud maximum, only a half to

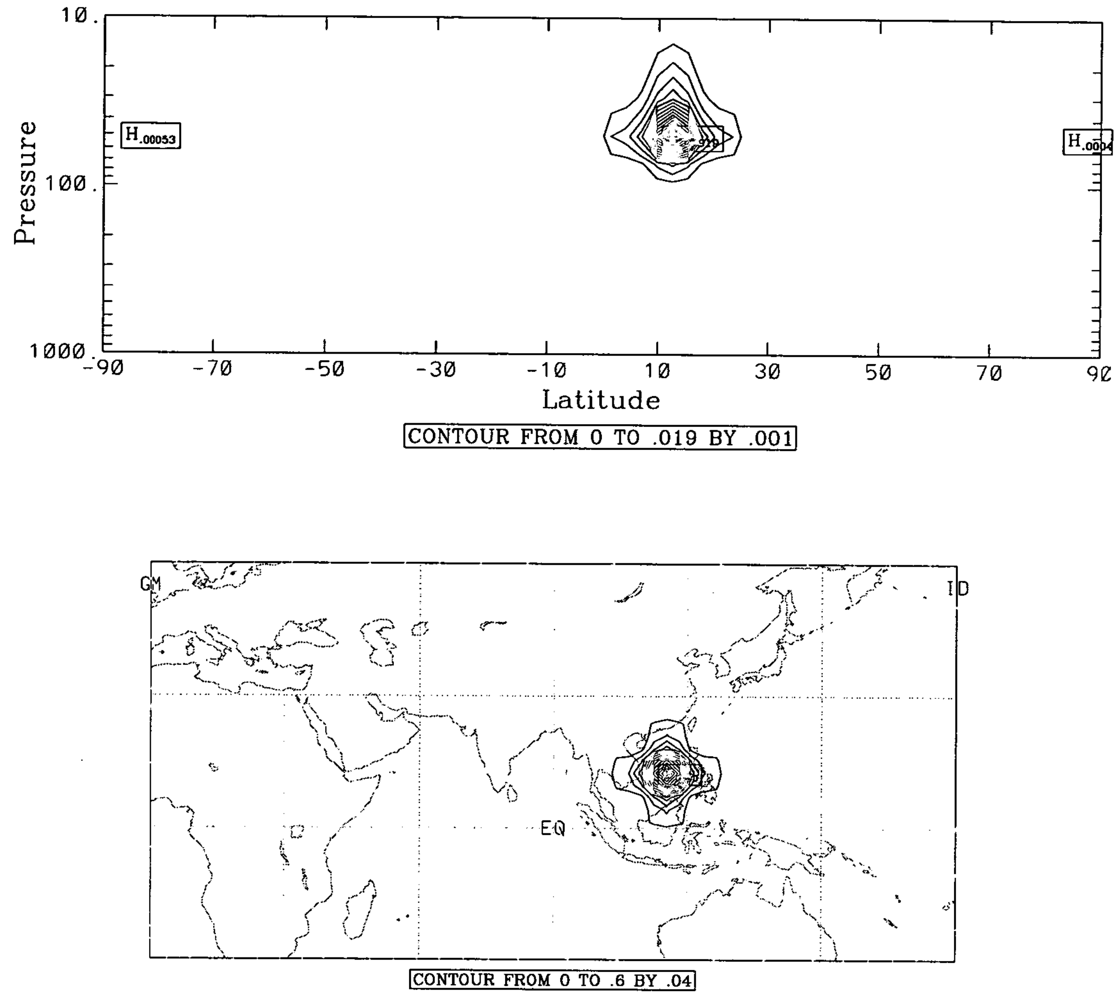

Figure 4.27: Initial distribution of the tracer (vmr) in Run A as seen in the model output fields. a) The zonally averaged distribution. b) the quasi-horizontal distribution (on the isentropic surface θ=500K, just below the highest values). The plot is for the limited area 30°S to 60°N (y-axis) and 0°E to 180°E (x-axis).

two thirds of the way round the Earth has been reached. This is also due to the distribution of zonal winds, this time the zonal winds becoming higher as altitude increases. As can be seen from Figure 4.30, at day 21 of Run A, the main part of the cloud is about to complete one circuit of the earth. This agrees very well with actual measurements of the cloud.

Figure 4.29 also shows the problems presented when using a model with such a low top level for an experiment such as this. Through diffusion and general circulation (upwelling in tropics) the tracer very quickly reaches the top of the model. However, while this creates difficulties later on, the opportunity to study the processes transporting aerosol into mid-latitudes from the tropics still presents

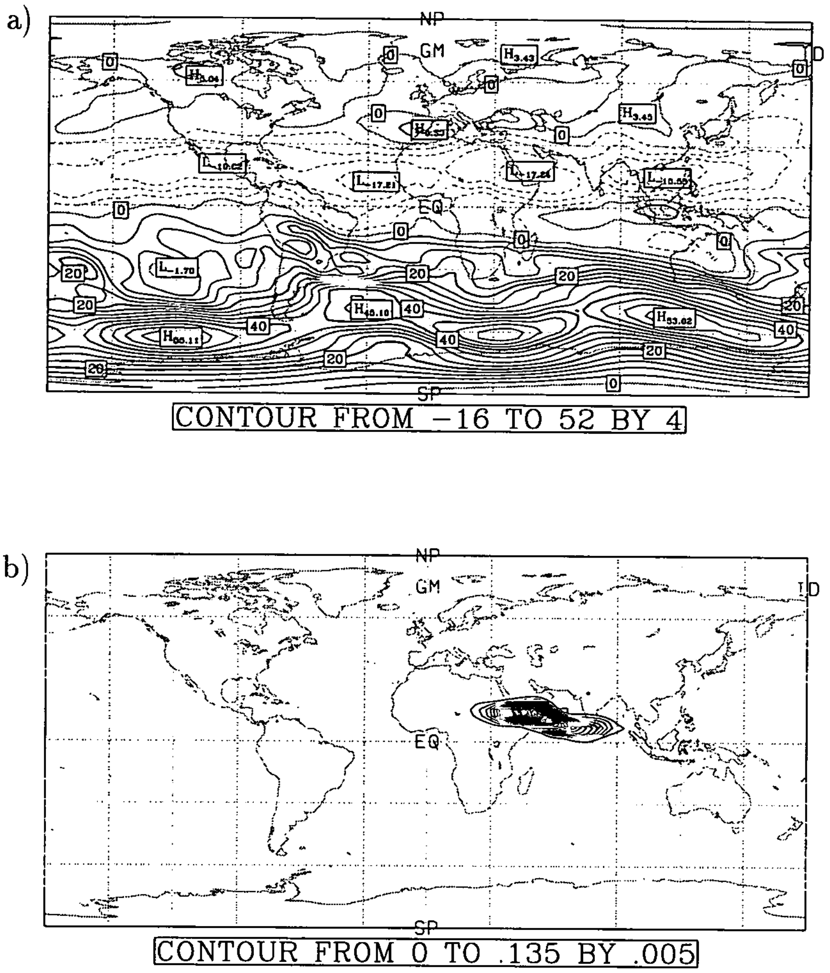

Figure 4.28: Isentropic map of a) zonal wind (in ms^{-1}) and b) tracer volume mixing ratio, 5 days into Run A, at a height of 500 K. Illustrates how the rate of longitudinal spread is dependent on latitude

itself.

4.4.2 Spread of tracer as seen from zonally averaged fields

The zonally averaged tracer fields are useful for looking at the general spread of the tracer with respect to latitude and altitude. The following analysis is based on Figures 4.31 and 4.32. In the first 5 days of the experiment there is very little change in the latitudinal distribution of the tracer. Material consistently lies between the Equator and 20/25°N. The tracer diffuses vertically, material quickly reaching the top of the model. The bottom of the cloud remains at the

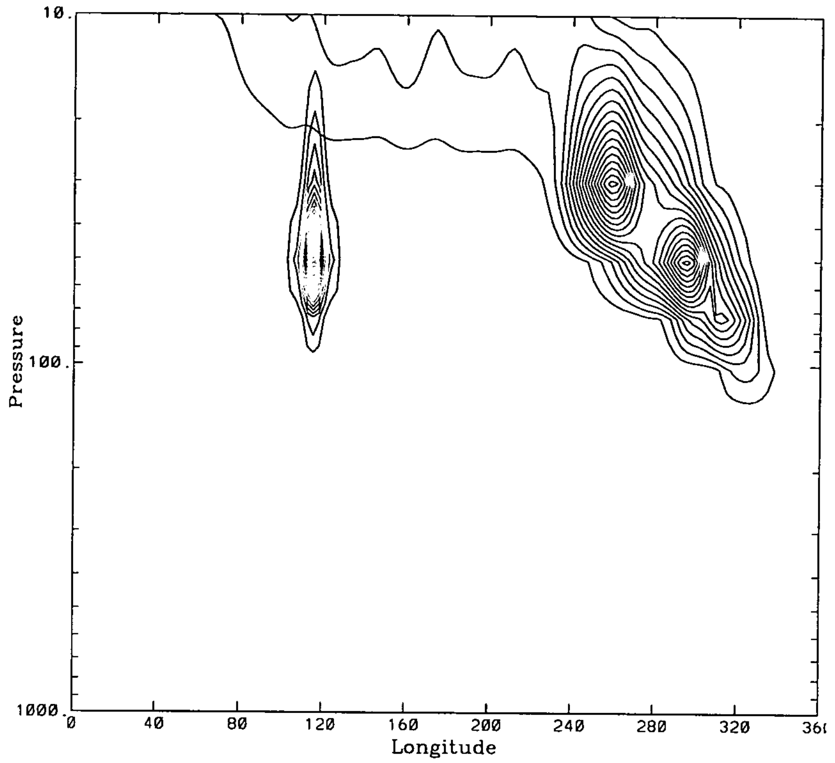

Figure 4.29: Latitude slice (longitude vs. pressure) at 12.5°N of tracer (vmr) on day 15 of Run A with the initial tracer distribution superimposed. The initial distribution is the narrow band of contours centred over 115°E.

100mb mark except for a very small amount of material above 20°N being drawn both downwards and northwards.

The movement of tracer northwards and downwards continues over the next 10 days at a gradual pace. During this time there is no other significant movement of tracer (particularly with respect to latitude) other than a slight diffusing. The rate that material is transported from the tropics into the northern mid-latitudes increases and by day 20, significant amounts of tracer can be found in the extra tropics. The distribution at day 20 of Run A (Figure 4.32a) gives the impression that the material in the northern mid-latitudes is now quite separate from that in the tropics.

The transport of material northwards appears to slow down after day 22 and material disperses gradually around the mid-latitudes resulting in the highest zonally averaged values in this area to have dropped by day 25. At this point no significant amount of material has been transported further north than 50°N.

Other than general diffusion with respect to both altitude and latitude, there

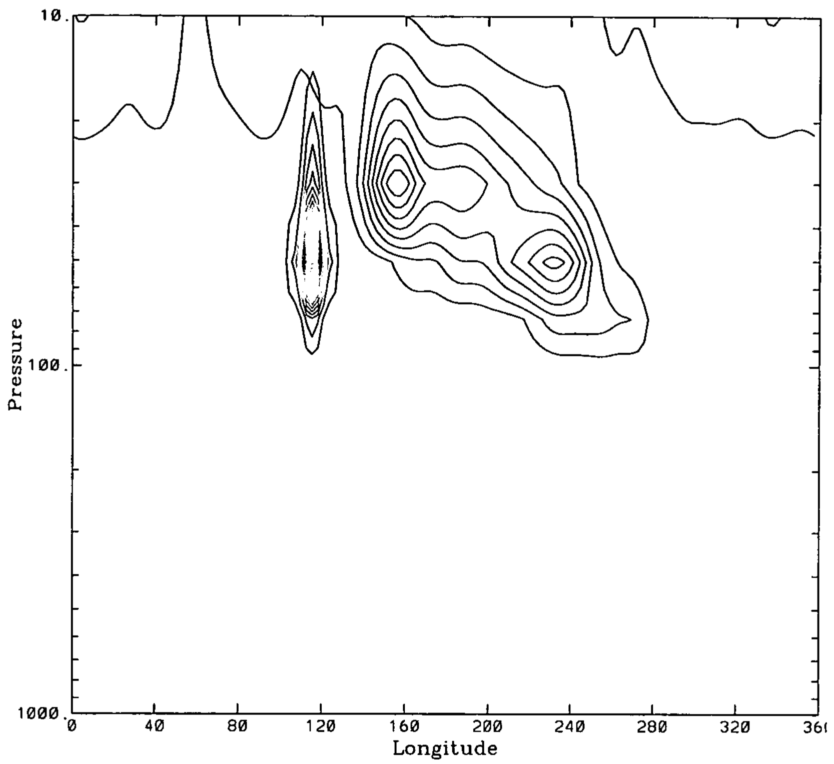

Figure 4.30: Latitude slice (longitude vs. pressure) at 12.5°N of tracer (vmr) on day 21 of Run A with the initial tracer distribution superimposed. The initial distribution is the narrow band of contours centred above 115°E.

is no change in distribution between day 25 and 30. During the first month of Run A, the highest values of tracer (which remain over 10°N throughout) rise up to the top of the model. This is a consequence of the top of the model being so low; close to where the cloud was initialised. The general circulation carries the tracer to the top level of the model where it is trapped, so it collects there. This is unrealistic as in the real atmosphere the material would loft higher. The collection of material at the top of the model is inevitable, but, in this case, the situation is exacerbated by a fairly poor vertical resolution near the top of the model (see Figure 2.8). The lack of settling velocities applied to the tracer may also be a reason for this problem. The effect of settling velocities on a volcanic cloud distribution is investigated in section 6.3.1.

Between day 30 and day 60, it is difficult to say whether any more tracer is transported northwards, out of the tropics. Some tracer does reach northern polar latitudes (around day 50) while material in the mid-latitudes further disperses. The widespread dispersion in the northern mid- and polar latitudes is what makes

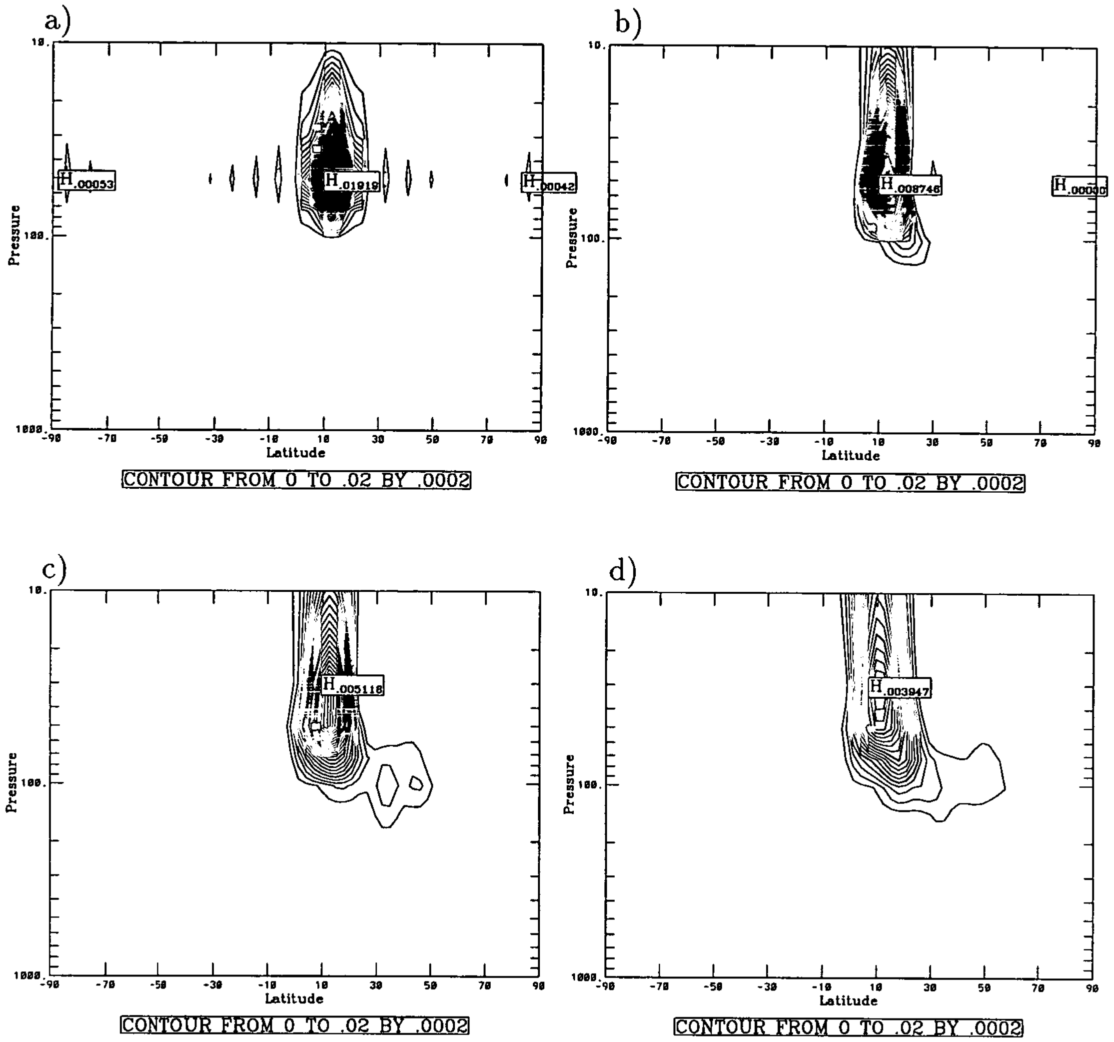

Figure 4.31: Zonally averaged tracer (vmr) from Run A at a) 0, b) 5, c) 10 and d) 15 days. The contour interval is 0.0002 for all four plots.

it difficult to determine the amount of material transported from the tropics using only zonal plots.

Throughout Run A, the tracer does not appear to move northwards from the tropics above 30mb. Some small traces of material may exist above this height in the northern mid-latitudes but I believe this to be a result of material, which has been transported to the mid-latitudes at a lower altitude, diffusing vertically (the model is susceptible to this due to the relatively low vertical resolution at the top of the model).

In the same period of Run A (days 30 to 60) material makes a fairly significant move southwards above 30mb. The material still does not manage to get south of the tropics though. The UGCM, although managing to show evidence of two

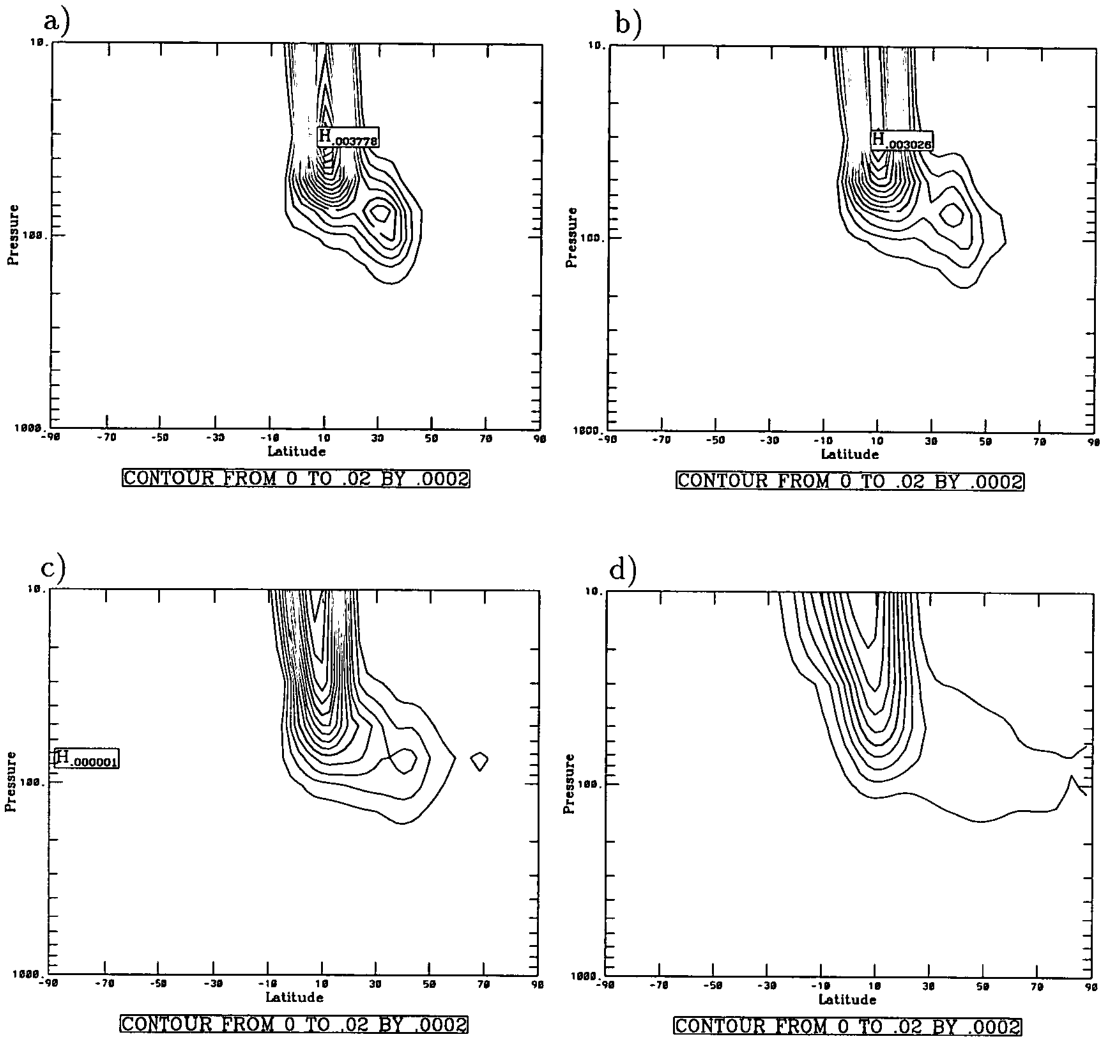

Figure 4.32: Zonally averaged tracer (vmr) from Run A at a) 20, b) 25, c) 30 and d) 60 days. The contour interval is the same as that for the previous figure.

different mixing regimes, does not exhibit the same rates of poleward transport seen in real measurements of aerosol spread. Even after 60, days the model has much more material in the northern hemisphere than in the southern hemisphere despite the fact that the distribution was centred slightly further south than in the real atmosphere. The distribution of the aerosol in the northern hemisphere is quite close to that seen in the measurements (see Figure 4.6).

After the first few months, the peak of tracer found at the top of the model above the tropics begins to drift northwards, eventually reaching the polar latitudes (see Figure 4.33). We discuss why this happens later, in section 4.4.5, when we look at the consequences of having the top level of the UGCM so low in the stratosphere.

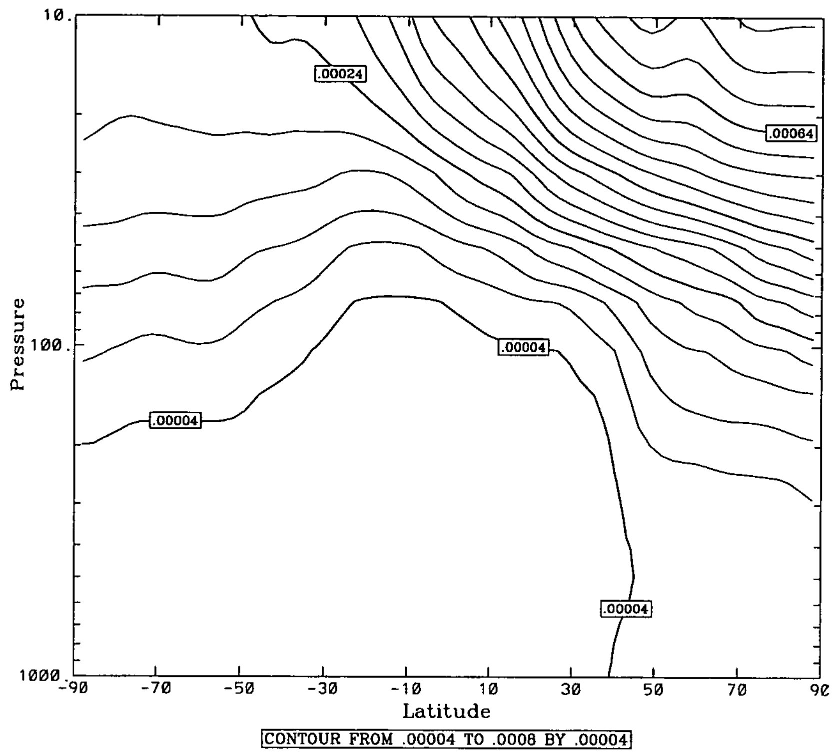

Figure 4.33: Zonally averaged tracer (vmr) on day 360 of Run A.

Despite the limitations of the UGCM with respect to this experiment, a height dependency of poleward dispersal was demonstrated and using latitude-longitude plots on isentropic surfaces we can make an initial investigation into the nature of the dynamics transporting material from the tropics into the mid-latitudes as simulated by the UGCM.

It is clear from Figures 4.31 and 4.32 that material, although confined to the tropics in a general sense, is managing to escape into the mid-latitudes. The next two sections try to establish the nature of the mixing events in the UGCM which allow tropical material to reach mid-latitudes.

4.4.3 Mixing events transporting material northwards

The next series of plots (Figures 4.34 to 4.36) show the evolution of the first mixing event to transport tropical material into the mid-latitudes. The winds for the same heights and times are superimposed on the tracer fields to give an idea of what dynamics are affecting the tracer. From Figure 4.34 we can see that the most northerly tip of the main cloud has been caught in the anticyclone centred

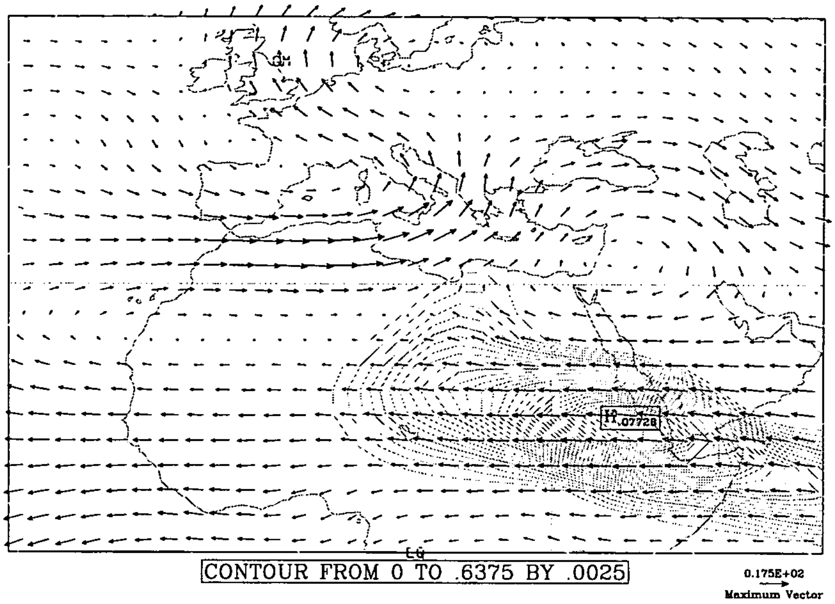

Figure 4.34: Latitude-longitude limited area plot (Eq. to 60°N and 30°W to 60°E) on the isentropic surface θ=450K (approx. 70mb) of tracer (vmr) on day 6 of Run A. Wind vectors are superimposed.

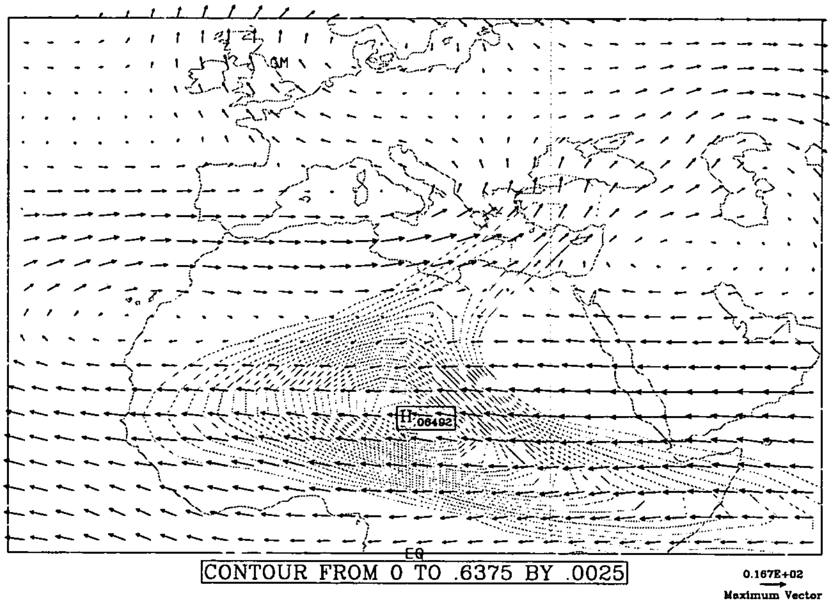

Figure 4.35: Latitude-longitude limited area plot (Eq. to 60°N and 30°W to 60°E) on the isentropic surface θ=450K (approx. 70mb) of tracer (vmr) on day 8 of Run A. Wind vectors are superimposed.

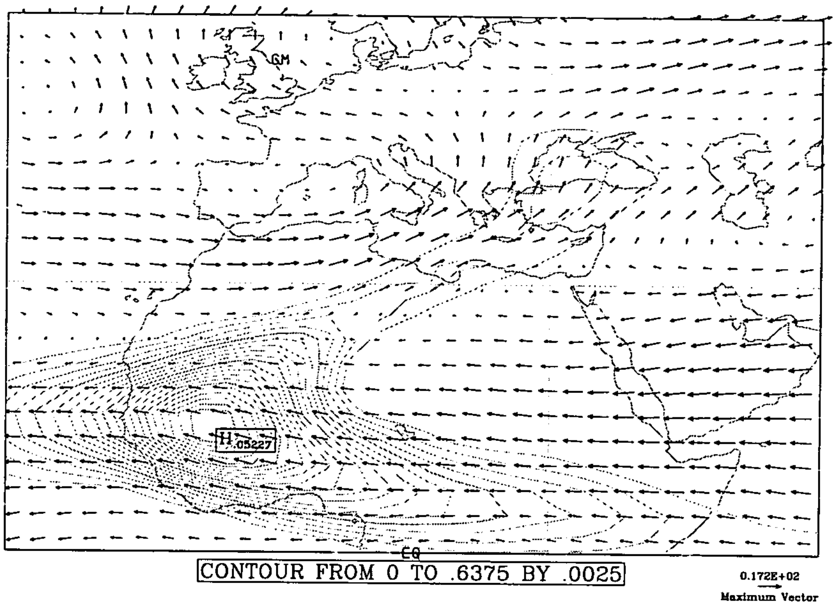

Figure 4.36: Latitude-longitude limited area plot (Eq. to 60°N and 30°W to 60°E) on the isentropic surface θ=450K (approx. 70mb) of tracer (vmr) on day 10 of Run A. Wind vectors are superimposed.

near 30°N, 30°E, helped by the slight northwards bias of the tropical jet at this longitude. The main part of the cloud continues westward in the tropics.

Two days later (Figure 4.35), the anticyclone has moved a few degrees westward and continues to pull the cloud north, reaching well into the mid-latitudes. Meanwhile, the main mass of the cloud is being carried along by the easterly flow in the tropics. These strong tropical easterlies combined with the strong westerlies in the sub-tropics form a shear, which starts to separate the tongue of cloud stretching into the mid-latitudes from the main cloud. This feature can be seen clearly in its more developed stage a further two days later (Figure 4.36).

At day 10, the tongue of tracer has nearly completely separated from the main cloud. The anticyclone which created the tongue is no longer in the vicinity and so no more material is pulled from the tropics. The northern-most part of the tongue is left to disperse in the middle latitudes with no route back to the tropics.

We can see anticyclonic events similar to that in Figure 4.34 in the ECMWF analyses (introduced earlier in the chapter). Figure 4.37 shows a vector plot for June 21st, 1991 taken from the ECMWF analyses data set. The vectors are plotted on the pressure surface 70mb; as you can see from Figure 4.22, this is a similar height to the isentropic surface, 450K, in Figure 4.34. Although not in the same

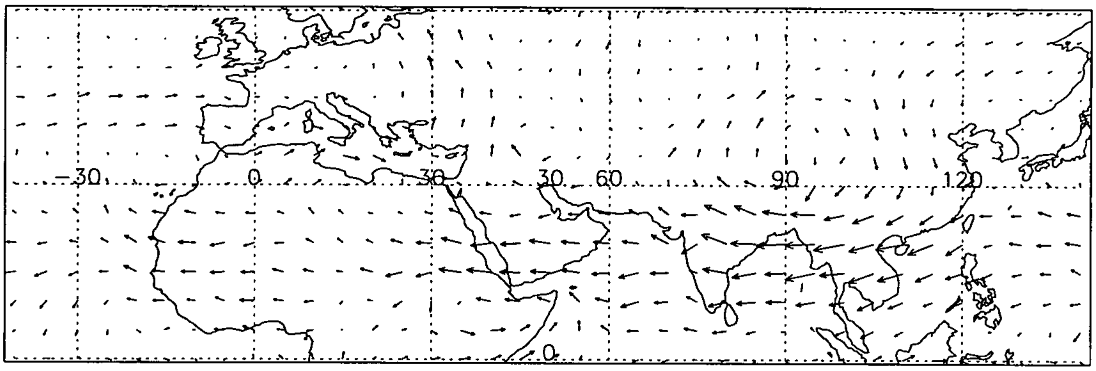

Figure 4.37: Latitude-longitude limited area plot (Eq. to 60°N and 40°W to 140°E) on the pressure surface 70mb of wind vectors on June 21st, 1991, taken from ECMWF analyses

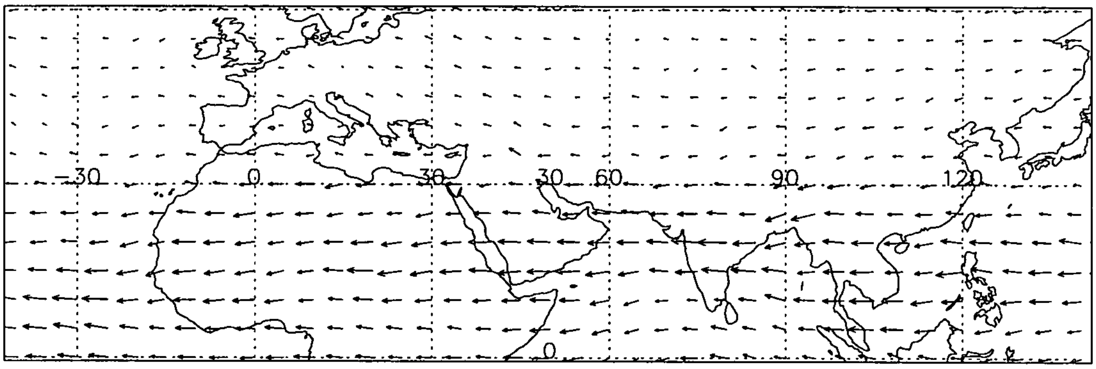

Figure 4.38: Latitude-longitude limited area plot (Eq. to 60°N and 40°W to 140°E) on the pressure surface 30mb of wind vectors on June 21st, 1991, taken from ECMWF analyses

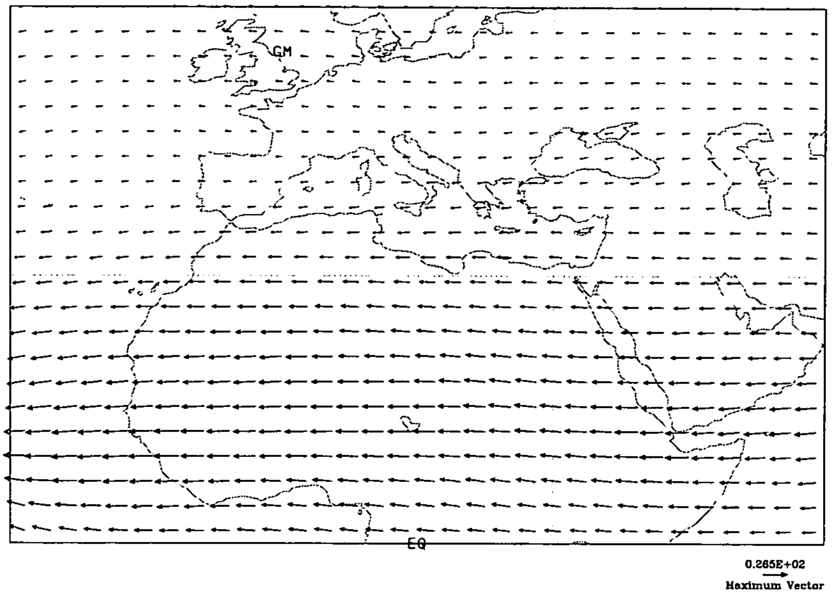

Figure 4.39: Latitude-longitude limited area plot (Eq. to 60°N and 30°W to 60°E) on the isentropic surface θ=650K (approx. 20mb) of wind vectors on day 6 of Run A.

position, there is a clear anticyclonic event centred at approximately 30°N, 90°W. There also some lesser events which look capable of transporting material from the tropics at round 30°W and 30°E. These anticyclonic events appear in the analyses at this height in most days in the months following the eruption, especially the main anticyclonic event (at 90°W) associated with the Asian monsoon.

The next plot (Figure 4.38) shows winds in the ECMWF analyses on the same day as Figure 4.37, but higher in the atmosphere, 30mb. The anticyclonic events evident lower in the analyses are not here, and this is true for the first few months following the eruption of Mt. Pinatubo. This is in good agreement with the concept of a two layer mixing regime which was discussed earlier; material below 20km in the tropics mixing northwards due to tropospheric-related events, while the material above 20km was confined to the tropics in the northern hemisphere.

Returning to Run A, Figure 4.39 shows winds for the same day and region as Figure 4.34, but at a higher altitude in the model, close to that of the analyses in Figure 4.38. The anticyclonic event which was detraining material from the tropics lower in the model is not at this height. Again, although this is a specific day, this holds for the weeks following the start of Run A. This shows that Run A is replicating the two-layer mixing scheme well (with respect to the northern

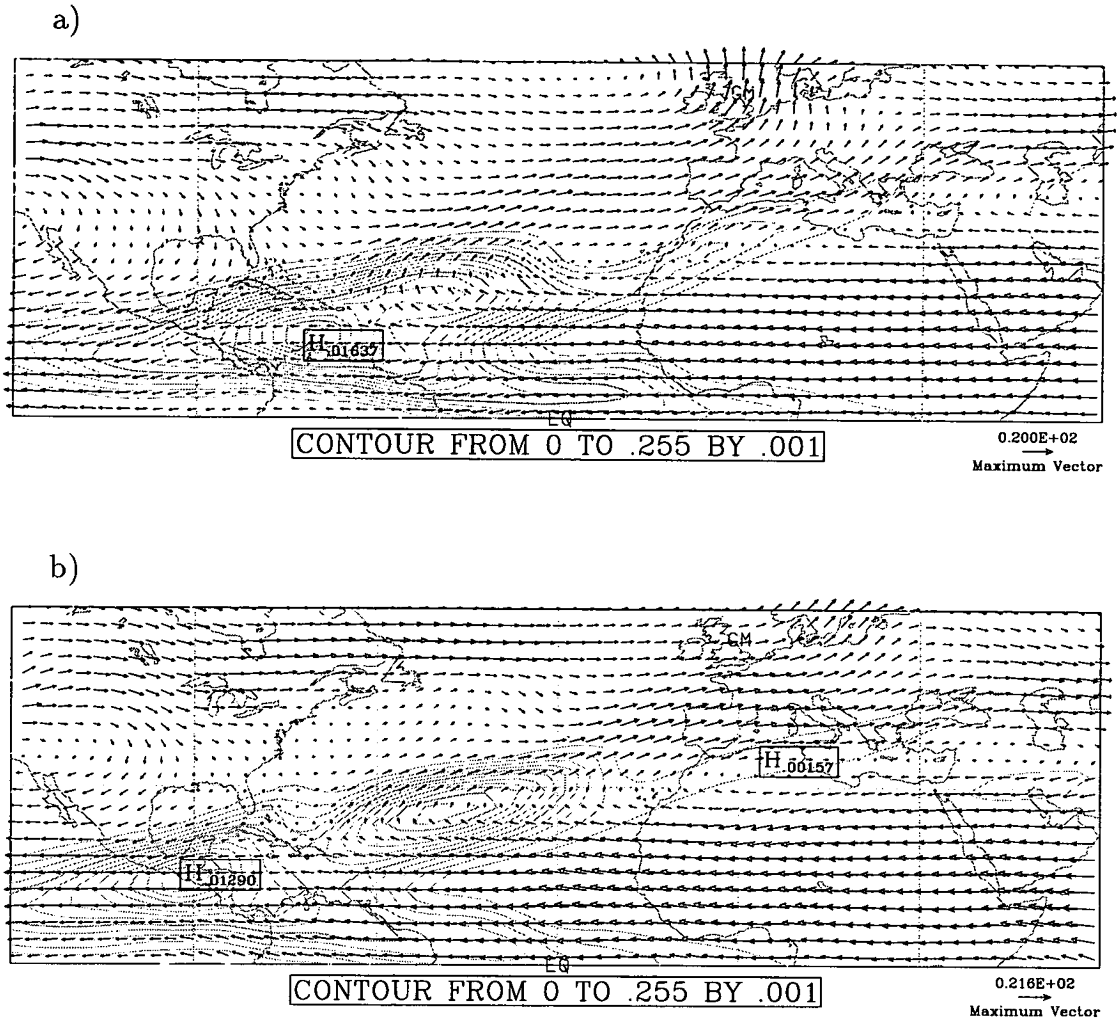

Figure 4.40: Latitude-longitude limited area plot (Eq. to 60°N and 120°W to 60°E) on the isentropic surface θ=450K (approx. 70mb) of tracer (vmr) on days a) 16 and b) 18 of Run A. Wind vectors are superimposed.

hemisphere) which is also in agreement with zonally averaged tracer fields shown earlier (Section 4.4.2).

Continuing with the spread of the tracer, the shearing mentioned in relation to Figure 4.35 is also responsible for a much larger event which occurs just a few days later, the start of which can be seen in (Figure 4.40a). The main cloud has continued westwards and the tongue of air described previously can still be seen, but not extending so far into the mid-latitudes (partly due to the larger contour interval used for the next few plots). The end of the tongue has broken off and mixed into the mid-latitudes. Around 15 to 30°W, a fairly strong northward flow is pulling material from deep within the main cloud into the extra-tropics.

The northward flow produced mainly between 30 and 60°W starts to pull a

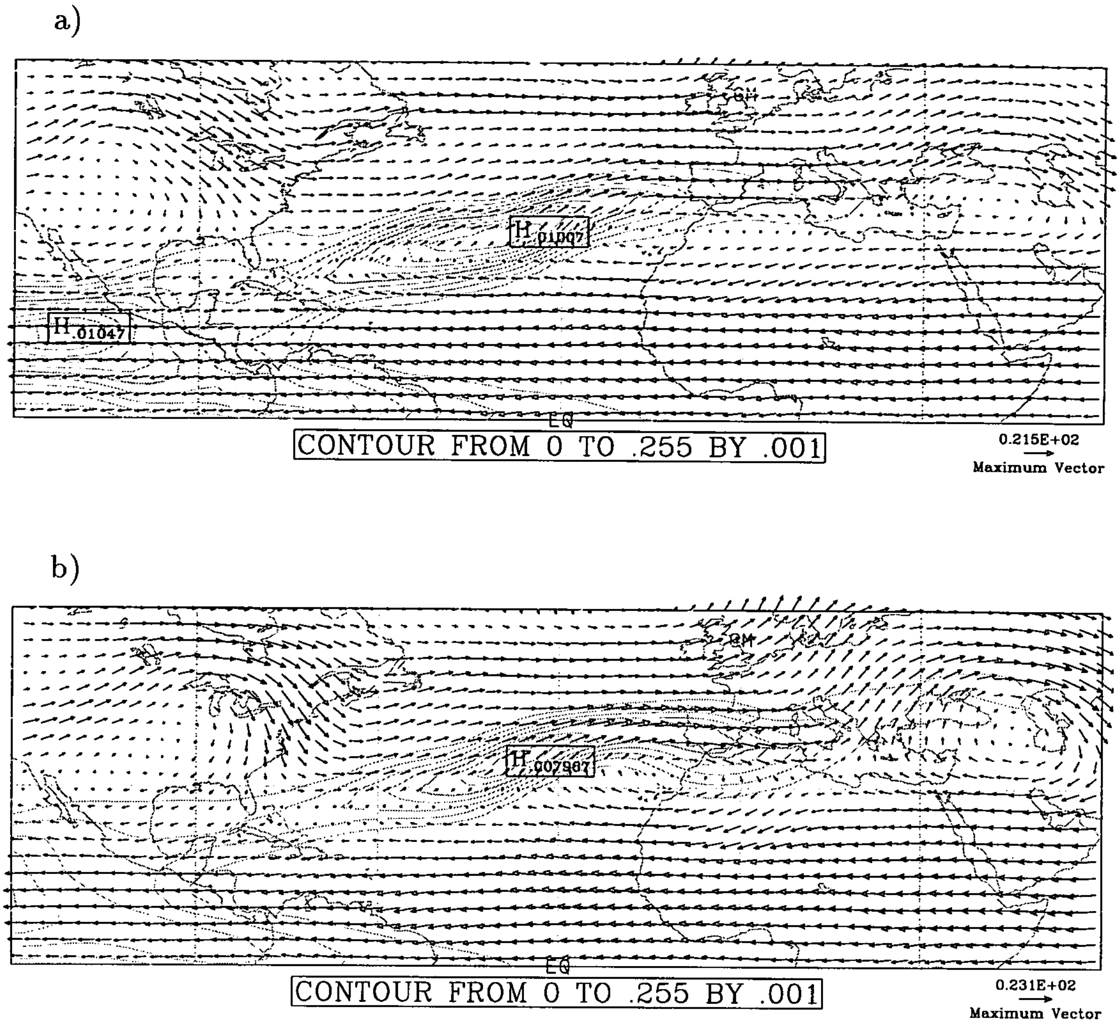

Figure 4.41: Latitude-longitude limited area plot (Eq. to 60°N and 120°W to 60°E) on the isentropic surface θ=450K (approx. 70mb) of tracer (vmr) on days a) 20 and b) 22 of Run A. Wind vectors are superimposed.

large fraction of the main cloud northwards. The southwards flow which occurs further west (approx. 90°W to 110°W) has an effect which is more apparent two days further into the run (Figure 4.40b). The main cloud is kept well in the tropics by the southward flow while the northward flow separates some of the material from the main cloud.

This event is far more significant than the first one and this is because material has been pulled from much deeper in the tropics, where the highest mixing ratios are. The mixing ratios in the northward moving material are only slightly less than those in the main cloud. When the material is pulled far enough north it gets caught in the strong north-eastward flow (see Figure 4.41a). This causes the separated material to stretch into a tongue, most of which reaches the mid-

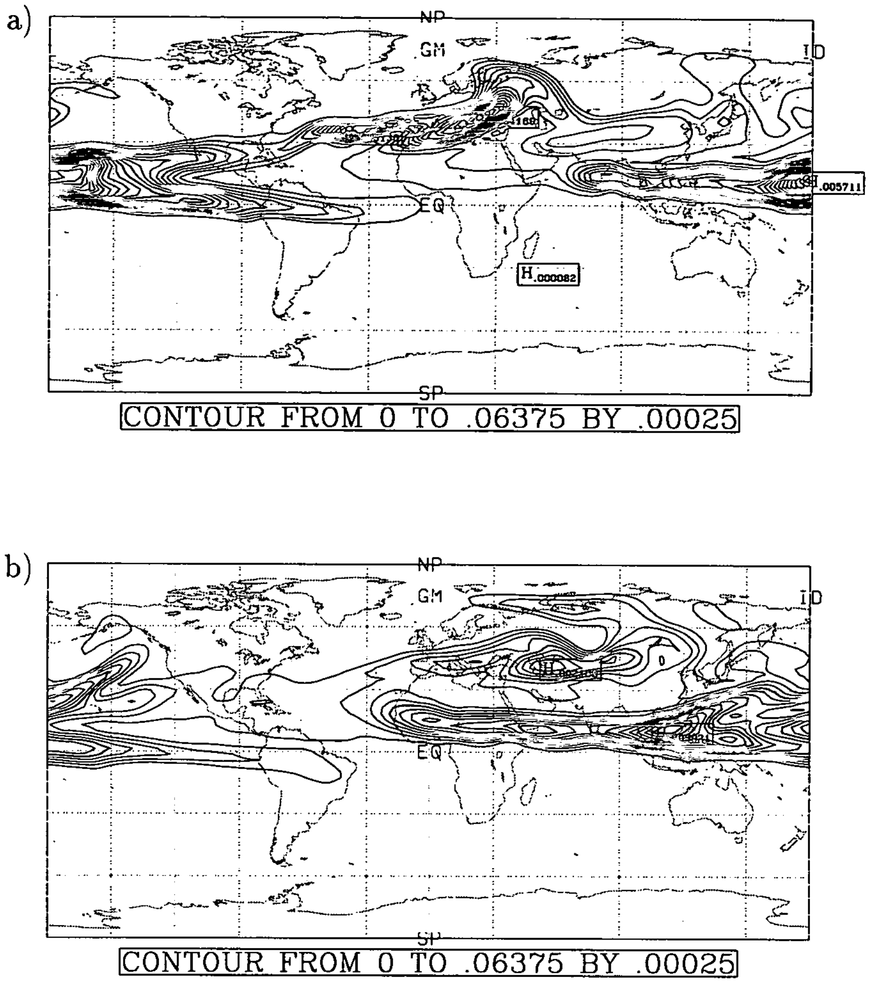

Figure 4.42: Global isentropic map (latitude-longitude) of tracer (vmr) at θ=450K (approx. 70mb) on days a) 25 and b) 30 of Run A.

latitudes. Some of this material becomes entrained in an anticyclone (near 30°N, 0°E) and it is through processes like this that the tropical air becomes well mixed in the mid-latitudes.

To put this event into context with what the rest of the cloud is doing we return to plots covering the entire latitude-longitude range. Figure 4.42 features two such plots, the first, three days later than plot 4.41b (day 25) and the second, day 30. From day 25, we can see that the mid-latitude material has almost entirely separated from the main cloud in the tropics. With the whole tracer field in view you can see just how large a proportion of the main cloud was transported north in just one mixing event.

At this point, on the isentrope θ=450K, the leading edge of the main cloud has more than completed its first circuit of the Earth. 5 days later the leading edge of the cloud has nearly caught up with the trailing edge, meaning that throughout the tropics material can be found at every longitude. The distribution, however, is by no means zonally symmetric. This zonal symmetry is not attained until around day 40 of the model run, a bit later than indicated by satellite observations.

Three more points can be made based on 4.42b. Firstly, a third event is developing around 180°W. A well-defined tongue of material is stretching out into the mid-latitudes in a strict north-east direction. We will not analyse this event, but it serves to indicate that these mixing events occur frequently in the UGCM (in the northern hemisphere).

The second point to be made involves the material cast into the mid-latitudes from the second mixing event. The mid-latitude cloud, having fully separated from the tropical material is drifting east. This cloud remains in mid-latitudes, quite separate from the cloud in the tropics and plot 4.42b shows this very well. A distinct gap remains between the mid-latitude and tropical material, enhanced by steep gradients of tracer either side of the space.

The final point also involves the material expelled from the tropics by the second mixing event. As well as the cloud having travelled east, some of the material has made a further northward movement, reaching the polar latitudes. Figure 4.43 shows how this occurs using a detail of the tracer field with wind vectors superimposed.

At day 25, there is some northward flow veering off from the main north-eastward flow which is how the material gets into the polar latitudes. As you can see from the plot, material carried by the northerly flow would also eventually travel in a westward direction. However, by day 27 the northward flow has ceased to exist. The tracer which has reached the polar latitudes is now stationary while the tongue of cloud in the mid-latitudes continues to be pulled east; pulling away from the polar material.

Meanwhile, the southern edge of the cloud at this height remains reasonably undisturbed, with only a very small proportion of the cloud lying south of the equator. The smooth southern edge of the cloud is similar to that described using observed data (see section 4.2.2), except here it is situated at 5 to 10°S rather than 20°S.

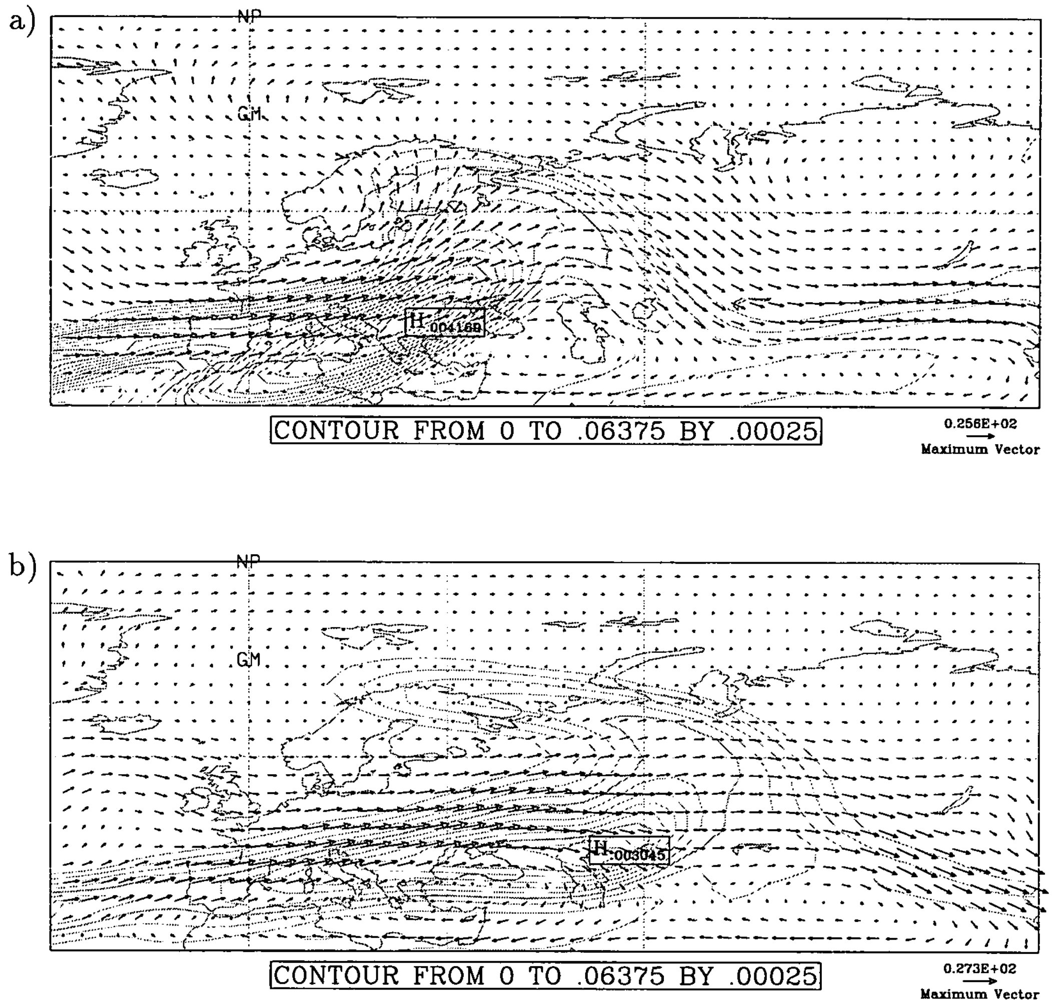

Figure 4.43: Latitude-longitude limited area plot (30°N to 90°N and 30°W to 120°E) on the isentropic surface θ=450K (approx. 70mb) of tracer (vmr) on days a) 25 and b) 30 of Run A. Wind vectors are superimposed.

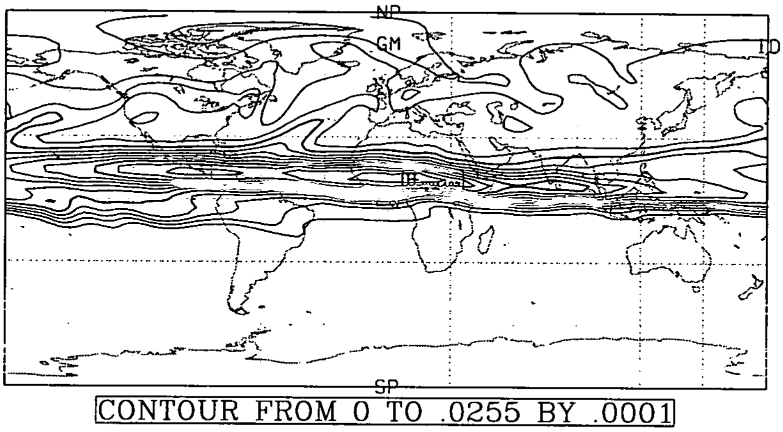

Figure 4.44: Global isentropic map (latitude-longitude) of tracer (vmr) at θ=450K (approx. 70mb) on day 60 of Run A.

Mixing events transporting tropical air into the northern mid-latitudes continue to occur throughout the model run after day 30, and the net effect of this can be seen in the tracer field for day 60 (Figure 4.44). The highest concentrations of material are still in the tropics. As was observed in the real atmosphere, the high latitudinal gradients of tracer found in the low latitudes help to illustrate the efficiency with which the tracer is confined to the tropics. The material which has reached north of the tropics is distributed well around the hemisphere (including polar latitudes), and evidence of filaments of tropical air stretching into the mid-latitudes is still apparent.

4.4.4 Mixing events transporting material southwards

According to *Trepte et al.*, [1993], the reverse of the above picture would be expected above 20km. That is, the aerosol still confined to the tropics but mixing events transporting material south instead of north. As we already know from the zonal plots though, there is not nearly enough material transported south in the first 60 days of Run A. In order to investigate this, the next series of latitude-longitude plots will be for the same model run but on the higher isentrope of θ=650K.

For the first 30 days of the run, at 650K there is no poleward mixing of any significance, north or south (Figure 4.45). As was previously mentioned, the tracer

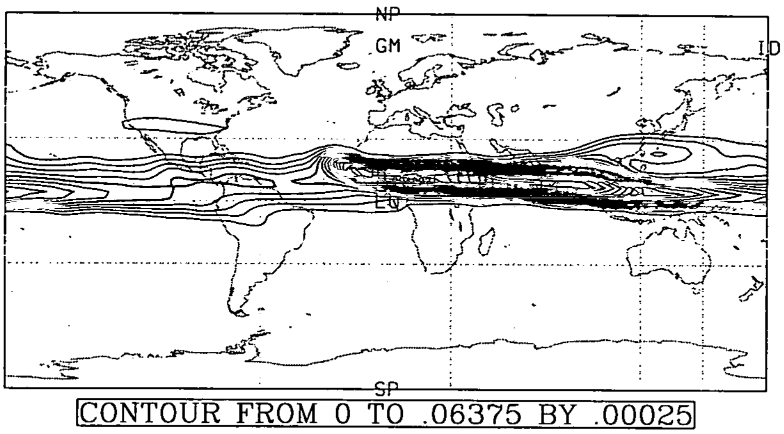

Figure 4.45: Global isentropic map (latitude-longitude) of tracer (vmr) at θ=650K (approx. 20mb) on day 30 of Run A.

encircles the earth at a greater rate at this height and by day 15 there were small amounts of material which had already circled the globe. For this reason, at day 30, although not totally zonal in nature, a well-defined band of material stretches round the Earth. The distribution is centred slightly further south than that at 450K and spans the latitude range 10°S to 20°N.

Day 34 of Run A (Figure 4.46a) presents the first clear evidence of tropical material being transported southwards. Here the material is leaving the main cloud only via a very narrow longitude range, a point strikingly made by the tight tracer gradients either side of the tongue. This tongue has been generated by an anticyclone which has penetrated far enough into the main cloud to pull off some material. The tongue follows the anticyclone round into the low latitudes but the material does not reach the middle latitudes. While this is happening, the anticyclone is moving west (see Figure 4.46b). The tail of the tongue of material reaches as far east as 120°E.

Two days later (Figure 4.47a), the anticyclone has dissipated and with it, the tongue of material, but a very small amount of tracer remains at 120°E. As interesting as this event may be, it is not nearly as significant as the events which are regularly occurring lower down, mixing material into the northern hemisphere. There is very little material transported, and the small amount which was did not reach any further south than 20°S. However, even though the event is weak, it does occur at the right time (half a month after northward transport - see section

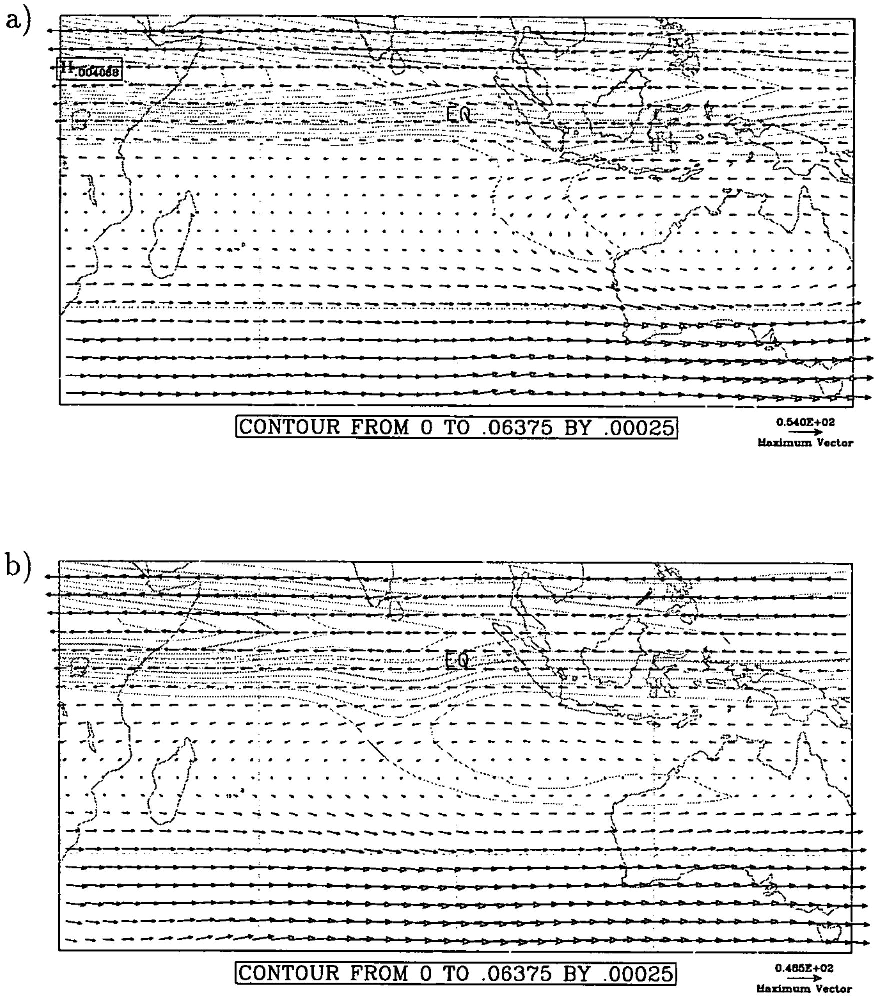

Figure 4.46: Latitude-longitude limited area plot (15°N to 45°S and 30°E to 150°E) on the isentropic surface θ=650K (approx. 20mb) of tracer (vmr) on days a) 34 and b) 36 of Run A. Wind vectors are superimposed.

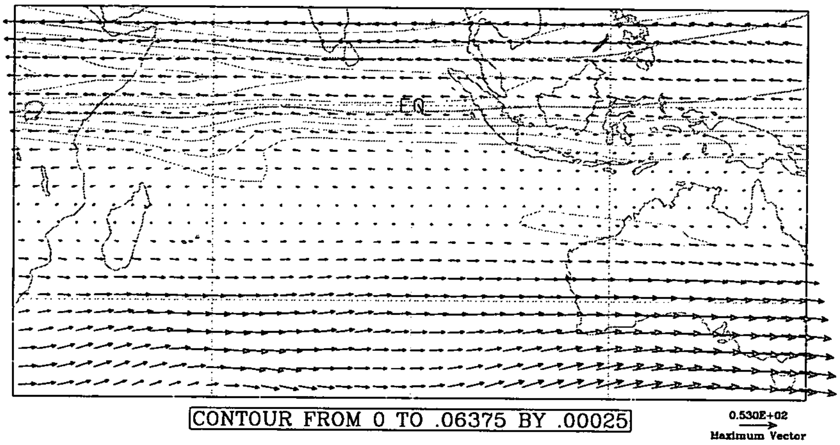

Figure 4.47: Latitude-longitude limited area plot (15°N to 45°S and 30°E to 150°E) on the isentropic surface θ=650K (approx. 20mb) of tracer (vmr) on day 38 of Run A. Wind vectors are superimposed.

4.2.3).

We can compare this event with a similar one in the ECMWF analyses. Figures 4.48, 4.49 and 4.50 present a series of wind maps taken from the ECMWF analyses data set at a height of 30mb, which is the nearest ECMWF model surface to the isentropic surface 650K. The event, in this case, occurs further west than the event just illustrated from Run A, but it occurs at around the same time of year; the plots are two days apart.

The first thing to comment on is the "kink" which occurs in the polar vortex, situated at the bottom of Figure 4.48. The particular event which we showed from Run A was not accompanied by this undulation in the polar vortex. Later (in Chapter 5), we will see examples of polar vortex undulation in the EUGCM which occur in conjunction with events detraining material from the tropics. Other aspects of the events are quite similar though. A strong jet exists in the tropics and the anticyclonic feature appears quite elongated in both Run A and the analyses. The lifespans of the events is also in agreement; just under a week. As the event in the analyses dissipates, the polar vortex becomes less undular (Figure 4.49) and is basically zonal in nature once the event has subsided (Figure 4.50). This occurrence of planetary wave mixing of this kind is believed to be facilitating the transport of aerosol from the tropics into the mid-latitudes (*Trepte et al., [1993]*).

We have seen from the ECMWF analyses that the model is able to simu-

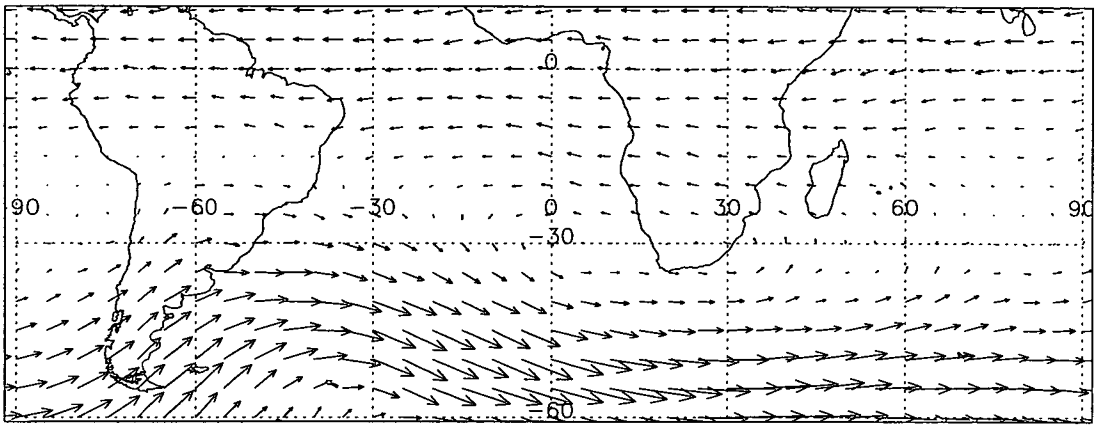

Figure 4.48: Latitude-longitude limited area plot (60°S to 10°N and 90°W to 90°E) on the pressure surface 30mb of wind vectors on July 14th, 1991, taken from ECMWF analyses

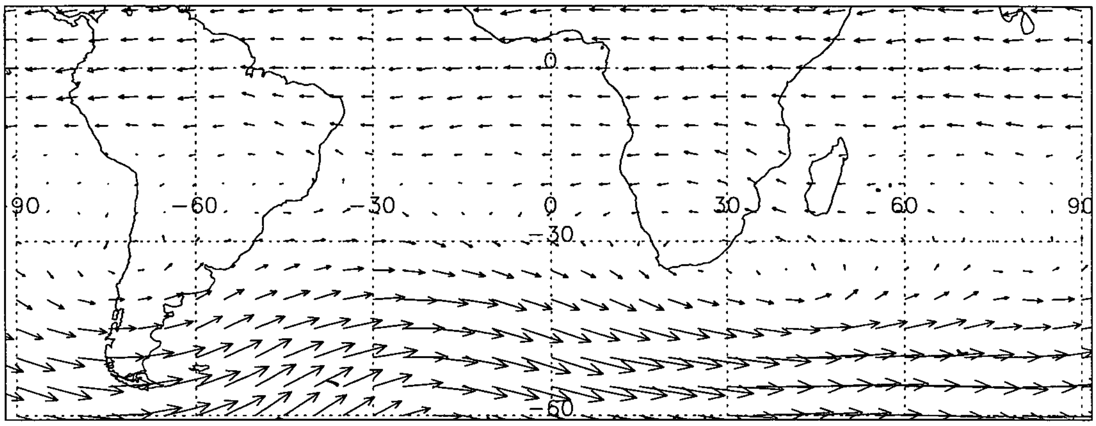

Figure 4.49: Latitude-longitude limited area plot (60°S to 10°N and 90°W to 90°E) on the pressure surface 30mb of wind vectors on July 16th, 1991, taken from ECMWF analyses

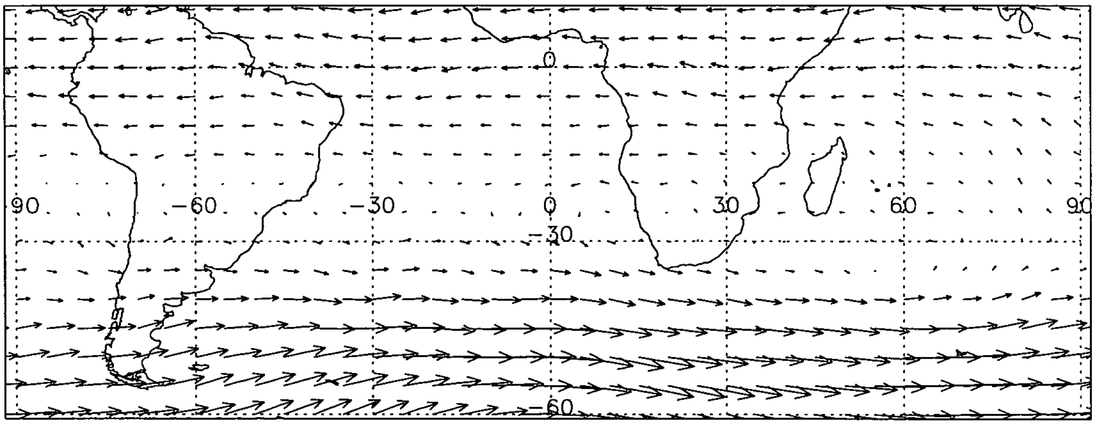

Figure 4.50: Latitude-longitude limited area plot (60°S to 10°N and 90°W to 90°E) on the pressure surface 30mb of wind vectors on July 18th, 1991, taken from ECMWF analyses

late many of the necessary dynamical phenomena which enable mixing from the tropics, in the same way as the real atmosphere.

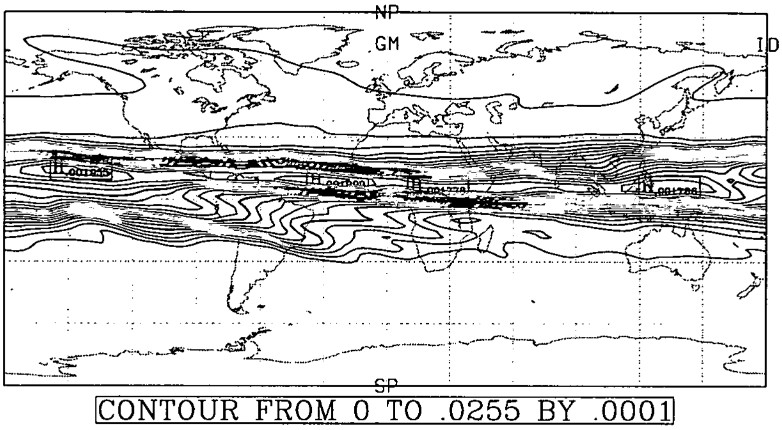

Figure 4.51: Global isentropic map (latitude-longitude) of tracer (vmr) at θ=650K (approx. 20mb) on day 60 of Run A.

By the 60th day of Run A the tracer at 650K is still confined to the tropics. Material has gradually progressed south of the equator but no significant tongues of material developed from the tropics. The plot for day 60 (Figure 4.51) shows an example of the kind of mixing which has been transporting material southwards. Over South America a ridge of material stretches in a south-eastward direction, from the equator to 30°S. This distribution of material is caused by two anticyclones on either side of the ridge in the southern tropics. Such events occur fairly constantly after the first southwards mixing event.

A large westerly jet exists in the southern mid-latitudes which proves impenetrable for any southward moving material, thus tracer remains in the tropics in the southern hemisphere.

To illustrate best the height dependency of poleward spread, Figure 4.52 shows two time series of the zonal averages of the Pinatubo-like tracer. The first is for the isentrope θ=450K, the second for θ=800K. These plots summarise well how the rate and direction of the poleward spread differs depending on height. The 450K plot shows clearly the large mixing event described earlier on in this section. Despite material mixing into the mid-latitudes the boundary between the tropics and mid-latitudes is well-defined by the higher tracer gradients. Confinement to the tropics is clear in both plots as a sharp gradient in the tracer field. The

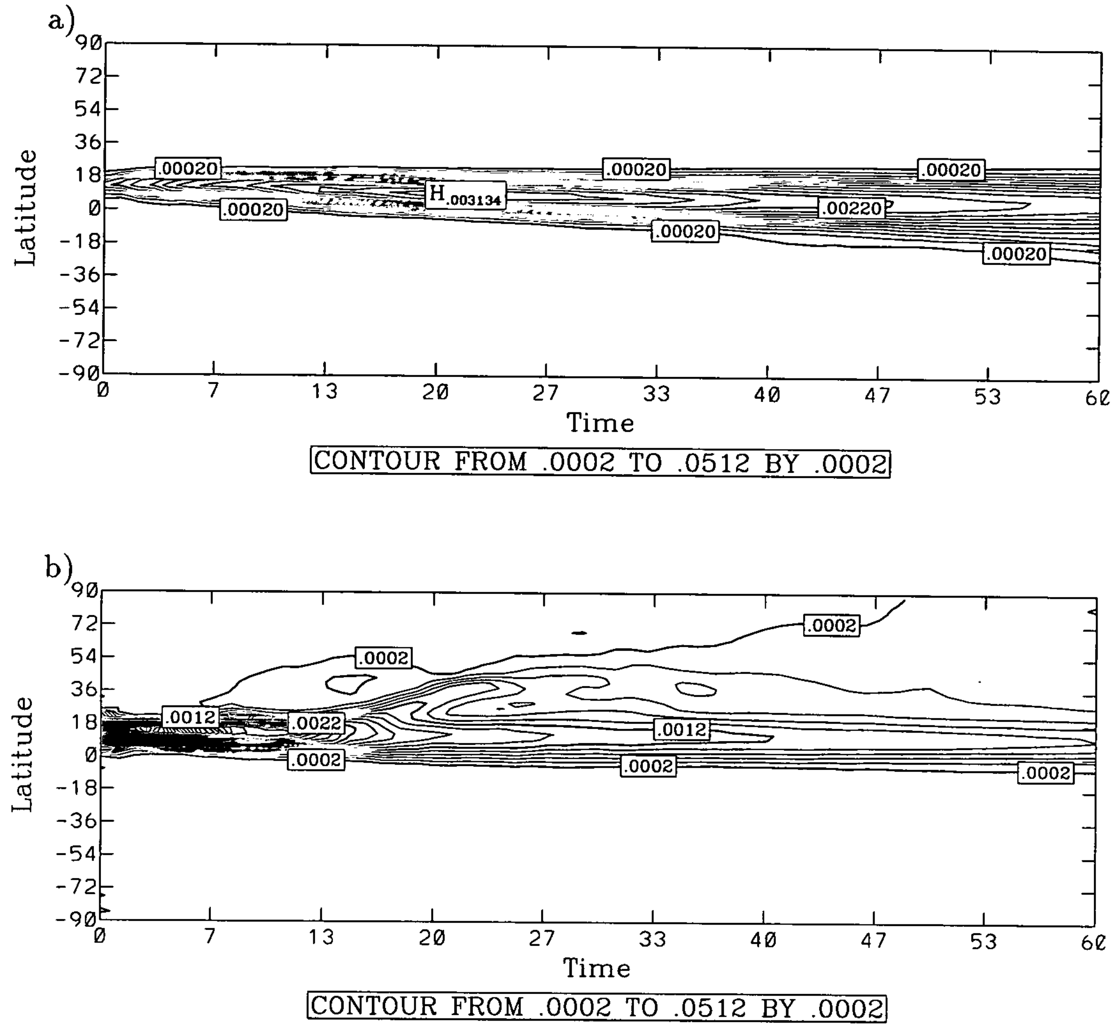

Figure 4.52: Time series plots of zonally averaged tracer (vmr) from day 0 to 60 at two different heights; a) θ=800K (approx. 10mb) and b) θ=450K (approx. 70mb)

tropical, stratospheric reservoir is mostly confined to the northern tropics at 450K. The 800K plot (same contour interval), which is virtually the top of the model, also shows good tropical confinement. The poleward movement at this height is a much more gradual process and does not penetrate so deeply into the mid-latitudes.

4.4.5 The limitation of Run A

We have already mentioned that Run A eventually produces a very unrealistic simulation. The following section looks at why the Run A fails to maintain the tropical reservoir of volcanic material.

Figure 4.53 shows a time series of zonally averaged tracer at a height of 10mb,

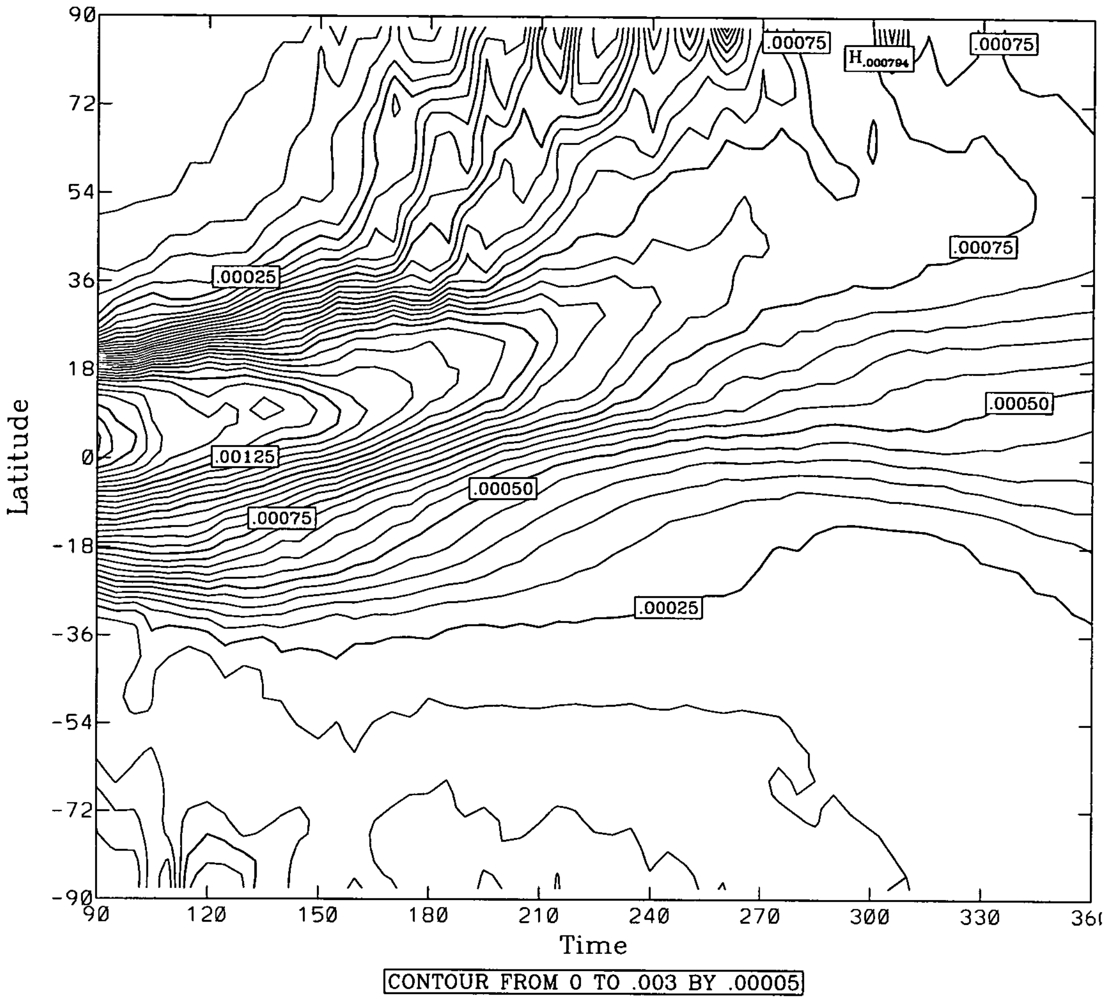

Figure 4.53: Time series of the zonally averaged tracer (vmr) from Run A at 10mb. The time series spans from day 90 to 360 of the model run (mid-September until June).

which is the top level of the model used for Run A. You can see clearly from this figure, the polewards progression of tracer after day 90 of the model run. After day 150 (around mid-November) the area of largest concentrations of aerosol begins a northwards movement. This movement persists throughout the northern winter at a fairly constant rate. To understand why this happens, we need to consider the meridional circulation in the stratosphere and how the 19 level model copes with it.

We can, at this point, refer back to the figure of meridional circulation presented in Figure 2.2. The diagram illustrates what is thought to be a typical meridional circulation for January and from this we can see the kind of circulation the model is trying to represent during the boreal winter. The model only

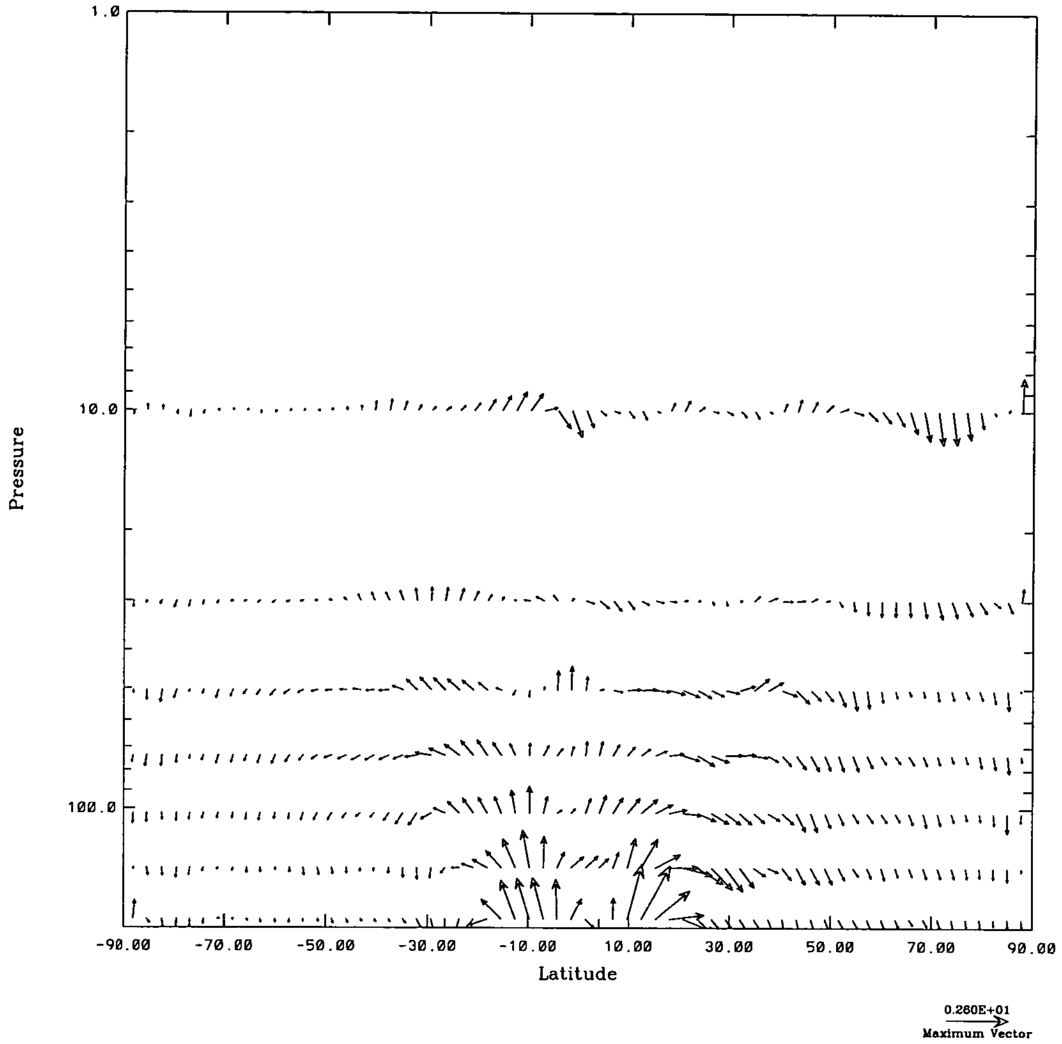

Figure 4.54: The transformed Eulerian mean of meridional velocity vectors time-averaged from mid-November to mid-December taken from the UGCM.

goes up to 10mb, which is approximately 30km. At this height in the figure, over the tropics many of the mass transport streamlines are directed upwards.

We now look at a similar plot for the UGCM. The vector plot in Figure 4.54 shows a typical residual meridional circulation in the 19 level model. Time-averaging the transformed Eulerian mean of the velocities provides us with an approximation to the mean advective transport of trace substances. The data have been time-averaged over 30 days, from mid-November to mid-December; the first month of the unrealistic northwards transport of the tracer at the top of the model.

You can see a few similar features in this plot as the mean circulation (Fig 2.2); upwards motion in the tropics and downwards motion over the poles with

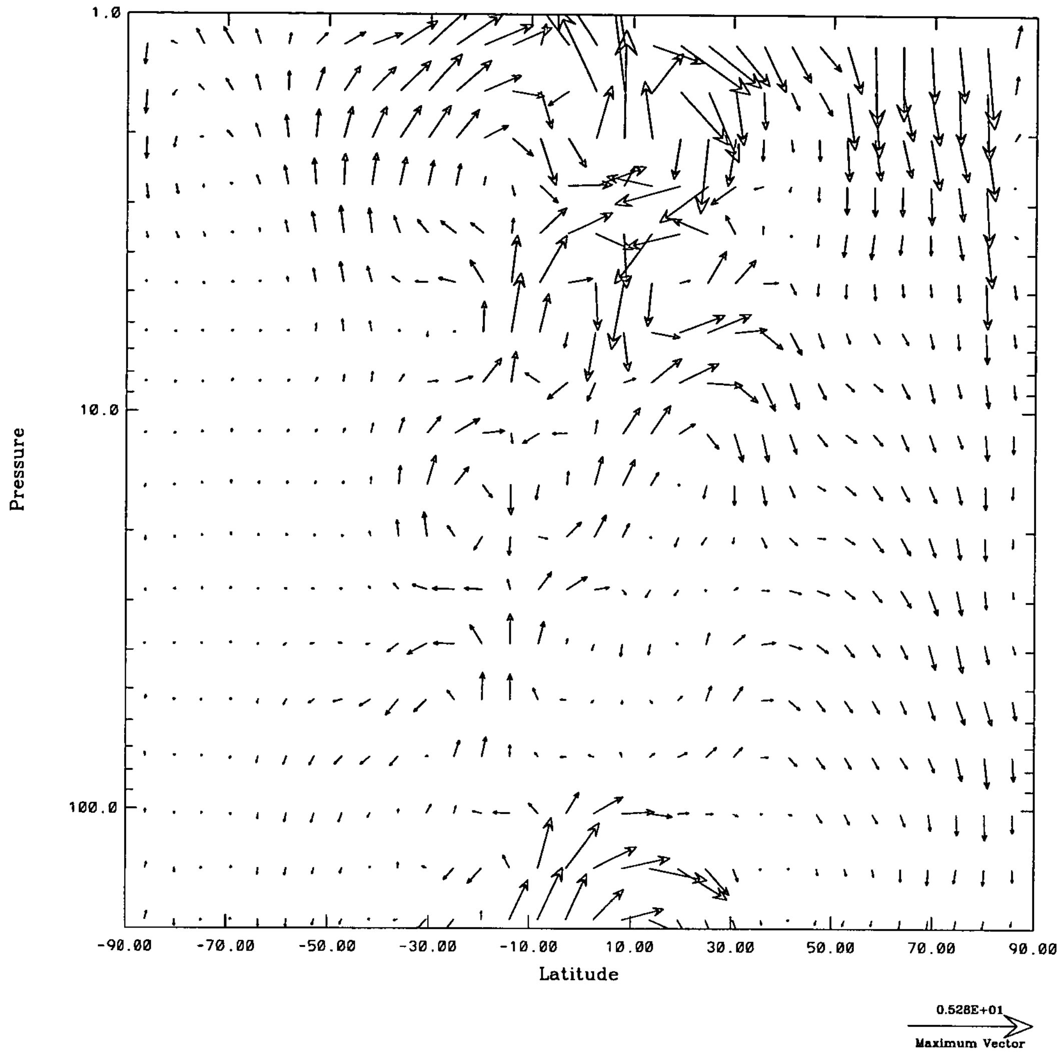

Figure 4.55: The transformed Eulerian mean of meridional velocity vectors time-averaged from mid-November to mid-December taken from the EUGCM.

poleward motion from the tropics in each hemisphere. At the top of the model, while there is some vertical variation, the vectors from the southern sub-tropics to the northern polar latitudes are all pointing northwards. The tracer is unable pass through the top of the model and so gets trapped at the top. The northwards movement forces the material along the lid of the model toward the north pole. We go on to quantify the motion at the top of the model to see if this statement can be confirmed, but first we turn to the EUGCM.

Figure 4.55 shows the equivalent circulation plot for the EUGCM, the model we use for Run B. Some similar features can be spotted between the circulations of the two models. Such features include the upwards motion over the tropospheric tropics and downwards motion over the northern polar regions. The circulation

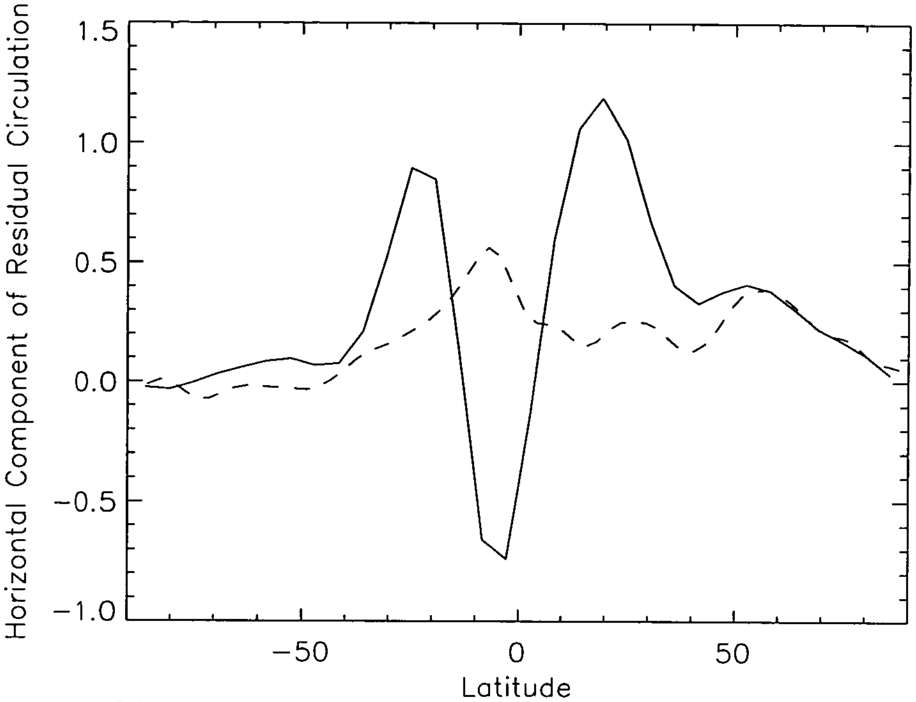

Figure 4.56: The transformed Eulerian mean of the horizontal component of meridional winds (ms^{-1}), at 10mb, time-averaged from mid-November to mid-December. The dashed line is the UGCM (Run A) and the solid line is the EUGCM (Run B).

over the tropics in the stratosphere seems less structured in the EUGCM than it did in the UGCM. There is some evidence of quite strong downwards motion over the tropics which we could. These downwards velocities could be construed as inertial instabilities occurring in the model (see *Harwood and Pyle*, [1975]) which are not necessarily unrealistic. To test this hypothesis however, is beyond the scope of this work.

Above 10mb there is clear upwards motion of the southern mid-latitudes which, as it reaches 1mb, becomes northwards. This branch of circulation continues over the tropics until and then starts descending over the winter polar latitudes. This arch of motion is in very good agreement with the circulation seen in Figure 2.2, although the area underneath the arch seems less uniform. This upper circulation, driven by wave forcing, cannot be represented by the UGCM due to it's low top level.

Figure 4.56 allows us to compare the horizontal component of the mean meridional winds at a height of 10mb in the two models more quantitative. You can see a rather large difference in the tropics of the two models. If we focus on Run A first, the meridional velocity where the largest concentrations of tracer were situated (tropics at the top of the model) ranges between 0.5ms^{-1} and 0.25ms^{-1} or between approximately 11 degrees latitude per month and 5.5 degrees latitude per month northwards. These velocities remain about the same (sometimes slightly higher) throughout the months that the centre of the tracer cloud progresses northwards. Referring back to Figure 4.53 we see that these figures are consistent with the general rate of polewards movement made by the largest tracer concentrations at the top of the model which is about 8 degrees latitude per month.

In the EUGCM at this time however, there is a strong southwards motion which is met by a strong northwards motion in the southern sub-tropics. The motion in the northern sub-tropics is stronger than that seen in the UGCM. However, from Figure 4.55 we can see that the motion here is also upwards. Any material being advected here would not get trapped as it did in the UGCM.

We have seen here that the stratospheric, meridional circulation, caused by eddy forcing, cannot properly be resolved by the model because the top level of the UGCM is only 10mb. As a result the Pinatubo simulation becomes very unrealistic. For a more realistic simulation we need to be able to include the rest of the stratosphere and so we move to the EUGCM for Run B.

4.4.6 Summary of Run A

Before studying Run B, we first give a summary of Run A. To review Run A we consider again the points listed in section 4.2.6.

The UGCM did demonstrate very good tropical confinement in the first 60 days of the run, although during this time, not much material enters into the southern hemisphere compared to the real atmosphere. The tropical stratospheric reservoir was bounded between 10°S and 30°N in the model, but the reservoir in the real atmosphere was between 20°S and 30°N one month after the eruption. Any material being mixed from the tropics agrees with the concept of two different mixing regimes, including the height dependence of the direction of mixing. The amount of tracer getting into the southern hemisphere is not as much as was seen in the real atmosphere. This seems to be related to material not getting into the southern tropics rather than a lack of planetary wave breaking in mid-latitudes. The last three points on the list cannot be commented upon due to useful fields only being available for the first two months of the model run.

Run A has been successful in simulating a few of the main features of the Pinatubo cloud, but height restrictions proved to be too limiting for a complete simulation. As the top of the EUGCM is much higher than the top level of the UGCM, and the vertical resolution is slightly greater where the tracer has been inserted, it is hoped that all the key features raised in section 4.2.6 can be assessed for Run B.

4.5 Analysis of Run B

Now we will examine Run B in the 47 level EUGCM. We begin as we did with Run A; the rate at which the cloud circles the globe.

4.5.1 Rate at which cloud circles the globe

From the latitude-slice at 12.5°N (Figure 4.57) we can see that there is a clear relationship between height and the rate at which cloud travels around the globe. The relationship is not as exaggerated as that observed in Run A (Figure 4.30). The very fast material at 10mb in Run A can be considered to be somewhat unrealistic as it is at the top of the model. The rate at which the cloud circles the Earth is also dependent on latitude, as we would expect after looking at Run A. This relationship is not illustrated here, but can be seen later in Figure 4.58a.

After 20 days the leading edge of the tracer distribution has completed one circuit of the Earth. The highest tracer mixing ratios are not far behind. This agrees well with the real atmosphere so the representation of the zonal flow in the tropics is satisfactory, at least in these initial stages of the experiment.

4.5.2 Spread of tracer with respect to latitude

Figure 4.58 shows an extremely interesting sequence of plots from day 20 to 35. They show strong northward movement from the tropics into the mid-latitudes followed by a cessation of such a movement and then further transport of material from the mid- to polar latitudes. The rate at which material reaches polar latitudes is quite rapid compared to the real atmosphere. The three main latitudinal divisions (tropics, mid-latitude and polar latitudes) of the northern hemisphere

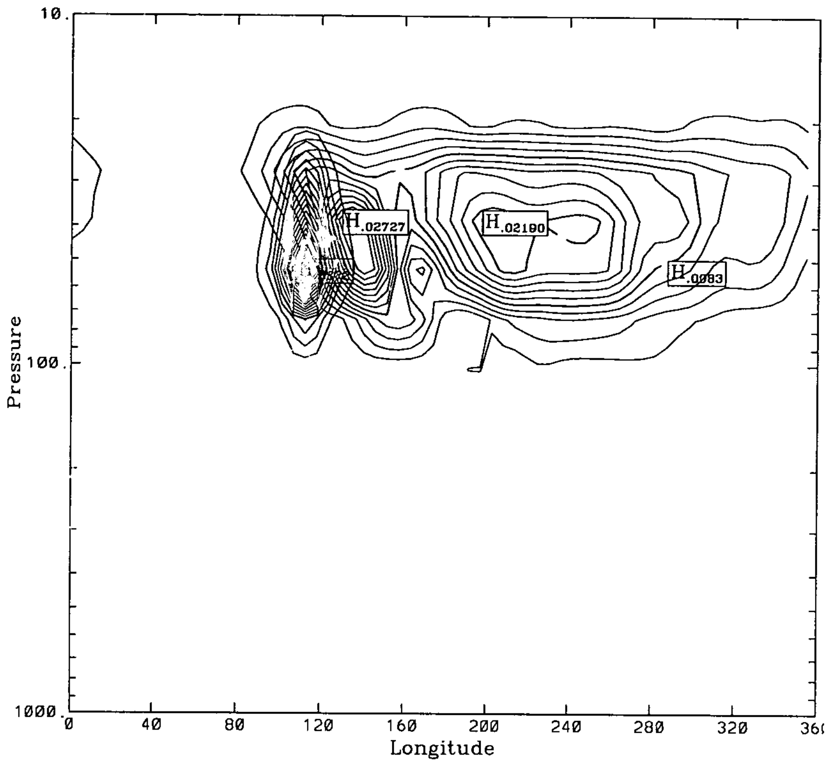

Figure 4.57: Latitude slice (longitude vs. pressure) at 12.5°N of tracer (vmr) on day 20 of Run B with the initial tracer distribution superimposed. The narrow band of contours centred above 115°E is the initial distribution.

can be identified by steep horizontal gradients in the tracer field on days 25, 30 or 35. Note that the height at which material is escaping (18km) northwards from the tropics, is the same as that which was observed (see section 4.2.3).

From day 35 to around day 60, there are no more large displacements of material between latitude regions (certainly not discernible on the zonal mean fields), but in the meantime, the material throughout the mid-latitude and polar regions becomes well mixed with respect to latitude.

So far, there is no movement of material to the south at all, the main tropical cloud being bounded between 10°S and 30°N.

Northward movement from the tropics begins again from around day 60, but this time it occurs over a larger altitude range (from around 17km to 26km) with the largest amounts of material escaping the tropics at 21km. At day 90, a significant proportion of material has reached the polar latitudes, but by day 95 the levels of material above the pole have dropped to what they were shortly before day 90 (Figure 4.59). The cause of this will be looked for when analysing

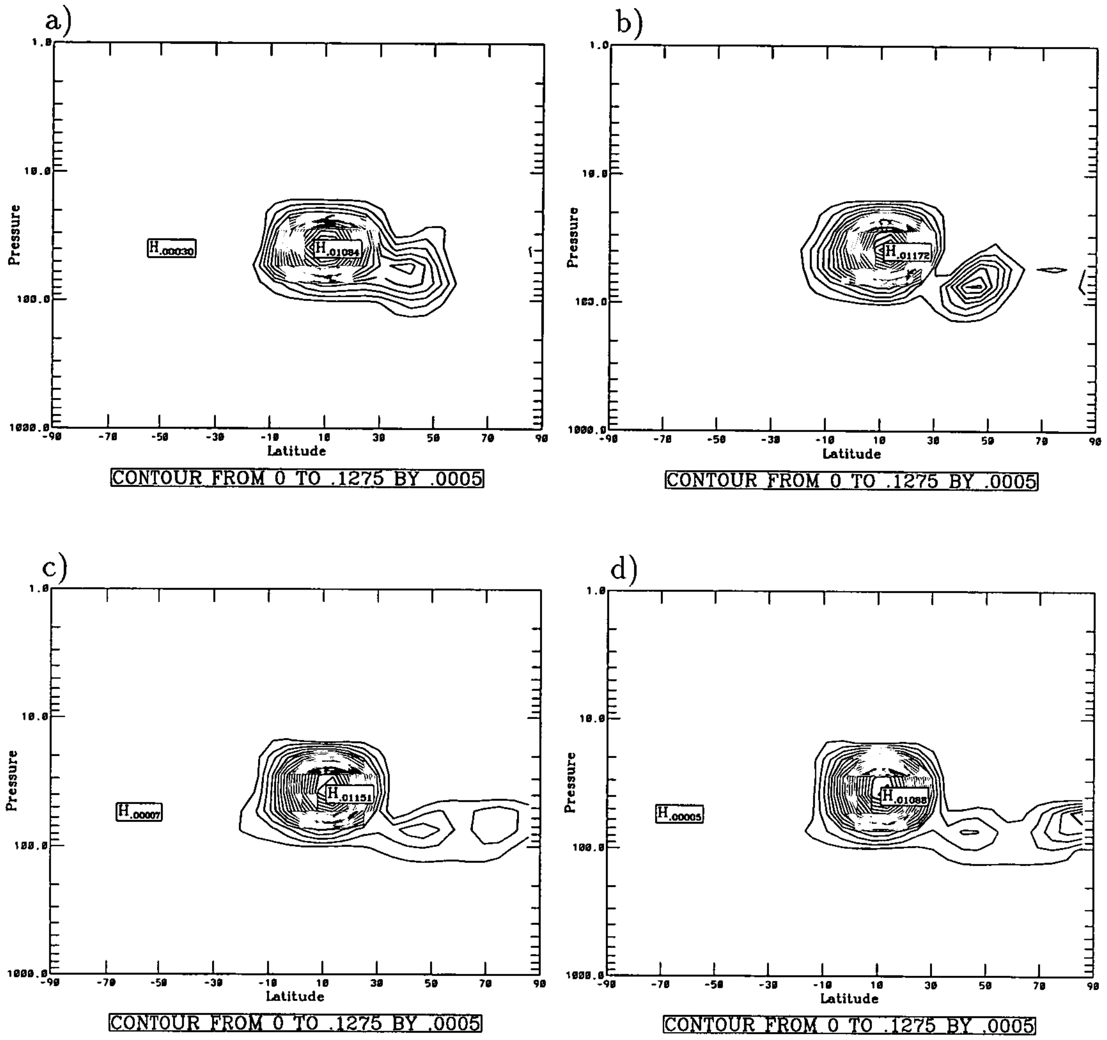

Figure 4.58: Zonally averaged tracer (vmr) from Run B at a) 20, b) 25, c) 30 and d) 35 days. The contour interval is 0.0005 for all four plots.

the latitude-longitude plots later on.

Beyond day 100 of Run B, the northern edge of the main tropical reservoir becomes less defined (see the plot for day 130 as an example - Figure 4.60). While the southern edge of the tropics continues to be marked by a tight latitudinal tracer gradient, the contour gradient over the northern low latitudes becomes shallower. This scenario will bear further investigation, using lat-long plots to see if this spreading of material in the low latitudes is due to a gradual movement by the cloud edge or a series of mixing events blurring the boundary of the cloud. This occurs at all altitudes at which the cloud exists in the tropics, not just where the lower mixing regime was.

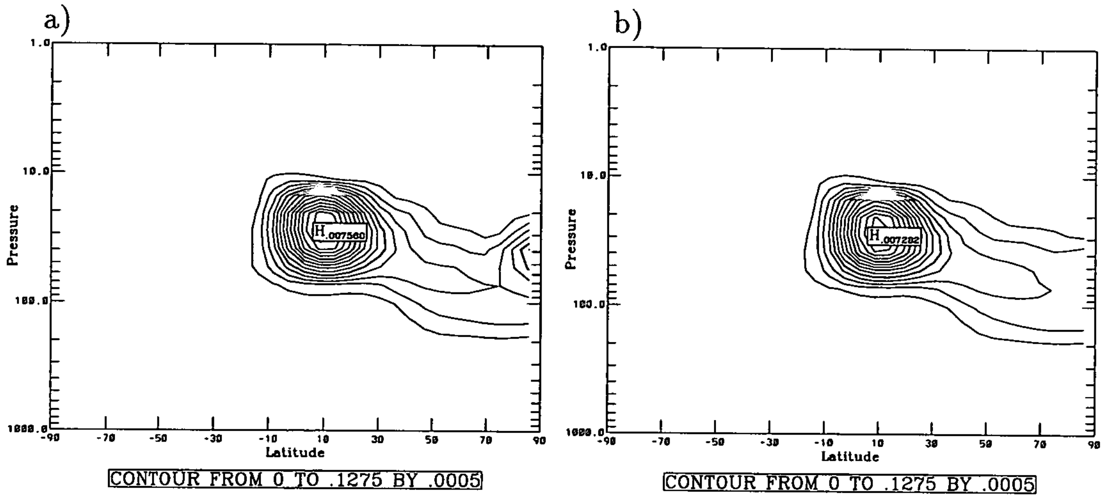

Figure 4.59: Zonally averaged tracer (vmr) from Run B at a) 90 and b) 95 days. Note the contour remains the same as in the previous figure.

In the zonal plot for day 180 (Figure 4.61a) there seems to be a latitudinal gradient present in the northern polar region. This could be construed as evidence for the polar vortex impeding the northward progress of material but it is difficult to say as the nature of the northern polar vortex is not very zonal and so a clear boundary might not be seen in zonal fields. The issue of the impermeability of the vortex edge in the UGAMP GCM is investigated in Chapter 5.

No matter what the conclusion regarding the polar vortex preventing poleward movement of tracer is, after day 180 the average mixing ratios of tracer to be found in the mid-latitudes and polar latitudes are not much less than those found in the tropics. This is certainly not the case in the real atmosphere (compare Figure 4.61b with Figures 4.6b and 4.6c, for example). Clearly, somehow, too much material is getting into the northern hemisphere. These highest levels of tracer in the northern hemisphere and the tropics very gradually drop as a general dispersion occurs throughout the model. In the northern hemisphere there are no other significant developments before the end of the run (with respect to latitude).

During this same period the southern-most part of the tropical reservoir edges from 10°S to 30°S which is where it is at day 340 of the run. After this, a sizable portion of material is transported into the southern mid-latitudes. The motion system that produced this transport could have happened the previous year but the tracer was not in it; the tracer was too far north. This will be an important area of investigation in Chapter 5. Interestingly though, the mixing has occurred

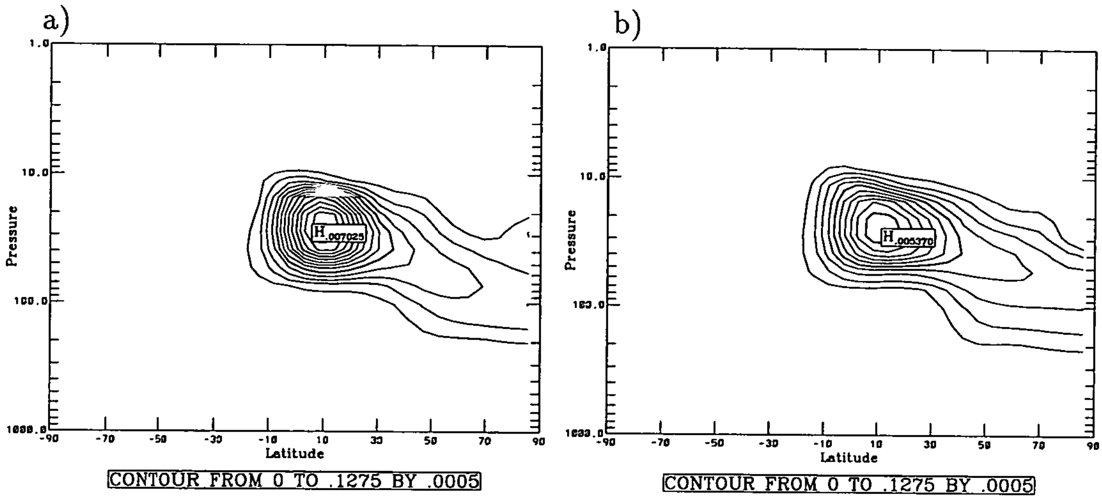

Figure 4.60: Zonally averaged tracer (vmr) from Run B at a) 100 and b) 130 days. Note the contour remains the same as in the previous figure.

at a higher altitude than the northward mixing before and this is in agreement with what was observed in the real atmosphere even though the timing is not.

The tropics during the second half of Run B are not well-defined with respect to the tracer field. This is partly due to the choice of contour interval in these plots but mainly due to the excessive transport of material northwards, across the sub-tropics.

4.5.3 Spread of tracer with respect to altitude

So far, the focus of the comparison has been the poleward spread of the tracer, but also important is the vertical distribution of the tracer field. This could not be considered much in Run A due to the height restriction of the UGCM.

At day 60 of Run B, the tracer above the tropics is between 100 and 10 mb. This corresponds to a height range of about 17 to 29km (see also Figure 4.63a) which is very similar to the heights at which the volcanic material was found in the real atmosphere in the first few months after the eruption (see section 4.2.4).

After day 60, all of the cloud above the tropics gradually moves upward. This upwards movement is not at a uniform rate though. Ascent depends on position of material in the tropics, and season.

For the bottom edge of the tracer cloud over the tropics, the rate of ascent is fairly constant. Between days 60 to 240, the rate is about .025 km/day after which ascent drops off. Also, at this time, the bottom edge of the cloud becomes tilted,

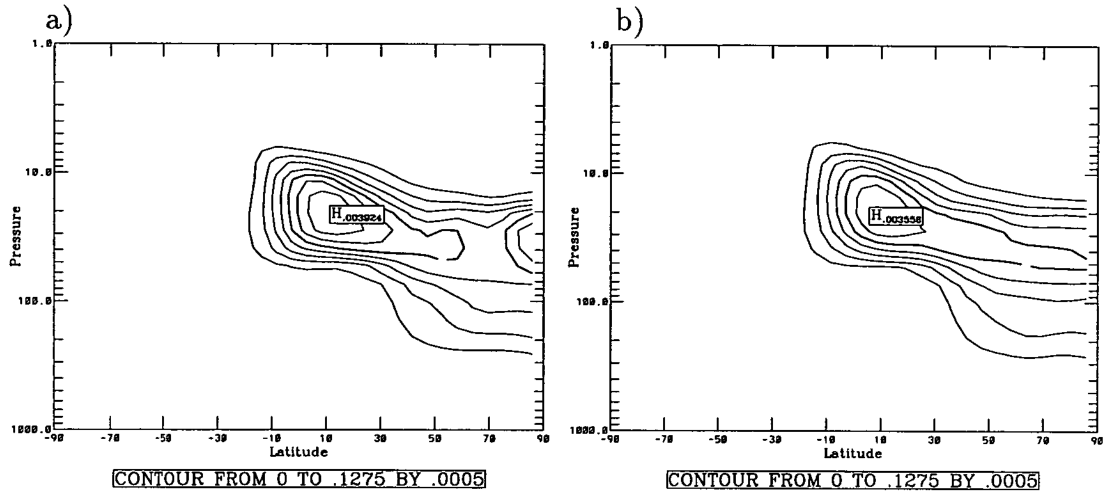

Figure 4.61: Zonally averaged tracer (vmr) from Run B at a) 180 and b) 200 days. Note the contour remains the same as in the previous figure.

material being found further down the further north you look (Figure 4.63d). This blurs the distinction between the tropics and mid-latitudes which could previously be identified by a sharp latitudinal gradient in the tracer fields (see Figure 4.58 for an example of this).

For the southern part of the tropical reservoir, the rate of ascent (using the top edge of the cloud as a measure) is fairly constant between days 60 and 260. The rate is .035 km/day. After day 260, the top edge of the cloud in the southern tropics fluctuates either side of 36km until the end of the run.

The northern section of the tropical reservoir behaves quite differently from the other parts of the cloud. The rate of ascent is not constant and sometimes the top of the cloud drops a little in altitude. The overall motion, up until day 240, is slowly upwards at an average rate of .012 km/day. The slower rate of ascent on the northern side causes the top edge of the tropical reservoir to be sloped (see Figure 4.63b). From day 240 onwards, the rate of ascent increases, and hasn't stopped increasing by the end of the run. The average rate of ascent during this period is .108 km/day and the rate of ascent on day 360 is .2 km/day.

On day 300 the opposite sides of the upper edge of the tropical cloud are at the same altitude again (as they were at day 60). At this point, a slight dip to the extent of half a kilometer can be seen in the top edge of the tropical cloud (see Figure 4.63c). This could tentatively be compared with the double peak seen in the observations presented by *Lambert et al.* [1993] (see Figure 4.6).

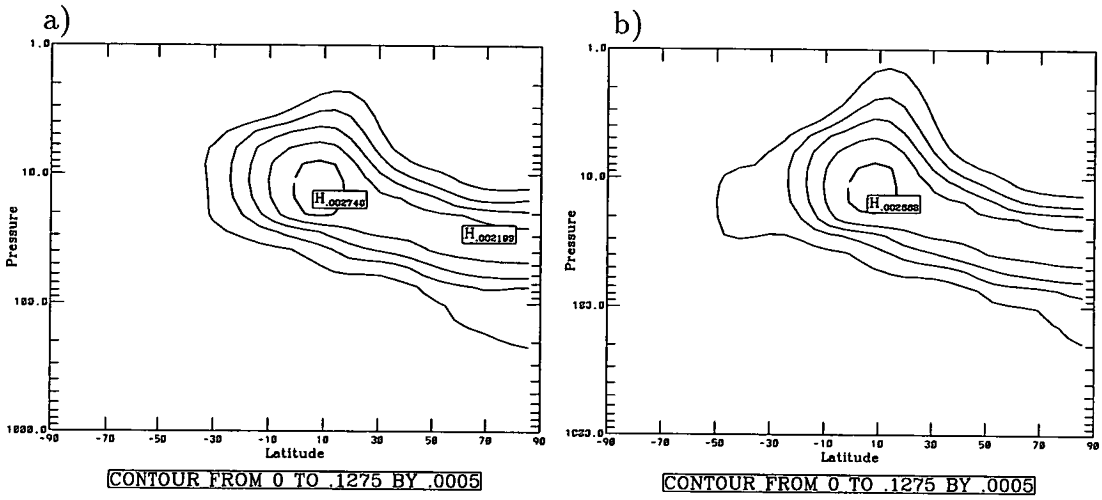

Figure 4.62: Zonally averaged tracer (vmr) from Run B at a) 340 and b) 360 days. Note the contour remains the same as in the previous figure.

By day 360 the top of the cloud has reached 44 km in altitude which is higher than any of the measurements placed the cloud.

That was the top edge of the cloud, but the bottom edge also provides some interesting information. From the plots it can be seen that the lower edge of the tracer distribution relaxes into the shape of the tropopause. After day 90 the lowest edge of the cloud very gradually descends over the high northern latitudes. It is particularly noticeable that during the boreal winter months, the tropics are very clearly bounded from the middle and high latitudes below 100mb.

Significant amounts of tracer do get low over polar regions but they don't appear to be below the tropopause. In the real atmosphere, when the aerosol cloud enters the troposphere it is rapidly washed out by rain (a time scale of the order of days). The model does not account for this but if tracer did get into the troposphere it would be mixed very quickly and would probably become quickly diluted.

4.5.4 Mixing events as seen on isentropic surfaces

In the zonal analysis, the period between days 20 and 35 was particularly noted for a very significant northward movement of material from the tropics. Figures 4.64 and 4.65 show tracer fields for the same time period on the isentropic surface, θ=450K. We can see from the plot of day 20 why the mixing event was so noticeable on the zonal fields. The event is pulling material from the area of the

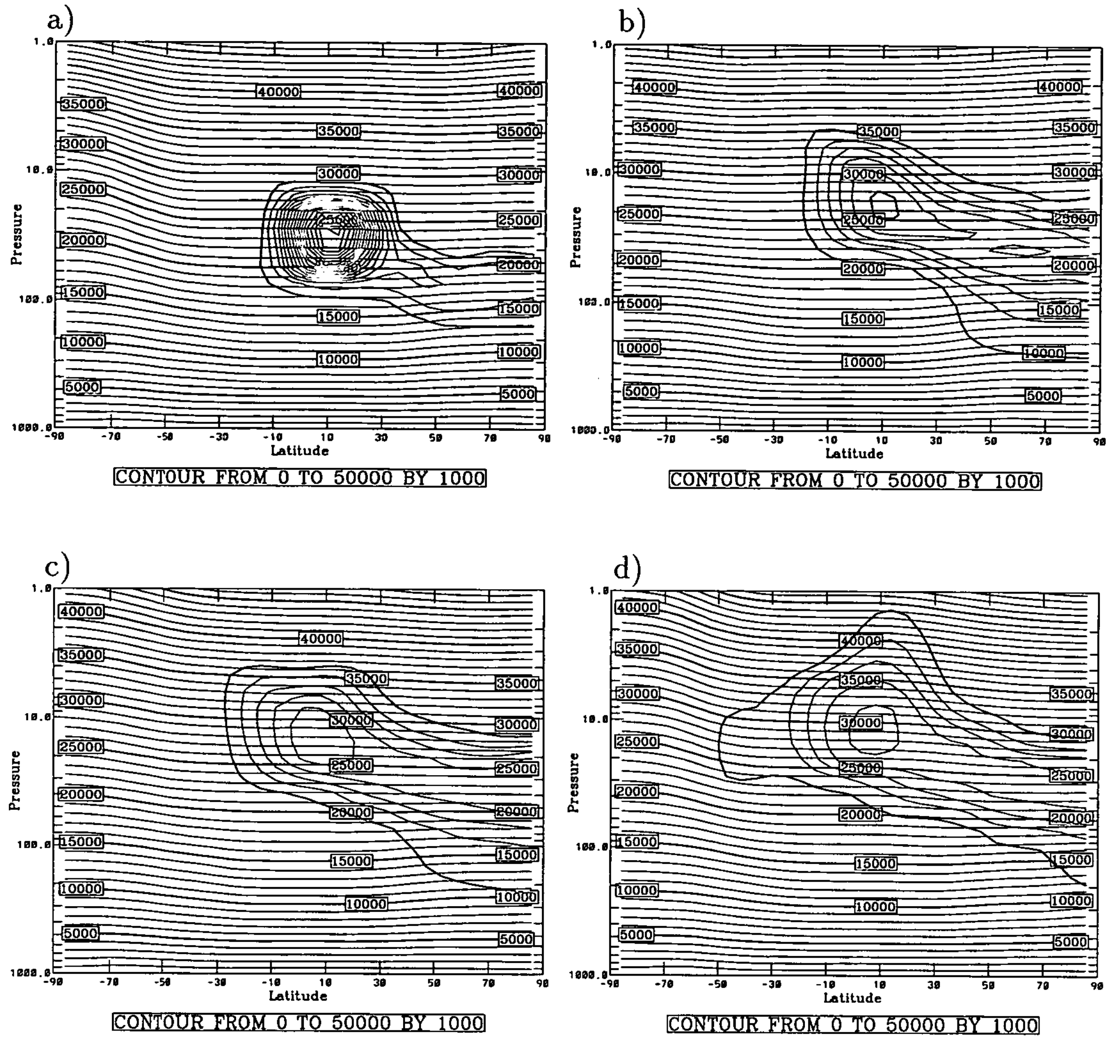

Figure 4.63: Zonally averaged tracer (vmr) from Run B at a) 60, b) 240, c) 300 and d) 360 days, with respective geopotential height (in meters) fields superimposed

tropics with the highest amounts of tracer.

The presence of this event is a reassuring sign that this model can represent mixing events which were also evident in the higher resolution version of the model. From the plots following day 20 we can also see that the mixing appears to be irreversible, the tropical material circling the Earth in the middle and polar latitudes.

The last of this sequence of plots shows another tongue transporting material north, also stemming from the highest values of tracer, promising another fairly large movement of material northwards. Perhaps more surprising though, is the tongue of material stretching from the tropics to the southern mid-latitudes. The

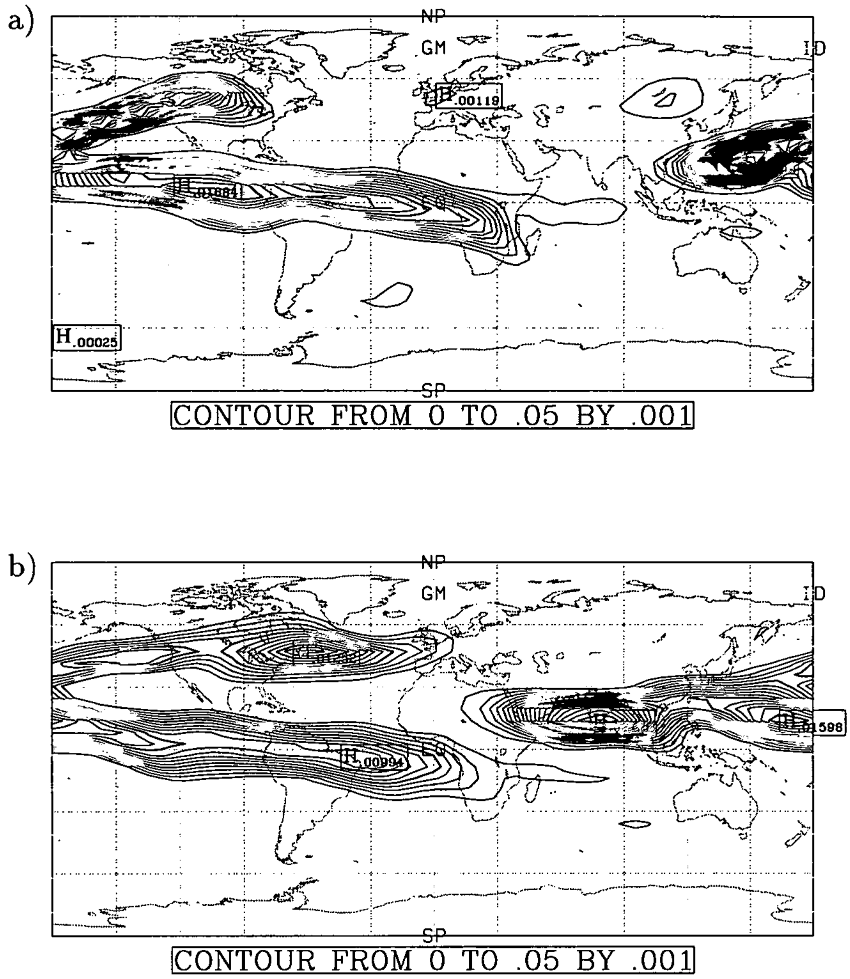

Figure 4.64: Global isentropic map (latitude-longitude) of tracer (vmr) at θ=450K (approx. 70mb) on days a) 20 and b) 25 of Run B.

event itself was not large enough to show up in the zonal plots of tracer and only a negligible amount of material remains in the mid-latitudes. Most of it remains around the subtropics (but still separate from the main tropical reservoir).

This southward mixing, despite transporting very little tracer, presents an issue which may help address the problem of the severe interhemispheric asymmetry in volcanic tracer. The point can be found in the following question: if the tropical reservoir was centred further south (as it was in the real atmosphere) then would that be enough to redress the balance of material between the hemispheres, bringing it in line with observations? This question will be investigated further in Chapter 5 (section 5.1).

Figure 4.66 contains plots of tracer on the isentrope, θ=650K, which is around

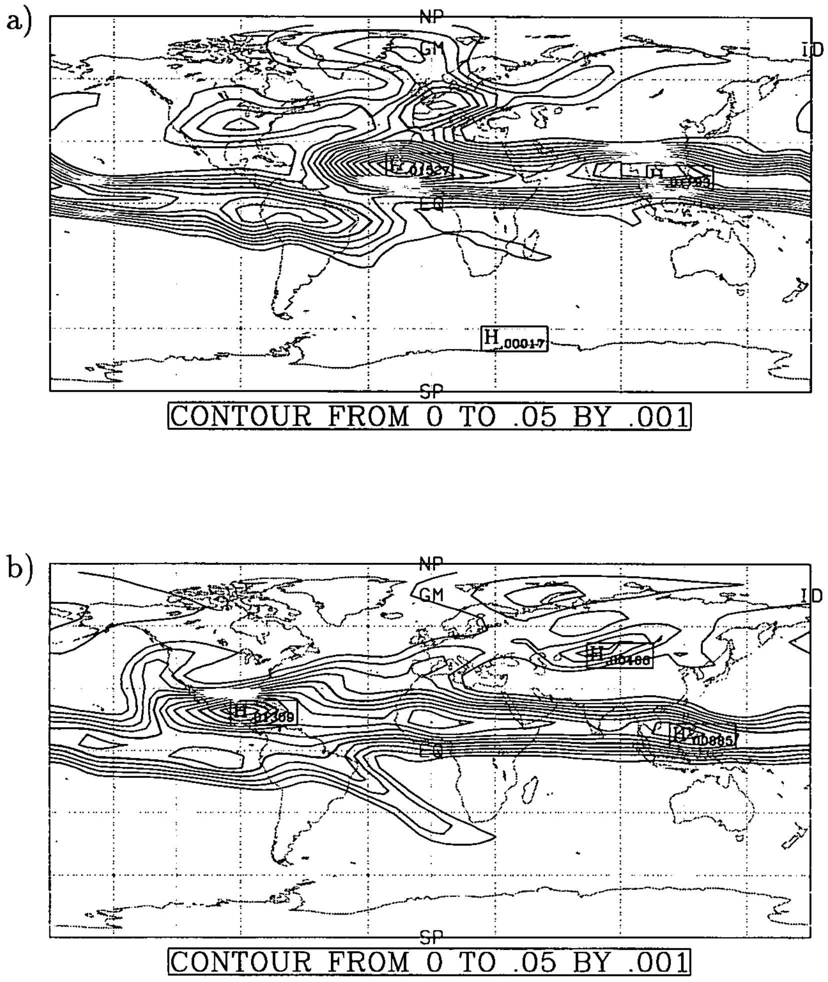

Figure 4.65: Global isentropic map (latitude-longitude) of tracer (vmr) at θ=450K (approx. 70mb) on days a) 30 and b) 35 of Run B.

the altitude at which southward mixing was occurring in the real atmosphere. These plots show that some material is being pulled off the main cloud, but fails to evolve into a tongue of material stretching into the southern mid-latitudes and thus no irreversible mixing occurs (although it does serve to push the southern edge of the cloud slightly further south).

The tropical reservoir as seen on the isentrope, θ=650K becomes zonally symmetric around day 50 of the run. Zonal symmetry at lower altitudes is not achieved until later in the run. On the isentrope θ=450K, it occurs a little after day 70 (plots not shown here). This is just over a month later than seen in the real atmosphere.

Again referring to our previous description of poleward motion through zonal

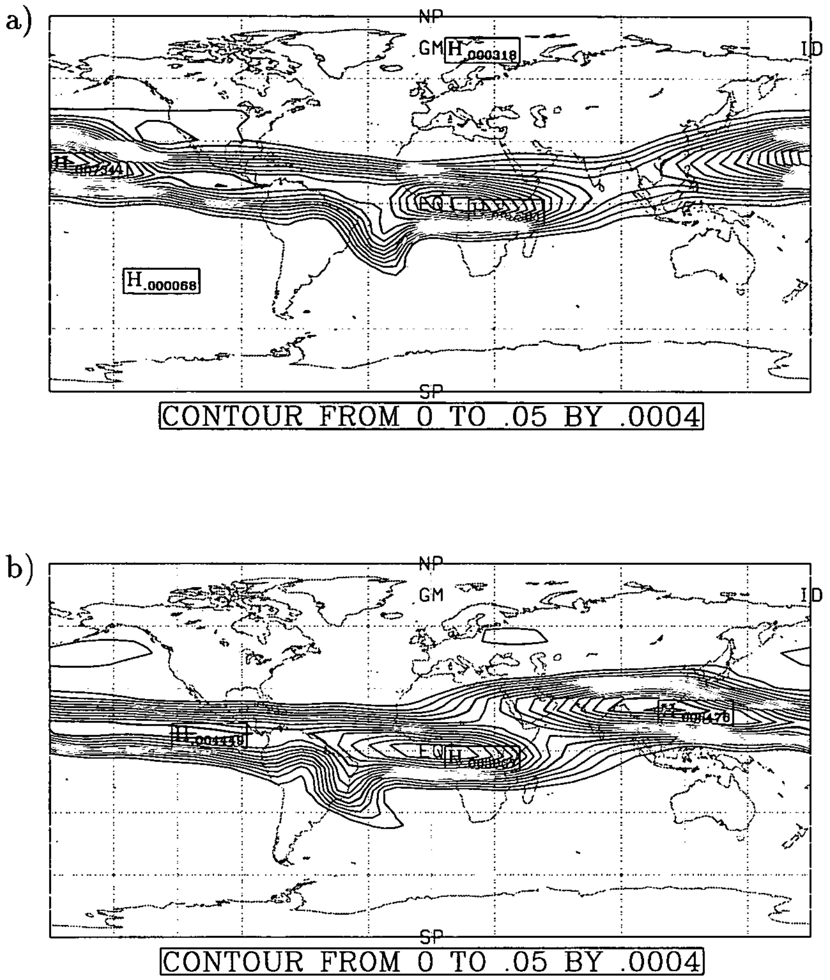

Figure 4.66: Global isentropic map (latitude-longitude) of tracer (vmr) at θ=650K (approx. 20mb) on days a) 35 and b) 40 of Run B.

mean tracer fields, days 60 to 95 were highlighted for an increase in northward movement from the tropics centred higher up in the model followed by a seemingly anomalous high of material over the north pole on day 90. The cause of this can be seen in the following latitude-longitude plots.

Figures 4.67 and 4.68 show a sequence of four plots of tracer on the isentrope, θ=500K, for days 80, 85, 90 and 95. At day 80 the start of the mixing event can be seen transporting tropical material northeast from around 180°W (note that this series of plots has 180°W in the centre to make this event easier to see). On day 85, due to some dynamical process, some of the tongue of tracer has reached as far as the northern polar region. This material covers the north pole on day 90 and is connected to the tropics by a band of material only about 60 degrees wide. So

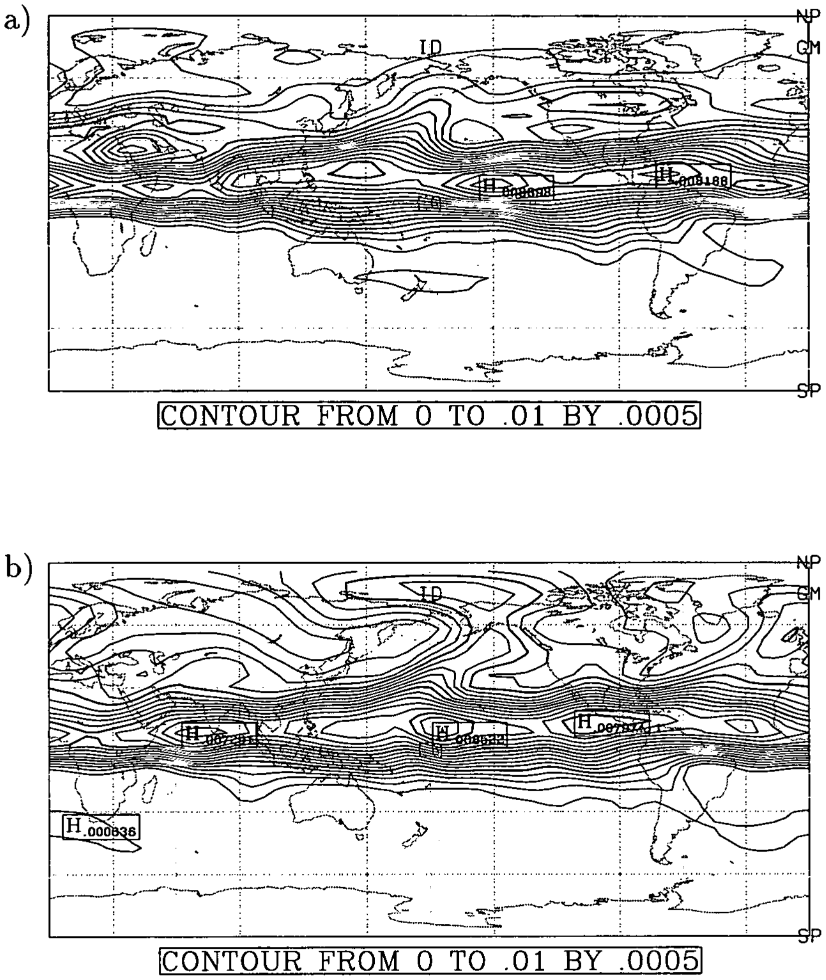

Figure 4.67: Global isentropic map (latitude-longitude) of tracer (vmr) at θ=500K (approx. 50mb) on days a) 80 and b) 85 of Run B.

the effect of zonally averaging this field would be to produce high values over the tropics and pole but considerably lower values over the mid-latitudes (see Figure 4.59 again). Although the high mixing ratios over the pole were exaggerated by the nature of zonally averaging this kind of field, the fact that the material reached the pole so quickly is significant and it still being connected to the tropics is an unusual feature. By day 95 the tracer is more thoroughly dispersed around the northern mid- and polar latitudes and so the zonal high of tracer has disappeared (Figure 4.68b).

Note that during the same period of time, a mixing event pulls a low amount of material from the main cloud into the southern mid-latitudes but by day 90 the small amount has dispersed to such a degree that it is no longer discernible to the

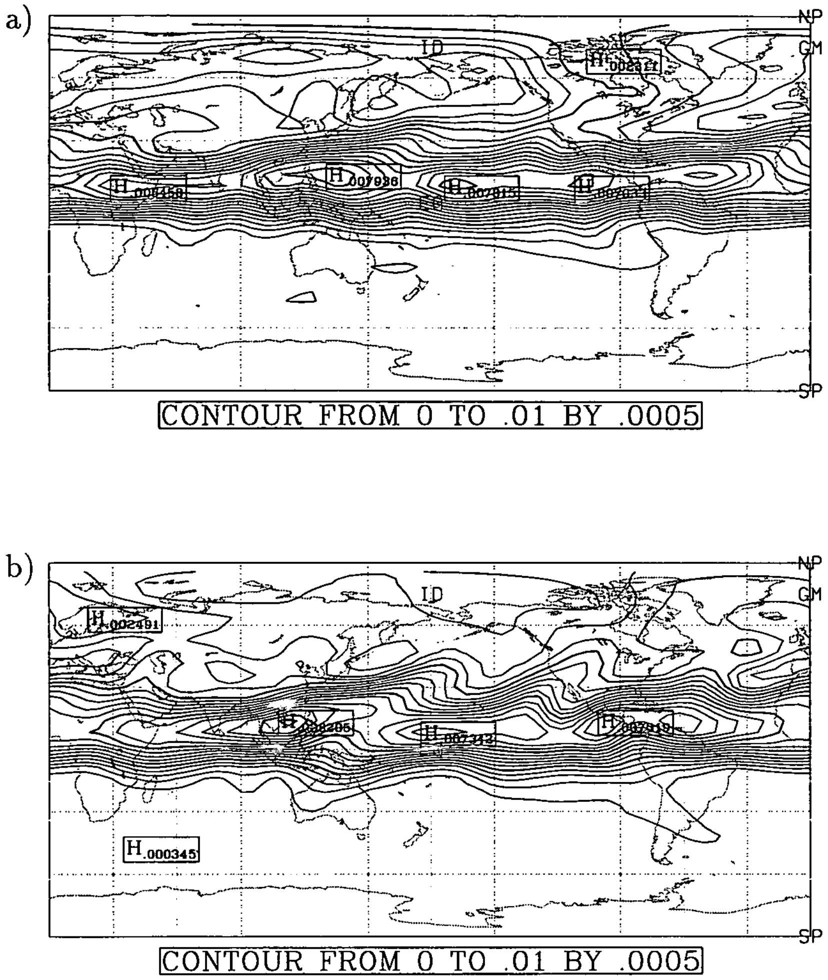

Figure 4.68: Global isentropic map (latitude-longitude) of tracer (vmr) at θ=500K (approx. 50mb) on days a) 90 and b) 95 of Run B.

chosen contour range. This is further evidence that perhaps if the distribution was centred further south then more material would escape into the southern mid-latitudes through events such as this.

Despite a significant quantity of material being transported northwards across the subtropics, the gradient in the tracer field between the tropics and mid-latitudes remains coherent. According to the zonal mean analysis this coherence decreases after around day 100. The quasi-horizontal tracer fields show why this is the case. For the period of Run B following day 100, the northern hemisphere is very active with mixing events transporting material from the tropics to the extra tropics. At times there are up to three mixing events occurring simultaneously, and at the same height. Not only has the frequency of events increased dramatically, but the amount of material transported has increased also.

Figure 4.69 presents an example of the the mixing events occurring during this period of Run B. On day 130, two mixing events are in progress, with a third having just finished (the remnants of which can be seen at 170°W). The tongue of material resulting from one of the mixing events stretches to the fringes of the polar region. The other event has transported a very high amount of tropical material into the mid-latitudes.

Five days later the two tongues of material are all but gone. A new event is underway around 150°W. A tight latitudinal gradient in the tracer field is in evidence but it is irregular in nature, not smooth (with respect to longitude). It can be seen though, that although the edge of the tropics is no longer apparent within the tracer field, the northern edge of the main reservoir of material is still coherent. The irregular pattern here seems identical to that seen in the real measurements in the first few months; a smooth southern edge of the cloud opposed to the northern, irregular edge. This also explains why there is no clear division between the northern mid-latitudes and tropics in the zonal tracer fields.

The last points I want to make using isentropic maps of tracer involve fields many months later in the model run. In the last couple of months of Run B a dramatic increase in southward movement of material occurs. The movement takes the form of tongues of material stretching from the tropics into the mid-latitudes and mixing irreversibly. It starts around day 295 but Figures 4.70 and 4.71 give an excellent example of what we had hoped to have seen in the first few months of the run.

On day 340 the tracer field at 650 K has many interesting features. A very important feature is that the tropics still contain the highest values of tracer and can be distinguished from the mid-latitudes in both hemispheres. Even in the northern hemisphere, where excessive mixing into the extra tropics means that there is only slightly less tracer than in the tropics, a subtropical gradient persists. On the southern side the subtropical gradient is incredibly steep, due to the small amount of tracer which has reached the southern mid-latitudes by this time.

That leads to the next point: some irreversible mixing has already occurred in the southern mid-latitudes (from day 295 onwards) but none of it has reached polar latitudes. In fact, it could be perceived that a boundary also separates the

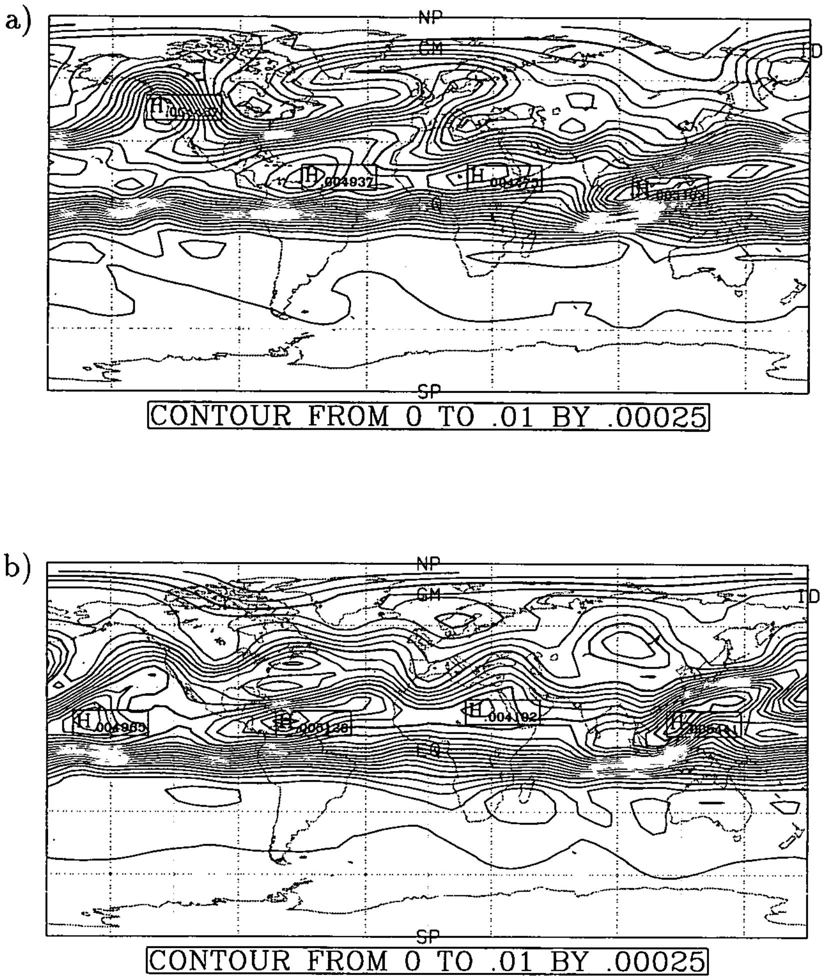

Figure 4.69: Global isentropic map (latitude-longitude) of tracer (vmr) at θ=500K (approx. 50mb) on days a) 130 and b) 135 of Run B.

polar latitudes from the rest of the hemisphere.

A southward movement of material has started, originating from deep within the tropics (intimated by the kink in the subtropical barrier, stretching over the length of South America). A tongue of material develops (Figure 4.70b) and by day 350 (Figure 4.71a) it stretches from the tropics to the edge of the polar region and from around 15°E to three quarters round the world, 120°E.

The tongue has mixed into the tropics by day 355 (Figure 4.71b). Despite the large increase in tracer loading within the mid-latitudes no material gets south of the polar boundary, previously noted. In fact, the boundary between the middle and polar latitudes has been enhanced by a steepening of the tracer gradient. This is further evidence that the polar vortex (stronger in the southern winter) is

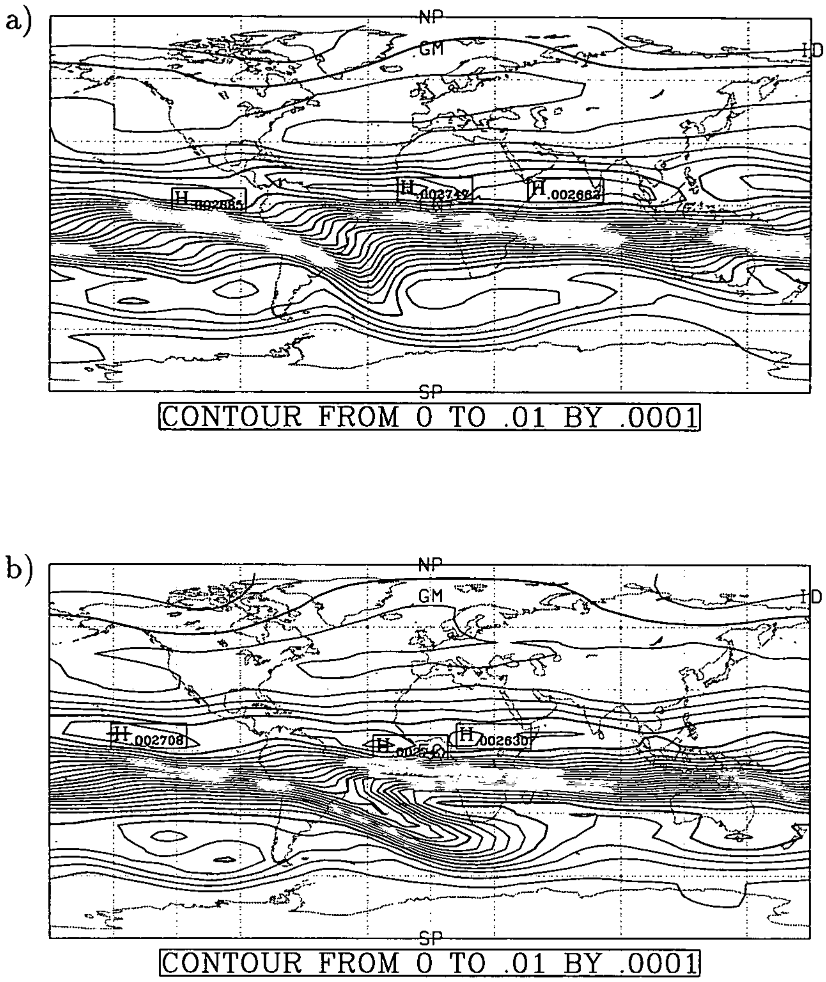

Figure 4.70: Global isentropic map (latitude-longitude) of tracer (vmr) at θ=650K (approx. 20mb) on days a) 340 and b) 345 of Run B.

inhibiting poleward movement.

4.5.5 Summary of Run B

In keeping with the summary of Run A, we will go through the points in section 4.2.6 with respect to Run B.

Run B did maintain a tropical stratospheric reservoir of material for the entire run although it did not exist throughout the entire tropics. Again, the tracer was reluctant to move southwards of 10°S. The tropical band of tracer was more uniform on its southern edge in the first few months of the run and this agrees with observations.

The height dependency of poleward spread is more difficult to determine since

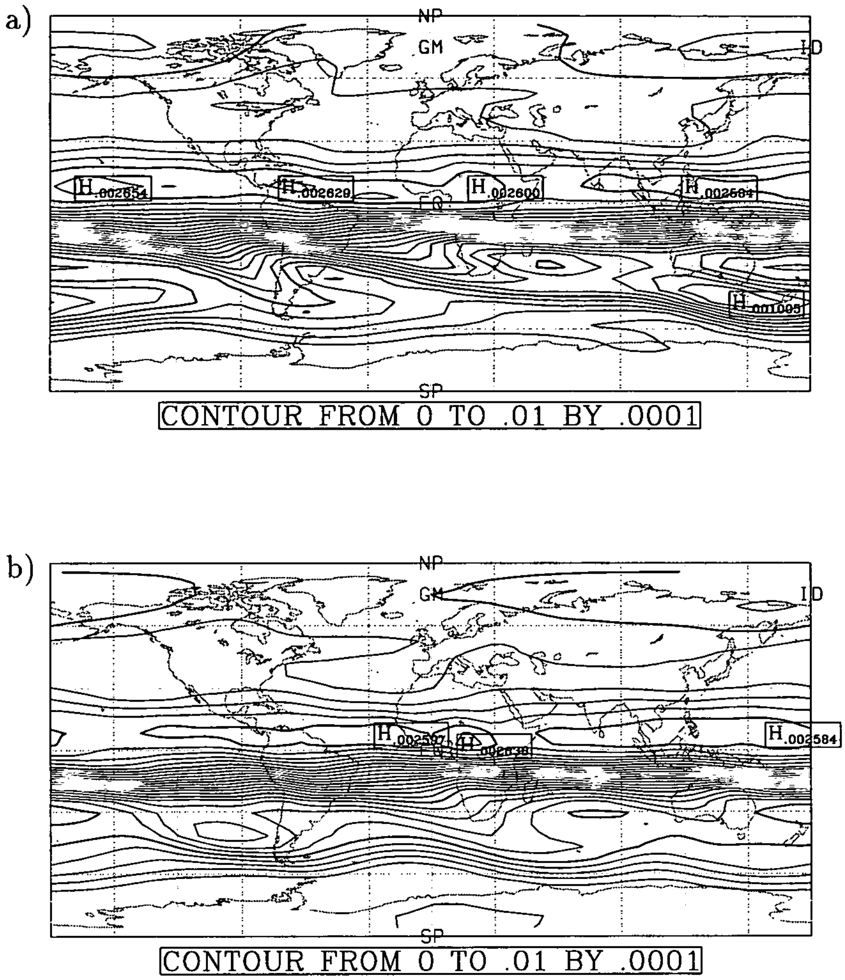

Figure 4.71: Global isentropic map (latitude-longitude) of tracer (vmr) at θ=650K (approx. 20mb) on days a) 350 and b) 355 of Run B.

there was very little tracer in the southern tropics to be mixed into the southern mid-latitudes. The initial northward mixing was very clear in the lower stratosphere, in the same altitude range as was seen in observations. What little evidence of mixing into the southern hemisphere there was did occur at higher altitudes but this cannot be taken as conclusive evidence that the EUGCM is demonstrating the two different mixing regimes reported in real measurements. Tracer experiments in the next chapter allow us to answer this question more authoritatively.

There was some evidence of the polar vortex inhibiting the spread of tracer in Run B, particularly in the southern hemisphere near the end of the run. Isentropic fields of potential vorticity will be used in the next chapter to confirm this.

The next point refers to the cloud rising suddenly over the tropics in December. In the EUGCM a fairly sudden rise did occur, but much later in the model run; around day 240 (beginning of February). Rates of ascent varied in each hemisphere, at one point forming a double peak in the tropics. The top of the cloud in the model is higher than that in the real atmosphere towards the end of the experiment. This can be attributed to the lack of settling velocities, but this is not considered to be too serious compared to the interhemispheric asymmetry.

The final point concerns where the model has diverged the most from the real atmosphere. An extreme inter-hemispheric asymmetry exists in the tracer fields after almost a year of Run B. In the real atmosphere, there was very little imbalance between the two hemispheres. In fact, slightly more material was found in the southern hemisphere. The cause of this unsatisfactory result will be the main focus for the Chapters 5 and 6.

4.6 Comparison with Boville et al

It is useful at this point to make a comparison between the Pinatubo simulations presented here with a similar simulation presented in the literature. *Boville et al.*, [1991], also use a general circulation model to simulate the spread of the Pinatubo cloud. The model is a spectral one with horizontal resolution T42 (the same as Run A and finer than Run B). There are 35 levels in the vertical about 2km apart. The model employs a semi-Lagrangian advection scheme, eliminating problems usually associated with spectral models (negative quantities of tracer, for example). The simulation is initialised on model day June 15th by inserting a passive tracer in the region of Mt. Pinatubo. This distribution is smoothed with its centre of mass at a height of 24mb. The model is run on annual cycle mode for 180 days.

The main points of the simulation can be summarised as follows (refer also to Figure 4.72). In the first month, the tracer spreads throughout the tropics to a similar extent as seen in the real atmosphere. Throughout the entire model run, tracer is fairly well confined to the tropics and the centre of mass remains at around 20mb. The model demonstrates the two-layer mixing regime well, with tracer mixing into the northern extra tropics only below 20km and tracer

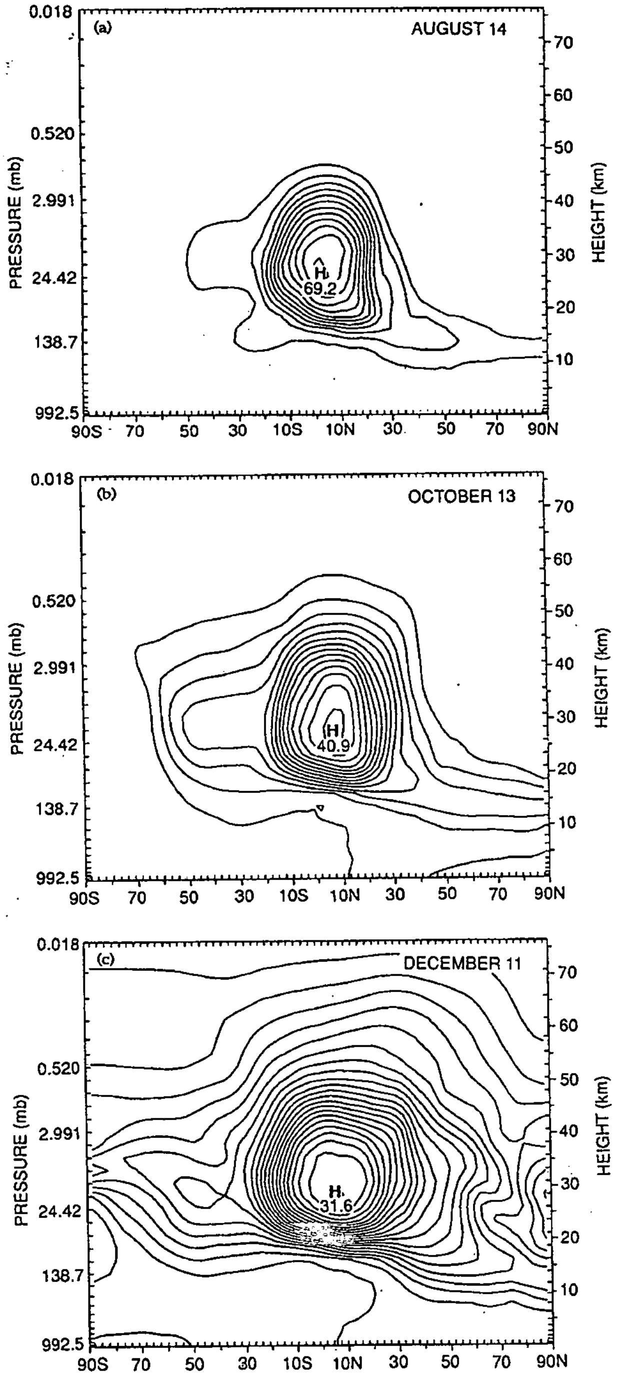

Figure 4.72: Latitude-height cross sections of zonally averaged tracer mixing ratio (ppbv) from the model run presented in *Boville et al.* [1991].

mixing into the southern extra tropics mainly occurring above 20km. By mid-December significant amounts of tracer can be found at all latitudes. The tracer distribution at this time does have more tracer in the northern hemisphere than the southern hemisphere, but the inter-hemispheric asymmetry is not nearly as severe as was found in Run B. This is the main difference between the the results of the two simulations. Another difference is that, in general, the tracer spreads in the vertical to a much greater extent in the *Boville et al.* experiment than in Run B. *Boville et al.* found small amounts material in the equatorial upper-troposphere within a month after the eruption despite the tracer being released at a higher altitude than in Run B. There was no evidence of this in Run B, or in measurements of the real atmosphere.

Other simulations of the Mt. Pinatubo cloud have been presented in the literature, but they also include the effects of radiative heating so those experiments are discussed later, in Chapter 6.

4.7 Conclusions of the Pinatubo simulation

Useful information has been gained from both runs, but especially Run B. There were several aspects of the simulation which reproduced the atmosphere well in both runs. One example of this is the rate at which the cloud completed its first circuit of the Earth. The leading edge of the cloud in each run took about three weeks to circle the Earth which corresponds well with observations.

Run A and Run B managed to simulate convincingly the tropical confinement of the highest mixing ratios of the volcanic cloud. This includes a high latitudinal gradient in the tracer fields over 10°S and 30°N. However, the southern edge of the reservoir is too close to the equator, compared with the real Pinatubo cloud. Also, both runs demonstrated the ability to reproduce the kinds of mixing events required to facilitate the tropical/mid-latitude exchanges seen in the real atmosphere.

There seemed to be no problem for either run to simulate the northward mixing exclusively below 20km. Run A managed to have some mixing into the southern hemisphere, and it did occur above 20km. Unfortunately though, there was not nearly enough southward mixing of tracer, although it was better than Run B in this respect. There was no significant mixing into the southern hemisphere until near the end of the Run B. Chapter 5 will establish whether the reason for this is because there was not enough wave breaking in the southern hemisphere at the start of Run B or the tropical reservoir was centred too far north to be reached by mixing events. At the end of Run B, southward mixing of the volcanic tracer did start in earnest, and at the height it should have occurred during the previous southern winter.

Prevention of the poleward spread of material due to a polar vortex was a major feature of the real measurements. Only Run B provided us with pertinent information on this dynamical occurrence. There is encouraging evidence that the tracer movement is halted when encountering a polar vortex edge, but this needs to be firmed up in the next chapter with the introduction of isentropic fields of PV into the investigation.

We have established in this chapter that the UGAMP GCMs (particularly the EUGCM) reproduce many of the dynamical processes necessary for simulating the transport of a volcanic cloud. Despite this, Run B fails to represent the global distribution of material after one year, showing instead a large interhemispheric asymmetry in the tracer field. The main problem is that the model is not getting enough material into the southern hemisphere. Of course, the model is also putting too much material into the northern hemisphere, but the two problems are probably related.

The next two chapters specifically examine the problem of the interhemispheric asymmetry. Chapter 5 looks at things like whether there is enough planetary wave mixing in the southern hemisphere and why the tropical reservoir is centred further north than it was in the real atmosphere. The Run B model configuration will be used again but with new tracer distributions designed for this investigation. Chapter 6 uses a two-dimensional numerical model to investigate the effect that radiative heating would have on the distribution of the volcanic cloud plus a look at the significance of settling velocities on the cloud.

Chapter 5

Factors Affecting the Poleward Spread of Tracer

The following experiments all go some way to addressing the issues highlighted by the simulation of the Mt. Pinatubo aerosol cloud in the previous chapter. The comparison between model and real data raised important questions about the dynamics of the atmosphere and how well the EUGCM is representing them. We saw that the EUGCM did produce many features similar to the real atmosphere:

- Cloud circles the globe in three weeks
- Northern mixing below 20km for a few months after the eruption
- Good tropical confinement throughout first year

In section 5.2 we look for evidence in the EUGCM of low-latitude, steep gradients of PV inhibiting polewards transport of volcanic material from the tropics.

Out of all the points listed in section 4.2.6, one was left unresolved with respect to the EUGCM simulation, namely, the prevention of poleward spread by the edge of the polar vortex. Analysis using isentropic PV fields in section 5.2 determines whether this does occur in the EUGCM.

The model also differed from the real atmosphere in the following ways:

- Significant southern transport did not occur above 20km (or at any height) in the first months after the eruption
- The EUGCM displayed a severe interhemispheric asymmetry in the tracer fields after a year

As the EUGCM was not initialised with June data from 1991, we would not expect the cloud dispersal to mimic the real Pinatubo cloud exactly due to interannual variability. However, the interhemispheric asymmetry is far too severe to be a result of interannual variability; it represents a serious problem in the model for which a solution has to be found. In section 5.1, a number of experiments are set up in the EUGCM to determine the importance of the cloud's tropical distribution in the first few weeks to the poleward spread of the cloud.

While these are the main issues being studied in this chapter, attention will also be given to the amount of planetary wave mixing in each hemisphere. We will want to see whether the interhemispheric asymmetry, seen last chapter, could be due to an unsatisfactory simulation of Rossby wave breaking by the EUGCM.

5.1 Sensitivity of simulation to where tracer is released

The observations show, 10 months to a year after the eruption, slightly more material in the southern hemisphere than the northern hemisphere while the model simulation showed a very strong bias towards the northern hemisphere. One possible cause of this interhemispheric asymmetry could be that the southern hemisphere is not sufficiently dynamically active. This is addressed in this section. Another line of reasoning would be that the mixing to the southern mid-latitudes does exist but no material is transported as there is none in the southern tropics due to a lack of cross-equatorial transport. Accordingly it was decided to perform some tracer experiments to investigate whether the fate of the aerosol depends strongly on the release position within the tropics.

There are four different tracer distributions in all, the main features of which are listed in Table 5.1. All the tracers used in this chapter are initialised with zonally symmetric distributions. That is to say, the distribution varies only with altitude and latitude but not with longitude. The reason for this change is that now we will be focusing on how material is transported latitudinally in the model and the zonal distributions serve us well in this respect as well as reducing problems with negative values. We will see that the zonally symmetric tracer based on the Pinatubo tracer from last chapter produces very similar looking zonal fields to the Pinatubo tracer.

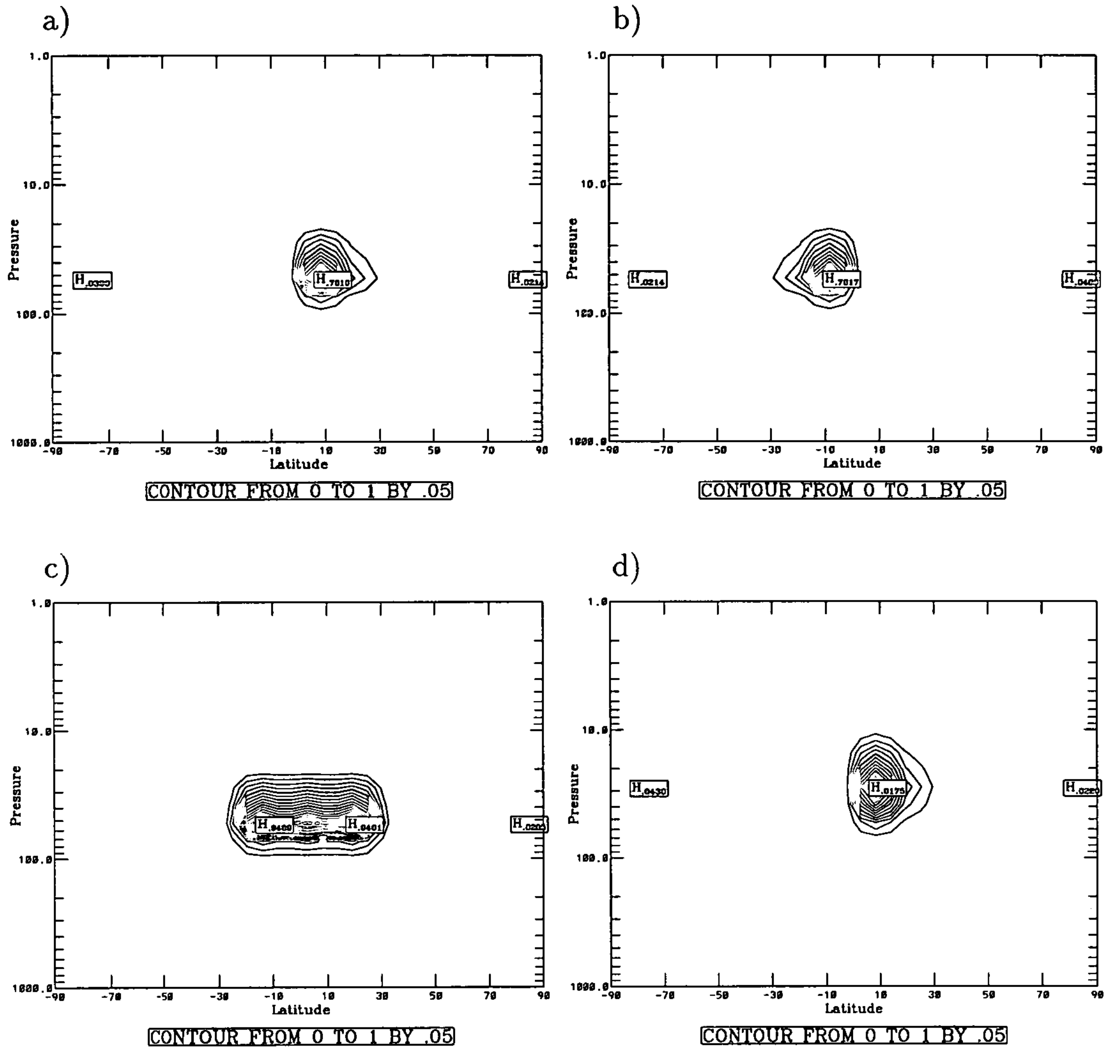

Figure 5.1: Initial latitude-height cross sections of zonally averaged tracer (vmr); a) Tracer 1 b) Tracer 2 c) Tracer 3 and d) Tracer 4. See Table 5.1 also.

Tracer 1 (Figure 5.1a) is based on the Mt. Pinatubo tracer used in Chapter 4, but extended around all longitudes. Tracer 2 (Figure 5.1b) is a reflection about the equator of Tracer 1. This will be useful to see if the lack of cross equatorial transport applies to material in the southern tropics as well. It will also serve to test the tropical/mid-latitude exchange due to planetary wave breaking in the southern hemisphere and it will be interesting to see if the distribution of Tracer 2 after a year is the same as that of Tracer 1 reflected about the equator.

Measurements tell us that the real Pinatubo cloud was transported south across the equator in the first few weeks after the eruption. The volcanic cloud,

Tracer	Centred at Height	Latitude Range
Pinatubo Tracer	50mb	Equator - 30°N
Tracer 1	50mb	Equator - 30°N
Tracer 2	50mb	30°S - Equator
Tracer 3	50mb	20°S - 30°N
Tracer 4	30mb	Equator - 30°N

Table 5.1: Brief description of the five different tracer distributions used throughout this chapter. The Pinatubo Tracer is that which was featured in Run B in Chapter 4.

a month after the eruption, spans from 20°S to 30°N. The model has not demonstrated this initial transport across the equator very well. The tracer distribution, a month after initialisation spans from only 10°S to 30°N, a latitude range very similar to that at the start of the simulation. Tracer 3 (Figure 5.1c) is distributed between 20°S and 30°N, similar to the fields observed a month after the eruption. From this we will be able to see whether, if the tracer had crossed the equator to produce a distribution similar to that in the real atmosphere, the simulation would go on to produce an accurate interhemispheric distribution after a year.

This experiment does not address the actual problem of the tracer's reluctance to cross the equator, but if the new tracer does achieve a global distribution similar to that in the real atmosphere then the severe interhemispheric asymmetry of the Pinatubo simulation would be entirely due to the lack of cross-equatorial transport. This would considerably simplify things by focusing attention onto why the tracer is not moving south across the equator. Either way, the problem of cross-equatorial transport needs to be considered further and it is, later in this chapter and again in Chapter 6, where possible influence of heating is considered.

As can be seen from Figure 5.1, Tracers 1 to 3 have the same distribution with respect to pressure. The last tracer to be considered here is initialised higher in the model. Both observations and model studies (see chapter 4) show evidence that the direction of poleward dispersal of material from the tropics is highly dependent on altitude. In the first few months after the eruption of Mt. Pinatubo, the bulk of tropical/mid-latitude exchange (in the southern hemisphere) occurs above 20km.

Initialising a tracer higher in the model allows us to see if height affects the amount of material mixing into the southern hemisphere. Tracer 4 (Figure 5.1d) is centred at approximately 24km (30mb) and is situated over the same latitudes as Tracer 1. One possibility is that radiative heating due to the volcanic aerosol would loft the cloud to higher altitudes. Chapter 6 will investigate the effects of radiative heating but meanwhile, Tracer 4 will test whether this would change the global dispersal of aerosol in the EUGCM.

5.1.1 Tracer 1 vs. Pinatubo Tracer

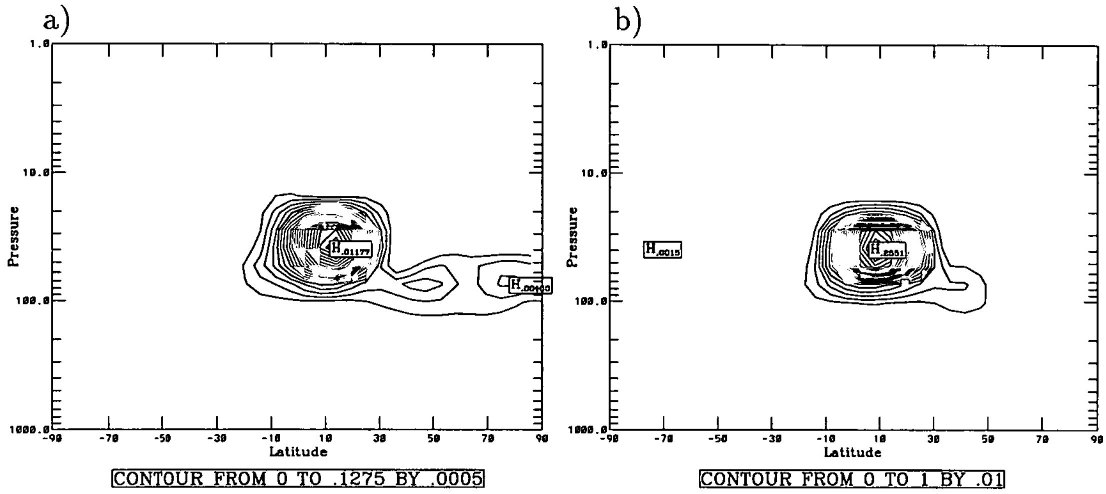

Figure 5.2: Latitude-height cross sections of zonally averaged tracer mixing ratio (vmr) on day 30 (July) of the model run: a) Pinatubo Tracer and b) Tracer 1.

First, a quick comparison is made between the tracer used for simulating Mt. Pinatubo in the EUGCM (last chapter) and Tracer 1. All the basic features of the zonally averaged distributions of both tracers are very similar throughout the entire model run. The one exception to this is in the first month, when proportionately less material mixes into the northern mid-latitudes in the case of Tracer 1 (see Figure 5.2). This is due to the event detailed in section 4.5.4 of Chapter 4 (Figures 4.64 and 4.65). The event which took such a huge proportion of the tropical Pinatubo Tracer into the mid-latitudes takes a smaller proportion of Tracer 1 which covers all the longitudes in the tropics. The difference between the proportions of the two tracers in the northern mid-latitudes dwindles to nothing in a matter of weeks.

Figure 5.3 shows the zonal fields for each tracer at the end of the model run. Clearly, the fields are quantitatively different as the tracer amounts assigned to just a few longitudes for the Pinatubo tracer are extended over all longitudes for

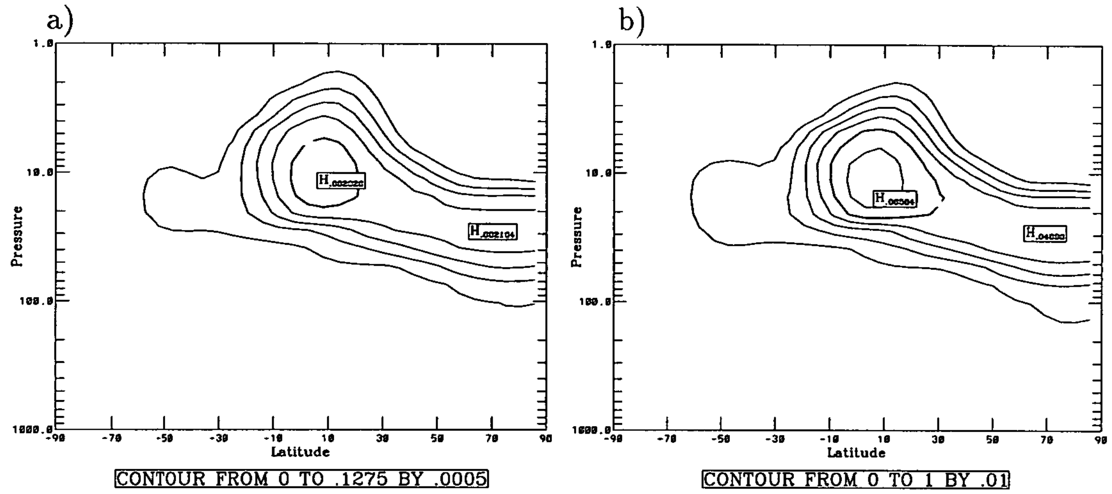

Figure 5.3: Latitude-height cross sections of zonally averaged tracer mixing ratio (vmr) on day 360 (mid-June) of the model run: a) Pinatubo Tracer and b) Tracer 1.

Tracer 1. The important thing is that the fields are proportionately very similar. This indicates that, in the long term, the rate of latitudinal spread in the model is not dependent on longitude. This, in turn, means that the evolution of the zonally symmetric tracers in this chapter can be compared with the Pinatubo tracer. For example, if Tracer 4 spread to each hemisphere equally, not only would it say something about the EUGCM in general, but we could reasonably conclude that if the Pinatubo tracer in the last chapter had been initialised higher, a more realistic hemispherical distribution would have been achieved.

5.1.2 Tracer initialised in northern tropics vs. tracer initialised in southern tropics

Just over a month into the model run, the zonal field for Tracer 2 is not simply the reflection about the Equator of Tracer 1 (Figure 5.4). Much more of Tracer 2 has been transported into the southern mid-latitudes than of Tracer 1 into the northern mid-latitudes. This is a result of a continuous flow of tracer from the tropics to extra-tropics throughout the first five weeks of the run. Clearly, there is not a lack of planetary wave breaking in the southern winter in the EUGCM. The mixing of Tracer 2 into the southern sub-tropics occurs over the entire altitude range which the tropical cloud covers. It appears that material drops in height when it enters the mid-latitudes (a feature associated with adiabatic transport).

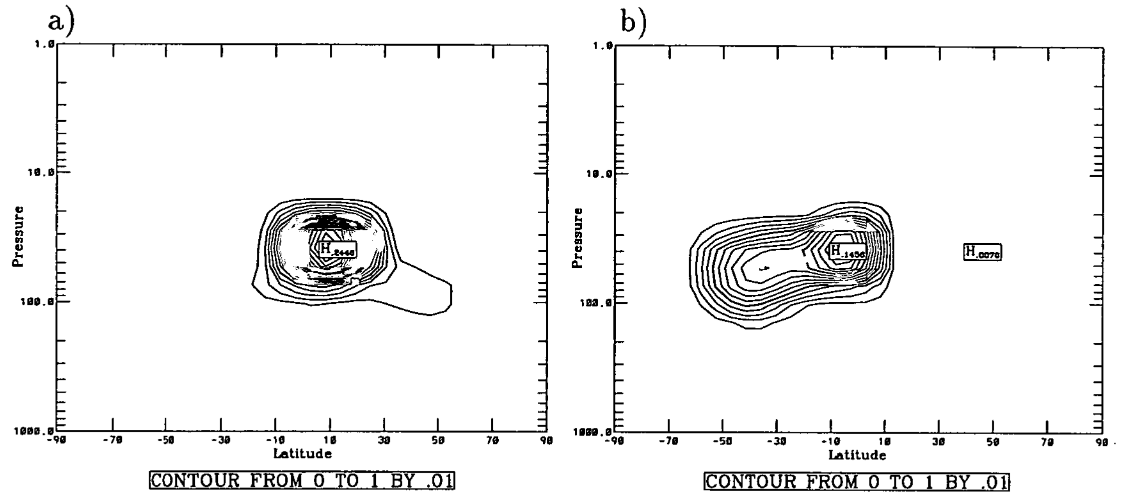

Figure 5.4: Latitude-height cross sections of zonally averaged tracer mixing ratio (vmr) on day 35 (July) of the model run: a) Tracer 1 and b) Tracer 2.

Once in the mid-latitudes, Tracer 2 does not continue into the polar latitudes, possibly due to the polar vortex preventing further southward transport (see later in this chapter for more on the polar vortex).

One particular feature of Tracer 2's distribution which agrees with the distribution of Tracer 1 at this stage is the lack of transport across the equator. The lack of cross-equatorial transport of Tracer 2 persists for several months. In fact, there is no significant movement by Tracer 2 until around day 115 of the model run.

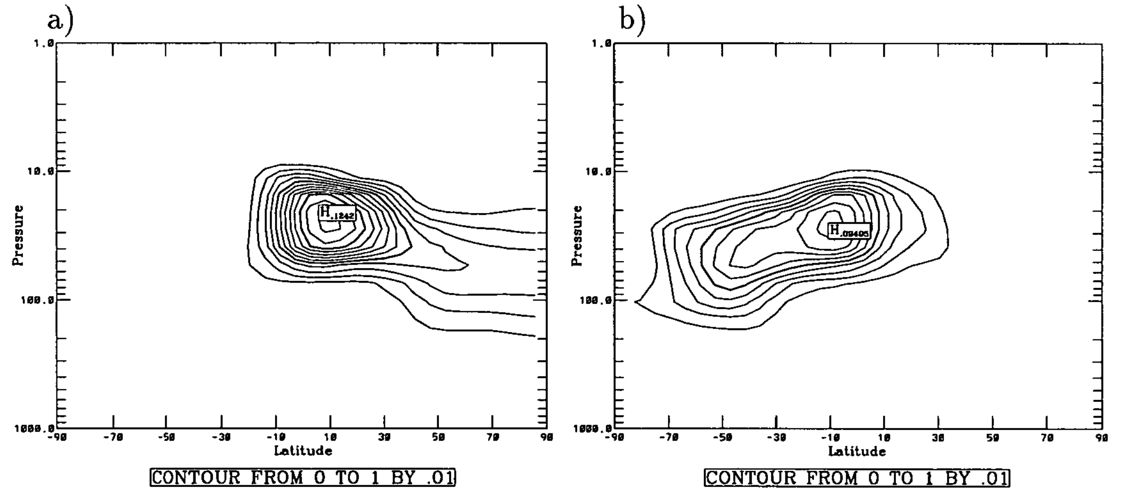

Figure 5.5: Latitude-height cross sections of zonally averaged tracer mixing ratio (vmr) on day 135 (October) of the model run: a) Tracer 1 and b) Tracer 2.

From day 115, the northern edge of the Tracer 2 cloud starts to advance northwards. This proceeds at a fairly gradual pace but by day 135, there is still no significant amount of Tracer 2 in the northern mid-latitudes (Figure 5.5b). Figure 5.5b also shows the first significant amounts of Tracer 2 to reach the southern polar region. Tracer 2 had reached the northern polar regions in just over two months from the start of the model run and so by day 135 there is much more of Tracer 1 over the north pole than there is of Tracer 2 of the south pole. Again, the field of Tracer 2 cannot be considered a reflection about the equator of Tracer 1. Tracer 2 reaches 30°N, but Tracer 1 only reaches 15°S which indicates that the transport in the northern tropics is more active than transport in the southern tropics.

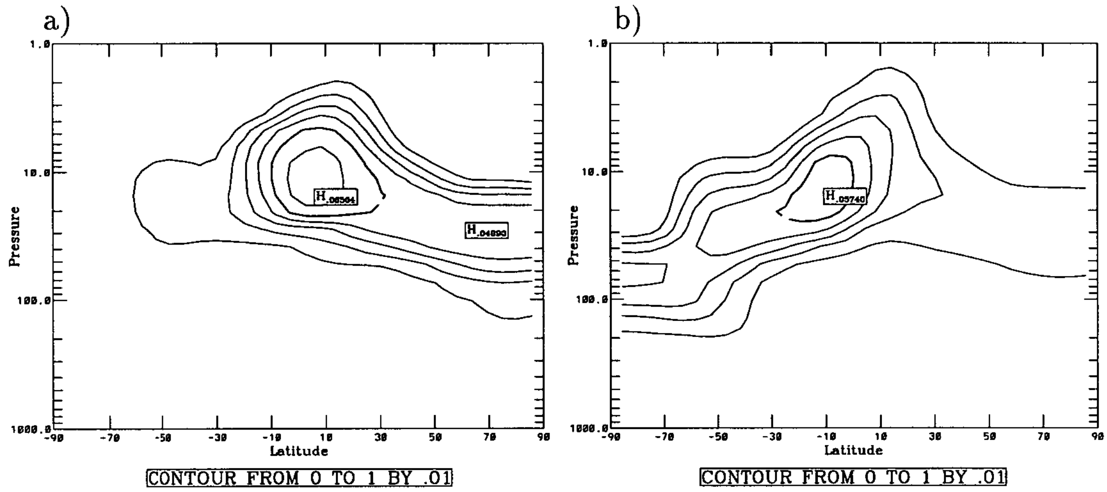

Figure 5.6: Latitude-height cross sections of zonally averaged tracer mixing ratio (vmr) on day 360 (mid-June) of the model run: a) Tracer 1 and b) Tracer 2.

The final zonal fields for both Tracer 1 and Tracer 2 are shown in Figure 5.6. If we compare one with the reflection of the other, then three differences stand out. The first has to do with the latitudinal distribution of the two clouds. Tracer 2 has reached the northern polar latitudes while Tracer 1 remains outside the southern polar region. The difference here is because of the southern polar vortex stopping Tracer 1 advancing any further south (i.e. associated with the season of the hemisphere).

Two other differences are related to distribution with respect to altitude. The distribution of Tracer 1 drops gradually in altitude from the tropics to the north pole. The distribution of Tracer 2 while sloping down into the southern mid-latitudes from the tropics, has a large step between the mid-latitudes and the polar region. The material over the south pole is very much lower than that over the north pole, indicating descent in the southern polar vortex. The step in the tracer distribution is where the polar vortex is situated.

Another difference is associated with where in the tropics material has been lifted. The prominent peak of material over the northern tropics is not just evident in Tracer 1 (which was initialised in the northern hemisphere) but is even more obvious for Tracer 2. This means that the peak in the distribution of Tracer 1 was not in the northern hemisphere just because that was where most of the material was released. The fact that Tracer 2's peak is more pronounced and Tracer 2's distribution in the tropics takes a more elongated shape implies that the flow of material causing the peak in the northern hemisphere must originate from lower in the southern tropics.

Quantitatively, Tracer 2 is showing a reflection of the interhemispheric asymmetry shown by Tracer 1 but to a slightly less extent. One feature which is very apparent is shared by both Tracer 1 and Tracer 2; the latitudinal position of the highest concentration of tracer never varies for either tracer. This is further evidence that in the tropics of the model there is virtually no meridional transport.

5.1.3 Tracer initialised throughout the tropics

The purpose of the experiment with Tracer 3 is to establish whether, if the Pinatubo Tracer had crossed the equator as it did in the real atmosphere, would the final global distribution look more realistic? We will be looking for similarities between the evolution of Tracer 3 and that of the real Pinatubo cloud. Tracer 3 cannot be considered a proper simulation of Pinatubo though, due to it starting with the distribution of the Pinatubo cloud one month after the eruption. However, it does serve as a good indication of whether the lack of transport across the equator is the sole reason for the extreme interhemispheric asymmetry in the Pinatubo simulation (Chapter 4). Tracer 3 extends from 20°S to 30°N and is not smoothed, so we would not expect to see fields which simply look like Tracer 1 and Tracer 2 added together, but we should expect to see many of the same features.

On day 35 of this model run, there are two distinct mixing regimes (as was seen in the first few months after the eruption in the real atmosphere). Mixing into the northern mid-latitudes is restricted to altitudes below 40mb and is most

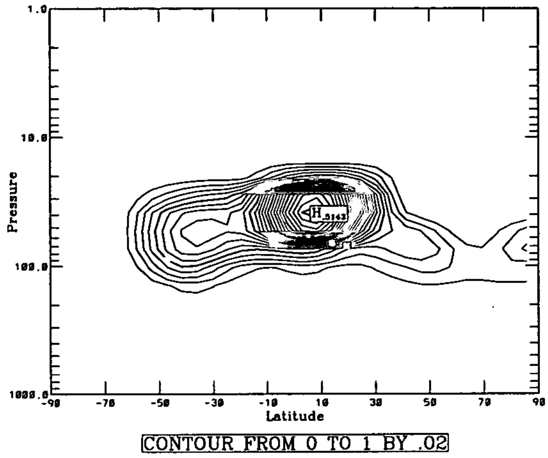

Figure 5.7: Latitude-height cross sections of zonally averaged tracer mixing ratio (vmr) on day 35 (July) of the model run: Tracer 3

prominent at a height of 60mb. Mixing into the southern mid-latitudes occurs over a greater altitude range, from 100mb to 20mb with the majority of mixing situated at 45mb.

More material has mixed into the southern extra-tropics than the northern extra-tropics. Despite the greater amount of material available in the southern mid-latitudes, Tracer 3 does not reach the southern polar latitudes, while it can be found in the northern polar region, even though the pool of mid-latitude material is less in the north than the south. This is good evidence that the southern polar vortex is inhibiting poleward transport of aerosol in the model.

By day 120 (about mid-October) poleward transport from the southern mid-latitudes has still not occurred (see Figure 5.8). This is in contradiction with the real measurements of the Pinatubo cloud (see Figure 4.6 in Chapter 4) which show material in the southern polar regions by this time. This is due to the EUGCM having a more persistent southern polar vortex than the real atmosphere in 1991. This is confirmed when looking at isentropic PV maps in the next section.

There appears to be no more material in the southern mid-latitudes at day 120 than at day 35. This suggests very little tropical/mid-latitude exchange in the southern hemisphere between those two points in the model run.

The northern extra tropics have gained more material by day 120, most of which was transported between days 65 to 85. It is reasonable to say that the amount of tracer to be found in each hemisphere, outside the tropics, is about

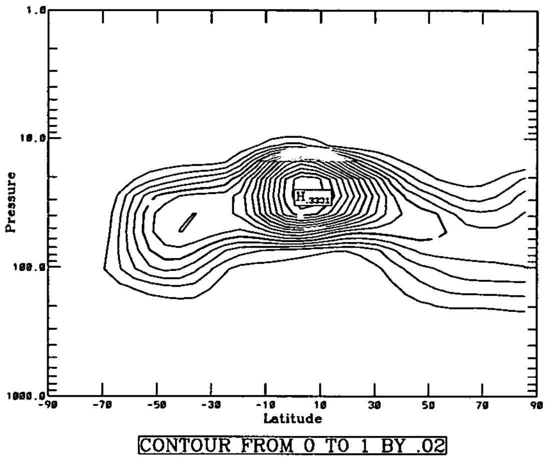

Figure 5.8: Latitude-height cross sections of zonally averaged tracer mixing ratio (vmr) on day 120 (October) of the model run: Tracer 3

equal, although the latitudinal distribution of the tracer in each hemisphere remains different. With respect to Tracer 3 in the first four months of the model run, the planetary-wave mixing into the southern mid-latitudes is just as effective as the lower mixing regime transporting material into the northern mid-latitudes. The tropical confinement is well defined, particularly in the southern hemisphere. The tropical stratospheric reservoir is bounded between 20°S and 30°N as the Pinatubo cloud was in the real atmosphere.

As we would expect from observing Tracer 2's evolution, Tracer 3 moves into the southern polar region after day 135. There is no evidence of tropical/mid-latitude exchange in the southern hemisphere following day 120 until nearly the end of the run when the Rossby wave breaking becomes active again. This inactivity in the southern mid-latitudes for such a long period emphasizes how important it is that the material is able to reach the southern extra tropics in the first few months of the model run if a realistic interhemispheric symmetry in the tracer distribution is to be achieved.

There is significant transport into the northern extra-tropics during the winter of that hemisphere. With this tracer distribution, evidence of the northern polar vortex preventing transport of material is clearer. Once the vortex has broken down, the tracer becomes evenly distributed (with respect to latitude) around the northern hemisphere, outside the tropics. After this, the flow of material from the tropics into the northern hemisphere is imperceptible and the distribution of

Tracer 3 in the northern hemisphere remains practically constant for the rest of the model run.

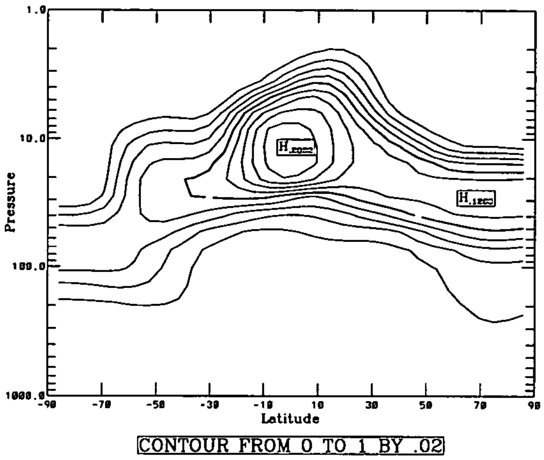

Figure 5.9: Latitude-height cross sections of zonally averaged tracer mixing ratio (vmr) on day 360 (mid-June) of the model run: Tracer 3

The zonal field of Tracer 3 for the last day of the model run can be seen in Figure 5.9. Clearly, the final field of Tracer 3 is much closer to the kind of picture we were seeing in the real data (Chapter 4) than Tracer 1 was. By this time the highest values over the tropics have shifted slightly south and are now situated directly over the equator. There is still some imbalance between the hemispheres, and so the lack of transport across the equator during the model run is not entirely responsible for the unrealistic asymmetry, but it is the major contributor to the problem.

5.1.4 Tracer initialised at a higher altitude

Tracer 4 will establish what difference, if any, initialising a tracer at a higher altitude will have on the poleward dispersal of material. Perhaps the cross-equatorial transport will not be so inhibited at higher altitudes in the EUGCM.

Comparing the zonally average fields for Tracers 1 and 4 on day 65 of the EUGCM run answers the last point (Figure 5.10). There is no more southwards transport across the equator for the higher distribution (Tracer 4) than there was for Tracer 1. Unlike Tracer 1, no significant amount of Tracer 4 has been transported north from the tropics. As has already been pointed out, the initial

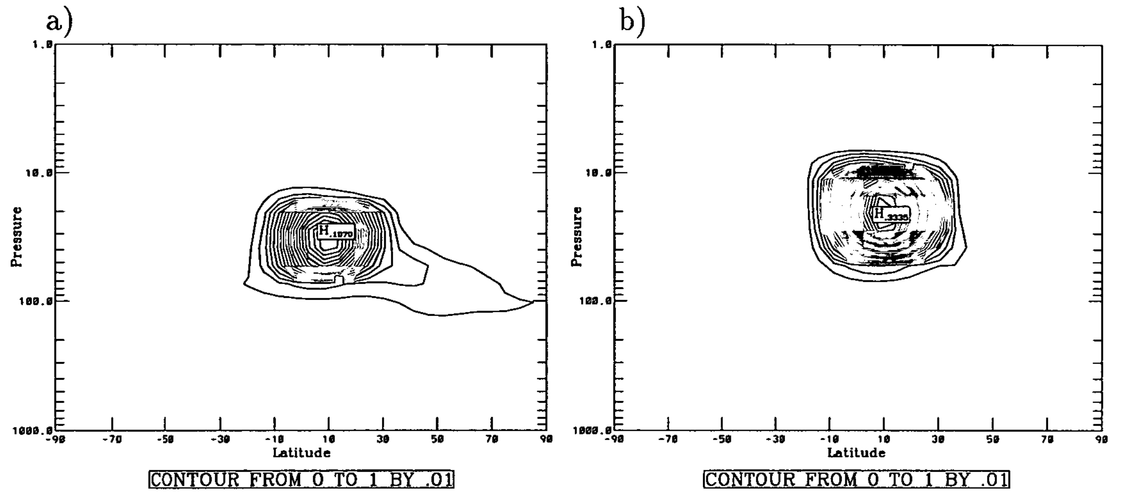

Figure 5.10: Latitude-height cross sections of zonally averaged tracer mixing ratio (vmr) on day 65 (August) of the model run: a) Tracer 1 and b) Tracer 4.

northwards transport from tropics occurs below 20km. There is a lot less Tracer 4 below 20km than there is Tracer 1.

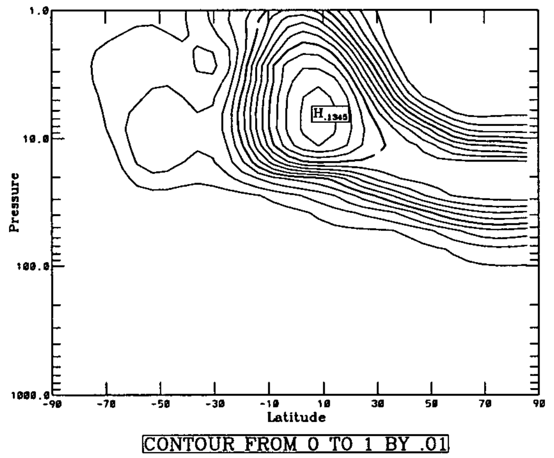

Figure 5.11: Latitude-height cross sections of zonally averaged tracer mixing ratio (vmr) on day 360 (mid-June) of the model run: Tracer 4

By the end of the model run there is not much difference between the two tracer distributions (see Figures 5.3 and 5.11), particularly with respect to latitude. The main difference is in altitude range covered; Tracer 4 reaches much higher than the real Pinatubo cloud.

A similar comparison was conducted between Tracer 3 and a tracer initialised with the same latitudinal distribution but at a higher altitude (not shown here). Again, the higher altitude made no overall impact on the final global distribution of material. These last two comparisons indicate that, in the case of the EUGCM, any change in altitude that occurs due to the aerosol heating has no effect on the long-term latitudinal dispersion. The effects of radiative heating on the volcanic aerosol cloud will be given more thought in Chapter 6.

Through this section, we have isolated the main cause of the interhemispheric asymmetry in the Pinatubo simulation; there is a lack of cross-equatorial transport in the model. We have also shown that if this problem was rectified then it would greatly improve the interhemispheric distribution by allowing tracer-rich air to enter the southern tropics which can then be transported into the southern mid-latitudes.

The next section looks at PV barriers inhibiting isentropic transport in the EUGCM. Particular attention will be given to transport of material from the tropics. If such barriers exist in the model the effectiveness of each hemisphere's barrier to inhibit transport will be quantified.

5.2 Using PV fields to examine the poleward transport of tracer

5.2.1 The concept of PV barriers

Chapter 2 introduced the idea that PV can be regarded as a measure of the inertial and static stability of the air [*Hoskins et al.* 1985]. *McIntyre* [1992] presents the concept that steep gradients of Potential Vorticity (PV) could inhibit the isentropic transport of an air parcel. The reasoning behind this is that in regions where the PV gradients on isentropic surfaces are sufficiently strong, the Rossby wave restoring mechanism suppresses Rossby wave breaking. This means that instead of irreversible mixing occurring, parcel displacement takes the form of reversible undulations. The sharp gradient of PV is effectively a barrier to isentropic transport of trace constituents, inhibiting irreversible mixing. This theoretical "PV barrier" to transport has been demonstrated in numerical models ([*Juckes and McIntyre* 1987, *McIntyre* 1989 and *Bowman* 1993 are good examples). There is also evidence in observations which suggest that PV barriers do exist in the real stratosphere, the prime example being the edge of the winter polar vortex preventing material entering the vortex. We will be trying to establish whether

PV barriers exist in the EUGCM as they would play an important role in the poleward dispersal of material.

Trepte and Hitchman [1992] and *Hitchman et al.* [1994] put forward the theory that the tropical reservoir of aerosol seen after the Pinatubo eruption is due to high PV gradients acting as barriers to transport between the tropics and mid-latitudes. Large gradients in PV are thought to exist in the subtropics partly as a manifestation of the dynamics driving the Quasi-Biennial Oscillation (QBO) but mainly as a result of mixing by planetary Rossby Waves which exist in the extratropical winter hemisphere. Figure 2.6 (Chapter 2) demonstrates the effect of planetary wave breaking on an isentropic PV field; a high PV gradient does develop in the subtropics, although not as strong as the polar vortex.

During the experiments presented here it has been clearly demonstrated that a tropical stratospheric reservoir exists in the model complete with sharp gradients in tracer fields at the edges of the tropics. The purpose of the following work is to establish what role, if any, steep PV gradients play in the restriction of the poleward transport of tracer in the EUGCM. The impermeability of the polar vortex edge will be investigated, but emphasis will be on the tropical confinement of tracer in order to test the hypothesis from *Trepte and Hitchman*, outlined above.

5.2.2 PV barriers in the EUGCM

In order to investigate the existence and role of PV barriers in the EUGCM, a number of isentropic maps of PV and tracer are studied.

The first period of analysis covers days 35 and 40 of the model run. Figure 5.12 shows isentropic fields of PV at 550 K for those two days. From either of these two plots, the southern polar vortex can easily be identified by the very strong PV gradient at the edge of the polar region. The vortex, as portrayed by the model, is both very strong and uniform. By uniform, I mean that the centre of the vortex is over the Pole and the edge of the vortex is fairly smooth. As well as the polar vortex, the surf zone is clearly represented in the model, and is most distinct in the PV fields at around 650 K (Figure 5.13a).

There is a tight PV gradient at the tropical edge of the surf zone and, as was shown in the theory (2.1.6), this gradient is not as steep as the gradient at the edge of the polar vortex. However, the position of the tropical gradient of PV does

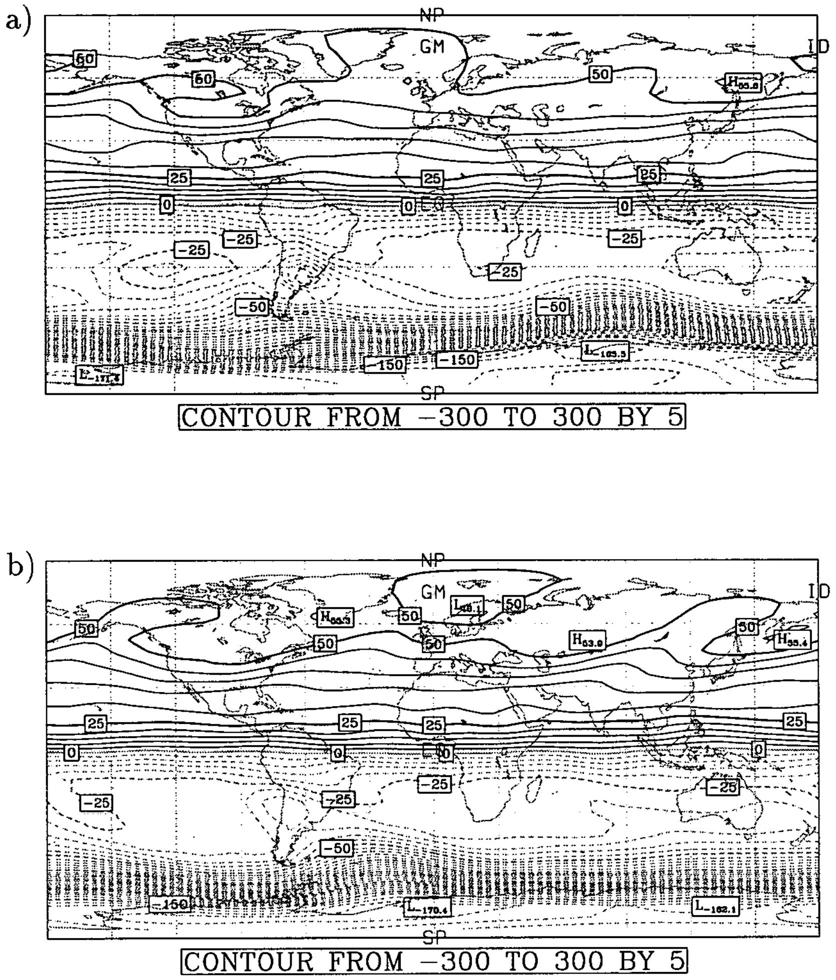

Figure 5.12: Global isentropic map (latitude-longitude) of Ertel's PV (pvu) at θ=550K (approx. 30mb) on days a) 35 and b) 40 (July) of the model run.

differ from expectations. The gradient is centred over the Equator and extends to no more than 20°S and 20°N from the start of the model run and during the period being looked at here. This is true at a range of heights in the EUGCM, not just at 550 K. In fact, Figure 5.13 demonstrates that all the different aspects of the PV field (at 550 K) discussed here, including the wave breaking event introduced below, are also featured at 450 K and 650 K.

As well as serving to point out some basic features of a PV field in the EUGCM, this specific period provides a good example of how planetary wave breaking is seen in an isentropic PV field. During this example, a relaxing of the tight, tropical PV gradient can be seen over central South America. If the sharp gradient of PV

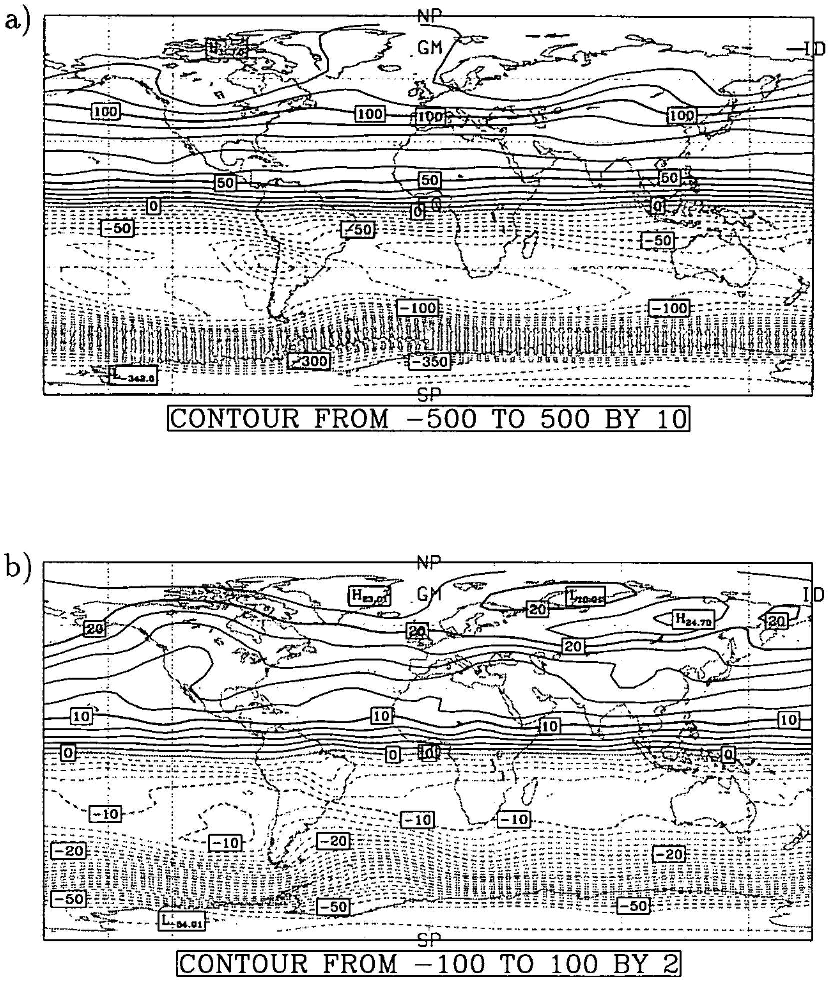

Figure 5.13: Global isentropic map (latitude-longitude) of Ertel's PV (pvu) at a) θ=650K (approx. 20mb) and b) θ=450K (approx. 70mb) on day 40 (July) of the model run.

is truly acting as a barrier to isentropic transport then we would expect material to be able to enter the southern mid-latitudes (from the tropics) only at this area of weaker PV gradient. To test this hypothesis we can use two of the tracer distributions introduced in section 5.1.

Figure 5.14 contains isentropic tracer fields at the same height and day as the PV field in Figure 5.12a. The two tracers featured in Figure 5.14 are Tracers 1 and 3, described in section 5.1. Looking first at the Figure 5.14a, we can see that Tracer 1 is very tightly confined north of 10°S at nearly all longitudes. A small tongue of material is very clear, extended from the longitude range where the

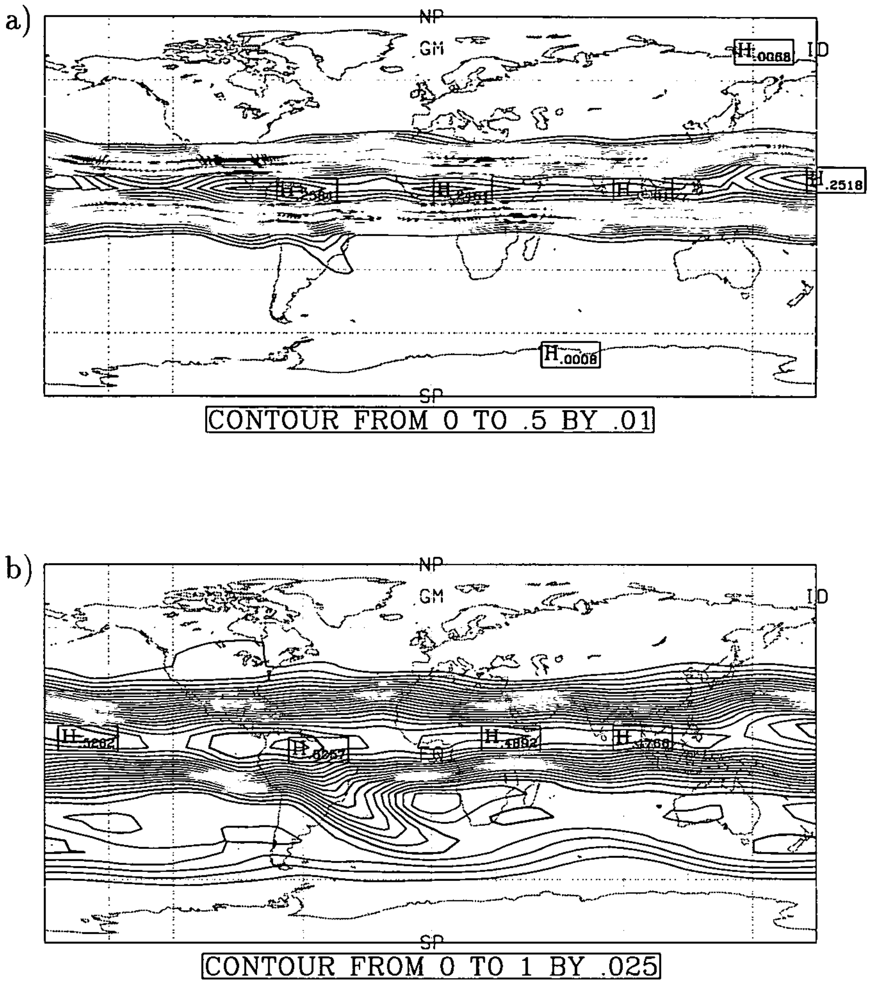

Figure 5.14: Global isentropic map (latitude-longitude) of tracer mixing ratio (vmr) at θ=550K (approx. 30mb) on day 35 (July) of the model run: a) Tracer 1 and b) Tracer 3.

weaker PV gradient exists.

The next plot (Figure 5.14b) is of Tracer 3, which was the tracer initialised over the latitudes 20°S to 30°N, the same latitude range which the Pinatubo cloud covered a month after the eruption. Even though material has reached the southern mid-latitudes, a clear distinction exists between the tropical stratospheric reservoir and the material in the mid-latitudes. The distinction takes the form of a steep gradient in the tracer field up to 20°S (the same position as the southern edge of the main Pinatubo cloud in the real atmosphere), corresponding with a steep gradient in the PV field. Again, an isolated tongue of material is visible, extending from the tropics and, in the case of this tracer, well into the southern mid-latitudes. The only region where the tracer is escaping the tropics is over central South America. At all other longitudes a sharp gradient exists in the tracer field, as it does in the PV field.

From this example, it is fair to say that the strong PV gradient in the tropics is acting like a barrier to transport from the tropics. In addition to this, an area of weaker PV gradient constitutes a break in the barrier through which material can freely flow.

Another feature can be seen in the PV fields in Figure 5.12. There is some kind of disturbance in the PV field at the vortex edge and it is situated in the same longitudes as the break in the PV barrier in the tropics. Whatever the disturbance is, it effectively creates a secondary PV barrier extending from where material is being emitted into the mid-latitudes to the vortex edge and about 90° further east. The tongue of Tracer 3 being detrained from the tropics (Figure 5.14) follows this secondary barrier its full length to the vortex edge. It does this without getting west of the secondary barrier and this is a further indication that, in the EUGCM, steepness of PV gradient can be a reliable measure of where material flow is inhibited.

A striking example of isentropic flow being curtailed by a steep PV gradient can be found in the southern polar vortex, also seen in the last plots. Tracer 3 is well mixed (except for the tongue just discussed) in the surf zone, but is clearly being stopped from progressing further southwards by the vortex edge. There are no significant amounts of tracer inside the vortex at all. Comparing closely Figures 5.12a and 5.14b reveals that the southern edge of Tracer 3's distribution follows exactly the shape of the vortex edge.

A final point from Figures 5.12 and 5.14 relates to the study in section 5.1. These plots spell out why Tracer 3 delivers a more Pinatubo-like distribution (no severe interhemispheric asymmetry) after a year than Tracer 1 does. The sharp gradient of PV over the equator means that any cloud released into the stratosphere north of the equator is going to have difficulty getting into the southern hemisphere. As a result of this, there is no material in the southern tropics for wave breaking events to transport into the mid-latitudes.

This is exactly what has occurred in our example here. The wave breaking event has pulled some material south from the main cloud for both Tracer 1 and Tracer 3, but the event pulls proportionately more of Tracer 3 south than Tracer 1. This is because the highest concentrations of Tracer 3 are situated further south than those of Tracer 1 and so the event is pulling material from an area where the air is richer in Tracer 3.

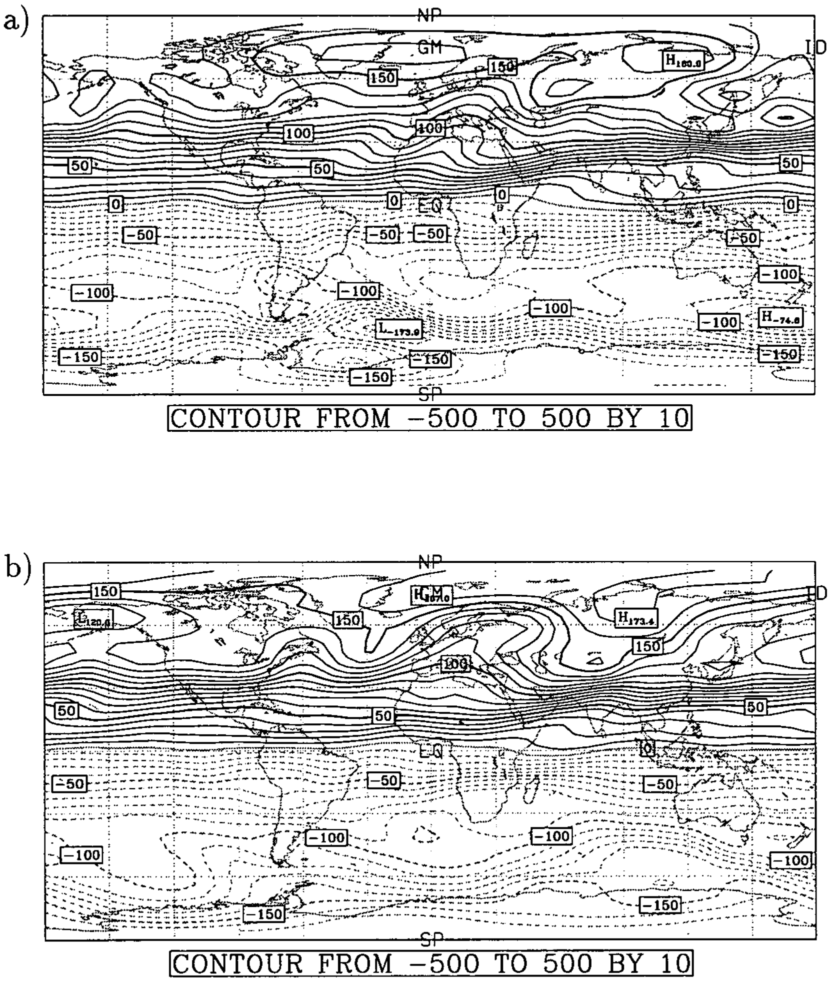

Figure 5.15: Global isentropic map (latitude-longitude) of Ertel's PV (pvu) at θ=650K (approx. 20mb) on days a) 120 and b) 125 (October) of the model run.

The next three plots (Figures 5.15 and 5.16a) are of PV on the isentropic surface, 650 K, and they cover days 120, 125 and 130 of the model run, during which the southern polar vortex breaks down. Figure 5.15a shows that the polar vortex is still present at 650 K, but it is considerably weaker than earlier in the model run. The sharp PV gradient still marks the vortex edge but it is not as

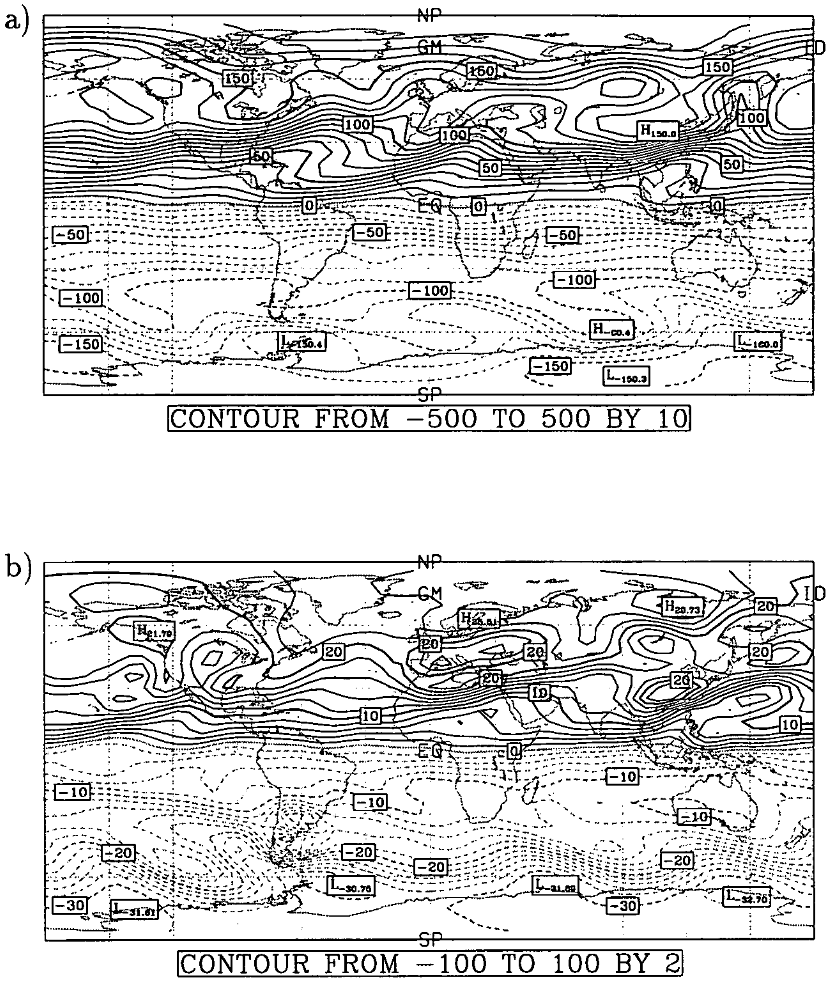

Figure 5.16: Global isentropic map (latitude-longitude) of Ertel's PV (pvu) at a) θ=650K (approx. 20mb) and b) θ=450K (approx. 70mb) on day 130 (October) of the model run.

broad or steep as it was and it is more irregular in nature (compare with Figure 5.13b).

The vortex edge becomes even less well-defined and more irregular as the model run continues (Figure 5.15b). Despite this though, the vortex edge is still identifiable in the PV field on day 125. The area of the surf zone is becoming less obvious.

Five days later the vortex has all but disintegrated. The PV field south of the tropics is highly irregular in nature with only small pieces of what was the vortex wall discernible in Figure 5.16a. Although the vortex has broken down at this height, lower down, at θ = 450 K, the vortex is still fairly coherent (see Figure 5.16b). In fact, the vortex does not break down at 450 K until 10 days later in the model run (not shown here).

During all this time, the tropical PV barrier is still very much in evidence. In fact, it has become broader, covering the entirety of the tropics. The PV gradient in the southern tropics looks more uniform (zonal) than the gradient in the northern tropics. From what we have already said about PV gradients and the inhibition of tracer transport, we could reasonably suppose from this series of PV fields that more material is transported north from the tropics as opposed to south.

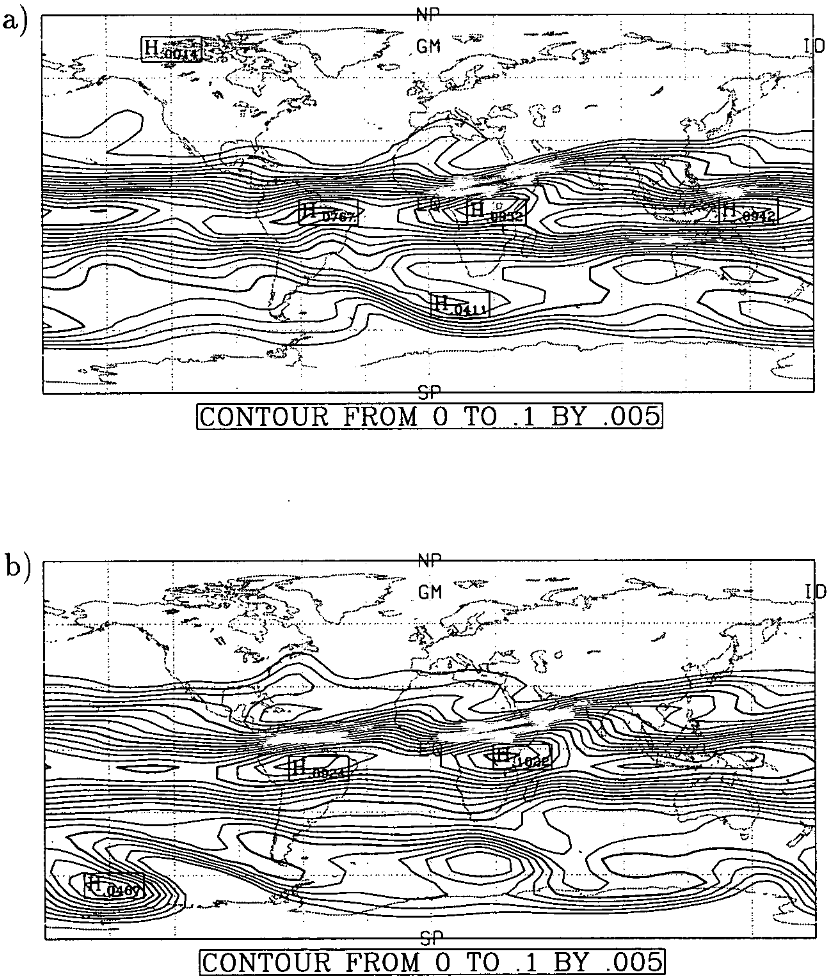

Figure 5.17: Global isentropic map (latitude-longitude) of tracer mixing ratio (vmr) at θ=650K (approx. 20mb) on days a) 120 and b) 135 (Oct/Nov) of the model run: Tracer 2.

The isentropic maps of Tracer 2 featured in Figure 5.17 will allow us to test this supposition. Both fields are on the isentropic surface 650 K, one on day 120, the other on day 135, representing before and after the vortex breakdown respectively. From Figure 5.17a we can see that Tracer 2, which was initialised in the tropics of the southern hemisphere, has been prohibited from entering the southern polar regions. The tracer is fairly well mixed in the mid-latitudes and has a reasonably distinct gradient at the vortex edge where further poleward dispersal is prevented. Two weeks later, after the vortex has broken down, significant amounts of Tracer 2 have reached the southern polar regions (Figure 5.17b). Following this, the tracer soon reaches the south pole (not shown here). This is further evidence that the vortex wall is impenetrable from the outside and material can only enter the polar regions once the vortex has broken down.

We move now to a time when the northern polar vortex has established itself. Figure 5.18 contains two plots of PV on the isentropic surface 650 K for days 205 and 210 of the model run. From these two plots, we can see that the northern polar vortex differs from its southern counterpart in two major ways.

The first difference is that the northern vortex is not centred over the pole. This is not always the case; the centre of the vortex shifting around the northern polar regions sometimes directly over the pole (not shown here). The southern polar vortex, throughout its existence from the beginning of the run, remained centred over the pole at all times. This kind of movement by the polar vortex has been recognised in observations [*Manney and Zurek*, 1993]. The off-pole vortex is better seen using polar stereographic projections, but since the main focus here is the transport of material from the tropics, we will continue to use the cylindrical projection which has been used up until now.

The other difference between the vortices of the two hemispheres is that the southern polar vortex is a lot stronger than the northern one. This too is a recognised feature of the atmosphere [*Schoeberl et al.* 1992].

The feature of the most interest, for the purposes of this investigation, is the wave breaking event which evolves throughout Figures 5.18a and 5.18b. There are actually two wave breaking events into the northern hemisphere at this time, but one is a lot stronger than the other. The strong PV gradient is still in the tropics and extends from 30°S to 30°N. The strong wave breaking event (situated around

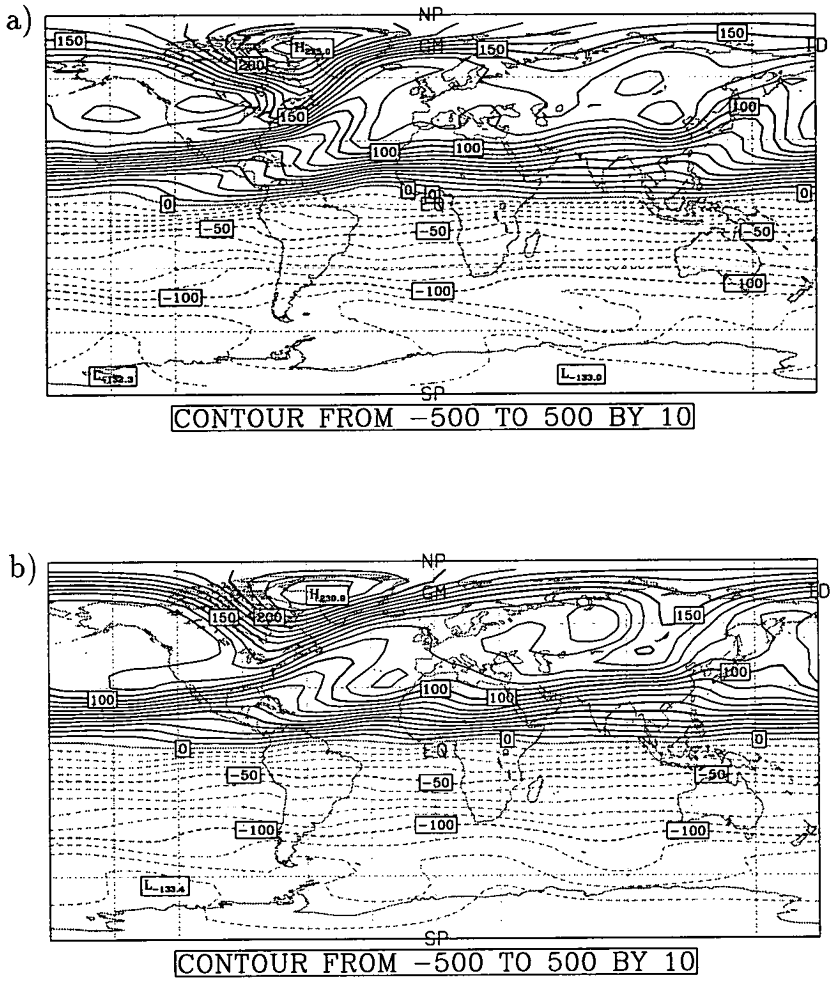

Figure 5.18: Global isentropic map (latitude-longitude) of Ertel's PV (pvu) at θ=650K (approx. 20mb) on days a) 205 and b) 210 (Dec-Jan) of the model run.

60°W) manages to create a channel of weak PV gradient through the tropical PV barrier. This channel starts at the northern sub-tropics and reaches as far as the equator. The second wave breaking event (situated around 150°E) does not penetrate so deep into the tropical PV barrier.

Again, we need to compare the PV fields with those of a tracer in order to see what relation there is between PV gradient and transport in the EUGCM. From what we have seen before we would expect tracer to be flowing from the tropics (from as deep as the equator) into the mid-latitudes via the afore-mentioned channel. Figure 5.19 provides us with the necessary tracer fields for such a comparison. The two plots in Figure 5.19 are exactly the same as the plots in Figure

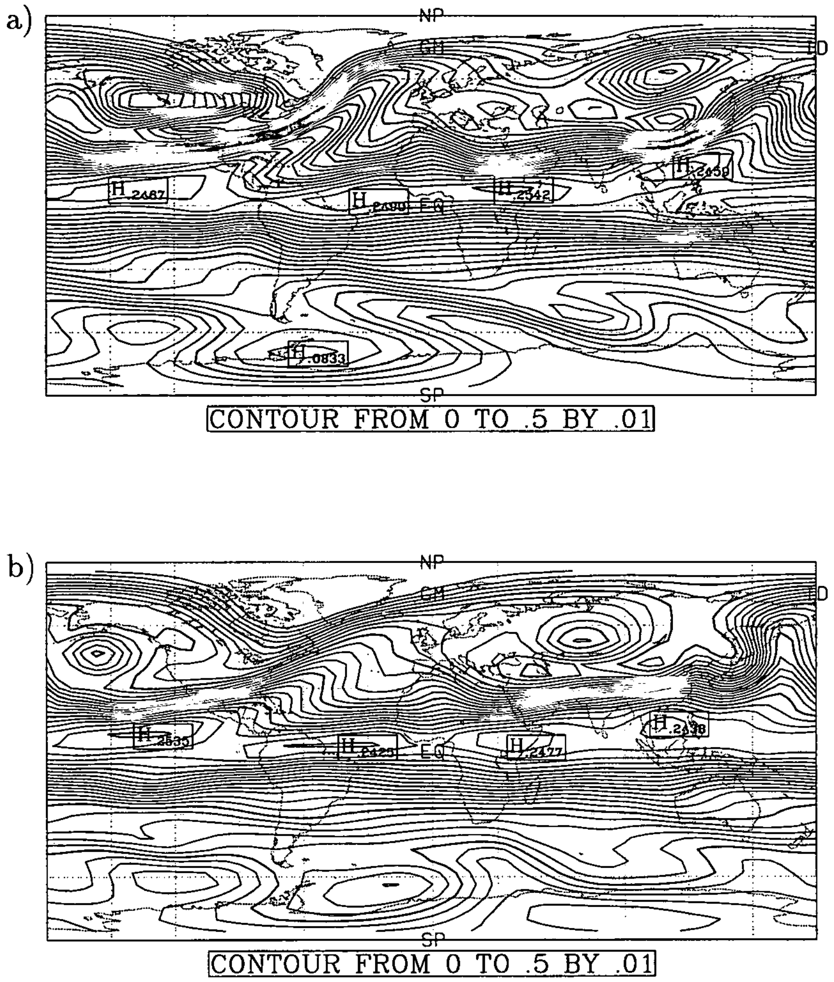

Figure 5.19: Global isentropic map (latitude-longitude) of tracer mixing ratio (vmr) at θ=650K (approx. 20mb) on days a) 205 and b) 210 (Dec-Jan) of the model run: Tracer 3

5.18, except they are of Tracer 3, not potential vorticity.

High tracer mixing ratios are, indeed, being drawn from the equator and along the low-PV channel to eventually form a tongue of tracer-rich air extending from the sub-tropics to the edge of the polar region. The same is true, to a lesser extent, for material being peeled off the tropics by the secondary mixing event. At all longitudes, other than where the tongues of material are extending from, the higher mixing ratios of tracer are confined to the tropics, as demonstrated by the high gradient in the tracer fields corresponding with the position of the high PV gradient.

It also appears that Tracer 3 is being efficiently held from the polar latitudes by the edge of the polar vortex. A situation is occurring which is very similar to that seen in the southern hemisphere in Figure 5.12. At the same longitudes where the tongue of material is extending from the tropics, the vortex edge comes well into the mid-latitudes (Figure 5.18a). A new PV barrier is formed, bridging the mid-latitudes between the sub-tropical PV barrier and the vortex edge. The path of the tongue of tropical air is dictated by this new, oblique PV barrier. The connection between tongues of material being detrained from the tropics and the polar vortex edge reaching low latitudes has also been seen in observations [*Leovy et al.*, 1985].

Following the progress of the tropical air in the mid-latitudes, we can see that some higher values of tracer have broken away from the main tongue and have travelled eastwards (Figure 5.19b). If you compare the tracer field for day 210 with the PV field for the same day, you can see that the tracer-rich air which has detached itself from the tongue corresponds with a similar patch of low-PV air which has been expelled from the tropics in the same mixing event. This is a good example of planetary wave breaking causing irreversible mixing of tropical material into the extra-tropics.

5.2.3 Seasonal variation of PV barriers in the EUGCM

We have seen that PV barriers to eddy advective transport do exist in the EUGCM and are typically situated at the vortex edge and throughout the tropics. It is apparent from the isentropic maps we have just studied that the steepness and thickness of these high PV gradients varies. For example, the tropical PV barrier in July of the model run covered a narrower latitude range than the one we saw about six months later in January (around day 210). The intention here is to characterise the variation in the attributes of the tropical PV barrier throughout the model run and to do this we will be using time series of zonally averaged PV at different isentropic heights.

The plots in Figure 5.20 are time series of the zonal mean of PV for the two isentropic surfaces, θ=450K and θ=650K. The time series start at the beginning of the model run and end on day 360, so almost an entire year is represented in each plot.

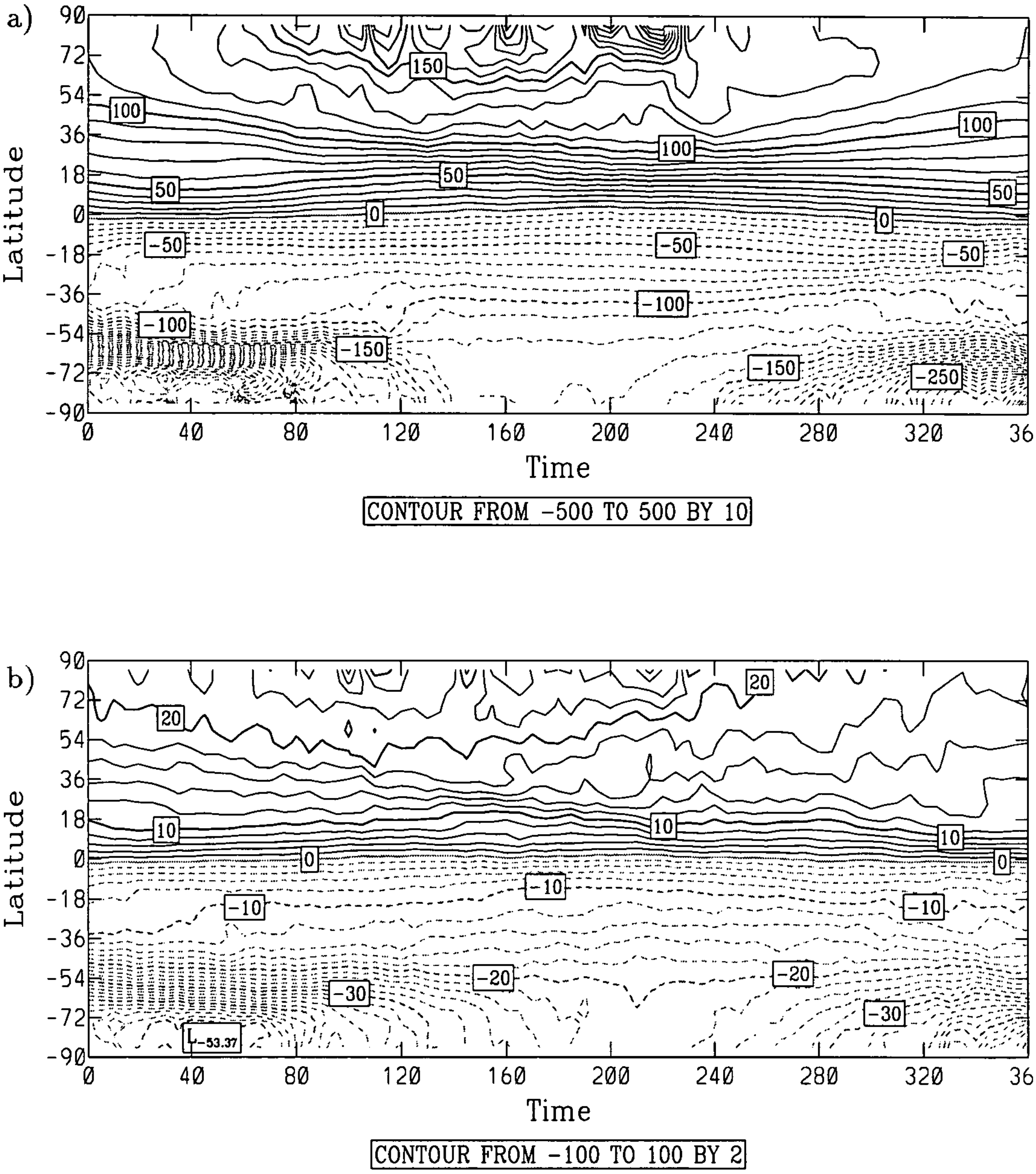

Figure 5.20: Time series over the 360 days of the model run of zonally averaged Ertel's PV (pvu) at isentropic heights of a) 650K (approx. 20mb) and b) 450K (approx. 70mb) .

Both plots show that the southern polar vortex is stronger and lasts longer than the northern polar vortex. The northern polar vortex looks particularly weak because it drifts off the north pole sometimes and the zonal mean does not give a proper impression of the local gradient at any particular longitude.

There is a clear seasonal variation in the PV gradients in the tropics at 650K (Figure 5.20a). The gradient over the equator is constant throughout the year; it is the sub-tropics where the variation occurs. In the northern sub-tropics, at the beginning of the run, there exists a PV gradient which is not as steep as the equatorial one. This sub-tropical gradient becomes steeper and narrower during the boreal winter. After the winter the gradient relaxes again and eventually reattains values similar to those at the start of the run. In the southern sub-tropics, a very similar thing happens. The broader, lesser gradient occurs in the austral winter and this gradually narrows down as the austral summer approaches.

Although the same thing seems to happen for the sub-tropical PV barrier of each hemisphere, it differs in a subtle way. In the northern hemisphere, the contours contained in the sub-tropical gradient remain the same throughout the year, whether the barrier is relaxed in the summer or steeper in the winter. The same is not true of the southern hemisphere. From austral winter to summer, the contours of the sub-tropical barrier do tighten slightly, but eventually leave the barrier and become part of the vortex edge. This means that, while the sub-tropical gradients of the respective summers of each hemisphere are very similar, the winter gradient in the southern hemisphere is virtually non-existent, compared with the strong gradient in the northern winter. This means that a steep PV barrier spans the entire northern tropics in boreal winter while a barrier, just as steep, spans only half the distance in the southern tropic during austral winter. The cause of this difference can be put down to the planetary waves being more active in the northern hemisphere winter than they are in the southern hemisphere winter.

Lower down in the stratosphere, at 450K (Figure 5.20b) the seasonal variation in tropical PV is not nearly as noticeable. The equatorial gradient is the dominant feature of the tropics, throughout the model run. The fact that the variation in the tropical PV gradients is a lot weaker than higher up is an interesting one and is good evidence that planetary wave breaking is the cause of the seasonal variation in the sub-tropical PV gradient. The planetary wave breaking is more prominent at 650 K than 450 K and this would explain why the seasonal variation is stronger at 650 K.

Evidence of steep PV gradients over the equator has been reported in the literature [*Chen et al.* 1994]. Figure 5.21 was produced from the same source of PV fields (UKMO analyses) as used by *Chen et al.* The plot is a time series of PV gradient from November 1991 to March 1994 at an isentropic height of 655K. The polar vortices of each hemisphere can easily be identified from this plot; further confirmation that the southern polar vortex lasts longer than its northern counterpart.

The equatorial PV barrier is clear and there is a distinct variation in strength with respect to time. There is strong evidence which links the strength of the equatorial PV barrier to the phase of the Quasi-Biennial Oscillation (QBO) [*Morrey*, personal communication]. Currently, the EUGCM does not reproduce the QBO and this could prove to be a serious issue with respect to tracer transport in the stratospheric tropics. Section 7.3.1 in the conclusions chapter discusses the QBO.

Another possible explanation if the equatorial PV barriers in the model are too strong is the lack of equatorial Kelvin waves. Some waves (Kelvin waves) cannot be resolved at the equator as the vertical resolution of the model is not adequate. This would mean that the tropics of the model are not as stirred up as the real atmosphere.

Note that there is also evidence in Figure 5.21 of the sub tropical PV barriers, but they are not as predominant as the equatorial one. There is a tightening and broadening of the sub-tropical PV barrier, depending on the season, similar to that seen in the EUGCM.

In this section it has been shown that PV gradients do act as a barrier to isentropic transport in the EUGCM. A PV barrier does exist in the sub-tropics but also over the equator, meaning that cross-equatorial transport is inhibited (the root of the interhemispheric asymmetry problem when simulating the Pinatubo cloud).

We now proceed to make a more quantitative comparison between the equatorial PV gradients in the EUGCM with those in the real atmosphere.

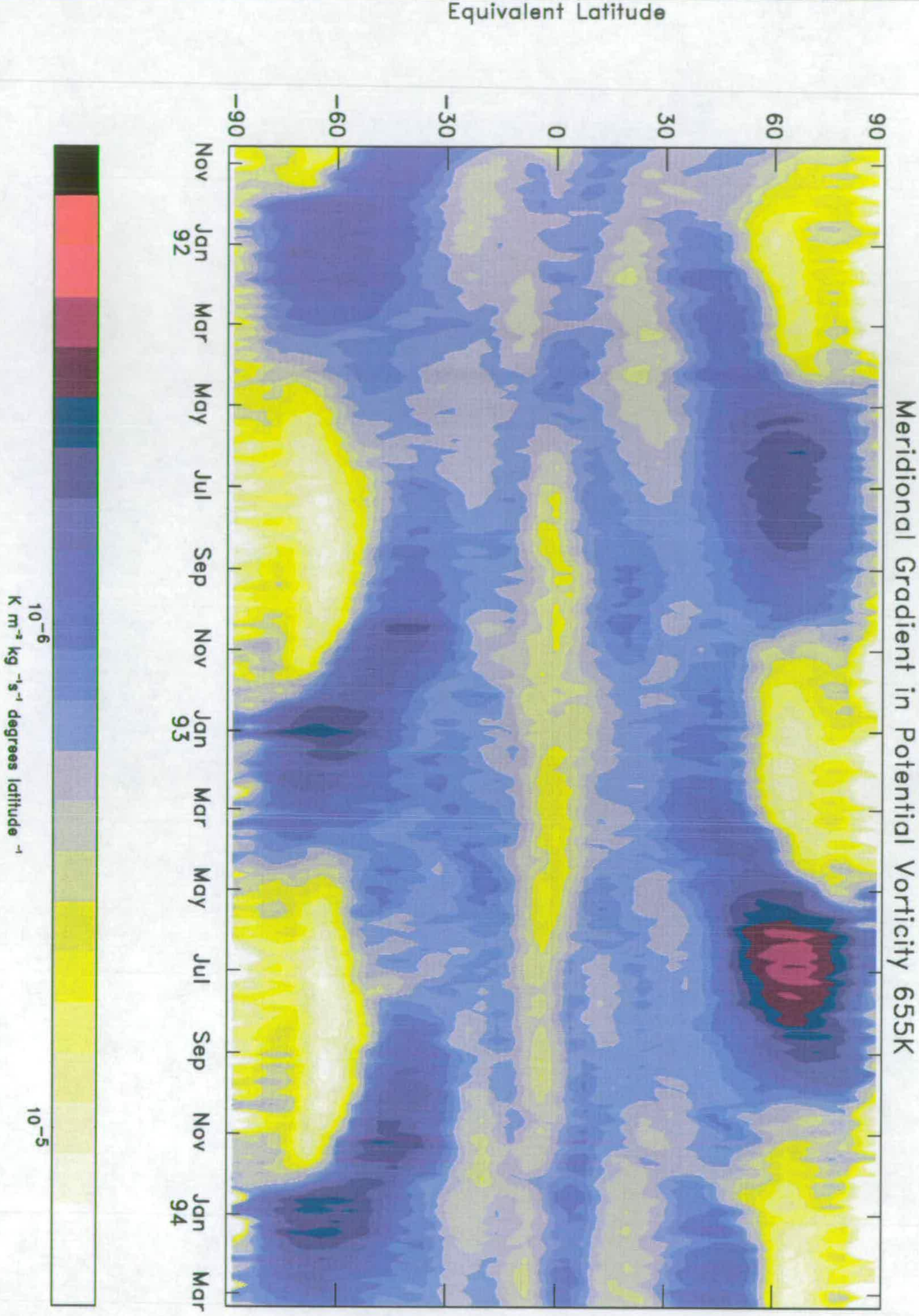

Figure 5.21: Time series of PV gradient ($\mathrm{Km^{-2}kg^{-1}s^{-1}}$degrees latitude^{-1}) at an isentropic height of 655 K (approx. 20mb). The lighter colours on the map represent areas of steep, meridional PV gradients. The PV is derived from UKMO analyses. This figure was produced by Martin Morrey and is used here with his permission.

5.3 Investigating equatorial PV barriers in the EUGCM

From our results, we see that there is good evidence to suggest that steep gradients of PV in the model are inhibiting meridional transport. In the Pinatubo experiment, material was inhibited to such a degree that an unrealistic, inter-hemispheric asymmetry developed in the tracer fields. The aim of this section is to establish whether the PV barriers observed in the EUGCM are too strong. If they are, then we want to find out why this is the case.

5.3.1 Comparison between the EUGCM and ECMWF analyses

We now need to determine how the equatorial gradients of PV in the model compare with those in the real atmosphere. To do this, we return to the ECMWF analyses which were used for our initial comparison between the model and the observed stratosphere in sections 4.3.2 and 4.3.3. Figures 5.22 and 5.23 show time series of the zonally-averaged, meridional PV gradient on the isentropic surface, 550K, taken from the model and analyses respectively. The isentropic surface 550K (approx. 30mb) is used throughout this section as this is the height at which most material entered the southern mid-latitudes in the first few months following the eruption of Mt. Pinatubo. The lighter areas of the plot are those with the steepest meridional PV gradients.

You can see from comparing Figures 5.22 and 5.23 that, in general, the model is producing stronger equatorial PV gradients than those seen in the analyses. In particular, the model has much steeper PV gradients at the beginning of the model run, January and the end of the model run (June). During the boreal winter, the steepest PV gradients are situated approximately 8° further north in the model than they are in the analyses. The subtropical PV barriers are in evidence in both plots, although they are less distinct in the model. There is good agreement southwards of 20°S and to a lesser degree northwards of 20°N.

Since our main concern is that there is a lack of cross-equatorial transport in the model in the first months of the Pinatubo simulation, a more quantitative comparison of this period is useful. Figure 5.24 shows the structure of the merid-

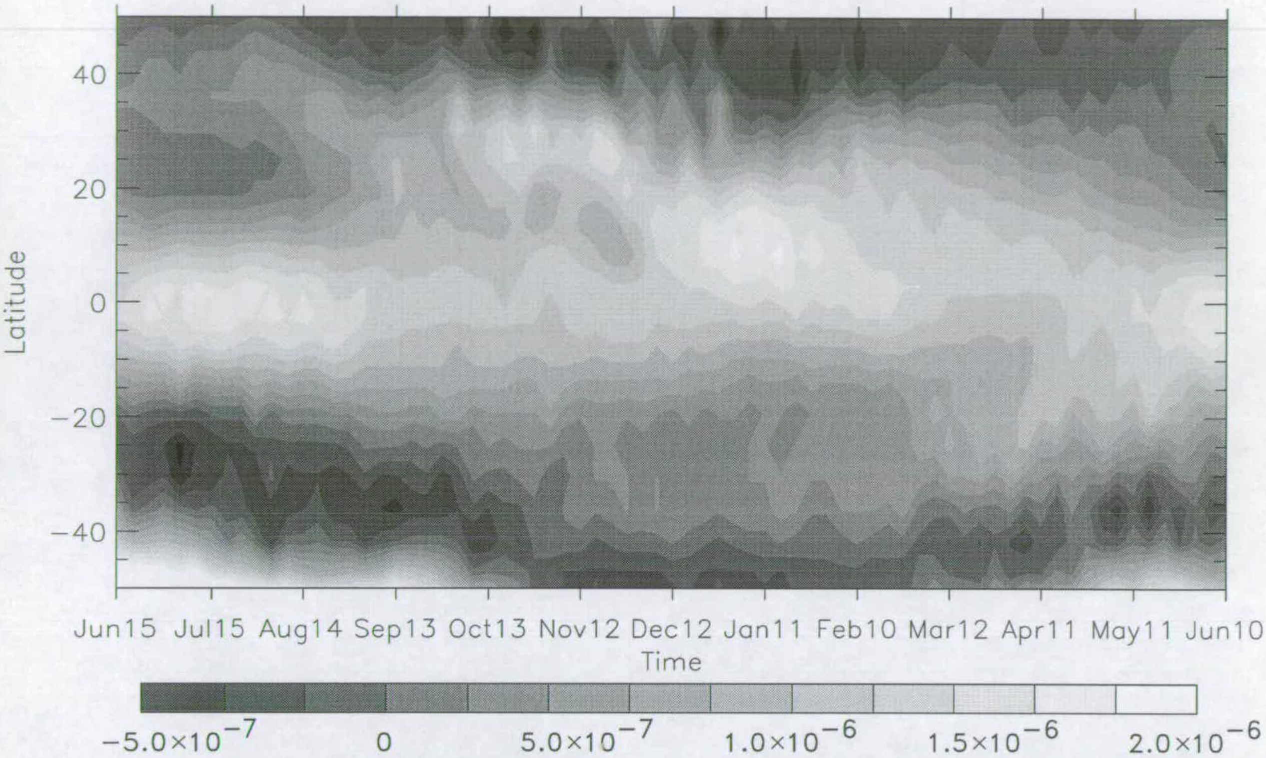

Figure 5.22: Time series of the meridional gradient of PV ($Km^{-2}kg^{-1}s^{-1}$degrees latitude^{-1}) on the isentropic surface 550K, taken from the EUGCM model. The latitude range of the plot is limited to 50°S to 50°N.

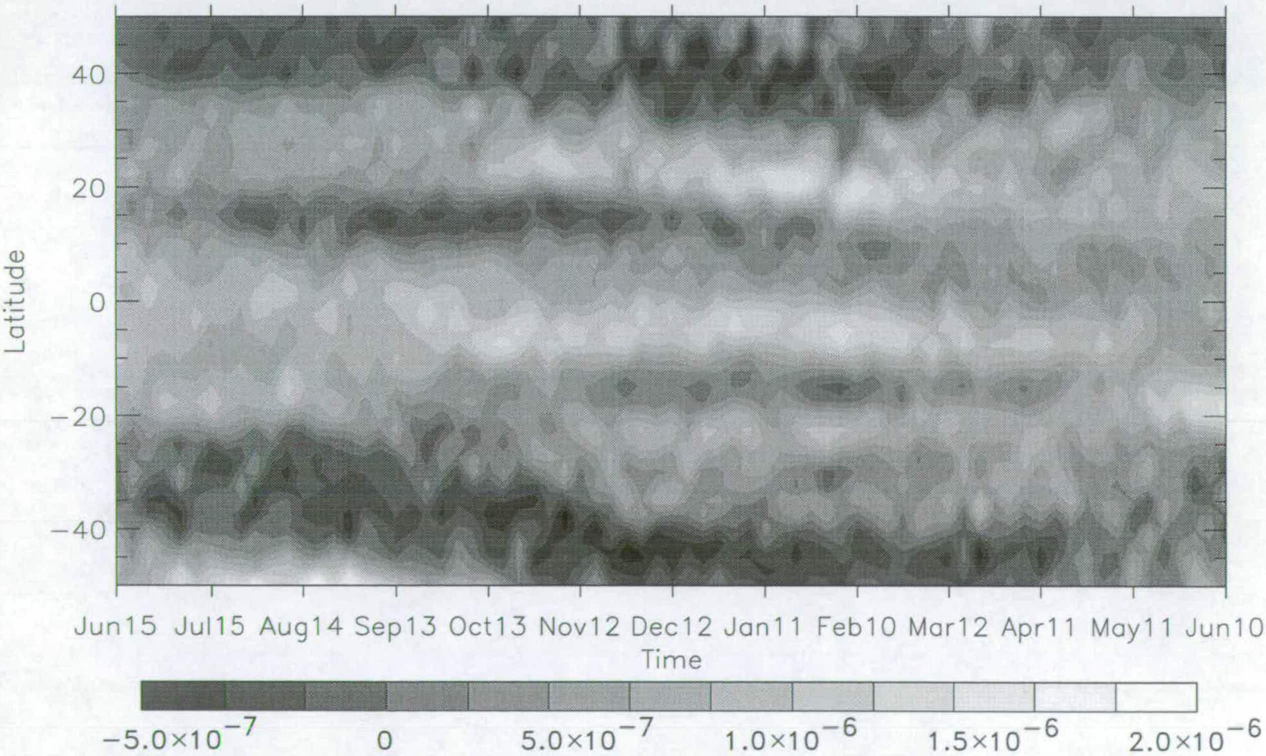

Figure 5.23: Time series of the meridional gradient of PV ($Km^{-2}kg^{-1}s^{-1}$degrees latitude^{-1}) on the isentropic surface 550K, taken from the ECMWF analyses. The latitude range of the plot is limited to 50°S to 50°N.

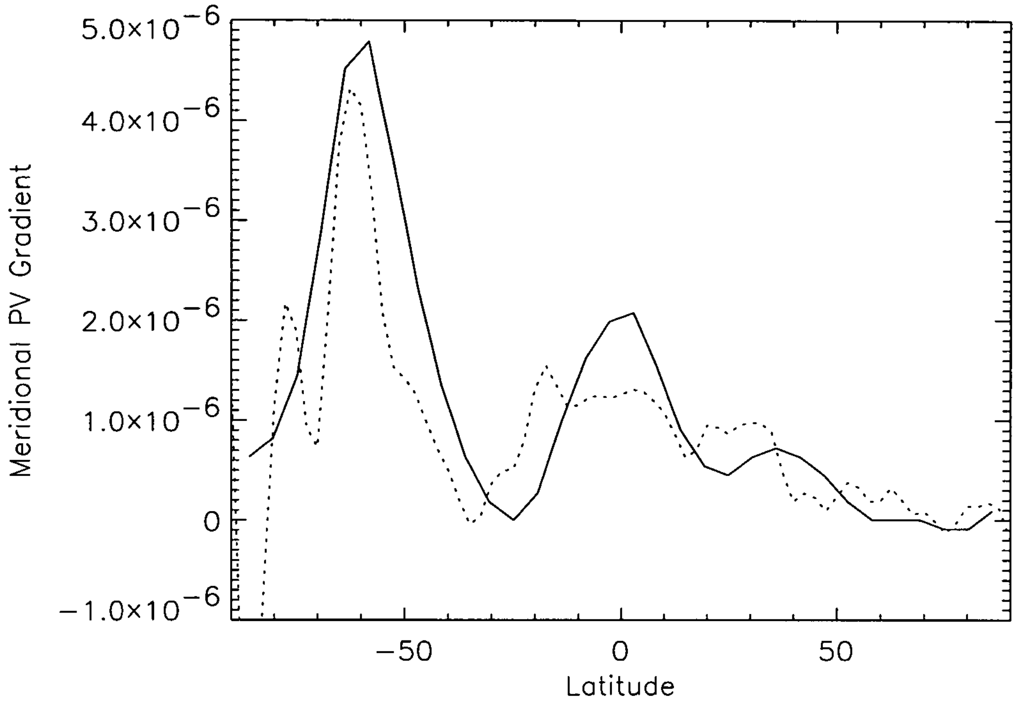

Figure 5.24: The meridional gradient of the zonal mean PV ($Km^{-2}kg^{-1}s^{-1}$degrees latitude^{-1}) with respect to latitude on the isentropic surface 550K, for the 30th June. The solid line is model data and the dotted line is the ECMWF analyses.

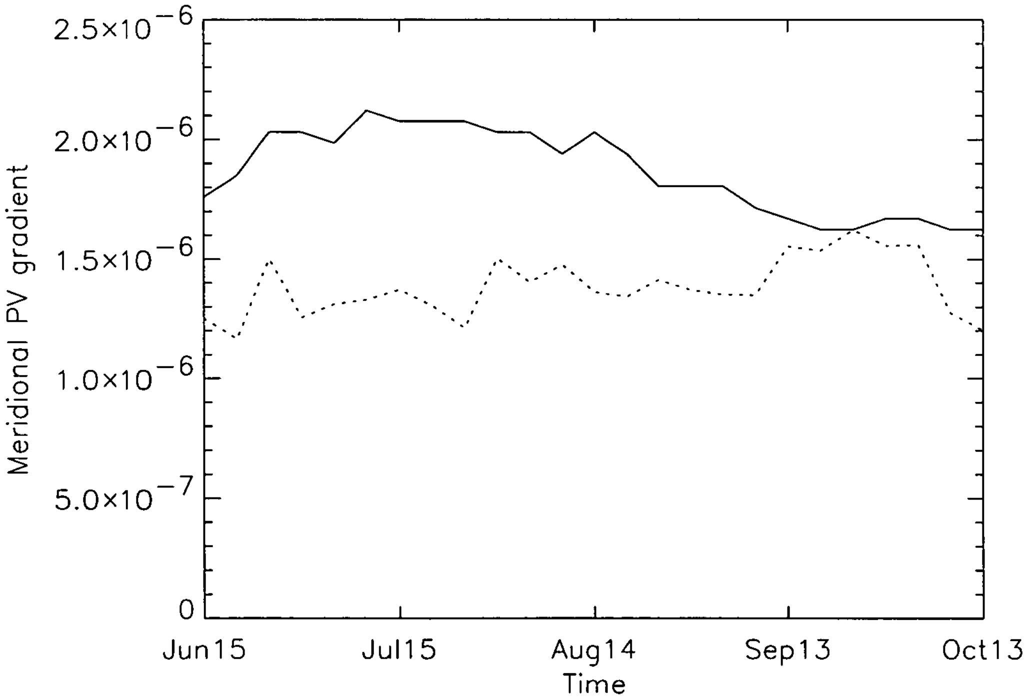

Figure 5.25: The meridional gradient of the zonal mean PV ($Km^{-2}kg^{-1}s^{-1}$degrees latitude^{-1}) with respect to time on the isentropic surface 550K, for the first 4 months following the Mt. Pinatubo eruption. The solid line is model data and the dotted line is the ECMWF analyses.

ional PV gradient with respect to latitude for both the model and the analyses on the 30th of June, just over two weeks after the eruption. Again, we can see that the equatorial PV barrier is stronger in the model than the analyses. What is clearer in this graph however, is that the sub-tropical PV gradients are a bit stronger in the analyses than the model. It does appear though, that the most obvious difference between the two data sets is over the equator. This difference over the equator is fairly consistent for the first few months following the Mt. Pinatubo eruption as can be seen in Figure 5.25. In the crucial first month following the eruption, the meridional PV gradient is approximately 50% greater in the model than in the ECMWF analyses.

5.3.2 Theoretical nature of PV barriers

We have now seen that the equatorial PV barriers in the model differ from those in the ECMWF analyses. Of particular relevance to the Pinatubo experiment is that the PV barriers in the model are significantly stronger in the months following the eruption than they are in the analyses. We need to determine why the model is not reproducing the PV barriers in a satisfactory manner. To do this we will compare the ECMWF analyses data and the model run further (next section), but first we use the ECMWF analyses to identify what quantities are important when considering high meridional gradients of PV, particularly in the tropics.

Figure 5.26 shows the meridional PV gradient with respect to latitude for the same date from two different years taken from the ECMWF analyses. The equatorial PV barrier for March 1993 is much stronger than that for the previous year. We confine this particular investigation to these two distinct cases; one with a strong equatorial PV gradient and the other with a weaker equatorial PV gradient.

Consider the isentropic-coordinate form of Ertel's potential vorticity taken from *Holton*, [1992]:

$$Q = (\zeta_\theta + f)(-g\partial\theta/\partial p) \tag{5.1}$$

where ζ_θ is the relative vorticity and f = $2\Omega\sin\phi$ is the Coriolis parameter. To make this analysis a bit simpler we shall consider the zonally averaged (with

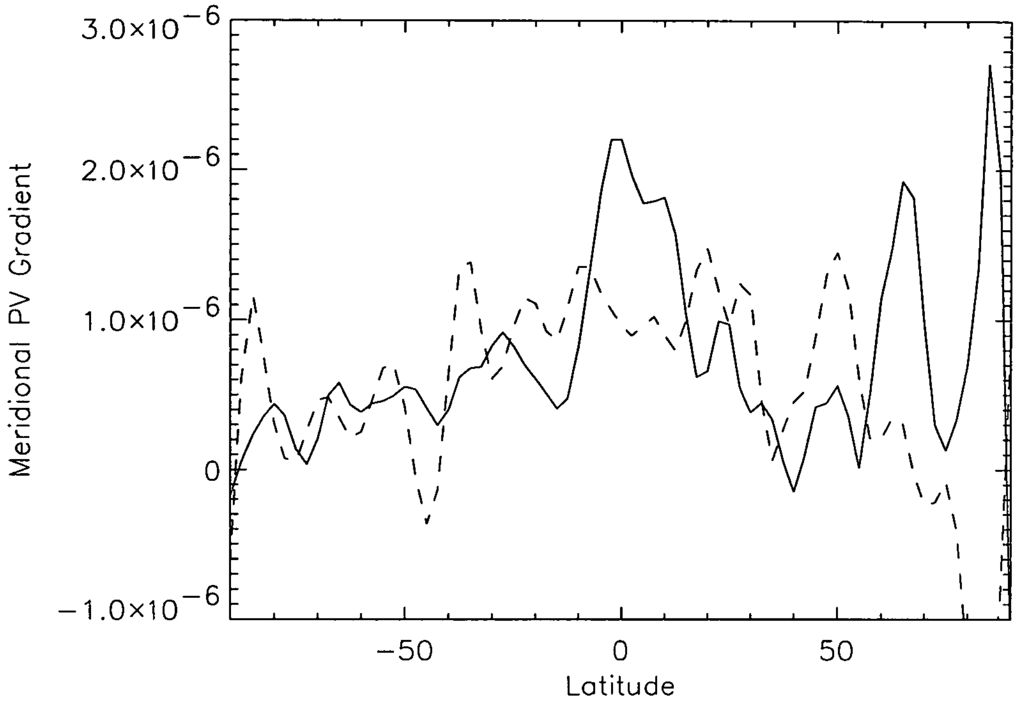

Figure 5.26: The meridional gradient of the zonal mean PV (Km^{-2}kg^{-1}s^{-1}degrees latitude^{-1}) with respect to latitude on the isentropic surface 550K taken from the ECMWF analyses. The dashed line is March 22nd, 1992, and the sold line is March 22nd, 1993.

respect to θ) PV:

$$\bar{Q} = (\bar{\zeta_\theta} + f)(-g\partial\theta/\partial\bar{p}) \tag{5.2}$$

Since we are trying to determine the significant terms contributing to the meridional gradient of PV we differentiate equation 5.2 with respect to latitude, ϕ:

$$\frac{\partial\bar{Q}}{\partial\phi} = \frac{\partial(\bar{\zeta_\theta} + f)}{\partial\phi}(-g\partial\theta/\partial\bar{p}) + (\bar{\zeta_\theta} + f)\frac{\partial(-g\partial\theta/\partial\bar{p})}{\partial\phi} \tag{5.3}$$

Before breaking these terms down further, we make an initial comparison between the two terms on the right-hand side of equation 5.3. We will call $\frac{\partial(\bar{\zeta_\theta}+f)}{\partial\phi}(-g\partial\theta/\partial\bar{p})$ "Term 1" and $(\bar{\zeta_\theta} + f)\frac{\partial(-g\partial\theta/\partial\bar{p})}{\partial\phi}$ "Term 2". Figure 5.27 compares these two terms for the case with the strong equatorial PV gradient taken from the ECMWF analyses. The data is taken from the isentropic surface 550K. We can see from this graph that the first term has the most impact on the gradient of PV, particularly over the equator.

This means that we can ignore Term 2 and focus on Term 1 in our search for the significant terms behind PV gradients. Figure 5.28 compares the meridional gradient of absolute vorticity with Term 1 (the meridional gradient of absolute

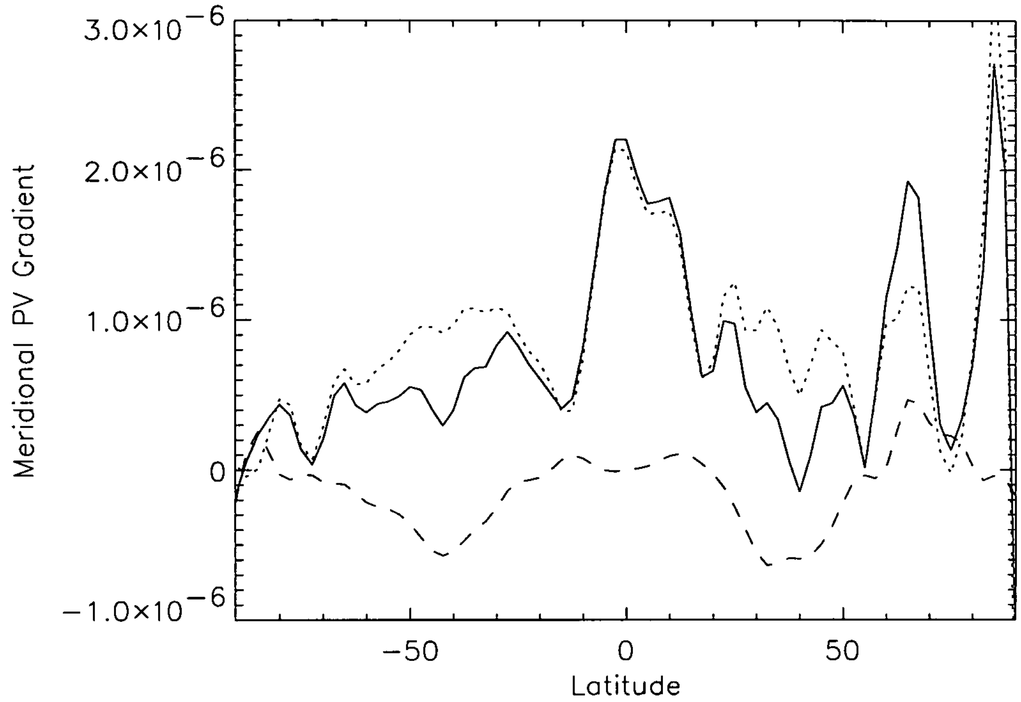

Figure 5.27: Comparison between the terms of equation 5.3. The data is taken from the ECMWF analyses at a height of 550K and is for March 22nd, 1993. The solid line is the meridional PV gradient ($Km^{-2}kg^{-1}s^{-1}$degrees latitude^{-1}), the dotted line is Term 1 from the right-hand side of the equation, and the dashed line is Term 2.

vorticity multiplied by the static stability). We can see that there is good correlation between the two terms and so we can conclude that the static stability has very little influence over whether there is a steep PV gradient or not.

So far we have seen that the meridional gradient of PV agrees closely with the meridional gradient of absolute vorticity. We now look at the different terms which make up the gradient of absolute vorticity. The gradient of absolute vorticity (zonally averaged) can be expressed:

$$\frac{\partial(\bar{\zeta}_\theta + f)}{\partial\phi} = -\frac{\partial(\partial\bar{u}/\partial y)}{\partial\phi} - \frac{\partial(\{\bar{u}\tan\phi\}/a)}{\partial\phi} + \frac{\partial f}{\partial\phi} \tag{5.4}$$

where a is the distance from the centre of the earth. The three terms on the right-hand side of equation 5.4 are plotted in Figure 5.29 for the scenario with steep equatorial PV gradients. From this plot we can see that there are two terms contribute greatly to the gradient of the absolute vorticity at the equator; the gradient in the Coriolis parameter and the gradient in the meridional wind shear. We know that the gradient of the Coriolis parameter is not going to vary with time, but the strength of the PV barriers does. We can conclude from this

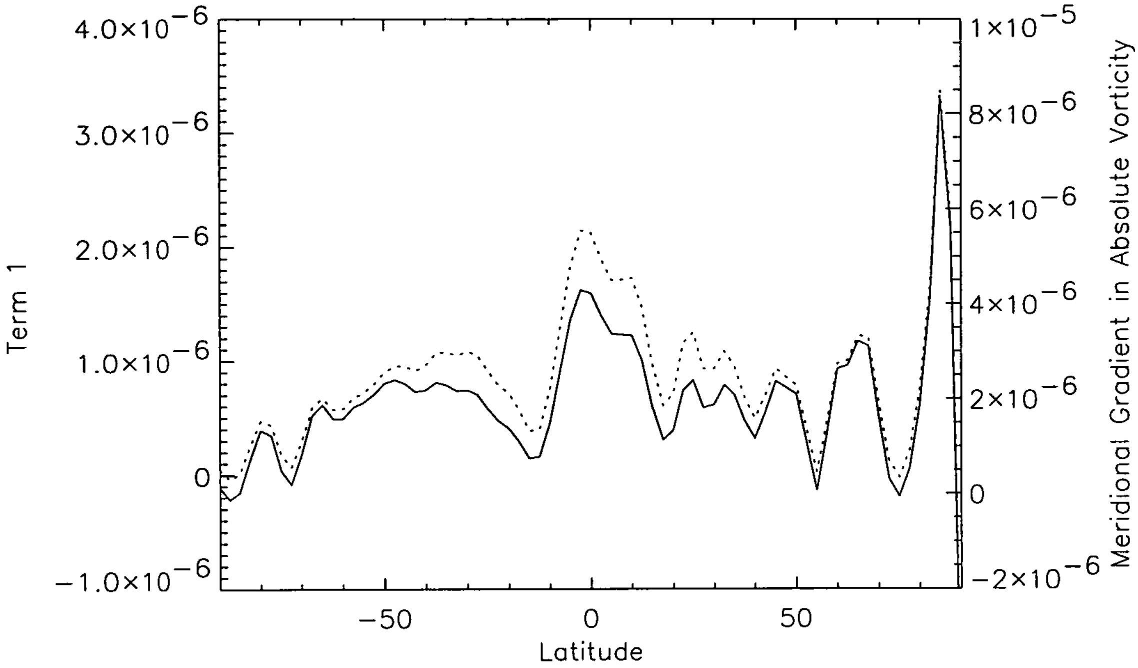

Figure 5.28: The data is taken from the ECMWF analyses at a height of 550K and is for March 22nd, 1993. The solid line is the meridional gradient of absolute vorticity (s^{-1}degree latitude^{-1}), the dotted line is Term 1 (Km^{-2}kg^{-1}s^{-1}degrees latitude^{-1}).

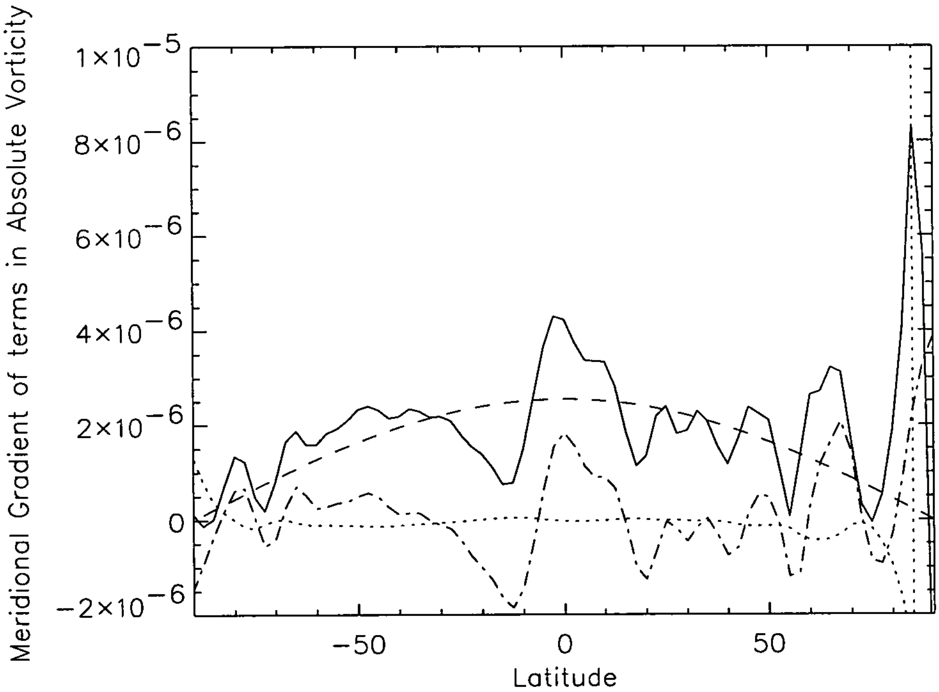

Figure 5.29: The data is taken from the ECMWF analyses at a height of 550K and is for March 22nd, 1993. The solid line is the meridional gradient absolute vorticity (s^{-1}degree latitude^{-1}), the dashed line is the gradient of the Coriolis parameter, the dot-dashed line is the term containing the gradient of meridional wind shear and the dotted line is the gradient of the term containing tan in equation 5.4

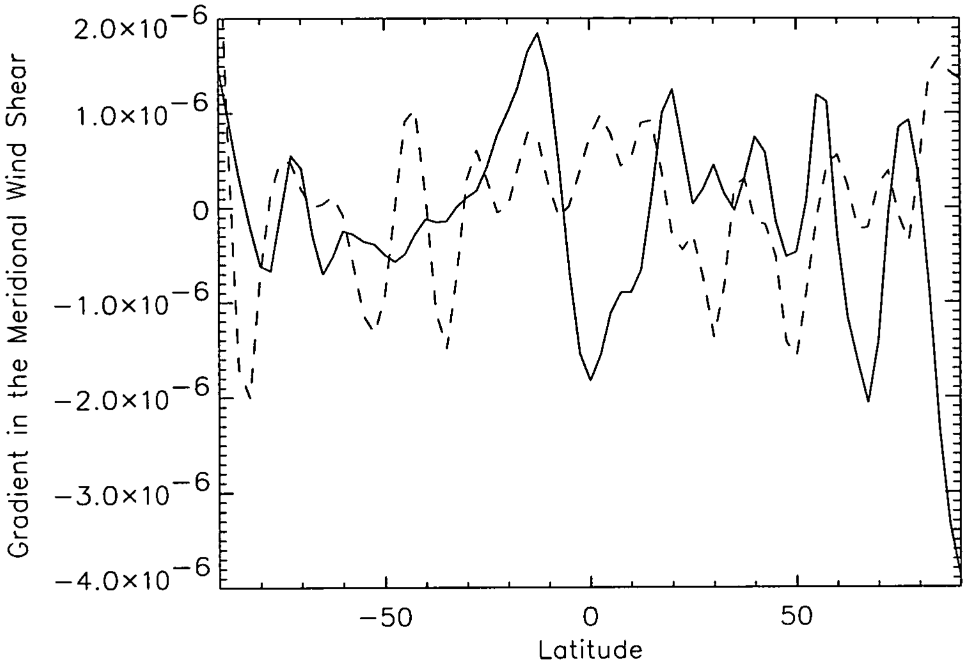

Figure 5.30: The gradient in meridional wind shear (s^{-1}degree latitude^{-1}) taken from the ECMWF analyses at a height of 550K. The solid line is for the case with strong equatorial PV barrier (March 22nd, 1993) and the dashed line is for the year before - the case with the weaker PV barrier.

that the gradient in the meridional wind shear is the significant dynamical term affecting the equatorial PV barriers. Steep PV gradients occur over the equator in the presence of steep negative gradients of meridional wind shear.

For confirmation, we compare the gradient in the meridional wind shear for the days with and without the strong equatorial PV gradients (see Figure 5.30). For the case with the strong equatorial PV barrier, the gradient in the meridional wind shear is strongly negative, while the case with the weaker equatorial PV gradient has a positive gradient in the wind shear over the equator.

Now we have a good idea under what conditions tropical PV barriers will appear. With this information we conduct another comparison between the ECMWF analyses and the EUGCM, but focusing on the the structure of zonal winds in the tropics.

5.3.3 Further comparison between model and analyses

Comparing the ECMWF analyses with the equivalent fields from the model run will hopefully give us some insight into why the model is failing to properly reproduce the PV barriers. We continue to pay particular attention to the first few

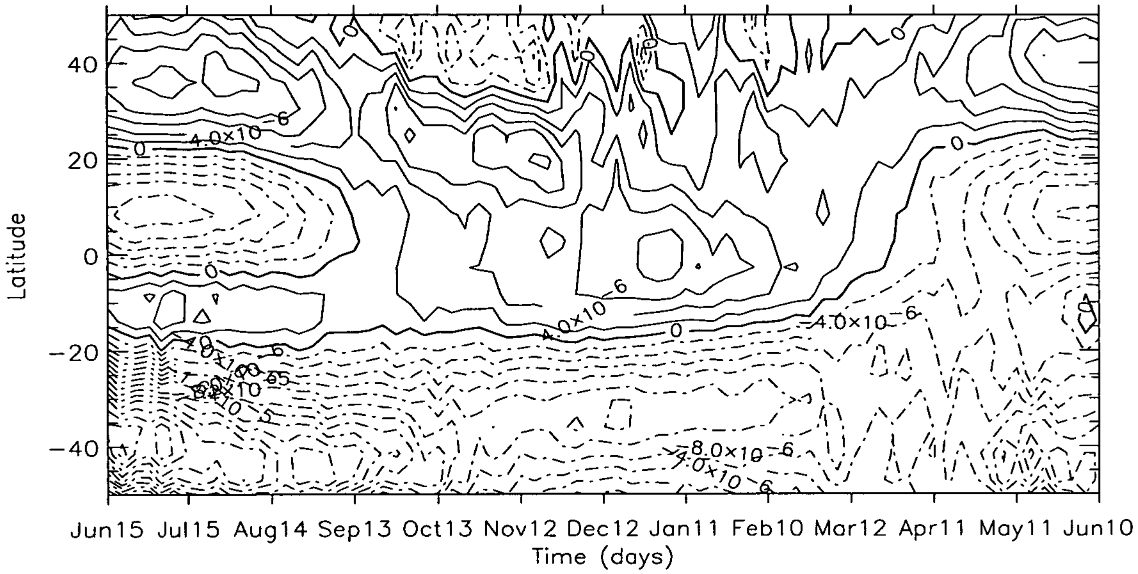

Figure 5.31: Time series of the meridional shear in zonal wind (ms^{-1}degree latitude^{-1}) at a height of 550 K (approx. 30mb) taken from the EUGCM. The latitude range of the plot is limited to 50°S to 50°N. The contour interval is 2×10^{-6}ms^{-1}degree latitude^{-1}.

months after the eruption, when cross equatorial transport is the most crucial. We have established that the equatorial PV gradient is strongly related to the gradient in the meridional wind shear; steep PV gradients occur when the gradient in meridional wind shear is steep and negative. Bearing this in mind, we look at the meridional wind shear first.

Figures 5.31 and 5.32 show time series of the gradient in zonally-averaged, zonal wind at a height of 550K for the model and the analyses respectively. You can see that the areas of steep, negative gradients in Figures 5.31 and 5.32 correspond well with the areas of large PV gradients in Figures 5.22 and 5.23 respectively. We turn our attention again to the first few months after the eruption, when the PV barriers in the model are too strong, compared to those in the ECMWF analyses. At this time in the model there is positive meridional wind shear situated in the southern tropics, while negative wind shear occurs in the northern tropics. This scenario means that a negative gradient in meridional wind shear exists over the equator, and hence steep, equatorial PV gradients occur. In ECMWF analyses, at the equivalent time, there is no positive wind shear anywhere in the tropics.

During the boreal winter, the scenario introduced above (westerly shear south

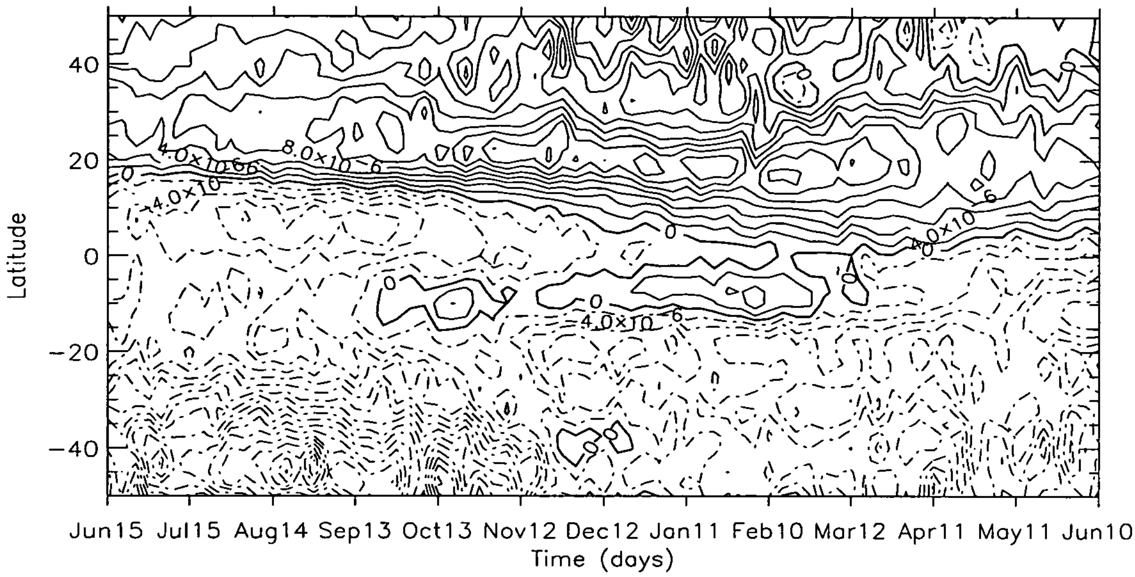

Figure 5.32: Time series of the meridional shear in zonal wind (ms^{-1}degree latitude^{-1}) at a height of 550 K (approx. 30mb) taken from the ECMWF analyses. The latitude range of the plot is limited to 50°S to 50°N. The contour interval is 2×10^{-6}ms^{-1}degree latitude^{-1}.

of the equator and easterly shear north of the equator) is in evidence in the analyses and this corresponds well with the enhanced PV gradients we see at this time in Figure 5.23. At this time in the model however, the tropics are dominated by westerly shearing, the maximum of which is situated on the equator. This gives a negative gradient in the wind shear north of the equator which is why we saw the PV barrier in the model further north than the analyses.

Nearly a year after the start of the model run, the structure of the meridional wind shear looks very similar to that at the beginning of the run. Westerly shearing in the southern tropics can just be made out. Again, the analyses at this time do not contain this positive, meridional wind shear. So, the problem of producing realistic equatorial PV barriers persists throughout the model run although it matters most for the simulation in the first months following the eruption of Mt. Pinatubo.

To find why the meridional gradient of horizontal wind shear should be so different in the model than it is in the analyses we look at time series of zonally-averaged zonal wind in both the model and analyses (Figures 5.33 and 5.34). In the first few months after the eruption the difference between the model and analyses is quite striking. In the model there is a split in the easterly jet over the

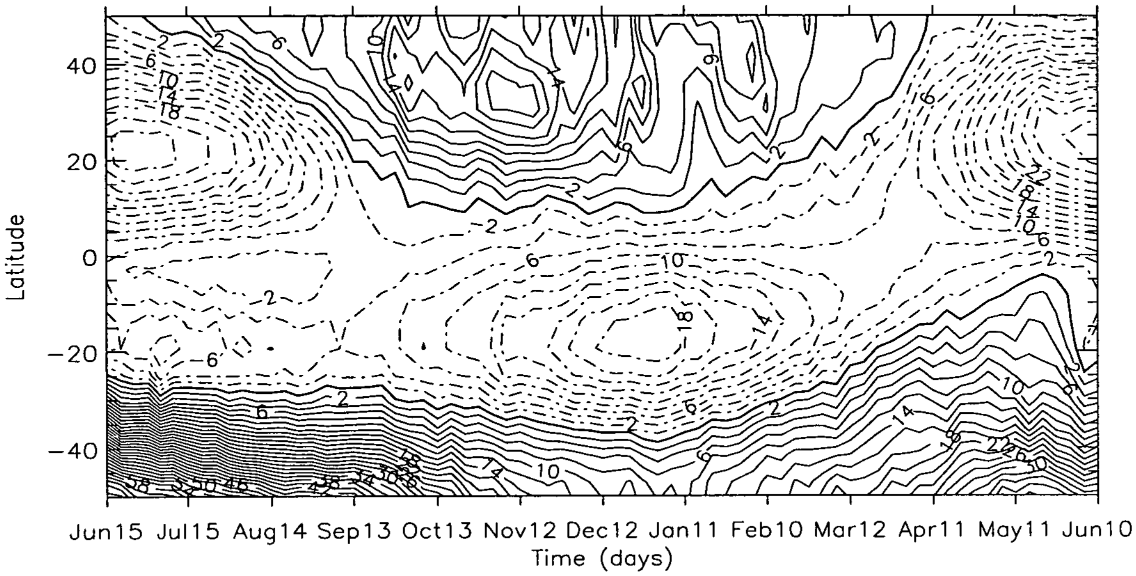

Figure 5.33: Time series of zonally averaged zonal wind (ms^{-1}) at a height of 550 K (approx. 30mb) taken from the EUGCM. The latitude range of the plot is limited to 50°S to 50°N. The contour interval is 2 ms^{-1}.

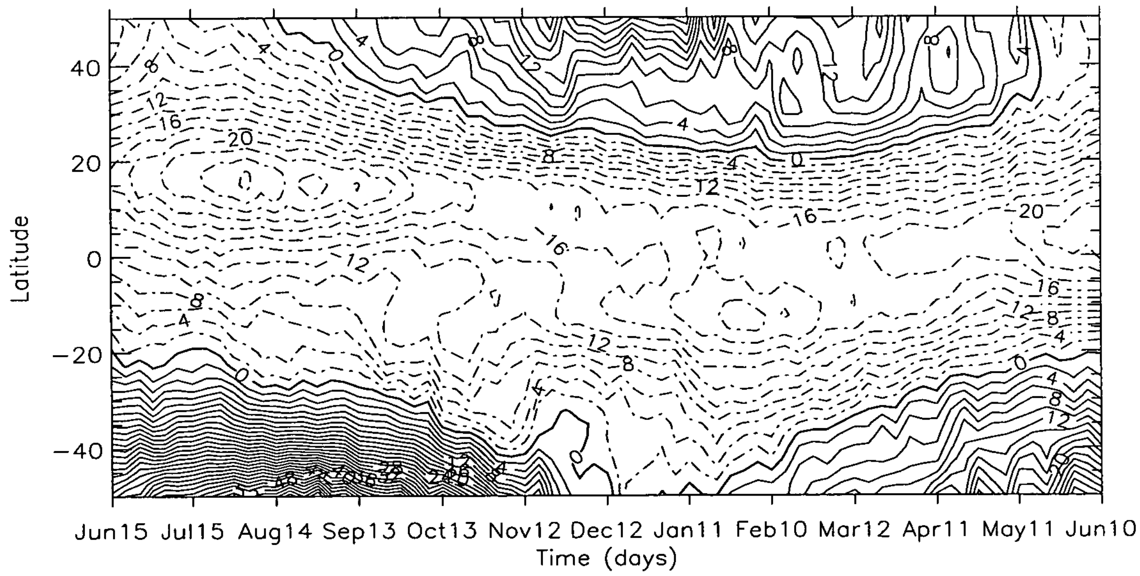

Figure 5.34: Time series of zonally averaged zonal wind (ms^{-1}) at a height of 550 K (approx. 30mb) taken from the ECMWF analyses. The latitude range of the plot is limited to 50°S to 50°N. The contour interval is 2 ms^{-1}.

equator which is not present in the analyses. It is this split in the jet which is causing the negative gradient in the meridional wind shear, and hence the strong PV barrier over the equator. For future experiments, care should be taken to ensure that the model is initialised with more realistic zonal winds, particularly at the altitudes where we expect most quasi-horizontal transport to occur.

5.4 Summary

Through a number of different tracer experiments, the EUGCM has been tested for dynamical features highlighted by the experiment in Chapter 4; the general aim being to investigate why the tracer dispersal in the EUGCM did not look like the Pinatubo aerosol in the real atmosphere.

It has been shown that the poleward dispersal of tracer is sensitive to the initial distribution in the tropics. Specifically, it is the variation of latitude which has a large impact on the final global distribution of material. The reason for this sensitivity to the latitudes over which the tracer is initialised was narrowed down to a lack of cross equatorial transport, particularly important in the first month of the model run. The comparison between Tracer 1 and Tracer 2 showed how striking the difference in tracer spread is when releasing material in the tropics of different hemispheres. From this work we could also see that the lack of cross-equatorial transport applied to tracer moving northwards as well as material moving southwards.

Tracer 3 demonstrated that if the Pinatubo tracer had achieved a realistic distribution in the tropics during the first month of the model run then a much more satisfactory global distribution would have been achieved after a year. It was seen that most mixing into the southern mid-latitudes occurred in the first month of the model run. If the radiative experiments in the next chapter do show an improvement in the tropical distribution of material (more goes into the southern tropics) in the 2-D model then we can conclude that this would improve the interhemispheric asymmetry in the EUGCM if the same heating was applied.

The evolution of Tracer 4 showed us that releasing a tracer at a higher altitude had little effect on the rate of poleward dispersal. This has implications for the next chapter which deals with the effects of radiative heating caused by the volcanic aerosol. According to this result, if the tracer was lofted to higher altitudes due to radiative heating then it would not affect the interhemispheric asymmetry of the tracer spread.

An investigation into the existence and effectiveness of PV barriers in the EUGCM revealed that a strong equatorial gradient of PV was the cause of material not crossing the equator. The model showed that sub-tropical PV barriers also existed and were inhibiting the transport of material from the tropics, thus maintaining the tropical stratospheric reservoir of volcanic tracer. Steep gradients in tracer fields were seen to correspond strongly with the steep gradients in PV fields. The sub-tropical PV gradients have a seasonal variation in steepness and width which is related to Rossby wave mixing. It was also shown that the vortex edge in the EUGCM is impermeable to transport of material from the mid-latitudes.

A further investigation into the strength of equatorial PV gradients in the model was carried out, using the ECMWF analyses as a basis for comparison. The model was found to have stronger equatorial PV barriers than the analyses, particularly in the first few months of the model run. Having determined that the structure of meridional wind shear was closely related to steep gradients in PV, the zonal winds in the model and analyses were examined. This revealed a split in the easterly jet over the equator in the model which was not present in the analyses, causing the enhanced equatorial PV barrier at the start of the model run. It is recommended for future experiments of this kind that the zonal winds used to initialise the model should be chosen with this in mind.

The EUGCM needs to be able to recreate the variation in strength of the equatorial PV barrier for the Pinatubo simulation (or any other tracer experiments involving trace gases around the tropics) to be accurate. Relating to this, a discussion on the effects of the QBO on tracer spread is included in the conclusions chapter. The next chapter deals with the effects of radiative heating due to volcanic aerosol on the spread of tracer in the tropics.

Chapter 6

Radiative Effect of Volcanic Aerosol on the Stratosphere

Chapter 4 showed that while the model was able to represent many facets of the evolution of the Mt. Pinatubo cloud, a large, unrealistic interhemispheric asymmetry occurred. Chapter 5 went on to state that if the cloud distribution in the tropics had been between 20°S and 30°N after a month (as seen in observations), then the distribution of the cloud after a year would not have such a severe hemispheric asymmetry. This chapter offers one solution to encourage cross equatorial transport in the model run.

So far the model experiments conducted in this thesis have neglected the effects of radiative heating due to the volcanic aerosol cloud. This chapter addresses the importance of such radiative heating on the stratosphere and ultimately on the distribution of the volcanic cloud itself. More specifically, the following hypothesis is tested; radiative heating due to the volcanic cloud promotes transport into the southern mid-latitudes from the tropics. If this is the case then mixing events into the southern mid-latitudes would have a richer source of tropical aerosol to draw from, improving the problem of asymmetry.

There are some conflicting opinions regarding this problem in the literature. *Young et al.* [1994], state that radiative heating is essential for accurately simulating the Mt. Pinatubo cloud but a good simulation by *Boville et al.* [1991], is achieved without the aerosol heating. Section 6.1 discusses these papers and other related literature associated with radiative heating.

The above hypothesis will be tested using a 2-D model, briefly described in section 6.2. The reason for using this model instead of the EUGCM is computational expense. Also, forcing the EUGCM with heating where the aerosol is situated, is not a trivial exercise. A simpler experiment was designed for the 2-D model to determine whether it is worthwhile to include heating in the EUGCM.

After some preliminary experiments presented in Section 6.3, we look at the difference between the evolution of two different tracers; one without additional heating, and one with extra heating. This experiment is the focus of this chapter and is detailed in Section 6.4.

6.1 Review of radiative heating due to volcanic aerosol

The fact that temperature increases occur in the stratosphere after volcanic eruptions is already well documented. The increase of stratospheric temperatures in the tropics after the Pinatubo eruption, as detailed by *Labitzke and McCormick* [1992] (see also Figure 4.2 in Chapter 4) would suggest an increase of about 2 to 4 Kelvin by October, 1991.

There have been a number of studies of heating rates due to volcanic aerosols: *Young et al.* [1994], *Kinne et al.* [1992], *Kinnison et al.* [1994], *Lacis et al.* [1992], *Lary et al.* [1994] and *Brasseur and Granier* [1992] to name a few. These studies differ in the treatment of aerosol size and whether solar radiation is important compared to infrared radiation.

Lacis et al. [1992] have computed the sensitivity of radiative heating to effective particle radius for aerosol layers in the stratosphere. They conclude that most factors can be ignored when calculating radiative heating of volcanic aerosol with the exception of optical thickness (how much aerosol there is) and particle size. They note that infrared heating is a strong function of particle size, an important factor considering the findings of *Kinne et al.* [1992].

Kinne et al. [1992] placed the heating rates due to the Pinatubo cloud in the order of tenths of Kelvin per day. They assign the cause of this heating to the absorption of upwelling infra-red (IR) radiation. In fact, they state that compared to the IR heating, the solar heating of the cloud is negligible. However, *Lary et al.* [1994] make a strong case for including the effects of solar heating of the SO_2 before it is converted into the sulphate aerosol. The heating rates calculated in

Lary et al., though short lasting, are about 1 K/day which could significantly alter the transport processes affecting the cloud transport.

Kinnison et al. [1994] calculate radiative heating due to volcanic aerosol also. Within the simulated cloud they have droplets of size 0.8 microns, 0.3 microns and 0.07 microns (background aerosol). In this experiment solar heating was not ignored. In fact, it contributes to just under half the total resulting radiative heating. This takes into account both the findings of *Kinne et al.* and *Lary et al.* and offers a compromise between the two.

Kinnison et al. estimate the peak radiative heating due to solar and infrared as 0.35 K/Day. According to their calculations using a 2-D model, this represents either a rise in temperature of 5-6K or a diabatic vertical velocity of 1.6 km per 100 days; in the real atmosphere, it would be a combination of the two effects. *Brasseur and Granier* [1992] assumed radiative heating of 0.4 K/day in the centre of the cloud, causing the cloud to rise 0.5km in 100 days. *Kinne et al.* [1992], using a radiative transfer model, calculated the radiative heating to be 0.3 K/day, mainly due to the absorption of infrared radiation. In a further simulation using a numerical model of the stratosphere, the calculated heating rate results in a 3°C rise in temperature after 90 days and the ozone profile is lifted by about 2km in 140 days. *Kinne et al.* also point out the importance of radiative heating in relation to the speed at which chemical reactions occur.

Using a combined 3-dimensional circulation model and aerosol microphysical/transport model, *Young et al.* [1994] show that radiative heating due to upwelling UV radiation from the troposphere can be very important in relation to the final distribution of the volcanic cloud. Two experiments were carried out. One simulation has the volcanic cloud as a passive tracer (as we did in Chapter 4) while the other has the cloud causing radiative heating. A particle size of 0.6 microns is assumed. This particle size is a compromise between ash particle size and aerosol particle size. The contribution to radiative heating by solar radiation is assumed to be negligible.

Without the effect of radiative heating, the volcanic cloud remains mostly north of the equator, the same problem we encountered in Chapter 4. When radiatively heated, the cloud is transported south of the equator within the first two weeks of the simulation. Indeed, following day 18 there was no more southward movement, so it appears that the first few weeks are crucial for the tropical distribution and ultimately, the global distribution of volcanic material. This experiment also showed temperature perturbations caused by aerosol heating within 1 to 4K of what was observed. *Young et al.* put forward the idea that the meridional circulations induced by aerosol heating were responsible for the transport of the cloud south of the Equator in the real atmosphere

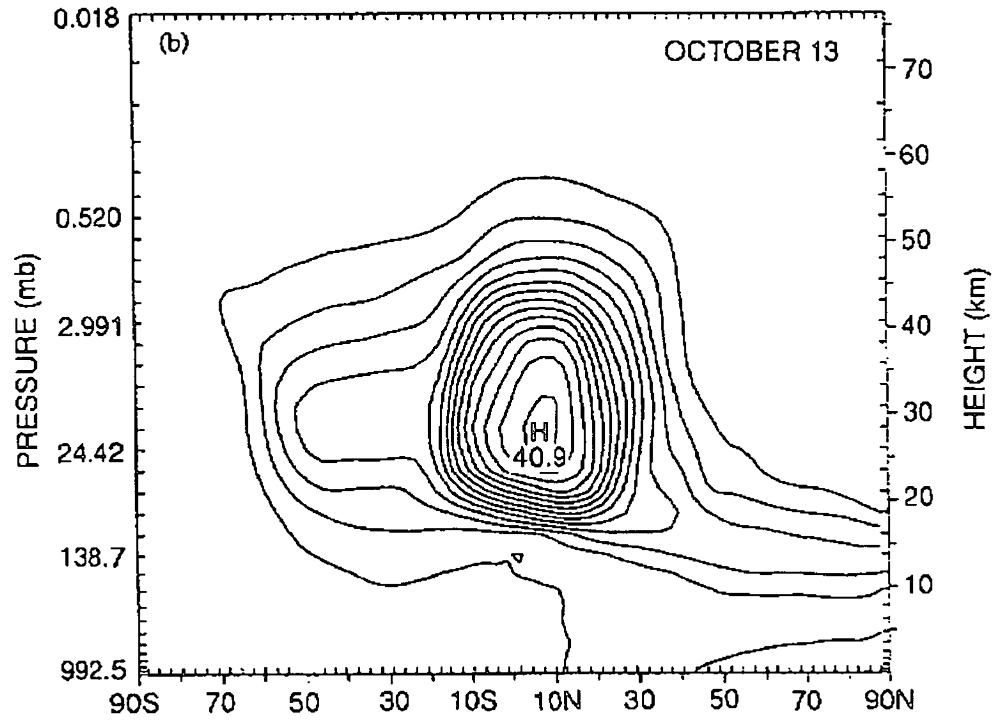

Figure 6.1: Latitude-height cross section of zonally averaged tracer mixing ratio (ppbv) on October 13 of the model run presented in *Boville et al.* [1991].

While *Young et al.* stressed the necessity of including aerosol heating in volcanic cloud simulations, previous studies have shown that the heating is not necessary for a good simulation. The experiment presented in *Boville et al.* [1991] is a good example of this. A passive tracer is initialised in a spectral general circulation model with an annual cycle. The fairly smooth tracer distribution was injected into the model stratosphere over the location of Mt. Pinatubo on model day June 15. The results of the model run show that in the first month, the tracer spreads throughout the tropics to a similar extent as seen in the real atmosphere. By October of the model run tracer has mixed well into the southern mid-latitudes (see Figure 6.1) and at a higher altitude than the northward mixing which is in good correspondence with real measurements. Throughout the simulation no additional heating was applied at all, and yet the tracer has no problem in transporting south across the equator in the first few weeks.

From this review we have seen that there is a lot of evidence to suggest that the dispersal of the volcanic cloud is affected by radiative heating. Most sources point towards the cloud being lifted to higher altitudes, but *Young et al.*, focusses on the heating enhancing the meridional circulation to promote the latitudinal spread of the cloud. It has also been demonstrated however [*Bolville et al.*, 1991], that it is not necessary to include the effects of radiative heating to simulate the evolution of the cloud accurately.

With conflicting opinions in the literature, it was decided to conduct our own experiment to establish the degree of importance that radiative heating has on the global distribution of volcanic material during simulated studies. The experiments use a simpler, more cost-effective, 2-D model with a view to following up the work by returning to the EUGCM if necessary. The interactivity between the radiation, dynamics and chemistry in the model will allow us to make a pertinent contribution to one side of the debate in the literature; is the inclusion of aerosol heating necessary to accurately simulate the volcanic cloud or not?

6.2 Description of the 2-D model

The model used for this experiment is an interactive chemical-dynamical isentropic two-dimensional model. A comprehensive description of the model can be found in *Kinnersley and Harwood* [1993], but the following summarises the important points.

The domain of the model extends from the ground to 100km and pole to pole. The vertical resolution is approximately 4km and gridpoints are about 9.6 degrees of latitude apart in the horizontal (20 from pole to pole).

The zonal mean temperature and zonal wind are both held on isentropic surfaces in the model. They are assumed to be in geostrophic balance at all times. This balance can be upset in two ways; the evolution of the temperature field due to radiative heating and wave drag on the zonal wind. The wave drag itself is due to both large-scale planetary waves and short scale gravity waves, calculated interactively in the model.

The thermal wind balance needs to be maintained and so a meridional circulation is required. The meridional circulation is calculated and used to update the zonal wind and temperature fields with a one hour time step. Of particular interest to us is that the meridional circulation is also used to update the modelled trace gases (including the Pinatubo like cloud) using an upwind advection scheme. The trace gases are also diffused along the isentropic surfaces where the planetary waves satisfy the breaking criterion (see below).

The radiation is handled in the following way: the heating due to absorption of solar radiation is calculated every 10 days using the O_2, O_3, and NO_2 calculated by the model. The scheme described by *Haigh* [1984], is used to calculate the heating due to absorption of solar energy near the infrared by H_2O, CO_2, O_2, CH_4 and NO_2. The same scheme is also used to calculate longwave cooling due to ozone, water vapour and nitric oxide. All the above calculations use the mixing ratios determined by the model. The heating rates are used to establish the evolution of temperature throughout the atmosphere.

The evolution of the zonal asymmetry in PV for the three longest planetary waves is explicitly modelled. The waves are forced near the tropopause using observed data. The waves are damped mechanically when the meridional PV gradient is locally negative. This is deemed to be wave breaking. This also results in the meridional diffusion of trace gases in the same region in the model. Horizontal winds are obtained by using the geostrophic balance condition to invert the PV for each wave. The horizontal winds are then used to integrate the non-linear PV equation with a 1-hour time step.

The gravity waves are assumed to be emitted from the troposphere in the model. They propagate vertically and when they become convectively unstable they are damped mechanically resulting in a drag on the zonal wind. The various properties of the waves (including emission probabilities and zonal wavelength) were determined through a combination of observations (which are rather limited) and tuning to give a fairly realistic model behaviour. The orographically-generated winds propagate through the zonally asymmetric model state defined by the zonal

Tracer	Latitude Range	Settling Velocities	Extra Heating
Tracer A	20°S - 20°N	No	No
Tracer B	20°S - 20°N	Yes	No
Tracer C	Equator - 30°N	Yes	No
Tracer D	Equator - 30°N	Yes	Yes

Table 6.1: Brief description of the four different tracer distributions used throughout this chapter.

mean winds and the three modelled planetary waves.

One of the most important aspects of this model is the interaction between dynamics, radiation and chemistry. This should provide us with realistic feedback when perturbing the heating rates due to the volcanic cloud; a property which gives this study considerable weight in the debate about the effect radiative heating on the transport of the volcanic cloud.

The 2-D model is going to be used specifically to ascertain the effects of radiative heating due to the volcanic aerosol on the dispersal of the volcanic cloud. Before conducting the main experiments we need to establish how results from the 2-D model will relate to the EUGCM volcanic cloud simulation.

6.3 Preliminary experiments

A number of different tracers will be used in the 2-D model, each with different attributes. The main features of each tracer are laid out in Table 6.1. The main experiment is a comparison between the evolution of two identical tracer distributions, one with additional heating (Tracer D) and the other without (Tracer C). Prior to this comparison, we investigate whether the tracer without heating is subject to the same interhemispheric asymmetry in the 2-D model as was found in the EUGCM (section 6.3.2). To do this, Tracer C will be compared to the Pinatubo Tracer from Chapter 4. A further consideration is the inclusion of settling velocities for the aerosol particles in the model run. The EUGCM managed to simulate the Pinatubo cloud reasonably well with respect to altitude without settling velocities, but the situation for the 2-D model proves to be different in this respect (section 6.3.1). Tracers A and B are used for this investigation.

Ideally, for the heating experiment to be relevant to the EUGCM, the 2-D model should demonstrate a similar latitudinal dispersion of inert tracer as the

EUGCM simulation did. If the same interhemispheric asymmetry in the tracer fields occurs then we can better judge how the aerosol heating will affect the interhemispheric asymmetry in the EUGCM.

Before this though, we are going to consider the issue of the settling velocities of the aerosol particles. The EUGCM simulation of the cloud did not suffer too much through the lack of settling velocities, the main problem was the lack of cross-equatorial transport and so the settling velocities did not concern us. However, as we will see in the 2-D model, the problems caused by the lack of settling velocities cannot be so easily ignored.

6.3.1 Settling velocities

The experiment here involves comparing the spread of two tracers with identical distributions (Tracer A and Tracer B in Table 6.1), one of which has settling velocities assigned to it. The settling velocities are based on the findings of *Kasten et al.* [1968]. We need to establish whether the inclusion of settling velocities is necessary before running further experiments associated with volcanic aerosol.

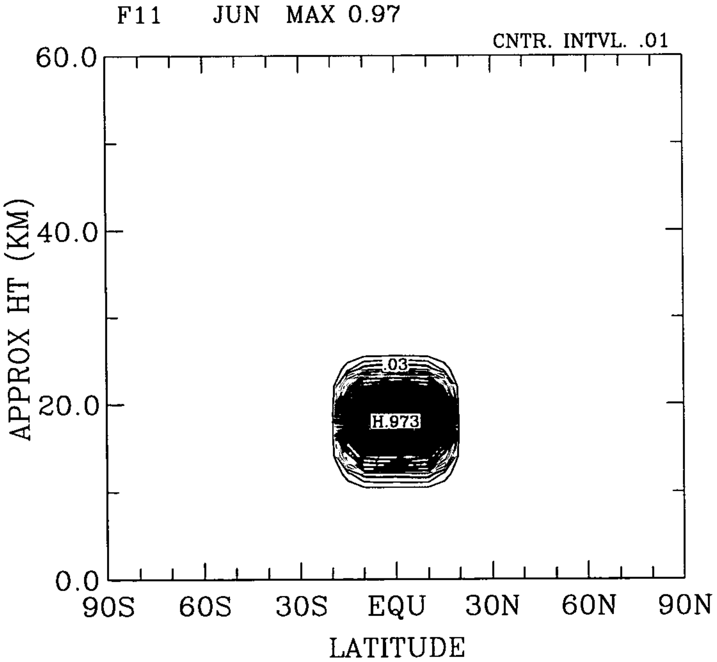

Figure 6.2: Initial latitude-height plots of zonally averaged tracer mixing ratio (vmr) at the start of the 2-D model run: Tracer A (the distribution of Tracer B is identical)

Kasten et al. [1968] provide settling velocities for aerosol particles depending on the particle radius and altitude of particle. For our purposes (within the limited altitude range between the tropics and 40km) an approximate expression based on the findings of *Kasten et al.* is used

$$w = 10^{(0.06125z+1.05logr-2.8)} \tag{6.1}$$

where w is the vertical velocity (downwards) in cms^{-1}, z is the altitude in km and r is the particle radius (microns).

The two tracers begin with identical initial distributions in this experiment (Figure6.2). In this case the tracer distribution is centred over the equator and at 18km. The second tracer (Tracer B) has settling velocities assigned to it based on the above equation. Assigning settling velocities to the tracer in this manner ignores the effects of coagulation. With time, aerosol particles merge to form larger particles which have increased settling velocities. With this in mind, a particle size of 0.3 microns is assumed, which is well within the range of particle sizes observed in the volcanic cloud.

Four months into the run, the difference the settling velocities makes to the tracer distribution is obvious (Figures 6.3a and 6.3b). Tracer A has reached 40km while the top edge of Tracer B sits at just over 30km. Considering that the Pinatubo cloud started off at a higher altitude and yet doesn't reach 40km until December, then the indications are that the cloud without settling velocities could be unrealistic. Incidentally, the amount of poleward spread displayed by both tracers is about the same.

After a year, the difference between the two tracers is huge (Figures 6.4a and 6.4b). Tracer A has reached the mesosphere which is very unrealistic (compare with the real measurements shown in Figure 4.6). The upper edge of the Tracer B distribution is around 35 km. This is lower than the upper edge of the Pinatubo cloud in the real atmosphere, but the distribution was initialised lower here.

Despite the additional settling velocities, Tracer B remains above the tropopause just as Tracer A does. This is encouraging as the real cloud remained above the tropopause too. So the addition of settling velocities gives a more realistic upper edge without adversely affecting the lower edge of the cloud. Clearly, for this atmospheric model, it is important to include the settling velocities of the aerosol

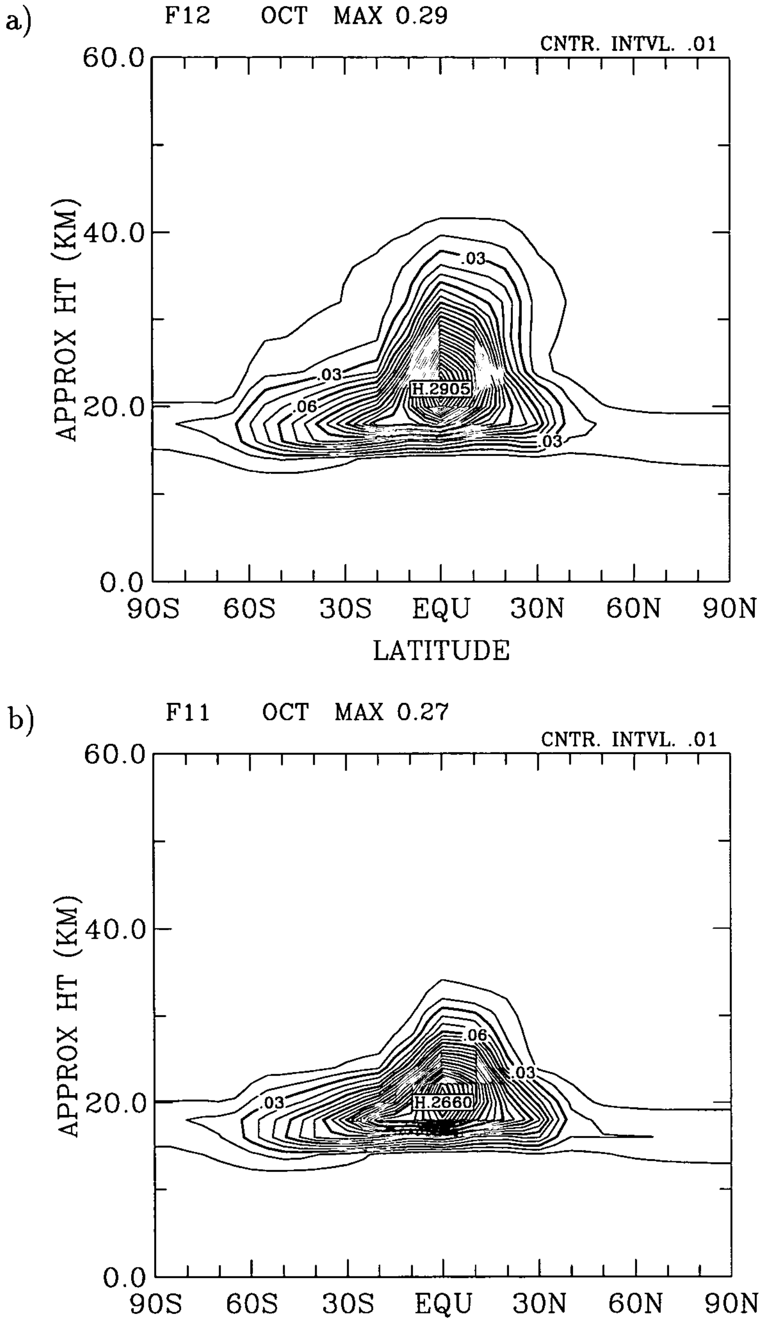

Figure 6.3: Latitude-height plots of zonally averaged tracer mixing ratio (vmr) in October of the 2-D model run: a) Tracer A and b) Tracer B. Tracer B has settling velocities while Tracer A does not.

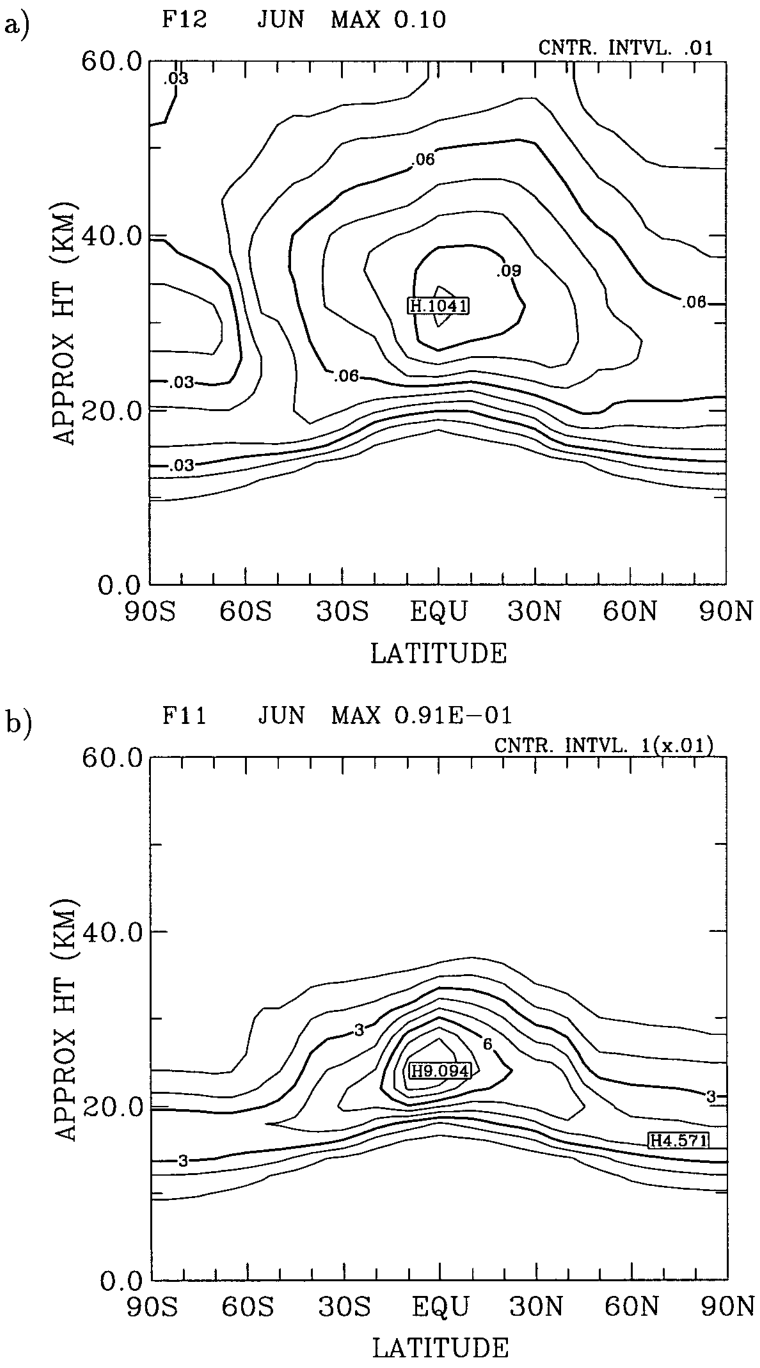

Figure 6.4: Latitude-height plots of zonally averaged tracer mixing ratio (vmr) in June, one year from the start of the 2-D model run: a) Tracer A and b) Tracer B. Tracer B has settling velocities while Tracer A does not.

cloud for believable simulations. The main experiment in this chapter will include settling velocities; not including settling velocities would make the 2-D model and the 3-D EUGCM non-comparable.

6.3.2 Comparison with the equivalent EUGCM run

Now, we briefly describe an experiment in the 2-D model equivalent to that carried out for the UGAMP GCM in Chapter 4. The effect of adding radiative heating will be better determined if this model shows the same hemispheric imbalance as the EUGCM did. If the two models produce similar results it would be easier to see that any improvements in tracer dispersal in the 2-D model due to radiative heating would apply to the EUGCM as well. The tracer used for comparison here (Tracer C in Table 6.1) will also serve as a good control run with which to compare the run with additional heating (Tracer D).

For this experiment we need to initialise a tracer in the 2-D model in a similar way to the initialisation of the EUGCM in Chapter 4. However, through model design (different gridpoint coordinates), the tracer cannot be initialised over the exact same latitude and height range but the closest approximation has been used. The most important aspect of the distribution of Tracer C, for our purposes, is that it is initialised north of the equator (Figure 6.5a). It is the distribution of the tropical reservoir with respect to the equator which has proved to be of importance in previous work (section 5.1). We have just established that, in this model, the inclusion of particle settling velocities is necessary for a realistic simulation, so in this respect the simulations in the two models also differ.

From the plot of Tracer C in August (Figure 6.5b) we can see that the 2-D model is showing evidence of two different mixing regimes, as was seen in the real atmosphere. Northwards mixing occurring at 20km and below, while the southwards mixing occurs mostly above 20km (compare Figure 6.5b here with Figure 4.4 in Chapter 4). The southward mixing, while occurring at the correct height, is not penetrating into the mid-latitudes; the same problem encountered with the EUGCM Pinatubo experiment.

By December (Figure 6.6a), only a small amount of Tracer C has reached southern mid-latitudes. Indeed, the amount of material south of 10°S has hardly changed since August. The picture in the northern hemisphere in December is

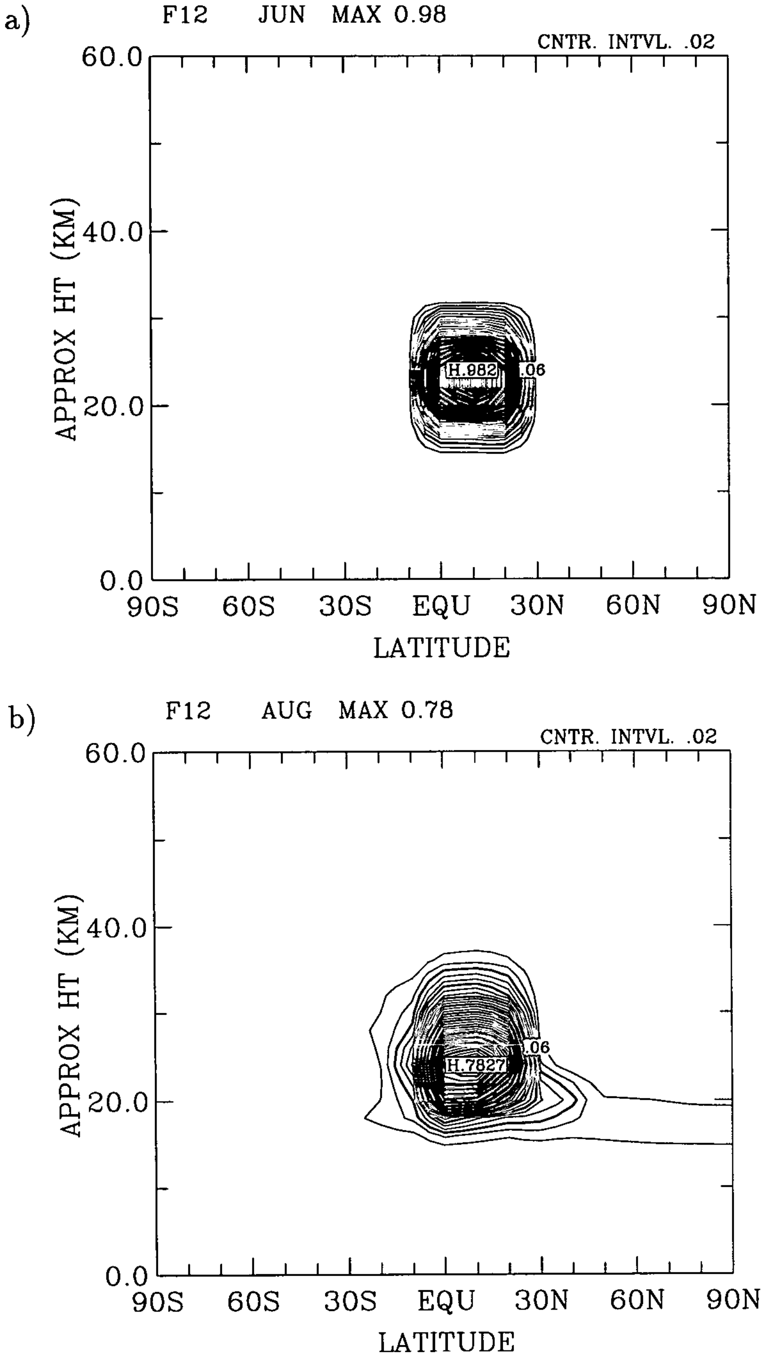

Figure 6.5: Latitude-height plots of zonally averaged tracer mixing ratio (vmr) in a) June at the start of the experiment and b) August of the 2-D model run: Tracer C.

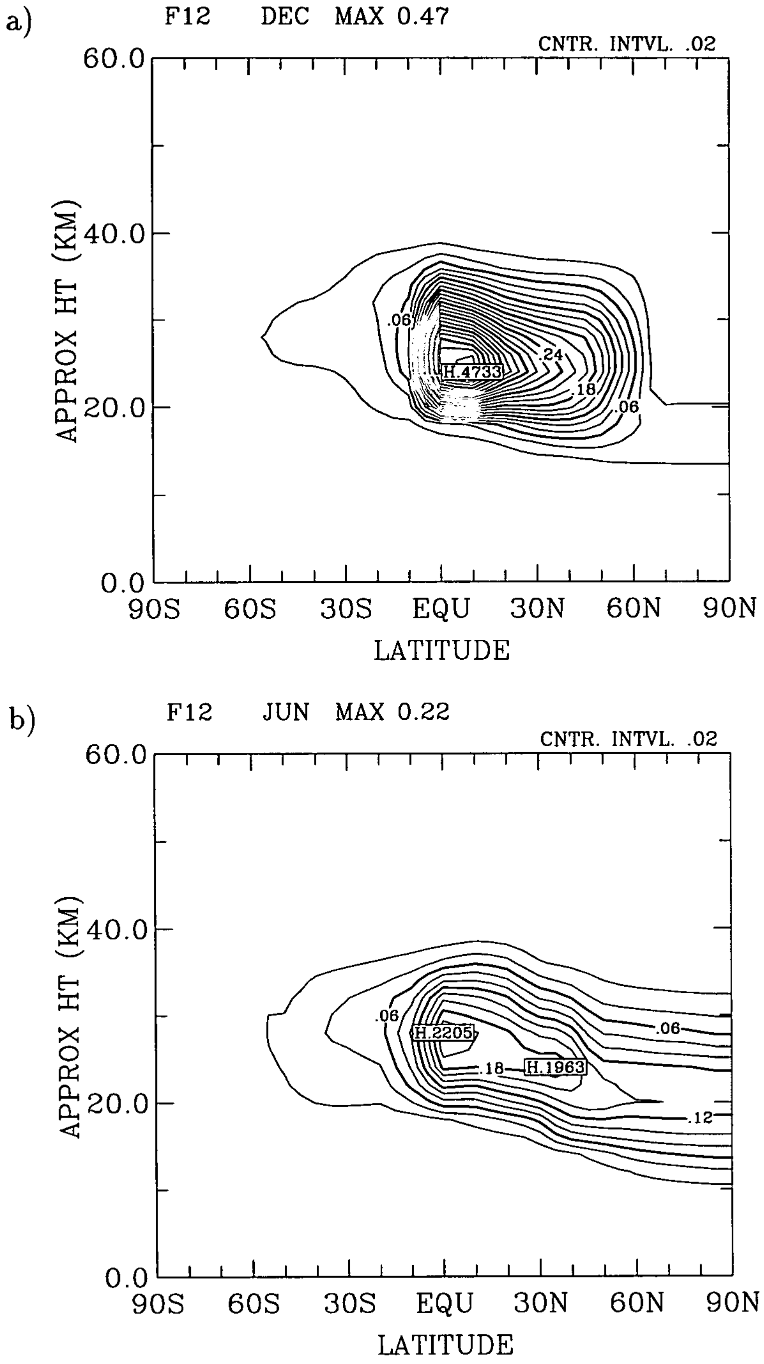

Figure 6.6: Latitude-height plots of zonally averaged tracer mixing ratio (vmr) in the 2-D model for December and b) one year after the start of the run, June: Tracer C.

quite similar to what it was in the EUGCM experiment. Mixing has transported large amounts of material into the northern mid-latitudes. This mixing takes place over the entire height range where the tropical reservoir of material exists. There is no clear distinction between the tropics and the mid-latitudes (lack of sharp meridional tracer gradient) but it does appear that the vortex edge can be seen at around 60°N (bar a small amount of material which reached the polar region early on in the model run).

Eventually a further portion of tropical material reaches the southern mid-latitudes but only a year after the tracer was initialised (see Figure 6.6b). There is a good distinction between the main cloud and the much smaller amounts of material in the southern hemisphere, but this distinction does not occur at the edge of the tropics, but rather closer to the equator. The highest values of Tracer C remain just north of the equator.

The material in the northern hemisphere after a year has become well distributed around the middle and polar latitudes and the amounts are just slightly less than those in the tropics. We are seeing the same degree of interhemispheric asymmetry that we saw in the EUGCM run. Therefore, the 2-D model is behaving sufficiently like the EUGCM for the results of the main experiment here to be pertinent to our previous studies with the EUGCM. The task now is to see if additional heating associated with volcanic aerosol affects the interhemispheric asymmetry to any extent.

6.4 Tracer evolution with additional heating

The following experiment is the main focus of this chapter and tests the hypothesis; radiative heating due to volcanic material promotes the transport of the material from the tropics into the southern mid-latitudes. We have already established that there are conflicting opinions related to this hypothesis in the literature and so this experiment aims to add weight to one side of the argument and to ascertain whether a more complex experiment in the EUGCM is warranted.

For the experiment we need to determine the differences between two tracer distributions, one of which has been subjected to radiative heating while the other has not (Tracer D and Tracer C respectively; see Table 6.1). If there is a difference between the two tracers we want to establish the cause. Is there enhanced mixing between the tropics and mid-latitudes because the radiative heating is increasing meridional circulation and does the radiative heating lift the aerosol to higher altitudes?

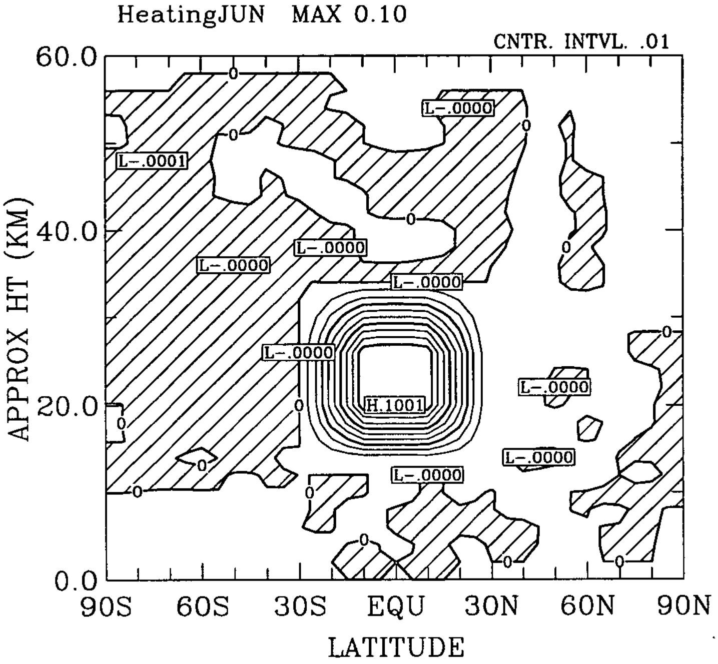

Figure 6.7: Additional heating (K/Day) in the model run containing Tracer D. The largest heating perturbation is 0.1 K/Day

The control run is that which we looked at in the last section (Tracer C). The new run consists of the same tracer distribution but with heating applied over the tropics at the altitudes where the tracer is situated (Tracer D).

The additional heating applied in this experiment is shown in Figure 6.7. A number of factors were considered when choosing the magnitude of the heating rate used in this experiment, the most important of which is how the heating is actually implemented in the model. As this is an initial investigation to establish the necessity of including the effects of radiative heating in the EUGCM, the additional heating is applied in a way such that its implementation was not so difficult.

The first simplification is that the heating applied is uniform across the tropics. The heating rates quoted earlier in this chapter are maximum values (caused by the highest concentrations of aerosol). To apply those heating rates uniformly across the tropics would give an overestimation in the amount of heating generated by the aerosol so we need a lower amount of heating in this experiment.

Another simplification is that the heating rate is applied constantly with respect to time. In the real atmosphere, the heating rates are relatively large immediately after the volcanic eruption and then they reduce gradually with time. For our experiment a heating rate needs to be chosen which is somewhat less than the larger reported heating rates so that exaggerated heating does not occur in the experiment.

Bearing these issues in mind, a figure of 0.1 K/Day was chosen for the additional heating in this experiment, a bit less than those quoted in the previous section. As well as ensuring no overestimation of the heating is made, choosing a conservative value for the heating rate has the advantage of testing the lower boundaries of the effect of heating. For example, if the cross-equatorial transport is encouraged by the additional heating the results will hold for any heating rates above this amount. If cross-equatorial transport is encouraged then further experiments are justified, such that a more sophisticated treatment of the heating can be implemented and thus a more quantitative assessment of the effect of the additional heating can be made.

6.4.1 The heating experiment results

Three months into the runs there is a clear distinction between the tracer with heating and the tracer without (Figures 6.8a and 6.8b). The most obvious difference is the greater amount of material to be found in the southern mid-latitudes of the run with Tracer D. Not only is the transport into the southern hemisphere enhanced with the extra heating, the largest amounts of tropical material are being transported south at a higher altitude.

Another difference is the nature of the northward mixing into mid-latitudes. As in the real atmosphere and the UGAMP model runs, the northward mixing is initially confined to below 20km. However, by September mixing of Tracer D is occurring above 20km as well. This occurred in the run without heating too, but a month later. So far, the additional heating is promoting poleward transport, both north and south.

As for the main cloud in the tropics, Tracer D has a lower maximum concentra-

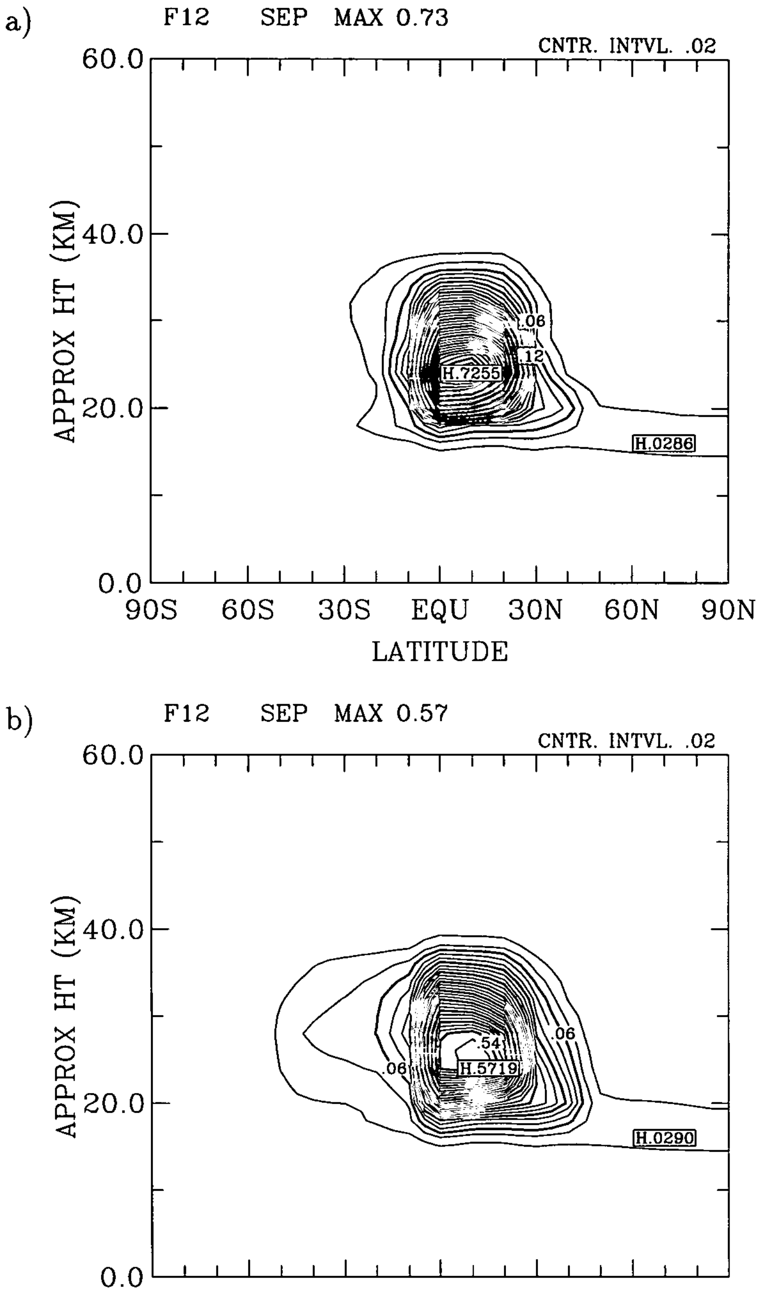

Figure 6.8: Latitude-height plots of zonally averaged tracer mixing ratio (vmr) in the 2-D model for September: a) Tracer C and b) Tracer D. The run with Tracer D has additional radiative heating.

tion, due mostly to the enhanced dispersal into both hemispheres. At this point, there is very little difference between vertical distribution in the tropics. Tracer D's greatest concentrations are a bit higher in altitude perhaps, but this is not the cause of the greater poleward mixing. This is true because, at the same height, the mixing ratios of Tracer C are not less than those in the maximum of Tracer D. In other words, the tropical air at this height is just as "tracer-rich" in the run without heating as the the run with heating so the greater flux of material into the southern mid-latitudes must be due to an increased meridional circulation.

The tropical, stratospheric reservoir of Tracer D has not moved significantly south so as to become more symmetrical about the equator and make more material available to be mixed into the southern mid-latitudes.

The plots for November of the same two experiments can be seen in Figures 6.9a and 6.9b. There is about twice the amount of material in the southern mid-latitudes in the heated run as in the non-heated run. The northern hemispheres look very similar; a little more dispersal can be seen in Tracer D. The highest mixing ratios are now over the equator in the heated run, but by this point most of Tracer D has drifted into the northern hemisphere. In both runs there is no further mixing into the southern mid-latitudes until the following May/June so the southward movement of the tropical cloud has taken too long to significantly affect the asymmetry between the two hemispheres in the tracer fields.

Despite the increase in southern mid-latitude material in the first few months of the heated run, there is very little difference between the evolution of Tracer C and Tracer D. The run with heating very quickly (first two to three months) reaches a new equilibrium. This new equilibrium is reached in the 2-D model in the following way.

Figure 6.10 shows the initial effect the additional heating has on the general circulation of the model. The plot shows the difference between the meridional circulation of the control run and that of the run with additional heating, giving the circulation resulting directly from the extra heating. From this, we would expect any material in the tropics to be lifted higher in the run with heating, as well as a little more transport polewards in both directions. However, this initial, uncomplicated circulation which results from extra heating very quickly disappears (within the space of month) and is replaced with something much more

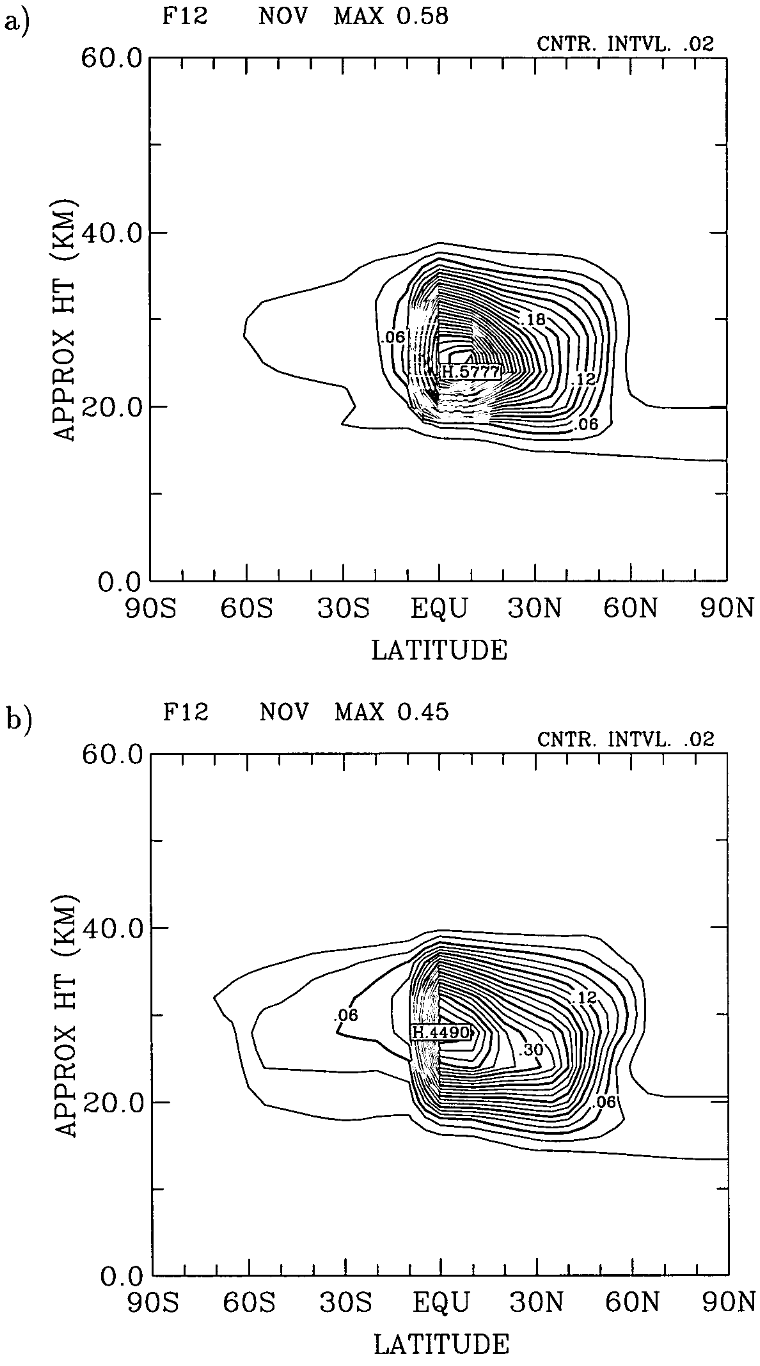

Figure 6.9: Latitude-height plots of zonally averaged tracer mixing ratio (vmr) in the 2-D model for November: a) Tracer C and b) Tracer D. The run with Tracer D has additional radiative heating.

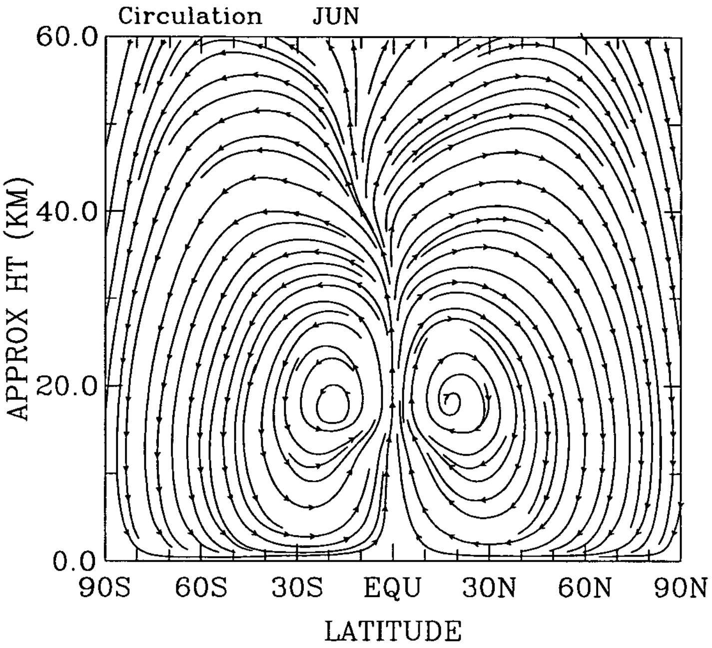

Figure 6.10: The circulation resulting from the addition heating due to the volcanic cloud. It has been obtained by taking fields from the heated run away from the equivalent fields of the control run

complex in nature.

The reason for this can be seen in the ozone profiles. Figure 6.11a shows the ozone profile as it would be without the aerosol heating. The next plot (Figure 6.11b) is the field produced by subtracting the ozone field in Figure 6.11a from the equivalent field from the run with additional heating. These two plots and the circulation resulting from the extra heating shown in Figure 6.10 enable us to understand what happens to the ozone field due to the aerosol heating.

As expected, the ozone profile is lifted which means that there is a reduction in ozone below where the highest ozone mixing ratios were. Note that there are increases in ozone in the mid-latitudes. This is due to the enhanced meridional circulation transporting more of the tropical, ozone-rich air polewards. A fairly dramatic decrease in ozone occurs in the area where most of the tracer is situated. This decrease in ozone has a significant effect on the radiative balance as can be seen in Figure 6.12. Where there is less ozone, radiative cooling occurs (the heating rates go down). The radiative cooling counteracts the effects of the aerosol heating and a new balance is established after about three months. The ozone

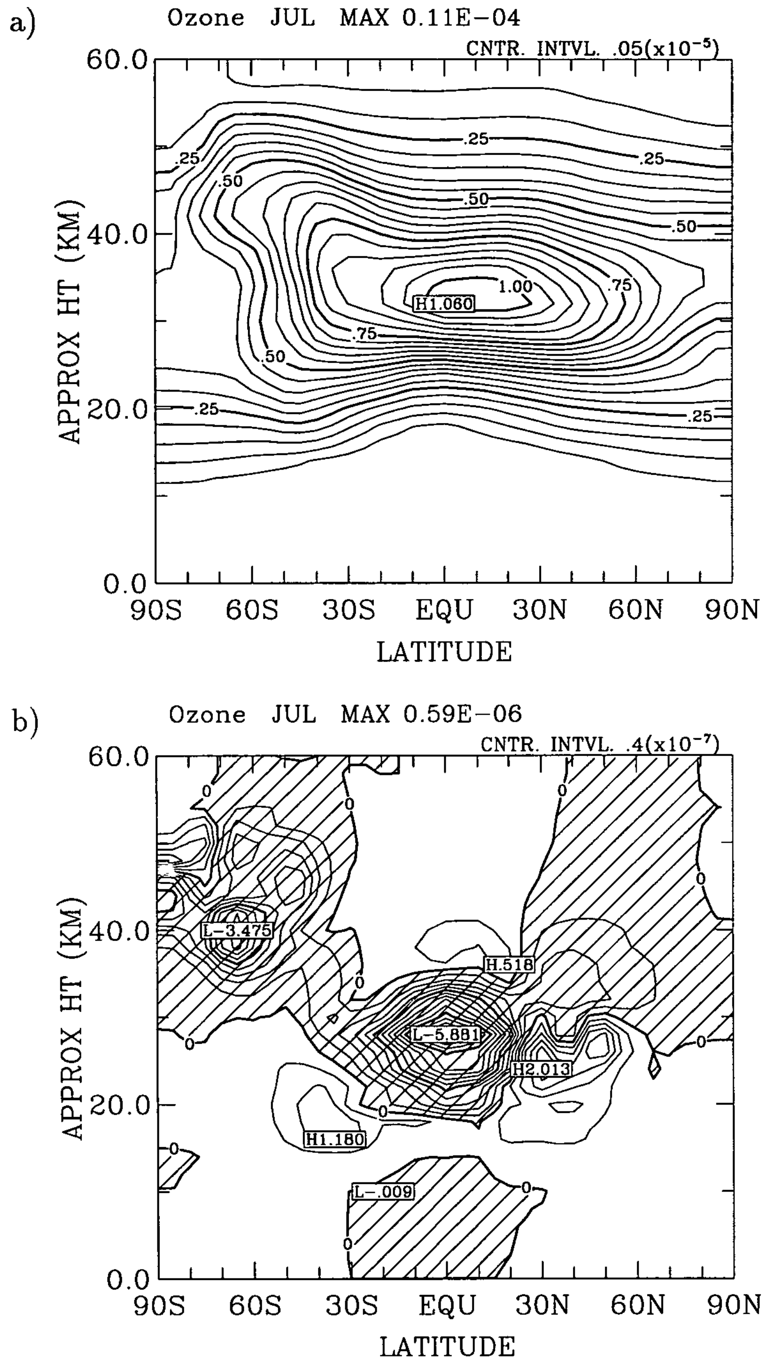

Figure 6.11: a) The ozone field as it appears in July of the control run. b) The ozone field in a) subtracted from the equivalent field from the run with heating gives us the change in ozone caused by the extra heating

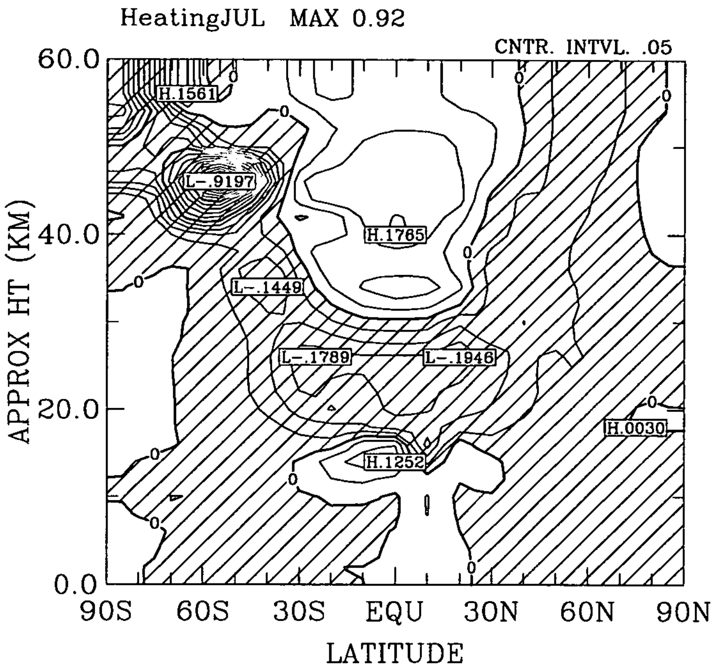

Figure 6.12: The net radiative heating (K/Day) for July of the 2-D model experiment (run with heating minus control run).

profile remains displaced by the same height above the tropics for the rest of the model run and, as a result, lower heating rates remain below 30km and above 30km the heating rates stay higher.

After a few months, the temperature of the tropical stratosphere in the run with heating settles to around 5 to 7°C higher than the control run throughout the rest of the experiment. As the new balance is established the additional poleward and upward movement of material due to aerosol heating is suppressed and tracer transport behaves as it did in the control run. So, it is in the first three months of the model run that the biggest differences due to volcanic heating are seen, before a new radiative balance is achieved. This can best be seen in the plots of circulation which have been derived in the same way as the plot in Figure 6.10, but for the months of August and September (Figures 6.13a and 6.13b).

In August there is clearly more southward movement (or less northward depending on the actual circulation) in the run with volcanic heating right across the tropics at a height of 27 km. This has already been seen in the tracer fields as enhanced transport of material into the southern mid-latitudes in Figure 6.8b. A month later, while this increase in southward flow still exists it no longer stretches

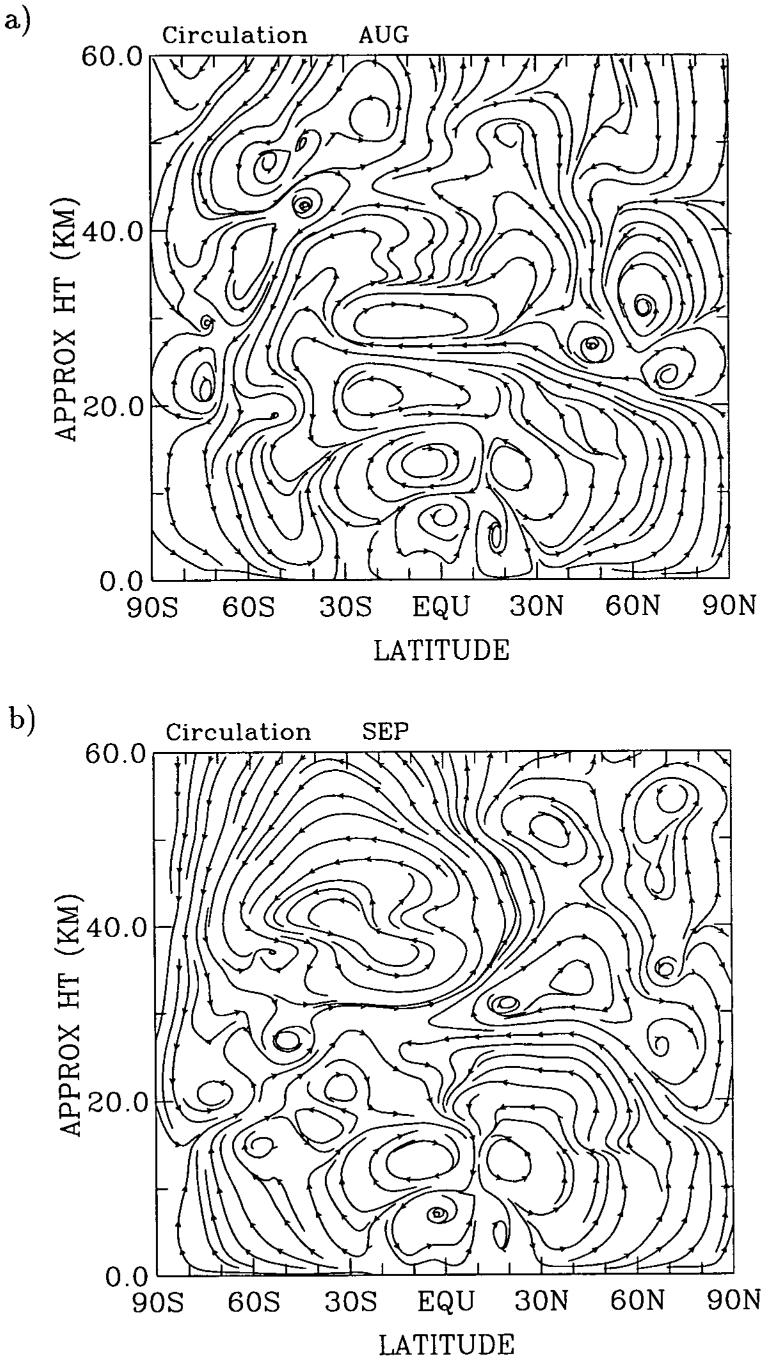

Figure 6.13: The change in circulation due to additional heating for a) August and b) September in the 2-D model run.

into the southern mid-latitudes. From this point on there is no evidence to suggest that the heating promotes any more transport into the southern hemisphere.

Figures 6.14a and 6.14b show that, after a year, the interhemispheric imbalance in the tracer fields has become slightly less severe due to the inclusion of aerosol radiative heating; any additional material found in the southern hemisphere due to extra heating got there within the first three months of the model run. In the real atmosphere, the aerosol cloud has crossed the equator and reached 20°S, one month after the eruption. This fact and our model results both suggest that it is crucial that a realistic aerosol distribution in the tropics is established early in the model run so that the final global distribution can be more accurate.

6.5 Summary

This study indicates that including the effects of radiative heating does improve the simulation of the Pinatubo cloud, but not to the extent as to produce realistic fields after a year. The amount of material transported into the southern mid-latitudes from the tropics increases and this is due to an enhanced meridional circulation.

These results show that the inclusion of heating is warranted. While this is true, a more sophisticated treatment of the heating is advisable. It would be ideal if the heating applied was in direct proportion with the tracer distribution. The highest amounts of heating would occur in the same place as the highest concentrations of aerosol. This would ensure a steeper meridional temperature gradient in the tropics which would hopefully enhance the meridional circulation.

The application of heating with respect to time could also be given a more sophisticated treatment. The heating rates in the real atmosphere were the highest in the first few months after the eruption, after which they gradually dropped as the aerosol concentrations decayed. In our experiment, the heating rates stayed constant throughout the year, which was what probably caused the edges of the tropical reservoir to become less well-defined. With this approach to applying the heating rates, a more active meridional circulation would occur in the first few months of the model run; the period of time in the real atmosphere when the Pinatubo tracer crossed the equator. A more realistic treatment of the heating

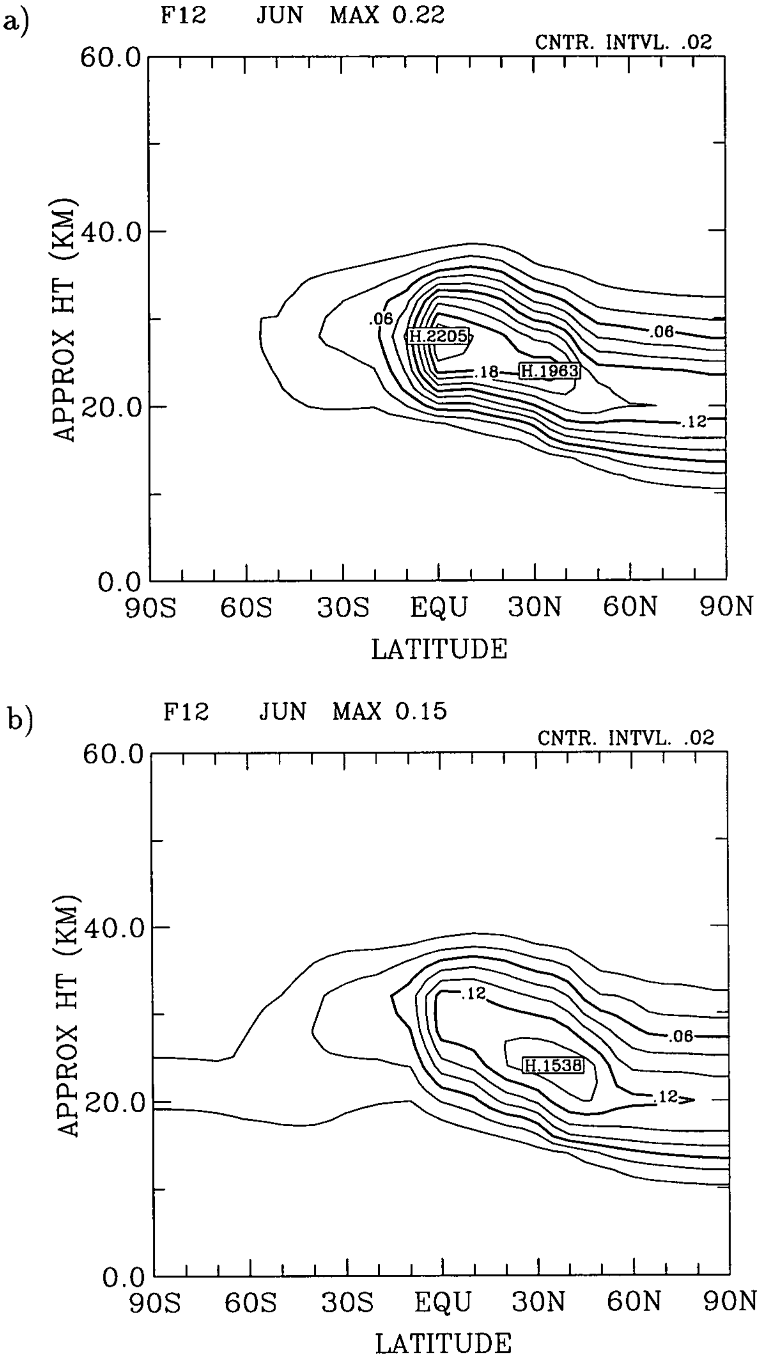

Figure 6.14: Latitude-height plots of zonally averaged tracer mixing ratio (vmr) in the 2-D model for June, one year from the start of the experiment: a) Tracer C and b) Tracer D. The run with Tracer D has additional radiative heating.

would mean that we would not need to be so cautious with the magnitude of the heating rates used.

Doing this experiment has established that the heating due to the volcanic cloud does matter, but more elaborate experiments are necessary. Using the 2-D model we were able to see how the extra heating affected the dispersal of the cloud and how the model attained a new balance. The extra heating affects the radiative balance as the ozone profile is lifted.

In relation to the EUGCM experiments, this chapter shows that the lack of cross-equatorial transport could be counteracted by the inclusion of radiative heating due to the volcanic cloud. This would mean a more realistic representation of the spread of a volcanic cloud within the UGAMP model. We can make these statements about the EUGCM with confidence because of the preliminary experiments conducted in section 6.3 which relates the 2-D model experiment with that of the EUGCM.

Chapter 7

Conclusions

Throughout this thesis, the circulations of the UGAMP models were tested by comparing model fields with measurements of trace constituents in the real atmosphere. Water vapour was used for an initial investigation and then more extensive comparisons were carried out using volcanic aerosol. Due to their chemical stability, both species are good for studying the dynamics of the upper-troposphere/lower-stratosphere in the numerical models. The UGCM was tested for an interhemispheric asymmetry in upper-tropospheric water vapour while both the UGCM and EUGCM were used to simulate the dispersal of the Mt. Pinatubo aerosol cloud. The volcanic tracer simulations presented us with questions about the dynamics of the GCM; the EUGCM was examined for the presence of PV barriers and the 2-D model was used to estimate the relevance that aerosol heating has on the poleward spread of volcanic material.

7.1 Upper-tropospheric water vapour in the UGCM

The upper-tropospheric fields of water vapour in the UGCM were compared with the aircraft measurements presented in *Kelly et al.* [1991]. The main purpose of this was to establish whether the model reproduced the interhemispheric asymmetry in the winter mid-latitudes reported by *Kelly et al.* The northern hemisphere contained 2 to 4 times more water vapour than the southern hemisphere. If the asymmetry is genuine, then it is important for the UGCM to reproduce it if the radiative balance is to be correct.

The UGCM did show an asymmetry between the two winter hemispheres although not to the same degree as in the real atmosphere. The asymmetry was shown to vary with latitude in the UGCM; the higher the latitude, the bigger the difference between the hemispheres. Although an asymmetry exists in the UGCM, typical mixing ratios of water vapour in the mid-latitudes of the boreal winter in the model were lower than those seen in the aircraft measurements (Figure 3.9). Measurements in the austral winter were in good agreement (Figure 3.8).

The investigation revealed that caution should be used when making conclusions based on just three measurement sites per hemisphere. The model fields showed that the variability of water vapour around the latitudes where measurements were taken could be enough to change the conclusions derived from them. These findings do not dispute that an asymmetry exists between the winter hemispheres, but they do cast doubt over the severity of the asymmetry.

As well as the comparison with aircraft measurements, UGCM water vapour fields were compared with satellite measurements. The measurements used were MLS retrievals, recently calculated for 215mb. The main reason for the comparison was that the MLS measurements cover the globe more extensively than the aircraft measurements in *Kelly et al.* They provided us with an independent measurement against which we could compare both the claims of *Kelly et al.* and the model behaviour.

The MLS data set and the UGCM compared well except in the polar regions where the UGCM was considerably drier than the MLS retrievals. As well as the good agreement quantitatively in the tropics, there were many structural similarities in the isobaric maps of MLS retrievals and model fields.

The MLS measurements did not show evidence of the interhemispheric asymmetry reported by *Kelly et al.* In fact, the amounts of water vapour in the mid-latitudes of the boreal winter are about equal to those in the austral winter. This further damages the credibility of the interhemispheric asymmetry presented by *Kelly et al.* It clearly existed in their measurements, but it now looks uncertain that the claim of interhemispheric asymmetry can be extended to all winters. A number of different winter hemispheres over several years needs to be compared.

A sensitivity study was carried out to ascertain what effect using a different convection scheme in the UGCM has on the comparisons summarised above. The default convection scheme in the UGAMP models is Kuo, but the more recently developed Betts-Miller scheme was used as an alternative for this exercise.

The upper-tropospheric water vapour in the tropics was very sensitive to the change of convective parametrization. This is due to the steep vertical gradient in the water vapour profile at this height. The Betts-Miller scheme produced dramatically higher mixing ratios of water vapour in the tropics of the UGCM. While water vapour fields produced by the Kuo scheme compared favourably with the MLS retrievals, the Betts-Miller fields look very different. Although the tropical upper-troposphere contains more H_2O using the Betts-Miller scheme, the polar regions remain drier than the MLS measurements. With respect to the MLS measurements, the Kuo scheme produces the best water vapour fields, but with respect to the claims made in *Kelly et al.* the change in convection scheme makes very little difference. There is slightly less asymmetry between the winter hemispheres for the Betts-Miller version of the model.

If we were to assume that the two measurement sets featured in this chapter are reasonably accurate then we would say that the Kuo convection scheme is the best for producing realistic upper-tropospheric water vapour fields. The fact that the Betts-Miller scheme produces such unsatisfactory water vapour should be a big concern for UGAMP modellers and further work addressing this is recommended.

7.2 Simulating the spread of a volcanic cloud

The majority of the experiments featured here focussed on the advection of volcanic tracers in two UGAMP models. Measurements of the Mt. Pinatubo cloud were used as a basis for comparing model dynamics with the dynamics of the atmosphere. The model failed to reproduce a realistic global dispersal of material and subsequent experiments were conducted to determine why this was the case. In the process of these experiments the EUGCM was also tested to see if steep PV gradients were acting as barriers to isentropic transport.

The ability of GCM's to simulate the impact a volcanic cloud has when reaching the stratosphere is very important for various model experiments. The sulphate aerosol which is produced when the volcanic SO_2 reaches the stratosphere has a number of effects on the atmosphere. The aerosol absorbs upwelling infrared radiation which causes a temperature increase in the vicinity of the cloud. The radiative heating also affects the ozone profile as aerosol rich air is lifted to higher altitudes. The presence of sulphate aerosol is also believed to promote ozone depletion through heterogeneous chemistry. This is of particular concern due to the position of the Pinatubo eruption. The ozone depletion occurs over the most populated areas: the tropics and mid-latitudes. Hence, it is desirable for model experiments associated with global warming or ozone profiles to include the effects of volcanic material reaching the stratosphere. The model should be able to simulate all aspects of a volcanic cloud, but we concentrated mainly on the dynamical representation.

7.2.1 Simulating the Mt. Pinatubo cloud in the UGAMP models

An attempt to simulate the Pinatubo cloud was made using the UGCM and the EUGCM. The UGCM, with an increased horizontal resolution, was useful for studying the transport processes mixing material into the extra tropics while the EUGCM provided the necessary altitude range to conduct a more complete simulation.

The UGCM (in a 60 day run) and the EUGCM (in a year-long run) were successful in simulating the following features of the spread of the Pinatubo cloud.

- Cloud circled the globe in three weeks
- Height dependence of poleward spread of material
- Tropical stratospheric reservoir of material

The fact that both models correctly simulated the rate at which the cloud circles the earth means that the zonal winds at that height in the tropics are the same as those in the real atmosphere.

Observations of the evolution of the Pinatubo cloud showed that, for the first few months after the eruption, material was getting into the northern mid-latitudes via synoptic scale disturbances below 20km while the southward mixing was centred at a higher altitude and was due to planetary-wave breaking. From these simulations, the height dependence of the poleward dispersal of tracer was clearest in the UGCM. The UGCM was also used to examine the nature of these events and examples of planetary-wave breaking mixing material into the southern latitudes and events mixing material into the northern mid-latitudes were seen. The mixing into the northern mid-latitudes was associated with shearing and anticyclonic disturbances near the edge of the tropics. Further work in Chapter 5 using different tracer initialisations revealed that the EUGCM was also recreating the two different mixing regimes.

The tropical confinement of volcanic material was one of the strongest features in the real atmosphere and it is evident in both model simulations. In both models, the edges of the tropical-stratospheric reservoir are characterised by a steep meridional gradient in the tracer field, although the southern edge of the reservoir was positioned too close to the equator compared with the real tropical-stratospheric reservoir. This property of the model runs presented the opportunity to investigate the mechanism which was maintaining the tropical, stratospheric reservoir. Specifically, the EUGCM was searched for evidence of steep gradients of PV preventing material from leaving the tropics. The issue of the prevention of tracer transport due to the vortex edge was studied in the same set of experiments.

The EUGCM failed to represent the following attribute of the cloud's dispersal:

- Interhemispheric balance of tracer distribution

In the measurements of the Pinatubo aerosol cloud, it was seen that, after a year, the volcanic material was almost equally divided between the two hemispheres. This was clearly not the case in the EUGCM experiment (the UGCM did not run long enough to be tested for this feature). The majority of material transported from the tropics went into the northern hemisphere, creating an acute interhemispheric asymmetry in the tracer fields. This problem with the simulation was one of the major motivations for the work which followed.

7.2.2 The cause of the interhemispheric asymmetry in the model

A number of new tracer experiments were designed to investigate the model for two things, the most important of which was to establish the cause of the interhemispheric asymmetry. The other task was to investigate the possibility that steep meridional gradients of PV were inhibiting eddy advective transport in the EUGCM.

It was quickly established that the root of the problem was a lack of cross-equatorial transport in the model. There was not much cross-equatorial transport throughout the entire model run, but it was the lack of transport in the first months of the model run which ultimately caused the interhemispheric asymmetry. According to observations, material crossed the equator in the month following the eruption such that the Pinatubo cloud covered latitudes 20°S to 30°N. This meant that mixing events caused by planetary-wave breaking in the southern hemisphere had a source of aerosol-rich air to pull into the mid-latitudes. The model simulations had material covering the latitudes 10°S to 30°N, so not enough tracer was available for transport from the southern tropics. The tracer experiments shown here demonstrated that if there had been tracer in the southern tropics at the start of the model run then it would have been transported south due to planetary-wave breaking.

It was concluded from the evolution of a tracer initialised between 20°S and 30°N that if the model had got the cross-equatorial right at the beginning of the run then the interhemispheric asymmetry at the end of the model run would be greatly improved, although not eliminated. This indicated that the lack of cross-equatorial transport was the main problem, but not the entire cause of the asymmetry.

7.2.3 PV barriers in the EUGCM

Many examples of PV barriers were seen in the EUGCM. There was a very strong correlation between steep meridional PV gradients and the prevention of tracer transport in the model. The steep PV gradient we most expected to see was at the edge of the polar vortex. In the EUGCM a very strong gradient was present there (particularly in the southern hemisphere) and it proved to be very effective at preventing material from entering the polar region. The northern polar vortex, although weaker and less uniform than its southern counterpart, also stopped material from getting inside the vortex.

Not only was the search for sub-tropical PV gradients successful, but a strong, equatorial PV gradient was found too. In the northern hemisphere steep PV gradients were situated in the low latitudes throughout most of the model run. This was not the case in the southern hemisphere where the steep PV gradients were only found in the low latitudes during the austral summer. The tropical edge of the southern winter surf zone was situated between 10°S and 20°S where the edge of a steep, equatorial PV gradient existed. Compelling evidence was presented showing the equatorial PV gradient acting as a barrier to isentropic transport. Specifically, tracer in the northern tropics was prevented from moving into the southern tropics. This barrier to cross-equatorial transport could be seen at all altitudes where the tracer was present. The sub-tropical PV gradients were also shown to inhibit isentropic transport; namely the transport from the tropics into the mid-latitudes. Material would escape into the middle latitudes only when a channel of low PV gradient existed in the PV barrier. The low PV gradient was the result of whatever process (e.g. planetary-wave breaking) caused the material to exit the tropics. Steep gradients in the tracer fields were present in the same positions as steep gradients in the PV fields.

The sub-tropical PV barriers have a seasonal variability relating to the breaking of planetary waves. The equatorial PV barriers have a variability believed to be related to the phase of the QBO; a feature which the EUGCM cannot currently emulate. A quantitative study of the strength of equatorial gradients of PV was carried out by comparing the EUGCM with the ECMWF analyses. It was found that the strength of the PV barriers in the model were stronger than those in the analyses. Further investigation revealed that the cause of this difference could be attributed to a split in the easterly jet over the tropics of the model which was not present in the analyses.

This study offers one possible solution to the interhemispheric asymmetry in the tracer fields: ensure the EUGCM is competently representing the strength of the equatorial PV barrier, whether it is related to the QBO or not. The work with the radiative effects of the volcanic cloud provided another possible solution.

7.2.4 The effect that the radiative heating of the volcanic cloud has on the tracer dispersal

There were conflicting views in the literature as to what effects the inclusion of radiative heating of the volcanic cloud would have on its dispersal. At least one model simulation of the cloud was accurate without including the additional radiative heating [*Boville et al.*, 1991] while another paper claimed that the aerosol heating is essential if the simulation is to be realistic [*Young et al.*, 1994]. The literature also indicates that the radiative heating could affect the dynamics in two ways: the lofting of air and/or an enhanced meridional circulation. The possibility of an enhanced meridional circulation encouraging material to cross the equator was the motivation for this piece of work.

A 2-dimensional model was used to establish what effects the aerosol heating would have on tracer transport and how that relates to the Pinatubo simulation in the EUGCM. The 2-D model has interaction between dynamics, radiation and chemistry, making it a valuable tool for assessing the effects of aerosol heating.

It was necessary to assign settling velocities to the tracer in the 2-D model for the fields to appear realistic with respect to altitude. This helped to make the 2-D experiment and the Pinatubo simulation comparable. A further experiment using a Pinatubo-like tracer in the 2-D model produced very similar fields to the equivalent EUGCM experiment, including the severe interhemispheric asymmetry. The fact that the 2-D model produced the same error as the EUGCM provided a strong link between the two models; any differences in the tracer dispersal due to extra heating in the 2-D model would apply to the EUGCM as well.

The amount of extra heating applied in this experiment was a very conservative estimate, testing the model reaction to the lower boundaries of heating perturbations due to aerosol. The additional heating was constant throughout the model run. The extra heating did make a difference to the poleward dispersal of tracer; more material entered the southern hemisphere in the first months of the model run with heating than that without extra heating. Considering this was a lower bound scenario, the conclusion from this experiment was that the inclusion of aerosol heating is needed for modelling the dispersal of a volcanic cloud. These results endorse the claim made by *Young et al.* [1994].

The 2-D model showed that the meridional circulation was enhanced by the extra heating and this was responsible for the increase in material reaching the southern latitudes. The extra heating also caused a redistribution of ozone with respect to latitude and altitude. This meant that the radiative heating below 30km in the model run with extra heating became less than that of the control run. The reverse was true above 30km. With this change, the model circulation reached a new equilibrium and the enhanced meridional circulation returned to what it had been in the control run. After the first three months, the differences between model fields of the two different runs remained fairly constant. For example, the maximum temperature difference between the two runs is approximately 6°C from September onwards.

This study showed that including the effects of radiative heating due to the volcanic aerosol is very important when modelling the dispersal of a volcanic cloud. While the extra heating did not eradicate the problem of the interhemispheric asymmetry, it did enable cross equatorial transport in the first months of the model run. This experiment used a very conservative estimate of the aerosol heating rate and it is reasonable to assume that even more material would have been transported south, across the equator, if the heating had been increased. Whether this would be enough to completely solve the interhemispheric asymmetry in the poleward dispersion of material is uncertain and requires further investigation, but we have seen here that the inclusion of heating does improve the asymmetry. Not only is the inclusion of aerosol heating deemed necessary for the modelling of the volcanic cloud, but a more sophisticated treatment of the heating is recommended.

7.3 Further Work

The work presented here, while having answered some questions, opens up new avenues of investigation. This section discusses some of the possibilities for further work based on the volcanic tracer experiments in this thesis.

7.3.1 The significance of the QBO

As mentioned in Chapter 4, the quasi-biennial oscillation (QBO) has not been fully considered in relation to the Pinatubo simulation. This is because the EUGCM does not currently represent this feature of the equatorial stratosphere. This was not of immediate concern as the tropical zonal winds in the model were very similar to those in the real atmosphere.

According to *Trepte et al.* [1992] and *Hitchman et al.* [1994], the phase of the QBO has an influence on the poleward spread of volcanic aerosol. This influence depends on the two different mixing regimes which transport tropical material into the mid-latitudes: the upper regime (above approx. 20km) and the lower regime.

We have already seen evidence of these two mixing regimes in the observations and the model runs conducted here. Detrainment from the tropics in the upper regime occurs more frequently during the QBO easterly shear. The strongest meridional divergence occurs at the level of maximum easterlies. Detrainment in the lower regime occurs more readily during westerly shear.

The Pinatubo eruption occurs at a time of predominant easterly shear in the stratosphere with some westerlies in the lower stratosphere. The EUGCM does not have the westerlies in the lower stratosphere at the start of the run. From the statements above in the previous paragraph, we can deduce that the northward mixing seen in the EUGCM experiment is too strong, contributing to the interhemispheric asymmetry near the end of the model run. Although the model has the easterly shear, we should consider that, without the QBO being represented properly, this shearing is not very accurate, resulting in an unsatisfactory poleward spread of material.

As we already know, this is not the whole solution to the interhemispheric asymmetry problem; the lack of cross equatorial transport means that not enough material reaches the southern tropics so that it is accessible to mixing into the mid-latitudes. It is suspected, however, that the QBO is linked to the equatorial PV barrier too.

7.3.2 The equatorial PV barrier

The equatorial PV barrier is a feature of the atmosphere which has seen little discussion in the literature but is clearly in need of further consideration, particularly in relation to the spread of volcanic aerosol. Having seen that these barriers are a feature of the ECMWF and UKMO analyses, the next task is to establish whether they are a feature of the real atmosphere. Although it is very likely that they are a feature of the real atmosphere, we should consider that they might be an artifact of the various models used in this thesis. However, it is worthwhile to try and realistically model the strength of these barriers. Our findings show that particular care should be taken with the zonal wind distribution used to initialise the model in future experiments.

Indications are that the barrier becomes weaker during the easterly phase of the QBO. The model has a strong barrier throughout most of the model run (with very little variation in strength) despite having easterlies in the tropical stratosphere during this time. This is perhaps another case where the QBO needs to be modelled properly to produce the desired outcome.

Another possible explanation for the strong equatorial PV barriers in the EUGCM is the lack of Kelvin waves in the model. The model's vertical resolution is too coarse to be able to simulate Kelvin waves. Propagating Kelvin waves in the tropical stratosphere would give the model a more active mean meridional circulation, diminishing the effectiveness of any PV barriers.

Whatever the cause of the variation in strength of the equatorial PV barrier, our studies have shown that it is necessary to model it properly. This affects the modelling of any trace species in the tropical stratosphere including H_2O as well as sulphate aerosol.

7.3.3 Radiative heating due to sulphate aerosols

In the conclusions of Chapter 6 it was advised that a more sophisticated treatment of the aerosol heating was required. The ideal solution would be to relate the amount of heating specifically to the mixing ratios of aerosol. Some initial work was carried out with this purpose in mind.

In time, the 2-D model will have an updated version of the Morcrette radiation scheme built in. The new scheme includes the effects of sulphate aerosol and the larger volcanic ash, present in the few weeks after an eruption. Tracer D in section 6.4 would be treated as a sulphate aerosol, complete with radiative effects instead of an inert tracer with additional heating forced in the model. A more ambitious experiment would have the cloud starting as ash in the model, slowly converting to sulphate aerosol, producing heating rates according to how much ash and aerosol there is in the cloud. The work to integrate the new radiative scheme with the 2-D model has already begun.

7.3.4 Representation of volcanic aerosols in the EUGCM

Having just discussed a more realistic treatment of sulphate aerosol in the 2-D model, the natural extension of this is the same in the EUGCM. It is becoming increasingly apparent that for many model experiments, especially those connected with ozone or tropical/mid-latitude transport, the model should be able to represent the impact of volcanic material reaching the stratosphere. This means the heterogeneous chemistry on the sulphate cloud as well as the radiative heating.

During the 1980s the amount of aerosol in the atmosphere hardly ever reached as low as the background loading [*Hitchman et al.*, 1994]. Due to the Mt. Pinatubo eruption, the 1990s are shaping up the same way. *Hitchman et al.* recommend using a decadal average of aerosol for climatology of numerical models instead of the previously accepted background levels.

7.4 Concluding Remarks

The aim of this thesis was to test whether the UGAMP model is realistically representing the circulation of the middle atmosphere. We can say with some confidence that this is the case, but there are some issues which need further attention in the modelling community.

The experiments featuring upper-tropospheric water vapour showed generally good agreement with measurements when the Kuo convection scheme was used. The Betts-Miller convection scheme produced H_2O mixing ratios which were very much greater than observations. The fact that the more recently developed convection scheme should cause such a big difference between model and measurements is worrying. If the scheme is going to be used in the UGAMP model then this problem needs to be rectified.

This thesis also showed that the spread of a volcanic cloud cannot be simulated with just an inert tracer; the effects of radiative heating due to the sulphate aerosol need to be included too. The appearance of equatorial PV barriers has opened up a new area of investigation. It has also provided an added incentive to develop a good representation of the QBO in the UGAMP model.

I believe that atmospheric models will need to simulate all the properties of sulphate aerosol (radiative and chemical) if their calculations of ozone depletion (especially in the more populated areas) are to be realistic. Getting the heterogeneous chemistry right will mean nothing if the aerosol is not distributed around the globe correctly and we should pursue this goal. This thesis provides plausible solutions to this end and they should be followed through.

Appendix A

The TVD Scheme

In the UGAMP GCM advected quantities are defined on model full levels while the vertical velocity is defined on half levels (interfaces). Vertical derivatives are generally expressed in terms of pressure, p, since the model level spacing, $\Delta\mathrm{p}(\mathrm{k}) = \mathrm{p}_{\mathrm{k}+1/2} - \mathrm{p}_{\mathrm{k}-1/2}$ are easily computed. When dealing with vertical advection in a mathematical model, a numerical scheme is needed to determine $\hat{\omega}(\partial \mathrm{q}/\partial \mathrm{p})$ in the equation

$$\frac{\partial q}{\partial t} + \hat{\omega}\frac{\partial q}{\partial p} = \text{otherterms} \tag{7.1}$$

where q can be any quantity to be advected like tracer mixing ratio or specific humidity and $\hat{\omega}$ is the vertical velocity relative to the model levels.

Previously, in the UGCM, a second-order centred difference scheme was used for vertical advection. Unfortunately such a scheme tends to produce spurious oscillations in the advected quantity, upwind of sharp increases of gradient. A sharp vertical gradient features in both water vapour fields and the volcanic cloud distribution. The problems of a centred difference scheme can be solved by using a total variation diminishing (TVD) scheme and such a scheme has now been implemented in the UGCM. The following summarises this scheme based on a more detailed description in *Thuburn* [1993].

The total variation of a function, q, on a set of grid points, k, at time step, n, is defined to be

$$\mathrm{TV}(q^n) = \sum_k |\Delta q^n_{k+1/2}| \tag{7.2}$$

where $\Delta \mathrm{q}_{\mathrm{k}+1/2} = \mathrm{q}_{\mathrm{k}+1} - \mathrm{q}_{\mathrm{k}}$. A scheme is total variation diminishing (TVD) if

$$\mathrm{TV}(q^{n+1}) \leq \mathrm{TV}(q^n). \tag{7.3}$$

In order to achieve this TVD property, a simple flux-limited scheme is used in the UGCM.

The following equation,

$$q_k^{n+1} = q_k^n - (F_{k+1/2} - F_{k-1/2})\frac{\Delta t}{\Delta p_k} \tag{7.4}$$

is an advection scheme in which the change in advected quantity is expressed as the convergence of a flux over a time step. The flux is related to some interfacial value of the advected quantity,

$$F_{k+1/2} = \hat{\omega}_{k+1/2} . q_{k+1/2} . \tag{7.5}$$

Various numerical schemes prescribe the interfacial value, $\mathrm{q}_{\mathrm{k}+1/2}$, in terms of the full level values (...$\mathrm{q}_{\mathrm{k}-1}$, q_{k}, $\mathrm{q}_{\mathrm{k}+1}$, ...) in different ways. This needs to be done in such a way as to give an accurate scheme which satisfies the TVD condition.

Thuburn [1993] shows that a scheme can be constructed in which the fluxes are given by a linear combination of fluxes from a first-order upwind scheme (superscript (L)) and fluxes from another, higher order scheme (superscript (H)),

$$F_{k+1/2} = F_{k+1/2}^{(L)} + \phi_k^+ (F_{k+1/2}^{(H)} - F_{k+1/2}^{(L)}). \tag{7.6}$$

The superscript '+' indicates $\hat{\omega} > 0$. The case for $\hat{\omega} < 0$ follows in an analogous manner. In the first-order upwind scheme the fluxes are given by

$$F_{k+1/2}^{(L)} = \hat{\omega}_{k+1/2} . q_k \tag{7.7}$$

when $\hat{\omega} > 0$.

If $\phi_{\mathrm{k}}^+ \equiv 0$ in equation 7.6 then the scheme becomes a first-order upwind scheme. The first-order upwind scheme satisfies the TVD property but it is very diffusive. Because of this diffusivity, the term in parenthesis is called the anti-diffusive flux which, when multiplied by ϕ, becomes the limited anti-diffusive flux. Thus, ϕ is called the 'flux limiter'. If $\phi_{\mathrm{k}}^+ \equiv 1$ the scheme reduces to the high-order scheme. In general ϕ_{k}^+ may take different values depending on the values of the field being advected.

Removing a factor of $\hat{\omega}_{\mathrm{k}+1/2}$ from equation 7.6 gives

$$q_{k+1/2} = q_k + \phi_k^+ (q_{k+1/2}^{(H)} - q_k) \tag{7.8}$$

For the higher order scheme, the UGCM uses the second-order centred differences scheme and so $q^{(H)}_{k+1/2}$ can be expressed as

$$q^{(H)}_{k+1/2} = \frac{1}{2}(q_k + q_{k+1}) \tag{7.9}$$

so $q_{k+1/2}$ can now be written,

$$q_{k+1/2} = q_k + \frac{1}{2}\phi^+_k(q_{k+1} - q_k). \tag{7.10}$$

The flux limiter used to ensure the scheme satisfies the TVD property was first proposed by *Van Leer* [1974],

$$\phi^+_k = \frac{r^+_k + |r^+_k|}{1 + |r^+_k|} \tag{7.11}$$

where $r^+_k + \Delta q_{k-1/2}/\Delta q_{k+1/2}$ and $\Delta q_{k+1/2} = q_{k+1} - q_k$. Now the interfacial value, $q_{k+1/2}$ is expressed in terms of full level values and the scheme is TVD. Due to the fact that this flux limiter is specific to each grid box, not only is the TVD property satisfied on a global scale, but locally, extrema cannot grow and no new extrema can appear, so the solution is free from spurious oscillations.

However, while this scheme allows us to determine $\partial(\hat{\omega}q)/\partial p$, equation 7.1 requires us to work out $\hat{\omega}(\partial q/\partial p)$. This can be achieved by writing

$$\left(\hat{\omega}\frac{\partial q}{\partial p}\right)_k = \left(\frac{\partial(\hat{\omega}q)}{\partial p}\right)_k - \left(q\frac{\partial\hat{\omega}}{\partial p}\right)_k \tag{7.12}$$

Thuburn [1993] gives a far more rigorous explanation of the TVD scheme and how things like mass conservation, boundary conditions and time stepping schemes affect it. Although this brief summary ignores these things it does serve to give an indication of what the TVD scheme does and how it does it.

The vertical advection scheme in the EUGCM is also TVD but uses a higher order scheme in the anti-diffusive flux term. The higher-order scheme is the fourth-order centred difference scheme and the flux limiter used is *Leonard's* [1988] 'universal limiter'.

References

Andrews, D. G., J. R. Holton and C. B. Leovy, *Middle Atmosphere Dynamics*, 498pp, Academic Press, San Diego, Calif., 1987.

Angell, J. K., Comparison of stratospheric warming following Agung, El Chichon and Pinatubo volcanic eruptions, *Geophys. Res. Lett., 20*, 715-718, 1993.

Ansmann, A., U. Wandinger and C. Weitkamp, One-year observations of Mount Pinatubo aerosol with an advanced Raman lidar over Germany at 53.5°N, *Geophys. Res. Lett., 20*, 711-714, 1993.

Betts, A. K. and M. J. Miller, The Betts-Miller scheme, *The representation of cumulus convection in numerical models of the atmosphere*, Eds K. A. Emanuel and D. J. Raymond, American Meteorological Society, 1993.

Bluth, G. J. S., S. D. Doiron, C. C. Schnetzler, A. J. Krueger and L. S. Walter, Global tracking of the SO_2 clouds from the June, 1991 Mount Pinatubo eruptions, *Geophys. Res. Lett., 19*, 151-154, 1992.

Bowman, K. P., Large-scale isentropic mixing properties of the Antartic polar vortex from the analyzed winds, *J. Geophys. Res., 98*, 23,013-23,027, 1993.

Boville, B. A., J. R. Holton and P. W. Mote, Simulation of the Pinatubo aerosol cloud in a general circulation model, *Geophys. Res. Lett., 18*, 2281-2284, 1991.

Brassuer, G. P. and C. Granier, Mount Pinatubo aerosols, chlorofluorocarbons, and ozone depletion, *Science, 257*, 1239-1242, 1992.

Cacciani, M., P. Di Girolamo, A. Di Sarra, G. Fiocco and D Fuà, Volcanic aerosol layers observed by lidar at south pole, September 1991 - June 1992, *Geophys. Res. Lett., 20*, 807-810, 1993.

Chandra, S., and R. S. Stolarski, Recent trends in stratospheric total ozone: implications of dynamical and El Chichon perturbations, *Geophys. Res. Lett., 18*, 2277-2280, 1991.

Charney, J. G. and P. G. Drazin, Propagation of planetary-scale disturbances from the lower into the upper atmosphere, *J. Geophys. Res., 66*, 83-109, 1961.

Chen, P., J. R. Holton and R. Swinbank, A quasi-permiable barrier in the equatorial lower stratosphere, *Geophys. Res. Lett., 22*, 259-262, 1995.

Deschler, T., D. J. Hofmann, B. J. Johnson and W. R. Rozier, Balloonborne measurements of the Pinatubo aerosol size distribution and volatility at Laramie, Wyoming during the Summer of 1991, *Geophys. Res. Lett., 19*, 199-202, 1992.

Dritschel, D. G., Contour dynamics and contour surgery: numerical algorithms for extended, high-resolution modelling of vortex dynamics in two-dimensional, inviscid, incompressible flows, *Computer Phys. Rep., 10*, 78-146, 1989.

Ertel, H., Ein neuer hydrodynamischer wirbelsatz, *Meteorol. Z. 59*, 277 ,1942.

Fels, S. B., Radiative-dynamical interactions in the middle atmosphere, *Issues in Atmosphere and Oceanic Modeling*, ed. S. Manabe, 277-300, Academic Press, Orlando, Fla., 1985.

Grant, W. B., J. Fishman, E. V. Browell, V. G. Brackett, D. Nganga, A. Minga, B. Cros, R. E. Veiga, C. F. Butler, M. A. Fenn and G. D. Nowicki, Observations of reduced ozone concentrations in the tropical stratosphere after the eruption of Mt. Pinatubo, *Geophys. Res. Lett., 19*, 1109-1112 ,1992.

Haigh, J. D., Radiative heating in the lower stratosphere and the distribution of ozone in a two-dimensional model, *Quart. J. Roy. Meteorol. Soc.,* 110, 167-185, 1984.

Haltiner, G. J. and R. T. Williams, *Numerical Prediction and Dynamic Meteorology*, 477 pp, John Wiley and Sons, New York, U.S.A., 1980.

Harwood, R. S., and J. A. Pyle, A two-dimensional mean circulation model for the atmosphere below 80km, *Quart. J. Roy. Meteorol. Soc.,* 101, 723-747, 1975.

Hayashida, S., and Y. Sasano, Stratospheric aerosol change in the early stage of volcanic disturbance by the Pinatubo eruption observed over Tsukuba, Japan, *Geophys. Res. Lett., 20*, 575-578, 1993.

Haynes, P. H., C. J. Marks, M. E. McIntyre, T. G. Shepherd and K. P. Shine, On the "downward control" of extratropical diabatic circulations by eddy-induced mean zonal forces, *J. Atmos. Sci., 48*, 651, 1991.

Hitchman, M. H., M. McKay and C. R. Trepte, A climatology of stratospheric aerosol, *J. Geophys. Res., 99*, 20689-20700, 1994.

Hofmann, D. J., and S. Solomon, Ozone destruction through heterogeneous chemistry, *J. Geophys. Res., 94*, 5029-5041, 1989.

Holton, J. R., *An Introduction to Dynamical Meteorology*, 511pp, Academic Press, San Diego, Calif., 1992.

Hoskins, B. J., M. E. McIntyre and A. W. Robertson, On the use and significance of isentropic potential vorticity maps, *Quart. J. Roy. Meteorol. Soc., 111*, 877-946, 1987.

Johnston, P. V., R. L. McKenzie, J. G. Keys and W. A. Matthews, Observations of depleted stratospheric NO_2 following the Pinatubo volcanic eruption, *Geophys. Res. Lett., 19*, 211-213, 1992.

Juckes, M. N. and M. E. McIntyre, A high resolution, one-layer model of breaking planetary waves in the stratosphere, *Nature,* 328, 590 ,1987.

Kasten, F., Falling speed of aerosol particles, *Journal of Applied Meteorology, 7*, 944-947, 1968.

Kelly, K. K., A. F. Tuck and T. Davies, Wintertime asymmetry of upper tropospheric water between the northern and southern hemispheres, *Nature, 353*, 244-247, 1991.

Kinne, S., O. B. Toon and M. J. Prather, Buffering of stratospheric circulation by changing amounts of tropical ozone: a Pinatubo case study, *Geophys. Res. Lett., 19*, 1927-1930, 1992.

Kinnersley, J. S., and R. S. Harwood, An isentropic two-dimensional model with an interactive parametrization of dynamical and chemical planetary-wave fluxes, *Quart. J. Roy. Meteorol. Soc., 119*, 1167-1193, 1993.

Kinnison, D. E., K. E. Grant, P. S. Connell, D. A. Rotman and D. J. Wuebbles, The chemical and radiative effects of the Mount Pinatubo eruption, *J. Geophys. Res., 99*, 25705-25731, 1994.

Kuo, H. L., Further studies of the parametrization of the influence of cumulus convection on large-scale flow, *J. Atmos. Sci., 31*, 1232-1240, 1974.

Labitzke, K., and P. M. McCormick, Stratospheric temperature increases due to Pinatubo aerosols, *Geophys. Res. Lett., 19*, 207-210, 1992.

Lacis, A., J. Hansen and M. Sato, Climate forcing by stratospheric aerosols, *Geophys. Res. Lett., 19*, 1607-1610, 1992.

Lambert, A., R. G. Grainger, J. J. Remedios, C. D. Rodgers, M. Corney and F. W. Taylor, Measurements of the evolution of the Mt. Pinatubo aerosol cloud by ISAMS, *Geophys. Res. Lett., 20*, 1287-1290, 1993.

Lary. D. J., M. Balluch and S. Bekki, Solar heating rates after a volcanic eruption: the importance of SO_2 absorption, *Quart. J. Roy. Meteorol. Soc., 120*, 1683-1688, 1994.

Leonard, B. P., Universal limiter for transient interpolation modeling of the advective transport equations: the ULTIMATE conservative difference scheme, *NASA Technical Memorandom 100061-ICOMP-88-11*, 1988.

Leovy, C. B., C. -R. Sun, M. H. Hitchman, E. E. Remsberg, J. M. Russell, L. L. Gordley, J. C. Gille and L. V. Lyjak, Transport of ozone in the middle stratosphere: evidence for planetary wave breaking, *J. Atmos. Sci., 42*, 230, 1985

Manney, G. L., and R. W. Zurek, Interhemispheric comparison of the development of the stratospheric polar vortex during Fall: a 3-dimensional perspective for 1991-92, *Geophys. Res. Lett., 20*, 1275-1278, 1993.

McCormick, P. M., and R. E. Veiga, SAGE II measurements of early Pinatubo aerosols, *Geophys. Res. Lett., 19*, 155-158, 1992.

McGee, T. J., P. Newman, M. Gross, U. Singh, S. Godin, A.-M. Lacoste and G. Megie, Correlation of ozone loss with the presence of volcanic aerosols, *Geophys. Res. Lett., 21*, 2801-2804, 1994.

McIntosh, D. H., and A. S. Thom, *Essentials of Meteorology*, 240pp, Wykeham Publications Ltd., London, 1983.

McIntyre, M. E., On the "wave momentum" myth, *J. Fluid Mech., 106*, 331, 1981.

McIntyre, M. E., Dynamics and tracer transport in the middle atmosphere: an overview of some recent developments, *Transport Processes in the Middle Atmosphere*, 1987.

McIntyre, M. E., On the Antarctic ozone hole, *J. Atmosph. Terr. Phys., 51*, 29-43, 1989.

McIntyre, M. E., Atmospheric dynamics: Some fundamentals, with observational implications, *The use of EOS for studies of atmospheric physics*, eds. J. C. Gille, and G. Visconti, 313-386, 1992.

McIntyre, M. E. and T. N. Palmer, The surf zone in the stratosphere, *J. Atmosph. Terr. Phys., 46*, 825-849 ,1984.

McKeen, S. A., S. C. Liu and C. S. Kiang, On the chemistry of stratospheric SO_2 from volcanic eruptions, *J. Geophys. Res., 89*, 4873-4881, 1984.

Morcrette, J.-J., Impact of changes to the radiation transfer parameterizations plus cloud optical properties in the ECMWF model, *Mon. Weather Rev., 118*, 847-873, 1990.

Norton, W. A., Breaking Rossby waves in a model stratosphere diagnosed by a vortex-following coordinate system and a technique for advecting material contours, *J. Atmos. Sci., 51*, 654-673, 1994.

Palmer, T. N., G. J. Shutts and R. Swinbank, Alleviation of a systematic westerly bias in general circulation and numerical weather prediction models through an orographic gravity wave drag parametrization, *Quart. J. Roy. Meteorol. Soc., 112*, 1001-1039, 1986.

Prather, M., Catastrophic loss of stratospheric ozone in dense volcanic clouds, *J. Geophys. Res., 97*, 10,187-10,191, 1992.

Randel, W. J., J. C. Gille, A. E. Roche, J. B. Kumer, J. L. Mergenthaler, J. W. Waters, E. F. Fishbein and W. A. Lahoz, Stratospheric transport from the tropics to middle latitudes by planetary-wave mixing, *Nature, 365*, 533-537, 1993.

Read, W. G., L. Froidevaux and J. W. Waters, Microwave Limb Sounder measurement of stratospheric SO_2 from the Mt. Pinatubo volcano, *Geophys. Res. Lett., 20*, 1299-1302, 1993.

Read, W. G., J. W. Waters, D. A. Flower, L. Froidevaux, R. F. Jarnot, D. L. Hartmann, R. S. Harwood and R. B. Rood, Upper-tropospheric water vapor from UARS MLS, *Bulletin of the American Met. Soc., 76*, 2381-2389, 1995.

Rodriguez, J. M., M. K. W. Ko and N. D. Sze, Role of heterogeneous conversion of N_2O_5 on sulphate aerosols in global ozone losses, *Nature, 352*, 134-137, 1991.

Rood, R., A. Douglass and C. Weaver, Tracer exchange between tropics and middle latitudes, *Geophys. Res. Lett., 19*, 805-808, 1992.

Rosen, J. M., N. T. Kjome and H. Fast, Penetration of Mt. Pinatubo aerosols into the north polar vortex, *Geophys. Res. Lett., 19*, 1751-1754, 1992.

Rosen, J. M., N. T. Kjome, R. L. McKenzie and J. B. Liley, Decay of Mount Pinatubo aerosol at mid-latitudes in the northern and southern hemispheres, *J. Geophys. Res., 99*, 25733-25739, 1994.

Schoeberl, M. R., L. R. Lait, P. A. Newman and J. E. Rosenfield, The structure of the polar vortex, *J. Geophys. Res., 97*, 7859-7882, 1992.

Schoeberl, M. R., P. K. Bhartia and E. Hilsenrath, Tropical ozone loss following the eruption of Mt. Pinatubo, *Geophys. Res. Lett., 20*, 29-32, 1993.

Shine, K. P., The middle atmosphere in the absence of dynamical heat fluxes, *Quart. J. Roy. Meteorol. Soc., 113*, 603-633, 1987.

Simmons, A. J., D. M. Burridge, C. Girard and W. Wergen, The ECMWF medium-range prediction models: Development of the numerical formulations and the impact of increased resolution, *Meteorol. Atmos. Phys., 40*, 28-60, 1989.

Slingo, J. M., K. R. Sperber, J. -J. Morcrette and G. L. Potter, Analysis of the temporal behaviour of convection in the tropics of the ECMWF model, *J. Geophys. Res., 97*, 18,119-18,135, 1992.

Stolarski, R. S., Watching a disappearing shield, *Aerospace America, 26*, 32-35, 1988.

Stowe, L. L., R. M. Carey and P. P. Pellegrino, Monitoring the Mt. Pinatubo aerosol layer with NOAA/11 AVHRR data, *Geophys. Res. Lett., 19*, 159-162, 1992.

Swinbank, R., and A. O'Neill, A stratosphere-troposphere data assimilation system, *Mon. Weather Rev., 122*, 686-702, 1994.

Thomason, L. W., Observations of a new SAGE II aerosol extinction mode following the eruption of Mt. Pinatubo, *Geophys. Res. Lett., 19*, 2179-2182, 1992.

Thuburn, J., Use of a flux-limited scheme for vertical advection in a GCM, *Quart. J. R. Met. Soc., 119*, 469-487, 1993.

Tiedke, M., W. A. Heckley and J. M. Slingo, Tropical forecasting at ECMWF: The influence of physical parametrization on the mean structure of forecasts and analyses, *Quart. J. Roy. Meteorol. Soc., 114*, 639-664, 1988.

Trepte, C. R., and M. H. Hitchman, Tropical stratospheric circulation deduced from satellite aerosol data, *Nature, 355*, 626-628, 1992.

Trepte, C. R., R. E. Veiga and M. P. McCormick, The poleward dispersal of Mount Pinatubo volcanic aerosol, *J. Geophys. Res., 98*, 18563-18673, 1993.

Van Leer, B., Towards the ultimate conservative difference scheme. II:Monotonicity and conservation combined in a second order scheme. *J. Comput. Phys., 31*, 335-362, 1974.

WMO, *Scientific Assessment of Ozone Depletion:1994*, Global Ozone Research and Monitoring Project–Report No 37, World Meteorological Organisation, Geneva, Switzerland, 1995.

Young, R. E., H. Houben and O. B. Toon, Radiatively forced dispersion of the Mt. Pinatubo volcanic cloud and induced temperature perturbations in the stratosphere during the first few months following the eruption, *Geophys. Res. Lett., 21*, 369-372, 1994.